Analytical Procedures for Estimating Structural Response to Acoustic Fields Generated by Advanced Launch Systems

Phase II

by

I. Elishakoff, Y.K. Lin, L.P. Zhu, J.J. Fang and G.Q. Cai

Technical Report submitted to
Kennedy Space Center

Center for Applied Stochastics Research
Florida Atlantic University

July, 1994

TABLE OF CONTENTS

EXECUTIVE SUMMARY

This report supplements a previous report of the same title submitted in June, 1992. It summarizes additional analytical techniques which have been developed for predicting the response of linear and nonlinear structures to noise excitations generated by large propulsion power plants.

The report is divided into nine chapters. The first two deal with incomplete knowledge of boundary conditions of engineering structures. The incomplete knowledge is characterized by a convex set, and its diagnosis is formulated as a multi-hypothesis discrete decision-making algorithm, with attendant criteria of adaptive termination.

Chapter 1 deals with rectangular plates. The boundary conditions are represented by transverse and rotational springs with uncertain spring constants, modeling possible damages along the boundary. Bolotin's dynamic edge effect method is applied to determine the natural frequencies. Chapter 2 is devoted to the identification of end conditions for beams, and their natural frequencies, using a finite element formulation.

Chapter 3 deals with free and forced vibrations of periodic multi-span beams. The concept of wave propagation in periodic structures of Brillouin is utilized to investigate the wave motion at the periodic supports. Chapter 4 discusses the vibrations of a two-dimensional grillage. Each periodic support of such a grillage is constrained by a rigid transverse support and two elastic rotational springs in two orthogonal directions. The elastic springs on each row are identical; thus, the grillage forms a two-dimensional periodic pattern. The four boundary edges of the grillage are assumed to be either simply supported or clamped. Again the wave

propagation concept is used for the analysis.

Chapter 5 studies the random vibration of a typical weather protection system for space shuttles at a launch site. It is shown that the Timoshenko-beam model captures the essential structural behaviors of such a system. The use of the conventional Bernoulli-Euler beam theory may result in an error of about 50% in the computed mean-square value of the bending moments.

Chapter 6 to 9 are devoted to the analysis of nonlinear structures. Although there exist known methods to obtain exact mean-square responses of non-linear systems, they are applicable only to systems subjected to highly idealized random excitations. Therefore, the approximate method of stochastic linearization remains the only practical means to deal with complex continuous structures under rather general random loadings. In this report, a new energy-based stochastic linearization method is developed. Chapter 6 discusses its applications to discrete systems, whereas Chapters 7 and 8 deal with elastic beams. The simplest cases, for which exact solutions are obtainable, are considered in Chapter 7. The results are compared with those obtained from the conventional and the new stochastic linearization techniques. It is shown that the new stochastic linearization technique yields more accurate results than those from the conventional one. Chapter 8 investigates the nonlinear response of a beam when an exact solution is unavailable. The results must then be compared with those of Mote Carlo simulations. Again, superior performance of the suggested approximation technique is demonstrated.

The damping force is assumed to be viscous and linear in Chapters 7 and 8. This assumption is abandoned in Chapter 9. When both damping and the restoring force are nonlinear, the method of partial stochastic linearization is preferable, in which only the non-linear damping force in the original system is replaced by a linear viscous damping, while the non-linear restoring force remains unchanged. The replacement is based on the criterion that the same

average work is performed by the nonlinear damping force in the original system and its linear counterpart.

The possibilities of future research on this general subject are diverse. General commercially available computer software for engineering structures do not include programs for rigorous random vibration or convex analyses. Development of comprehensive finite element programs to incorporate random vibration and convex analyses into general purpose codes is therefore a must, especially for application to large-scale structures. It is hoped that these tasks can be addressed in phase III.

CHAPTER # 1:

Diagnosis of Local Modifications in the Boundary Conditions of a Rectangular Plate

DIAGNOSIS OF LOCAL MODIFICATIONS IN THE BOUNDARY CONDITIONS OF A RECTANGULAR PLATE

Isaac Elishakoff and Jianjie Fang

Center for Applied Stochastics Research
and Department of Mechanical Engineering
Florida Atlantic University
Boca Raton, FL 33431-0991, USA

1. INTRODUCTION

There is a vast literature on the free vibrations, as well as forced vibrations, either due to deterministic or random excitations, of thin rectangular plates. To the best of our knowledge, in all these studies the boundary conditions along the edges of the plates are assumed as known. Hence the investigators consider all possible combinations of boundary conditions along edges, namely those of simply supported (SS), clamped (C), free (F), or, more generally, elastically supported (ES) conditions. The natural question arises: How to identify the "true" boundary conditions? In addition, the integrity of plate-like structures is often determined by the condition at the junction of the plate with the remainder of the structure. Diagnosis of the integrity of the junction can be performed by estimating the existing boundary conditions.

In this study the boundary condition diagnosis is formulated as a discrete multi-hypothesis decision problem. This facilitates diagnostic determination of global features of the boundary conditions, without the necessity of detailed full reconstruction of the boundary condition profile along the entire perimeter of the plate. In particular, we concentrate on diagnosis of localized alteration of the boundary conditions due to some adverse effects, including the high level

excitation. The boundary conditions are modeled in general as translational or rotational springs. In particular, the aims of the diagnosis are (a) to identify the interval along the boundary within which the spring stiffnesses deviate from the nominal values, and (b) to diagnose the best nominal value of the stiffness along the adversely attached boundary. This diagnosis is based on measurement of a certain number of natural frequencies of the plate. In this study, the boundary condition is specified by the torsional stiffness at each point of the continuous interface between the plate and the structure. Translational stiffness at the boundary is identified with infinity, for the sake of simplicity. This implies that the transverse displacement vanishes identically along the perimeter of the plate.

It must be stressed that diagnosis of the boundary conditions does not imply the complete identification of these continuous functions. Indeed, total reconstruction of the boundary stiffness functions is not only quite challenging but also unnecessary for many operational or maintenance decisions. Rather, diagnosis of the boundary condition means identification of the adversely affected region on the boundary and estimation of limits on the magnitude of the stiffness change. In other words, the diagnosis will be considered satisfactory even though the characterization of the boundary condition is still partial or fragmentary. We utilize convex models to represent the degree of uncertainty in the boundary condition modification which can acceptably remain after completing the diagnosis. This implies that diagnosis of the boundary condition in fact means identification of the *convex model* to which the actual boundary stiffness profile belongs.

This will then allow us to precisely formulate the diagnosis as a discrete multi-hypothesis decision problem with attendant formulation of the adaptive termination of this algorithm. The cornerstone of the method is the ability of evaluating the frequency spectrum of a plate with

specified boundary conditions, which can be performed analytically or numerically. This is necessary for implementing the minimum-distance decision algorithm upon which the diagnosis is based. In the present study we employ the generalized Bolotin's dynamic edge effect method to determine the approximate natural frequencies and normal modes of elastically supported isotropic, uniform rectangular plates. The entire procedure of diagnosis of local modifications is implemented with numerically simulated diagnosis.

2. CONVEX MODELS OF UNCERTAINTY

As indicated above, diagnosis of the boundary condition means, in this study, identification of the affected region on the boundary and estimation of limits on the magnitude of the stiffness change. It is assumed that only the torsional stiffness is modified by boundary condition failure. Convex models put forward by Ben-Haim and Elishakoff [1] will be used to specify the degree of precision required in the diagnosis of the boundary torsional stiffness profile.

A convex model is a set of functions. Each element of the set represents a possible realization of an uncertain quantity of interest. In our case, these functions are the torsional stiffness profiles $k(s)$, where s is the position around the periphery of the plates. The diagnosis will be considered satisfactory when the uncertainty in the boundary condition has been reduced to an acceptable preselected level. Convex models will represent the acceptable uncertainty in the boundary condition. This means that diagnosis of the boundary condition is in fact no more than identification of the convex model to which the actual boundary stiffness profile belongs. It should be stressed again that the actual stiffness profile will not be identified; only the convex

model to which it belongs is sought by the diagnosis.

While several different convex models are available (see Ben-Haim and Elishakoff, [1]), the following simple model is particularly suitable for representing uncertain localized failures. Let S represent the boundary of the plate and let I_n , $n = 1,...N$ denote subsets of the boundary S. The sets I_n may be simple connected intervals, or unions of such intervals. Let $\bar{k}(s)$ be the nominal torsional stiffness profile, $s \in S$. We define convex models which are sets of stiffness profiles which deviate from the nominal profile only in a particular interval I_n. Specifically, the convex model C_{mn} is the following set of hypothesized stiffness profiles [2]:

$$C_{mn} = \left\{k(s) : k(s) = \bar{k}(s),\ s \notin I_n;\ |k(s) - K_m| \le \delta,\ s \in I_n\right\} \tag{1}$$

In other words, C_{mn} is the set of torsional stiffness profiles $k(s)$ which are equal to the nominal function $\bar{k}(s)$ outside the region I_n, but which deviate by as much as $\pm\delta$ from the constant value K_m throughout the region I_n. One recognizes that C_{mn} is a *localized uniform bound convex model.*

3. MULTI-HYPOTHESIS DECISION

The reference values K_m in the convex models in Eq. (1) can assume any of the M different values $K_1, ...,K_M$. Likewise, failure (i.e. "weakening" of the boundary conditions intended in the original design) can occur in any of N different boundary intervals, $I_1, ..., I_N$. Thus diagnosis of the boundary condition involves deciding which of the MN convex models contains the true boundary stiffness profile. This decision is based on a multi-hypothesis formulation.

In its simplest form the multi-hypothesis decision algorithm requires the choice of one representative or *hypothesized* stiffness profile from each convex model. It should be noted that in its more general form, more than one hypothesized stiffness profile is chosen for each convex model. Let $h_{mn}(s)$ denote the hypothesized stiffness profile from convex model C_{mn}. That is, $h_{mn}(s) \in C_{mn}$. Let $\omega^{(mn)} = (\omega_1^{(mn)},...\omega_J^{(mn)})$ indicate a vector of J natural frequencies of a plate whose boundary stiffness profile is $h_{mn}(s)$. Furthermore, let $\Omega = (\Omega_1, ...\Omega_J)$ represent the vector of measured natural frequencies of the same modes. Let $\|x\|$ denote a norm of the vector x.

The distance from the measured natural frequency vector Ω to the anticipated natural frequency vector $\omega^{(mn)}$ based on the *mnth* hypothesis is :

$$H_{mn} = \|\Omega - \omega^{(mn)}\| \tag{2}$$

It is reasonable to conclude that the true stiffness profile is likely to belong to the convex model whose anticipated spectrum of natural frequencies is closest to the measured spectrum. Let the pair of indices m_0 and n_0 satisfy:

$$H_{m_0 n_0} = \min_{m,n} H_{mn} \tag{3}$$

The multi-hypothesis decision is that the true stiffness profile belongs to the convex model $C_{m_0 n_0}$.

4. DIAGNOSIS PROCEDURE

The decision algorithm implied by Eq. (3) will always reach a decision, regardless whether or not the least distance, H_{mn}, is small. In other words, the multi-hypothesis will choose

the most likely one from among the available options, but none may be particularly convincing, due to unsatisfactory choice in the preliminary analysis.

Based on the assumption that all needed low-order frequencies of the plate are measured, the diagnosis procedure which we follow, in broad outline, is as follows:

1. *Construct* the convex model of the unknown boundary conditions by taking advantage of the available prior knowledge of the range of values which can reasonably be expected to occur. If such a knowledge is unavailable,

2. *Calculate* all the natural frequencies of interests for each hypothesized stiffness profile $h_{mn}(s)$ by employing the generalized Bolotin's dynamic edge effect method, or any other approximate, analytical, or purely numerical technique.

3. *Compute* the distances between the measured frequencies and the ones corresponding to hypothesized stiffnesses according to the general definition given in Eq. (2).

4. *Decide* which convex model is the most likely one, on the basis of minimum distance algorithm relation (3). If H_{mn} is larger than a specified threshold value θ then decision is deferred, and a new choice of the mostly convex model is made. The diagnosis process is terminated if

$$H_{mn} \leq \theta \tag{4}$$

As is seen, one of the cornerstone of the method is the ability to determine the natural frequencies of plates under arbitrary boundary conditions. This problem is addressed in the following section.

5. CALCULATION OF EIGENFREQUENCY SPECTRA

There exists an ample literature on vibration of elastic plates, as described in definitive

reviews by Leissa [3-5]. For plates with two opposite edges simply supported but with arbitrary boundary conditions along the remaining edges, exact solution is available. This class of vibration problems is referred to as *Lévy problems*. For *non-Lévy problems* exact solutions are presently unavailable and approximate techniques should be resorted to. Energy based techniques, like methods of Rayleigh, Rayleigh-Ritz, Galerkin, or the finite element methods are accurate and relatively incumbersome for the determination of the lower end of frequency spectrum. However, for higher frequencies use of energy methods becomes computationally expensive and cumbersome.

For higher frequencies, Bolotin [6] proposed so called *dynamic edge effect method.* It is based on the physical observation, that for high frequencies the mode shapes of plates of different boundary conditions have a somewhat similar behavior except in the zones near edges, where the effect of the boundary conditions is prominent. Bolotin therefore suggested to construct solutions emanating from each edge. In the interior region he "tailored" these solutions to yield two simultaneous characteristic equations. This method found ample popularity both in the East and the West (for appropriate bibliography one may consult review article by Elishakoff [7]). It turned out, however, that for certain instances it was impossible to construct solutions, having sufficient number of decaying terms, to converge to an interior solution. This phenomenon was called by Bolotin *degeneracy of the dynamic edge effect method.* The "cure" for such a situation was provided by Vijayakumar [8] and Elishakoff [9]. In particular in Ref. 9 it was suggested to solve two auxiliary Levy-type problems in conjunction with the relationship between the natural frequency and the modal numbers. In this formulation Bolotin's idea of necessity of decaying solutions towards the interior region was abandoned, and solution was

required to be valid in hypothesized "strips", somewhat similar to the original idea of Germaine (modified by Lagrange) to derive the very equations for the plate. Here we follow the generalization of Bolotin's dynamic edge effect method for the elastically supported plates, but in the framework of Ref. 9.

Differential equation of motion of Kirchoff-Love plate reads

$$D\nabla^2\nabla^2 w + \rho h\frac{\partial^2 w}{\partial t^2} = 0 \tag{5}$$

where D is the flexural stiffness, ρ-material density, h-thickness, $w(x,y,t)$ - displacement $\nabla^2 = \partial^2/\partial x^2 + \partial^2/\partial y^2$ Laplace operator, x and y space coordinates, t - time. The boundary conditions for rotationally restrained rectangular plate are

$$\gamma_1 M_x = \alpha_1\frac{\partial w}{\partial x} \qquad x = 0 \tag{6}$$

$$-\gamma_2 M_x = \alpha_2\frac{\partial w}{\partial x} \qquad x = a \tag{7}$$

$$\delta_1 M_y = \beta_1\frac{\partial w}{\partial y} \qquad y = 0 \tag{8}$$

$$-\delta_2 M_y = \beta_2\frac{\partial w}{\partial y} \qquad y = b \tag{9}$$

$$w = 0 \qquad on \qquad S \tag{10}$$

where a and b are side lengths of the plate,

$$M_x = D\left(\frac{\partial^2 w}{\partial x^2} + \nu\frac{\partial^2 w}{\partial y^2}\right) \tag{11}$$

$$M_y = D\left(\frac{\partial^2 w}{\partial y^2} + \nu\frac{\partial^2 w}{\partial x^2}\right) \tag{12}$$

are the bending moments per unit length. Coefficients α_1 and α_2 are stiffnesses of rotational springs in the x direction; β_1 and β_2 are stiffness of rotational springs in the y direction. In addition, artificial parameters γ_1, γ_2, δ_1 and δ_2 are introduced. They take values either zero or unity, in order to accommodate various possible ideal boundary conditions. For example $\gamma_1 = 0$, $\alpha_1 \neq 0$ corresponds to the edge $x = 0$ being clamped; combination $\gamma_1 \neq 0$, $\alpha_1 = 0$ corresponds to simply supported edge.

For free vibrations we seek solution of the Eq. (5) in the form

$$w(x,y,t) = W(x,y)e^{i\omega t} \tag{13}$$

where $W(x,y)$ is the vibration mode and ω is the sought natural frequency. Eq. (5) becomes

$$D\nabla^2\nabla^2 W - \rho h\omega^2 W = 0 \tag{14}$$

Consider first the plate which is simply supported all round S, with boundary conditions

$$W = 0\,, \qquad \nabla^2 W = 0 \tag{15}$$

The mode shape

$$W_{uv} = \sin\frac{u\pi x}{a}\sin\frac{v\pi y}{b}\,, \quad (u, v = 1, 2, \cdots) \tag{16}$$

satisfies both the governing differential equation (14) and the boundary conditions (15). The

serial numbers u and v are positive integers, representing, respectively, number of half waves in x - and - y - directions. The substitution of Eq. (16) into Eq. (14) yields the expression of the natural frequency

$$\omega_{uv}^2 = \frac{D}{\rho h}\left[\left(\frac{u\pi}{a}\right)^2 + \left(\frac{v\pi}{b}\right)^2\right]^2 \tag{17}$$

We introduce the nondimensional frequency parameter λ_{uv} defined by

$$\lambda_{uv} = \omega_{uv} a^2\sqrt{\rho h/D} = \pi^2\left[u^2 + (a/b)^2 v^2\right] \tag{18}$$

Consider now the plate with original boundary conditions specified in Eqs (6-10). Following the spirit of the Bolotin's dynamic edge effect method [6] as well as its generalization by Elishakoff [9], we represent the relationship between the natural frequency squared and modal numbers in a manner similar to the Eq. (17)

$$\omega^2 = \frac{D}{\rho h}\left[\left(\frac{p\pi}{a}\right)^2 + \left(\frac{q\pi}{b}\right)^2\right]^2 \tag{19}$$

where under new circumstances p and q, are unknown positive decimal numbers rather than integers. Similar to Eq. (18), the corresponding nondimensional frequency λ is

$$\lambda_{pq} = \omega a^2\sqrt{\rho h/D} = \pi^2\left[p^2 + (a/b)^2 q^2\right] \tag{20}$$

Eq. (14) becomes

$$\nabla^2\nabla^2 W - \left[\left(\frac{p\pi}{a}\right)^2 + \left(\frac{q\pi}{b}\right)^2\right]^2 W = 0 \tag{21}$$

The solution of this equation can be represented as composed of solutions W_1 and W_2 of following problems

$$\left\{\nabla^2 + \left[\left(\frac{p\pi}{a}\right)^2 + \left(\frac{q\pi}{b}\right)^2\right]\right\} W_1 = 0 \tag{22}$$

$$\left\{\nabla^2 - \left[\left(\frac{p\pi}{a}\right)^2 + \left(\frac{q\pi}{b}\right)^2\right]\right\} W_2 = 0 \tag{23}$$

These will be determined, as suggested by Elishakoff [9], from two auxiliary problems discussed below.

FIRST AUXILIARY PROBLEM

Consider the first auxiliary problem, referred to as *X-Problem*. We seek for the solution of Eq. (21) in the form

$$W(x,y) = X(x) \sin\frac{q\pi y}{b} \tag{24}$$

with boundary conditions, (6), and (7) and (10). Instead of Equations (22) and (23) we arrive at

$$\frac{d^2}{dx^2} X_1 + \left(\frac{p\pi}{a}\right)^2 X_1 = 0 \tag{25}$$

$$\frac{d^2}{dx^2}X_2 - \left[\left(\frac{p\pi}{a}\right)^2 + 2\left(\frac{q\pi}{b}\right)^2\right]X_2 = 0 \tag{26}$$

The solution for the function $X(x)$

$$X(x) = X_1(x) + X_2(x) \tag{27}$$

reads

$$X(x) = A_1 \sin\frac{p\pi x}{a} + A_2 \cos\frac{p\pi x}{a} + A_3 \sinh\frac{r\pi x}{a} + A_4 \cosh\frac{r\pi x}{a} \tag{28}$$

where the first two terms are associated with Eq. (25) and the last two terms are associated with Eq. (26). In Eq. 26 the following notation has been used

$$r = p\sqrt{1 + 2\left(\frac{q}{p}\right)^2\left(\frac{a}{b}\right)^2} \tag{29}$$

and A_j are constants of integration.

Boundary conditions (6), (7) and (10) lead following conditions for $X(x)$

$$X = 0, \quad at \quad x = 0, \quad x = a \tag{30}$$

$$\gamma_1 D\frac{d^2X}{dx^2} = \alpha_1\frac{dX}{dx} \quad at \quad x = 0 \tag{31}$$

$$-\gamma_2 D\frac{d^2X}{dx^2} = \alpha_2\frac{dX}{dx} \quad at \quad x = a \tag{32}$$

In writing Eqs (31) and (32) we have used the boundary conditions (6) and (7). Satisfaction of boundary conditions leads to:

$$A_2 + A_4 = 0 \tag{33}$$

$$A_1 s_1 + A_2 c_1 + A_3 S_1 + A_4 C_1 = 0 \tag{34}$$

$$A_1\phi_1 + A_2\gamma_1 p\pi + A_3 R\phi_1 - A_4 R^2\gamma_1 p\pi = 0 \tag{35}$$

$$\begin{aligned} &A_1(\phi_2 c_1 - \gamma_2 p\pi s_1) - A_2(\phi_2 s_1 + \gamma_2 p\pi c_1) \\ &+ A_3(\phi_2 R C_1 + \gamma_2 R^2 p\pi S_1) + A_4(\phi_2 R S_1 + R^2 p\pi\gamma_2 C_1) = 0 \end{aligned} \tag{36}$$

where

$$\phi_1 = \frac{\alpha_1 a}{D}, \qquad \phi_2 = \frac{\alpha_2 a}{D}, \qquad R = \frac{r}{p} \tag{37}$$

$$s_1 = \sin(p\pi), \quad c_1 = \cos(p\pi), \quad S_1 = \sinh(r\pi), \quad C_1 = \cosh(r\pi)$$

ϕ_1 and ϕ_2 are nondimensional rotational spring stiffnesses.

Requiring that A_j's do not vanish simultaneously results in a frequency determinant of the *X-problem*

$$\begin{vmatrix} 0 & 1 & 0 & 1 \\ s_1 & c_1 & S_1 & C_1 \\ \phi_1 & \gamma_1 p\pi & R\phi_1 & -R^2\gamma_1 p\pi \\ \phi_2 c_1 - \gamma_2 p\pi s_1 & -(\phi_2 s_1 + \gamma_2 p\pi c_1) & \phi_2 R C_1 + \gamma_2 R^2 p\pi S_1 & \phi_2 R S_1 + R^2 p\pi\gamma_2 C_1 \end{vmatrix} = 0 \tag{38}$$

This equation contains two unknowns p and q. We will obtain a needed companion equation for determining these two unknowns by solving an analogous problem in the y direction.

SECOND AUXILIARY PROBLEM

Consider now the second auxiliary problem referred to as an *Y-Problem.* We seek for the solution of Eq. (21) in the form

$$W(x,y) = Y(y)\sin\frac{p\pi x}{a} \tag{39}$$

with boundary conditions (8) and (9). Instead of Equations (22) (23) and (10) we have

$$\frac{d^2Y_1}{dy^2} + \left(\frac{q\pi}{b}\right)^2 Y_1 = 0 \tag{40}$$

$$\frac{d^2Y_2}{dy^2} - \left[\left(\frac{q\pi}{b}\right)^2 + 2\left(\frac{p\pi}{a}\right)^2\right] Y_2 = 0 \tag{41}$$

The solution for the function $Y(y)$

$$Y(y) = Y_1(y) + Y_2(y) \tag{42}$$

is given by

$$Y(y) = B_1\sin\frac{q\pi y}{b} + B_2\cos\frac{q\pi y}{b} + B_3\sinh\frac{z\pi y}{b} + B_4\cosh\frac{z\pi y}{b} \tag{43}$$

where

$$z = q\sqrt{1 + 2\left(\frac{p}{q}\right)^2\left(\frac{b}{a}\right)^2} \tag{44}$$

Note that z is obtained from the expression (29) for r, by formal replacement of p by q, of q by p, of a by b, and of b by a.

The boundary conditions (8), (9), (10) read

$$Y = 0, \quad at \quad y = 0, \quad y = b \tag{45}$$

$$\delta_1 D\frac{d^2Y}{dy^2} = \beta_1\frac{dY}{dy} \qquad at \quad y = 0 \tag{46}$$

$$-\delta_2 D\frac{d^2Y}{dy^2} = \beta_2\frac{dY}{dy} \qquad at \quad y = b \tag{47}$$

Satisfaction of the boundary conditions leads to following set of equations

$$B_2 + B_4 = 0 \tag{48}$$

$$B_1 s_2 + B_2 c_2 + B_3 S_2 + B_4 C_2 = 0 \tag{49}$$

$$B_1\psi_1 + B_2\delta_1 q\pi + B_3 Z\psi_1 - B_4 Z^2\upsilon_1 q\pi = 0 \tag{50}$$

$$\begin{aligned} &B_1(\psi_2 c_2 - \delta_2 q\pi s_2) - B_2(\psi_2 s_2 + \delta_2 q\pi c_2) \\ &+ B_3(\psi_2 Z C_2 + \delta_2 Z^2 q\pi S_2) + B_4(\psi_2 Z S_2 + Z^2 q\pi\delta_2 C_2) = 0 \end{aligned} \tag{51}$$

where

$$\psi_1 = \frac{\beta_1}{D}b, \quad \psi_2 = \frac{\beta_2}{D}b, \quad Z = \frac{z}{q} \tag{52}$$

$$s_2 = \sin(q\pi), \quad c_2 = \cos(q\pi), \quad S_2 = \sinh(z\pi), \quad C_2 = \cosh(z\pi)$$

Moreover, ψ_1 and ψ_2 are nondimensional rotational constants.

Requirement of nontriviality of the constants of integration yields the following determinant

$$\begin{vmatrix} 0 & 1 & 0 & 1 \\ s_2 & c_2 & S_2 & C_2 \\ \psi_1 & \delta_1 q\pi & Z\psi_1 & -Z^2\delta_1 q\pi \\ \psi_2 c_2 - \delta_2 q\pi s_2 & -(\psi_2 s_2 + \delta_2 q\pi c_2) & \psi_2 Z C_2 + \delta_2 Z^2 q\pi S_2 & \psi_2 Z S_2 + Z^2 q\pi \delta_2 C_2 \end{vmatrix} = 0 \qquad (53)$$

In contrast to classical free vibration problems [3], here two equations in terms of determinants, namely Eq. (38) and Eq. (53), should be solved simultaneously to determine the decimal modal numbers p and q. Their substitution into Eq. (19) yields the desired natural frequencies. It should be borne in mind that in contrast to energy based methods the determination of higher natural frequencies does not constitute a more difficult task than that of the low natural frequencies. In fact, the numerical effort for numerical evaluation of *any* natural frequency is essentially identical. The additional advantage of the present generalization of the Bolotin's method consists in the possibility of evaluation of any *preselected* natural frequency. This is important in particular due to the diagnostic method adopted in section 3. The validity of the present generalization of Bolotin's dynamic edge method is verified by comparing the present results with the results due to Leissa [4]. The comparisons are tabulated in the Appendix.

6. NUMERICAL EXAMPLE

1) Example 1

For simplicity, we first concentrate on the boundary condition diagnosis of a square plate (a=b) with three edges clamped and the fourth edge elastically supported (C-C-C-ES) (see Fig. 1). The uncertain rotational stiffness of the latter edge of the plate, β_2, is represented by the convex model, given in Eq. (1). We need some partial information on the plate boundary

condition, i. e. on β_2, to proceed with the diagnosis. Since no experimental results were available to present investigators, the simulated situation was constructed.

To simulate possession of some information about the to-be-diagnosed plate, we proceed as follows. We first investigate the extreme case with all four edges being clamped. The natural frequency parameter of the fundamental frequency by the present approximate analytical method is $\lambda_1=35.113$. The plate under consideration is an aluminum plate ($\rho=268.7\ kg/m^3$) with both side lengths fixed at $a=b=10\ m$, and thickness at $h=0.1\ m$. We first determine, by numerical evaluation of the generalized Bolotin's method, the value of the rotational stiffness β_2^* such that the first mode frequency will be some fraction (say, 97%) of the corresponding first mode frequency of the all-round clamped plate, namely $\lambda_1=34.060$. Numerical search yields the value of the nondimensional rotational stiffness $\beta_2^* = 1.522\times10^7\ N$. We note that in this case the numerical solution of Eq. (36) and Eq.(51) gives the values $p=1.3417$ and $q=1.2848$. For values of β_2 greater than β_2^* the natural frequencies will be identified with those of essentially C-C-C-C plate. One would expect that beyond this value of the rotational spring coefficient identification of the "true" boundary condition would be difficult since all the plates with various $\beta>\beta_2^*$ actually are the same.

As it was mentioned above, performing actual experimental measurements was beyond the scope of the present study. In order to simulate the actual situation, we suppose that we may get, in principle, all needed measured frequencies of the plate whose rotational stiffness coefficient β_2 along the fourth edge should be identified. Let us visualize that the set of

measured nondimensional natural frequencies is given in Table 1. The notation $\lambda_{(i)}$, where i is the sequence number of the frequency, is introduced in addition to the two index notation of frequency λ_{pq}, because repeated frequencies are considered as a single frequency in this study. We note in passing that the frequency parameters in Table 1 were obtained by setting $\beta_2=10^6 N$. We visualize that this actual value of the rotational stiffness is unknown to us in our hypothetical experiment and we should identify the convex model which represents it in a best way.

Table 1 The first six nondimensional frequency parameters of the to-be-diagnosed plate, simulating the results of measurements

$\lambda_{(1)}$	31.942
$\lambda_{(2)}$	64.119
$\lambda_{(3)}$	71.088
$\lambda_{(4)}$	101.052
$\lambda_{(5)}$	117.479
$\lambda_{(6)}$	130.355

Since within the present procedure we assume that the alteration of the boundary conditions occurs along the entire length of the side, we set that $N=4$ in Eq. (1) since the plate has four sides. Accordingly the subsets of the boundary S, I_n, $n=1, \cdots, 4$, are α_1, β_1, α_2, β_2. Here the nominal values of torsional stiffness are denoted by $\bar{\alpha}_1$, $\bar{\beta}_1$, $\bar{\alpha}_2$, $\bar{\beta}_2$. As mentioned before, we assume three edges of the square plate to be clamped and the remaining edge (edge 4 in this case) to be elastically supported. Therefore, the nominal values of torsional stiffness

corresponding to the three clamped edges, denoted by $\bar{\alpha}_1$, $\bar{\beta}_1$, $\bar{\alpha}_2$, are infinite, that is $\bar{\alpha}_1 = \bar{\beta}_1 = \bar{\alpha}_2 \to \infty$. The fact that the nominal value of the elastically supported edge, β_2, is unknown and is to be identified suggests that it may need several estimations to reasonably represent the convex model for the stiffness β_2. We denote these reference values $\bar{\beta}_{2,m}$, where m indicates the number of estimated nominal values. Then the general convex model set in Eq.(1) becomes

$$C_{m,4} = \{\alpha_i, \beta_i, i = 1,2:\ \alpha_i = \bar{\alpha}_i = \infty,\ i = 1,2;\ \beta_1 = \bar{\beta}_1 = \infty;\ |\beta_2 - \bar{\beta}_{2,m}| \le \delta_m\} \tag{54}$$

or, simply

$$C_{2,m} = \{\beta_2:\ |\beta_2 - \bar{\beta}_{2,m}| \le \delta_m\} \tag{55}$$

since only β_2, the stiffness of the elastically supported edge, is considered to be unknown.

The natural question arises: Is the convex modeling of the uncertain elastic supports along the fourth edge able to "uncover" the best convex model closest to this simulated situation?

To answer the above question it appears to be instructive to consider another question: "How to reasonably construct the convex model?" Conceivably, if the convex model of stiffness β_2 is constructed that can include the true value of β_2, the answer is "yes". Otherwise it makes no sense to try to single out the "best" stiffness from the wrong ones. It is quite natural to state that the estimated stiffness is likely to be far from the true one if the true stiffness can not be exactly or approximately represented by the elements of the hypothesized convex model. This happens since even the closest stiffness element in the convex set can be quite different from the

true one. Thus it is necessary to develop guidelines as how to choose the proper convex models, namely those which will *necessarily* contain possible realizations of an uncertain quantity of interest, and hence able to represent the uncertainty of the boundary conditions.

To illustrate the procedure to construct the convex model, we will investigate a quite general example in this section.

First we hypothesize the nominal value of stiffness β_2, say $\bar{\beta}_{2,1} = 0.65\times10^6 N$, and also set $\delta_1 = 0.15\times10^6 N$. The according convex model is $(0.5\times10^6, 0.8\times10^6)N$. As we will see later, the diagnosed stiffness will be identified at the upper bound of the interval (see Table 2). This implies that either this upper limit is a true value of β_2, or it is closest to the true β_2. Since it is improbable to "hit" the true value at the first trial, we conclude that the present convex model is not comprehensive and needs to be improved. The fact that the diagnosed value of β_2 lies at the upper bound of the interval suggests that a larger reference value $\bar{\beta}_{2,1}$ should be chosen. Next we select $\bar{\beta}_{2,2} = 2.5\times10^6 N$ and set $\delta_2 = 0.5\times10^6 N$. Then the corresponding interval becomes $(2\times10^6, 3\times10^6)N$. As we can see from the results, the diagnosed stiffness β_2 in this case lies at the lower bound of the interval (see Table 3). Again we conclude that either this lower limit is the true value of β_2 or it is closest to β_2 within this "wrong" interval. This leads to creation of the final convex model $(0.8\times10^6, 2\times10^6)N$ (see Fig. 2), and we can be confident that it is able to include the true value of stiffness β_2. In practical situations, we may need several estimated models to construct the "final" convex model. Obviously the above situation represents the typical case that may occur. The procedure, in detail, is as follows:

1. *Measure* all the "necessary" natural frequencies of the actual plate (In this study, we assume

that they are all provided and listed in Table 1.)

2. *Construct* a convex set of boundary conditions. In this example it is $(0.5\times10^6, 0.8\times10^6)N$. The lower bound of boundary stiffness interval is denoted by β_2^a, and the upper one by β_2^b.

3. *Calculate* the natural frequencies of the plate with the boundary stiffness β_2 equal to the mid-point value of the interval, $\beta_2^1 = 0.65\times10^6 N$ in this example.

4. *Compute* the distances H between the measured and calculated natural frequencies with $\beta_2 = \beta_2^1 = 0.65\times10^6 N$. It is well known that boundary conditions have a more pronounced effect in the range of the low frequencies than in the high frequency region. This means that we should put more "weight" when defining the norm on the low frequencies. Thus the distance between the natural frequencies in Eq. (2) can be defined specifically as:

$$H_{mn} = \|\Lambda - \lambda^{(mn)}\| = \sum_{i=1}^{4} \frac{|\Lambda_i - \lambda_i|}{\Lambda_i} \tag{56}$$

where Λ is the vector of nondimensionalized measured natural frequency Ω, and $\lambda^{(mn)}$ is the calculated one for the hypothesized stiffness.

5. *Compute* the distance H at values $\beta_2^1 = \beta_2^1 + \Delta\beta$, denoted by $H(\beta_2^1 + \Delta\beta)$ following the same way as step 4. We set $\Delta\beta$ at $1.0\times10^3 N$. The derivative of the distance H with respect to β_2 can be approximately estimated by

$$\frac{dH(\beta_2^1)}{d\beta_2^1} \approx \frac{H(\beta_2^1 + \Delta\beta) - H(\beta_2^1)}{H(\beta_2^1)} \tag{57}$$

6. *Decide* search direction of β_2 by the following manner:

a) If $H(\beta_2^1 + \Delta\beta) - H(\beta_2^1) < 0$, the stiffness β_2 should be increased.

b) If $H(\beta_2^1 + \Delta\beta) - H(\beta_2^1) > 0$, the stiffness β_2 should be decreased.

7. *Choose* the new search interval. In this study, it is always one half of the last search interval, and is created in such a way that the actual β_2 is always in the new interval, which is decided by the directional search. That is, if $dH(\beta_2^1)/d\beta_2^1 \leq 0$, the next diagnostic interval is (β_2^1, β_2^a); if $dH(\beta_2^1)/d\beta_2^1 \geq 0$, the next diagnosis interval is (β_2^a, β_2^1).

8. *Calculate* the natural frequency with the mid-point stiffness β_2' of the new interval, in the procedure following from step 3 to step 7 until the following criterion for termination is satisfied

$$|\beta_2^{(n+1)} - \beta_2^{(n)}| \leq \varepsilon \tag{58}$$

where $\beta_2^{(n)}$ denotes the nth diagnosed stiffness and $\beta_2^{(n+1)}$ the (n+1)th, from the next new interval following $\beta_2^{(n)}$. The value of ε is chosen as $10^4 N$ in present example. Since the diagnosed β_2 seems to be on the upper bound of the interval (see Table 2), we have to choose a larger reference value of β_2, say $\bar{\beta}_{2,2}$. Let $\bar{\beta}_{2,2} = 2.5\times10^6 N$ and $\delta_2 = 0.5\times10^6 N$. Therefore a second interval $(2\times10^6, 3\times10^6)N$ is created.

9. *Repeat* the same procedure for the second model interval $(2\times10^6, 3\times10^6)N$ as for the interval $(0.5\times10^6, 0.8\times10^6)N$. The lower and upper bounds of diagnosed interval are also denoted by β_2^a,

and β_2^b, respectively.

10. *Establish* the convex model. Now one may notice that the diagnosed β_2 for the first interval tends to increase monotonically till 0.8×10^6N while for the second interval it decreased till 2.0×10^6N. This implies that the true β_2 may lie in the range between 0.8×10^6N and 2.0×10^6N. It is straight-forward to determine the final possible small range of β_2 by employing the procedure indicated in steps 3 to 8. The above general procedure is illustrated in Fig. 2.

Tables 2, 3, and 4 show the diagnosed intervals of every step for both initial hypothesized stiffness models and the final convex model, as well as the frequency distances at the corresponding mid-point values.

Table 2

step	lower bound $\times10^{-6}$	upper bound $\times10^{-6}$	distance at midpoint β_2^1	distance at $\beta_2^1 + \Delta\beta$	sign of difference
1	0.5	0.8	1.0385	1.0374	-
2	0.65	0.8	0.8113	0.8095	-
3	0.725	0.8	0.6968	0.6935	-
4	0.7625	0.8	0.6403	0.6391	-
5	0.78125	0.8	0.6104	0.6096	-
6	0.79062	0.8			

Table 3

step	lower bound $\times 10^{-6}$	upper bound $\times 10^{-6}$	distance at midpoint β_2^1	distance at $\beta_2^1 + \Delta\beta$	sign of difference
1	2.0	2.5	3.6642	3.6672	+
2	2.0	2.25	3.1345	3.1345	+
3	2.0	2.125	2.8555	32.8564	+
4	2.0	2.0625	2.7120	2.7154	+
5	2.0	2.0313	2.6414	2.6514	+
6	2.0	2.0156	2.6135	2.6158	+
7	2.0	2.0078	2.5915	2.5929	+

Table 4

step	lower bound $\times 10^{-6}$	upper bound $\times 10^{-6}$	distance at midpoint β_2^1	distance at $\beta_2^1 + \Delta\beta$	sign of difference
1	0.7906	2.0078	1.1006	1.1043	+
2	0.7906	1.3992	0.2735	0.2766	+
3	0.7906	1.0949	0.1644	0.1527	-
4	0.9428	1.0949	0.0617	0.0635	+
5	0.9428	1.0188	0.0518	0.0491	-
6	0.9808	0.9998	0.0007	0.0021	+

From the above example, the following guidelines are suggested to construct the convex model:

a) *Initial Hypothesis*: We first hypothesize one reference, nominal value of stiffness $\bar{\beta}_{2,m}$ and specify a certain δ_m. As a result, a interval as in Eq.(54), $(\bar{\beta}_{2,m} - \delta_m, \bar{\beta}_{2,m} + \delta_m)$, is constructed and investigated by the present method. If the diagnosed β_2 belongs to this interval, the search process should identify it and thus the searching process should be terminated. This β_2 should be considered as the true value of stiffness. However, in most cases, due to the insufficient information, the reference value $\bar{\beta}_{2,m}$ may not be correct since the true value β_2 may not be included in the search interval. This situation will lead to the diagnosed value of stiffness β_2 to occur either at the upper or lower bound of the convex set. This would imply that more reasonable reference values have to be estimated and the previous convex model needs a correction or checking if the upper or lower bounds represent the true value.

b) *Correction*: When the hypothesized convex model needs to be corrected, we have to create other convex model(s) which will include the true value of stiffness β_2. Let us assume the diagnosed stiffness β_2 obtained in the initially hypothesized step lies at the lower bound of the interval, which means the true value of β_2 is equal or it is less than the lower bound of the interval. In the next step, we choose such a convex model among where all its values are less than those of the previous one. If the diagnosed stiffness β_2 of this convex model set also lies at the lower bound of the set, then we have to move the interval further to the left. Usually it is quite easy to create a convex model, such that the identified value of β_2 will suggest the upper bound of the interval, as long as the reference value $\bar{\beta}_{2,m}$ is small enough.

c) *Final Hypothesis*: Once having such two alternative convex models, a final convex model can be constructed with the two previous diagnosed stiffnesses β_2's representing the upper and lower bounds. As a result the "true" β_2 is "caught" inside this model.

2) Example 2

In the second example, we will investigate the diagnosis of the alteration in the boundary condition of a square plate (a=b) with two adjacent edges clamped and the other two edges elastically supported (C-C-ES-ES) (see Fig.3). The uncertain rotational stiffnesses of the two elastically supported edges, α_2 and β_2, are represented by the convex model, given in Eq.(1). As in the example 1, the simulated situation (natural frequencies and corresponding underlying rotational stiffnesses) is constructed since experimental measurements have not yet been performed.

Following the steps of imitating the real situation in the first example, we visualize that the set of measured nondimensional natural frequencies is given in Table 5. We note in passing that the frequency parameters in Table 5 were obtained by setting $\alpha_2=1\times10^6$N, $\beta_2=2\times10^6$N. The notations are same as that in example 1.

Table 5 The first six nondimensional frequency parameters of the to-be-diagnosed plate, simulating the results of measurements

$\lambda_{(1)}$	28.678
$\lambda_{(2)}$	62.882
$\lambda_{(3)}$	94.693
$\lambda_{(4)}$	117.162
$\lambda_{(5)}$	148.056
$\lambda_{(6)}$	191.336

As discussed before, the nominal values of torsional stiffnesses are denoted by $\bar{\alpha}_1$, $\bar{\beta}_1$, $\bar{\alpha}_2$, $\bar{\beta}_2$. Then the convex model set in Eq.(1) is as follows

(59)

$$C_{m,4} = \{\alpha_i, \beta_i, i = 1,2:\ \alpha_1 = \bar{\alpha}_1 = \infty,\ \beta_1 = \bar{\beta}_1 = \infty;\ |\alpha_2 - \bar{\alpha}_{2,m}| \le \delta_m,\ |\beta_2 - \bar{\beta}_{2,m}| \le \delta_m\}$$

or, simply

(60)

$$C_{2,m} = \{\alpha_2, \beta_2:\ |\alpha_2 - \bar{\alpha}_{2,m}| \le \delta_m,\ |\beta_2 - \bar{\beta}_{2,m}| \le \delta_m\}$$

since only α_2 and β_2, the stiffnesses of the elastically supported edges, are considered to be unknown.

We will omit the intermediate steps to create the "final" convex model, since they are similar to those in example 1. Thus, we assume that we have arrived at the following convex model, $\alpha_2 \in (0.1\times10^6, 10\times10^6)$N, $\beta_2 \in (0.1\times10^6, 10\times10^6)$N, which is large enough to include the

true values of stiffnesses α_2 and β_2. The procedure, in detail, is as follows:

1. We measure all the "necessary" natural frequencies of the actual plate (In this study, we assume that they are all provided and listed in Table 5.)

2. We construct a convex set for altered boundary conditions. In this example it is α_2, $\beta_2 \in (0.1\times10^6, 10\times10^6)N$. The lower bounds of boundary stiffness intervals are denoted by α_2^a and β_2^a, whereas the upper bounds are indicated by α_2^b and β_2^b, respectively.

3. We divide (α_2^a, α_2^b) and (β_2^a, β_2^b) into a number of equal intervals (20 intervals in this study). For each interval's separation point α_2^i $(i = 1, 2, \cdots, 20)$ in (α_2^a, α_2^b), we calculate the distances H_j between the measured and the calculated natural frequencies at all values of β_2^j $(j = 1, 2, \cdots, 20)$, and select the combination $(\alpha_2^{i_*}, \beta_2^{j_*})$ at which the distance H_j reaches minimum. This step is actually equivalent to choosing $(\alpha_2^{i_*}, \beta_2^{j_*})$ among the 400 dividing points of α_2 and β_2 such that H_j attains its minimum. This may considerably save the storage due to the fact that some data becomes of no use once they are compared and need not to be stored any more.

5. We redefine a searching rectangular range with the identified $(\alpha_2^{i_*}, \beta_2^{j_*})$ at step 4 as a center. The side length of this rectangular area is twice the divided interval length. It can be readily seen that the present area of α_2 and β_2 is one percent of the former one (see Fig. 4 & Fig. 5).

6. We repeat the procedure of step 3 through step 5 until certain convergence criterion is satisfied. In this example, the criterion was chosen as the increment in values of α_2 and β_2

between one search to another not to exceed 1×10^3N. The numerical results for α's and corresponding β's at which the distances H_j reach minimum in different searching areas are listed in tables 6-9.

Table 6 The values of α and β at which Distances H_j reach Minimum (First Searching Region)

	α	β at which H is min.	H
1	0.100	3.565	2.3826
2	0.595	2.080	0.7270
3	1.090	2.080	0.4194
4	1.585	1.585	0.7438
5	2.080	1.090	1.2431
6	2.575	1.090	1.7717
7	3.070	0.595	2.1220
8	3.565	0.100	2.3838
9	4.060	0.100	2.7720
10	4.555	0.595	3.2664
11	5.050	0.100	3.4329
12	5.545	0.100	3.7206
13	6.040	0.100	3.9796
14	6.535	0.100	4.2172
15	7.030	0.100	4.4345
16	7.525	0.100	4.6350
17	8.020	0.100	4.8179
18	8.515	0.100	4.9910
19	9.010	0.100	5.1491
20	9.505	0.100	5.2994
21	10.000	0.100	5.4382

Table 7 The values of α and β at which Distances H_j reach Minimum (Second Searching Region)

	α	β at which H is min.	H
1	0.5950	2.4270	0.5836
2	0.6445	2.4270	0.5006
3	0.6940	2.3280	0.4316
4	0.7435	2.2290	0.3654
5	0.7930	2.2780	0.2850
6	0.8425	2.1790	0.2144
7	0.8920	2.1300	0.1448
8	0.9415	2.0310	0.0834
9	0.9910	2.0310	0.0642
10	1.0410	1.9810	0.0569
11	0.1090	1.9320	0.1238
12	1.1400	1.8330	0.1791
13	1.1890	1.7830	0.2424
14	1.2390	1.7340	0.3046
15	1.2880	1.6840	0.3651
16	1.3380	1.6350	0.4241
17	1.3870	1.5850	0.4824
18	1.4370	1.5850	0.5494
19	1.4860	1.5850	0.6155
20	1.5360	1.5850	0.6798
21	1.5850	1.5850	0.7438

Table 8 The values of α and β at which Distances H_j reach Minimum (Third Searching Region)

	α	β at which H is min.	H
1	0.9910	2.011	0.0119
2	0.9959	2.006	0.0068
3	1.001	2.001	0.0038
4	1.006	1.996	0.0083
5	1.011	1.991	0.0147
6	1.016	1.981	0.0212
7	1.021	1.976	0.0279
8	1.026	1.971	0.0341
9	1.031	1.966	0.0407
10	1.036	1.956	0.0466
11	1.041	1.951	0.0539
12	1.045	1.946	0.0598
13	1.050	1.941	0.0669
14	1.055	1.932	0.0723
15	1.060	1.932	0.0793
16	1.065	1.932	0.0873
17	1.070	1.932	0.0939
18	1.075	1.932	0.1009
19	1.080	1.932	0.1089
20	1.085	1.932	0.1159
21	1.090	1.936	0.1237

Table 9 The values of α and β at which Distances H_j reach Minimum (Fourth Searching Region)

	α	β at which H is min.	H
1	0.9959	2.004	0.0046
2	0.9964	2.004	0.0041
3	0.9969	2.003	0.0032
4	0.9974	2.003	0.0029
5	0.9979	2.003	0.0022
6	0.9984	2.001	0.0021
7	0.9989	2.001	0.0006
8	0.9994	2.001	0.0008
9	0.9999	2.000	0.0005
10	1.000	2.000	0.0009
11	1.001	2.000	0.0016
12	1.001	1.998	0.0025
13	1.002	1.999	0.0027
14	1.002	1.999	0.0036
15	1.003	1.997	0.0038
16	1.003	1.998	0.0045
17	1.004	1.996	0.0051
18	1.004	1.996	0.0060
19	1.005	1.996	0.0064
20	1.005	1.997	0.0074
21	1.006	1.996	0.0083

6. DISCUSSION AND CONCLUSIONS

The generalized Bolotin's dynamic edge effect method, combined with the approach of the convex modeling of uncertainty, has been employed to estimate the convex models associated with the alteration of the boundary conditions of thin uniform rectangular plates. For determination of the natural frequencies the generalized version [7] of the Bolotin's dynamic edge-effect method [6] was employed. The essential advantage of this general method is the possibility of finding the natural frequencies for *any* preselected pair of mode numbers. We have shown in the Appendix, by comparing the nondimensional frequency parameters with those due to Leissa [4] and Gorman [10], that the use of "postulate" (20) and of two Levy's type solutions to approximate natural frequencies leads to very accurate results.

The main idea implemented in the present paper is the convex modeling of uncertainty, as applied to the diagnosis of local modifications in the boundary conditions. In order to describe the alteration in the boundary stiffness of the plate, convex models are utilized to specify the possible realizations of boundary conditions. In the next step the multi-hypothesis decision is implemented, based on the minimum distance algorithm.

For the sake of simplicity, plates with one or two edges elastically supported and the rest clamped were investigated. Two possible kinds of convex models for the stiffness of the elastically supported edge were constructed. The multi-hypothesis diagnosis, in conjunction with the generalized dynamic edge effect method, proved to be a fairly successful technique.

ACKNOWLEDGMENT

This study has been supported by the NASA Kennedy Space Center, through Cooperative Agreement No. NCC10-0005, S1 to the Florida Atlantic University; technical monitor: Mr. R. Caimi. This support is gratefully appreciated. Senior author acknowledges invaluable discussions and contributions of Dr. Yakov Ben-Haim of the Technion-Israel, Institute of Technology, Haifa, and Professor H. Günther Natke of the University of Hannover, Federal Republic of Germany to Sections 2-4 of this study. The joint work on diagnosis of general mixed boundary conditions along the edges is underway and will be published elsewhere.

REFERENCES

[1] Y. Ben-Haim and I. Elishakoff, Convex Models of Uncertainty in Applied Mechanics, (Elsevier Science Publishers, Amsterdam, 1990).

[2] Y. Ben-Haim and H. G. Natke, Personal Communications to I.E., 1991.

[3] A. W. Leissa, Vibration of Plates, NASA SP, U.S. Government Printing Office, Washington, D.C., 1969.

[4] A. W. Leissa, Plate Vibration Research, 1976-1980: Complicating effects, The Shock and Vibration Digest, 13 (10) (1981) 19-36.

[5] A. W. Leissa, Recent studies in plate vibrations: 1981-1985. Part II. Complicating effects, The Shock and Vibration Digest, 19 (3) (1987) 10-24.

[6] V. V. Bolotin, An asymptotic method for the study of the problem of eigenvalues for rectangular regions, in "Problems of continuum mechanics; Contributions in honor of the seventieth birthday of academician N. I. Muskhelishvili", SIAM, Philadelphia (1961) 56-68.

[7] I. Elishakoff, Bolotin's dynamic edge - effect method, The Shock and Vibration Digest, 8 (1976) 95-104.

[8] K. Vijayakumar, A new method for analysis of flexural vibration of rectangular orthotropic plates, Journal of the Aeronautical Society of India, 23 (1971) 197-204.

[9] I. Elishakoff, Vibration analysis of clamped square orthotropic plate, AIAA Journal, 12 (1974) 921-924.

[10] D. J. Gorman, Free vibration analysis of rectangular plates, (Elsevier Science Publishers Amsterdam, 1982).

APPENDIX

The numerical procedure of solving the first and the second auxiliary problems, resulting in Eq. (38) and Eq. (53), is carried out by applying Newton-Raphson method. Here Eqs. (36) and (51) are denoted as

$$F(p, q) = 0 \tag{A·1}$$

$$G(p, q) = 0 \tag{A·2}$$

They can be put in the expanded form as follows

$$\begin{aligned}&\pi^2\gamma_1\gamma_2 s_1 S_1 p^2 R^4 + 2\pi^2\gamma_1\gamma_2 s_1 S_1 p^2 R^2 + \pi^2\gamma_1\gamma_2 s_1 S_1 p^2 + \pi\gamma_2\phi_1 C_1 s_1 pR^3 + \\ &\pi\gamma_1\phi_2 C_1 s_1 pR^3 - \pi\gamma_2\phi_1 c_1 S_1 pR^2 - \pi\gamma_1\phi_2 c_1 S_1 pR^2 + \pi\gamma_2\phi_1 C_1 S_1 pR + \\ &\pi\gamma_1\phi_2 C_1 s_1 pR - \pi\gamma_2\phi_1 c_1 S_1 p - \pi\gamma_1\phi_2 c_1 S_1 p + \phi_1\phi_2 s_1 S_1 R^2 + \phi_1\phi_2 s_1^2 R + \\ &\phi_1\phi_2 c_1^2 R - 2\phi_1\phi_2 c_1 C_1 R - \phi_1\phi_2 S_1^2 R + \phi_1\phi_2 C_1^2 R - \phi_1\phi_2 s_1 S_1 = 0\end{aligned} \tag{A·3}$$

$$\begin{aligned}&\pi^2\delta_1\delta_2 s_2 S_2 q^2 Z^4 + 2\pi^2\delta_1\delta_2 s_2 S_2 q^2 Z^2 + \pi^2\delta_1\delta_2 s_2 S_2 q^2 + \pi\delta_2\psi_1 C_2 s_2 qZ^3 + \\ &\pi\delta_1\psi_2 C_2 s_2 qZ^3 - \pi\delta_2\psi_1 c_2 S_2 qZ^2 - \pi\delta_1\psi_2 c_2 S_2 qZ^2 + \pi\delta_2\psi_1 C_2 S_2 qZ + \\ &\pi\delta_1\psi_2 C_2 s_2 qZ - \pi\delta_2\psi_1 c_2 S_2 q - \pi\delta_1\psi_2 c_2 S_2 q + \psi_1\psi_2 s_2 S_2 Z^2 + \psi_1\psi_2 s_2^2 Z + \\ &\psi_1\psi_2 c_2^2 Z - 2\psi_1\psi_2 c_2 C_2 Z - \psi_1\psi_2 S_2^2 Z + \psi_1\psi_2 C_2^2 Z - \psi_1\psi_2 s_2 S_2 = 0\end{aligned} \tag{A·4}$$

According to Newton-Raphson method, the above two equations are approximately replaced by

$$F(p, q) \approx F_i + \left(\frac{\partial F}{\partial p}\right)_i (p - p_i) + \left(\frac{\partial F}{\partial q}\right)_i (q - q_i) = 0 \tag{A·5}$$

$$G(p, q) \approx G_i + \left(\frac{\partial G}{\partial p}\right)_i (p - p_i) + \left(\frac{\partial G}{\partial q}\right)_i (q - q_i) = 0 \tag{A·6}$$

where p_i and q_i are the values of roots of Eqs. (A·1) and (A·2) in ith iteration and $F_i = F(p_i, q_i)$, $G_i = G(p_i, q_i)$. The $(i+1)$th iteration of the above solution yields

$$p_{i+1} = p_i + \frac{a_{12}G_i - a_{22}F_i}{a_{11}a_{22} - a_{12}a_{21}} \tag{A·7}$$

$$q_{i+1} = q_i + \frac{a_{21}F_i - a_{11}G_i}{a_{11}a_{22} - a_{12}a_{21}} \tag{A·8}$$

where a_{11}, a_{12}, a_{21}, and a_{22} denote, respectively,

$$a_{11} = \left(\frac{\partial F}{\partial p}\right)_{p=p_i,\ q=q_i}, \qquad a_{12} = \left(\frac{\partial F}{\partial q}\right)_{p=p_i,\ q=q_i} \tag{A·9}$$

$$a_{21} = \left(\frac{\partial G}{\partial p}\right)_{p=p_i,\ q=q_i}, \qquad a_{22} = \left(\frac{\partial G}{\partial q}\right)_{p=p_i,\ q=q_i} \tag{A·10}$$

The derivatives $\partial F/\partial p$, $\partial F/\partial q$, $\partial G/\partial p$, $\partial G/\partial q$ were evaluated analytically using the computerized symbolic algebraic code REDUCE. In the p-q plane, the square defined by the lines $p=m$, $p=m+1$, and $q=n$, $q=n+1$, where m and n are any positive integers, there is only one root of Eqs. (A·1) and (A·2) (see Fig. 3). This allows us to find the natural frequency for any given pair of numbers m, n so long as the initial values of p and q are properly chosen.

In Tables *A-D* the results are presented for the frequency parameters $\lambda=\omega a^2\sqrt{\rho h/D}$ computed using both the present generalization of Bolotin's dynamic edge effect method, and the Rayleigh-Ritz method adopted by Leissa [4]. In cases where Leissa's results are not available, the results by Gorman [10] are cited and denoted by the star. It should be noted that the mode sequence numbers, cited from Ref. [4], are somewhat different from those in Ref. [4], because repeated frequencies are considered here as one.

Table A

Comparison of frequency parameters $\lambda=\omega a^2\sqrt{\rho h/D}$ (SS-C-SS-SS Plates)

Mode Sequence	a/b=2/3		a/b=1.0		a/b=1.5	
	Ref. 3	Present	Ref. 3	Present	Ref. 3	Present
1	15.578	15.578	23.646	23.646	42.528	42.528
2	31.072	31.072	51.674	51.674	69.003	69.003
3	44.564	44.564	58.646	58.646	116.267	116.267
4	55.393	55.393	86.135	86.134	120.996	120.995
5	59.463	59.463	100.270	100.270	147.635	147.635
6	83.438	83.606	113.228	113.228	184.101	184.101

Table B

Comparison of frequency parameters $\lambda=\omega a^2\sqrt{\rho h/D}$ (C-C-C-C Plates)

Mode Sequence	a/b=2/3		a/b=1.0		a/b=1.5	
	Ref. 3	Present	Ref. 3	Present	Ref. 3	Present
1	27.010	26.582	35.992	35.113	60.772	59.809
2	41.716	41.191	73.413	72.899	93.860	92.682
3	66.143	66.172	108.27	107.444	148.82	148.245
4	79.850	78.766	131.64	131.701	179.74	179.978
5	100.85	103.730	165.00[*2]	163.170	226.92	213.053

[1]After Gorman's [10] result (λ=41.25) is multiplied by four, since the side lengths in Ref. 10 are taken as 2a and 2b.

Table C

Comparison of frequency parameters $\lambda=\omega a^2\sqrt{\rho h/D}$ (C-C-C-SS Plates)

Mode Sequence	a/b=2/3		a/b=1.0		a/b=1.5	
	Ref. 3	Present	Ref. 3	Present	Ref. 3	Present
1	25.861	25.692	31.829	31.438	48.167	47.622
2	38.102	37.837	63.347	63.054	85.507	84.990
3	60.325	60.111	71.084	70.879	123.99	123.657
4	65.516	65.447	100.83	100.460	143.99	143.681
5	77.563	77.357	116.40	116.292	158.36	211.054
6	92.154	98.374	130.37	130.262	214.78	220.072

Table D

Comparison of Frequency Parameters $\lambda=\omega a^2\sqrt{\rho h/D}$ (C-C-SS-SS plates)

Mode Sequence	a/b=2/3		a/b=1.0		a/b=1.5	
	Ref. 3	Present	Ref. 3	Present	Ref. 3	Present
1	19.952	19.853	27.056	26.867	44.893	44.669
2	34.024	33.907	60.544	60.549	76.554	76.290
3	54.370	54.326	92.865	92.665	122.33	122.233
4	57.517	57.429	114.57	114.568	129.41	129.215
5	67.815	67.694	146.0*	145.786	152.58	152.313
6	90.069	90.013	188.5*	188.469	202.66	203.303

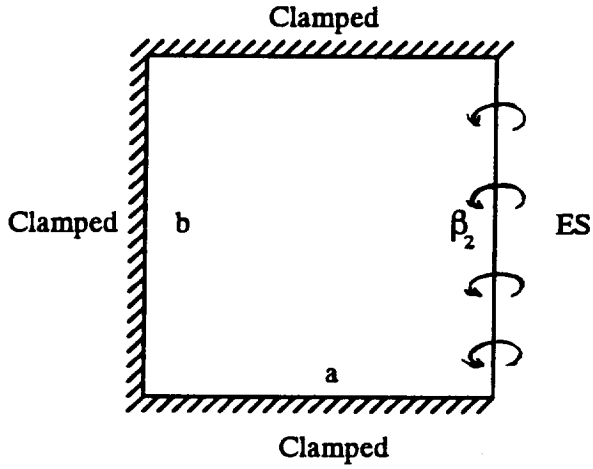

Fig. 1 A plate with three edges clamped and the fourth edge elastically supported (ES).

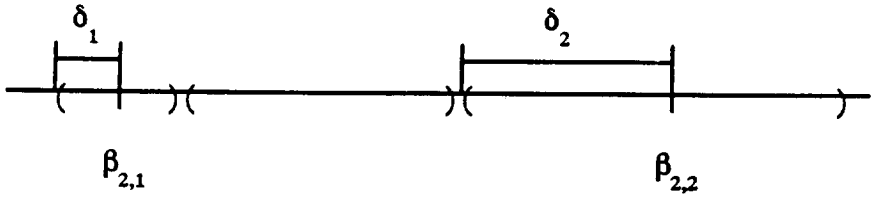

Fig. 2 The process of creating the "final" convex model.

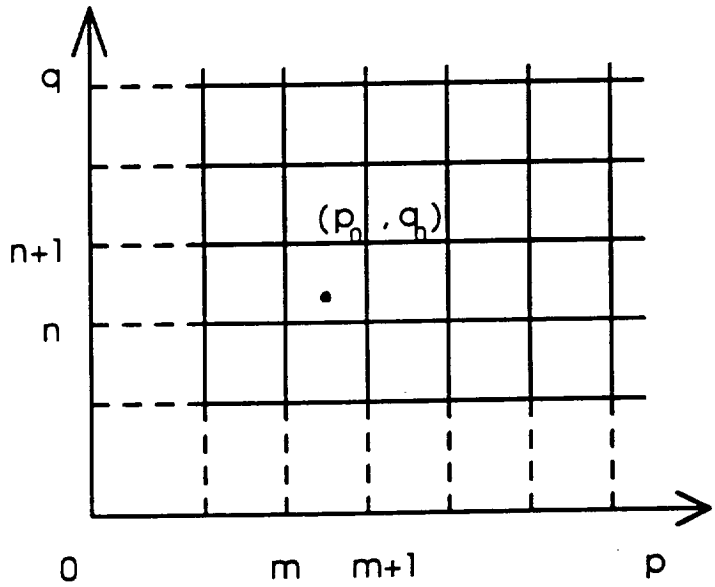

Fig. 3 The mode sequence numbers by generalized Bolotin's dynamic edge effect method.

CHAPTER # 2

Convex Identification of Boundary Conditions by Finite Element Method

CONVEX IDENTIFICATION OF BOUNDARY CONDITIONS BY FINITE ELEMENT METHOD

Jianjie Fang and Isaac Elishakoff

Center for Applied Stochastics Research
and Department of Mechanical Engineering
Florida Atlantic University
Boca Raton, FL 33431-0991, USA

Abstract: The study deals with the identification of the boundary conditions by the finite element method. The identification of the convex model, to which the boundary stiffnesses belong, rather than the total reconstruction of the boundary conditions, is performed. Two example problems of the beams, one uniform and the other nonuniform, both clamped at one end and elastically supported at the other, are considered and numerically evaluated in detail.

1. INTRODUCTION

The vibration problems of beams, either due to deterministic or random excitations, have been widely investigated. To the best of our knowledge, in most of these studies the boundary conditions at the ends of the beam are assumed as known (Gorman, 1975; Weaver, Timoshenko, and Young, 1990). Most investigators consider all possible combinations of boundary conditions at the ends, namely those of simply supported (SS), clamped (C), free (F), or, more generally, elastically supported (ES) ends. However, in practical problems, engineers usually do not have the exact information associated with the boundary conditions; they may, however, possess some fragmentary knowledge about those boundary conditions, such as the probable ranges of the boundary springs' stiffnesses. The natural question arises: How to identify the "true" boundary conditions based on the partial knowledge?

Boundary conditions have traditionally been modeled as axial and torsional springs or translational and rotational springs at the boundaries. Identification of parameters such as spring

stiffnesses has usually been considered within the context of identifying mass and stiffness matrices from measured eigenvectors (Baruch, 1982; Kabe, 1985; Baruh and Meirovitch, 1985; Dong, Cheng, and Qi, 1991). Identification of eigenvalues and eigenvectors form the system response is a popular subject and there are several methods available, such as those in Refs. (Ibrahim, 1983; Ewins and Gleeson, 1982; Juang and Pappa, 1985). Baruh and Boka (1993) recently presented a procedure for the identification of the spring constants, by assuming that a number of eigenvalues and eigenvectors are known and making use of identified eigenvectors and orthogonality conditions.

To the best of the authors' knowledge, the convex treatment of the uncertainty in boundary conditions was addressed only by Ben-Haim and Natke (1992, 1993). They represented this uncertainty by convex models, which are sets of mathematical entities such as functions, vectors or matrices (for more details about convex modeling of uncertainty one may consult the monograph by Ben-Haim and Elishakoff (1990)). For example, in Ref. (Ben-Haim and Natke, 1993), an adaptive diagnosis procedure was developed and furthermore, the performance of this procedure with uncertainty characterized by the convex models was studied.

In this study, the incomplete or partial knowledge about the boundary conditions is characterized by the convex model. The main idea about convex models for uncertainty is stated in the following section. It must be stressed that diagnosis of the boundary conditions within the convex modeling does not imply the complete identification of the spring constants in the beam problem. Indeed, total reconstruction of the boundary stiffnesses is not only quite challenging but may be unnecessary for many operational or maintenance decisions. Rather, diagnosis of the boundary conditions may mean identification of the adversely affected boundary (x=0 or x=L, where x is the axial coordinate and L is the length of the beam), and moreover, estimation of limits on the magnitude of the stiffness change of the elastic strings modeling the actual boundary conditions. Once convex models of the boundary conditions are constructed, the diagnostic process in fact implies identifying, in the convex model, the element to which the actual boundary stiffness belongs.

This will then allow us to precisely formulate the diagnosis as a discrete multi-hypothesis decision problem with attendant formulation of the adaptive termination of this algorithm. The boundary conditions are generally modeled in terms of both translational and rotational springs.

The present diagnosis is based on measurement of a certain number of natural frequencies of the beam. The integral part of the method is the subprocess of evaluating the frequencies of a beam with specified boundary conditions, which can be performed analytically for the uniform beams, or numerically for the non-uniform beams, by using the versatile finite element method or other approximate techniques. The class to which the "true" boundary stiffness belongs, can then be identified by the convex modeling and implementing the decision algorithm of the suitably chosen minimum distance between natural frequencies, or other suitable criteria.

2. CONVEX MODELS OF UNCERTAINTY

As indicated above, identification of the boundary condition means identifying in the convex model the element to which the actual boundary stiffness belongs. In this study, convex models developed by Ben-Haim and Elishakoff (1990) are employed to specify the degree of precision required in the diagnosis of the boundary translational and rotational stiffnesses.

A convex model is a set possessing certain convexity properties. Each element of the set represents a possible realization of an uncertain quantity of interest. In our case, these elements are intervals within which the "true" stiffnesses, K_i's, are possibly located, where i=1,2 are associated with translational and rotational stiffnesses, respectively. Therefore, elements in this convex model can represent the acceptable uncertainty in the boundary condition. The diagnosis will be considered satisfactory when the uncertainty in the boundary condition has been "reduced" to an preselected level, i.e. when the interval with sufficient small length has been found to yield corresponding actual measured frequencies of the beam. This means that diagnosis of the boundary condition is in fact no more than identification of the interval to which the actual boundary stiffness belongs. It should be stressed again that the actual stiffness will not be identified; only the interval to which it belongs is sought by the diagnosis.

While several different convex models are available (Ben-Haim and Elishakoff,1990), the following simple model is particularly suitable for the beam problem. Let $K_i^{(m)}$ be the nominal stiffnesses, where m=1, ···, M is the total number of convex models, and i=1, 2, corresponding to the translational and rotational stiffnesses, respectively. We define the convex model as a set of stiffness intervals whose centers are located at the nominal values. Specifically, the convex

model C is the following set of hypothesized stiffness intervals:

$$C = \{c_m,\ m=1,2,\cdots,M\} \tag{1}$$

where c_m is

$$c_m = \{K_i :\ |K_i - K_i^{(m)}| \le \delta_i,\ i = 1,2\} \tag{2}$$

In other words, c_m is the set of translational and rotational stiffness intervals which deviate by as much as $\pm\delta$ from the constant value $K_i^{(m)}$. One recognizes that C is a *uniform bound convex model.*

3. MULTI-HYPOTHESIS DECISION

The reference values $K_i^{(m)}$ in the convex models in Eq. (1) can assume any of the M different values $K_i^{(1)}$, $K_i^{(2)}$...,$K_i^{(M)}$. Thus diagnosis of the boundary condition involves deciding which of the M convex models contains the true boundary stiffness. This decision is based on a multi-hypothesis formulation (Wald, 1947).

In its simplest form the multi-hypothesis decision algorithm requires the choice of one representative or *hypothesized* stiffness from each element in the convex model. It should be noted that in its more general form, more than one hypothesized stiffness is chosen for each convex model. Let h_m denote the hypothesized stiffness from the element c_m. That is, $h_m \in c_m$. Let $\omega^{(m)} = (\omega_1^{(m)},...\omega_J^{(m)})$ indicate a vector of the first J natural frequencies of a beam whose boundary stiffness is h_m. Furthermore, let $\Omega = (\Omega_1, ...\Omega_J)$ represent the vector of measured natural frequencies.

The "distance" from the measured natural frequency vector Ω to the anticipated natural frequency vector $\omega^{(m)}$ based on the *mth* hypothesis is :

$$H_m = \mathcal{F}(\Omega, \omega^{(m)}) \tag{3}$$

where $\mathcal{F}$ denotes some measure of deviation between Ω and ω^m. One of the possible choices can be the following

$$\mathcal{F}(\Omega, \omega_m) = \|\Omega - \omega^{(m)}\| \tag{4}$$

where $\|x\|$ denotes a norm of vector x.

It is reasonable to conclude that the true stiffness is likely to belong to the convex model whose anticipated natural frequencies are the "closest" to the measured ones. Let the index m_0 satisfy:

$$H_{m_0} = \min_m H_m \tag{5}$$

The multi-hypothesis decision is that the true stiffness belongs to the element of c_{m_0}.

4. DIAGNOSIS PROCEDURE

The decision algorithm implied by Eq. (5) can always reach a decision, no matter whether the least distance, H_{m_0}, is small or not. In other words, the multi-hypothesis decision will choose the most likely stiffness interval from the available options.

As expected, in practical situation, it is assumed that all needed frequencies of the to-be-identified beam have been measured. We need to establish a convex model to which the boundary conditions belong. It should be pointed out that we have many definitions of the distance of frequencies given by Eq.(3), depending on the definition of the norm of vectors. The fact that the lower order natural frequencies can be measured more accurately than higher ones, allows us to reasonably define the distance as a sum of relative errors of frequencies over the first several natural frequencies, i.e,

$$\mathcal{F}(\Omega, \omega_m) = \sum_{i=1}^{N} \frac{|\Omega_i - \omega_i^{(m)}|}{\Omega_i} \tag{6}$$

where N is the number of measured frequencies. Note that the distance in Eq. (6) does not represent the norm, yet it appears to be a preferable criterion, from the physical point of view.

The diagnosis procedure is as follows:

1. *Measure* all the necessary natural frequencies of the beam.

2. *Construct* the convex model of the unknown boundary conditions by taking advantage of the available preliminary knowledge of the range of values which can be reasonably expected to occur. In this study, a specific convex model with general form of Eq.(1) is established. We set δ_1=0.005 N/m for the translational stiffness, and δ_2=0.005 N·m for the rotational stiffness. This implies that the stiffness differing from each other by less than or equal to 0.005 N/m will be treated as coinciding with each other. However, the number of elements in the convex model, M, is taken as infinite, and as a result $K_1^{(m)}$ and $K_2^{(m)}$ can take infinite number of values. But they do have a finite range, which is $K_1^{(m)} \in [0,10^4]\, EI_0/L^3$ N/m, $K_2^{(m)} \in [0,100]\, EI_0/L$ N·m in our example problem, where [a,b] denotes an interval. Since there are infinite numbers of elements, we can not afford testing all the elements in the convex model. The adaptive process of producing sub-intervals from original large intervals is utilized to reach the element of interest efficiently, without the necessity of checking all the elements. In this process the lower bounds of the boundary stiffness intervals are denoted by K_1^a and K_2^a, and the upper ones by K_1^b and K_2^b respectively. We note that in the first procedure K_1^a=0 N/m, K_1^b=10^4 EI_0/L^3 N/m, K_2^a=0 N·m, K_2^b=100 EI_0/L N·m.

3. *Divide* intervals $[K_1^a, K_1^b]$ and $[K_2^a, K_2^b]$ into a number of equal intervals (20 intervals were chosen in this study).

4. *Compute* the distances $\mathcal{J}$ between the measured frequencies and the ones corresponding to hypothesized stiffnesses according to the general definition given in Eq. (3) for every interval separation point K_1^i (i=1,2,..., 20) in $[K_1^a, K_1^b]$ at all K_2^j's (j=1,2,...,20) in $[K_2^a, K_2^b]$, by employing the finite element method (Petyt, 1990).

5. *Identify* the point $(K_1^{i_0}, K_2^{j_0})$ from the multi-hypothesis decision of Eq. (5) after obtaining all the distances in step 4.

6. *Reset* a searching range of K_1 and K_2, which is a rectangle in two dimensional space, with the identified vector $(K_1^{i_0}, K_2^{j_0})$ from step 4 as the center, and the side length of this rectangular is taken as twice the divided interval length of the preceding step. It can be readily seen that the present area of K_1 and K_2 is one percent of the preceding one.

7. *Repeat* steps 3 through 6 until an interval is found such that, on the basis of minimum distance algorithm decision Eq. (5), H_m is smaller than a specified threshold value θ. In other words, the process of diagnosis is terminated if the following inequality is satisfied

$$H_m \leq \theta \tag{7}$$

In the present example, this step is implemented as choosing $(K_1^{i^*}, K_2^{j^*})$ among the 400 dividing points of K_1 and K_2 such that H is minimum.

As we can see, one of the cornerstones of the method is the ability to determine the natural frequencies of beams under arbitrary boundary conditions. The finite element method, which is addressed in Appendix A, is applied to solve this problem.

5. NUMERICAL EXAMPLE

As an example, we will investigate the beam which is clamped at one end and elastically supported at the other.

5.1 **Uniform Beam**

Consider a uniform beam with length L, Young's modulus E, material density per unit length ρ, moment of inertia I and cross-sectional area A. In this case, we visualize that only the first two nondimensional natural frequencies were measured, which are given as follows

$$\lambda_1 = 18.0 \tag{8}$$

$$\lambda_2 = 50.0$$

The relation between the natural frequencies and their nondimensional counterparts λ_i is

$$\omega_i = \frac{\lambda_i}{l^2}\sqrt{\frac{EI}{\rho A}} \tag{9}$$

where ω_i is the natural frequency of the beam.

We note in passing that the exact frequencies for the uniform C-C (i.e., with both ends clamped) beam are

$$\lambda_1 = 22.37 \qquad \lambda_2 = 61.67 \tag{10}$$

$$\lambda_3 = 120.9 \qquad \lambda_i \approx (i+1/2)^2\pi^2 \quad , \ for \ \ i \geq 4$$

and for a C-F uniform beam are

$$\lambda_1 = 3.516 \qquad \lambda_2 = 22.03 \tag{11}$$

$$\lambda_3 = 61.70 \qquad \lambda_i \approx (i-1/2)^2\pi^2 \quad , \ for \ i \geq 4$$

These cases are of interest since C-C and C-F are two extreme cases of C-ES.

The results of the identified intervals in various steps are summarized in Table 1.

Table 1

step number	Interval for k_3	Interval k_4
1	$[0, 10]\times10^3$	[0, 100]
2	$[1.0,2.0]\times10^3$	[1,10]
3	$[1.15,1.25]\times10^3$	[4.5,5.5]
4	$[1.22,1.23]\times10^3$	[4.9,5.0]
5	$[1.2215,1.2225]\times10^3$	[4.965,4.975]
6	$[1.2216,1.2217]\times10^3$	[4.970,4.972]

where the nondimensional stiffnesses are

$$k_1 = \frac{K_1 L^3}{EI_0}, \quad k_2 = \frac{K_2 L}{EI_0}, \quad k_3 = \frac{K_3 L^3}{EI_0}, \quad k_4 = \frac{K_4 L}{EI_0} \tag{12}$$

Thus, the final result is $k_3 \in [1.2216, 1.2217]\times10^3$, $k_4 \in [4.970, 4.972]$. One can take the mid-points of these intervals $k_3=1.22165\times10^3$, $k_4=4.971$ as the identified boundary stiffnesses.

The first three nondimensional natural frequencies, obtained by finite element method for above k_3 and k_4, are λ_1=18.0000, λ_2=49.9999, λ_3=94.0661.

The above results are verified by the weighted residuals method which is given at Appendix B of the paper. The single term weighted residuals method yields λ_1=18.0637, which constitutes an error of only 0.3539%. This is also verifiable through the exact solution, which is obtained by solving the following characteristic equation (Weaver, Timoshenko, and Young, 1990):

$$\begin{vmatrix} 0 & 1 & 0 & 1 \\ 1 & 0 & 1 & 0 \\ -\lambda^{\frac{3}{2}}\cos\sqrt{\lambda} - k_3\sin\sqrt{\lambda} & \lambda^{\frac{3}{2}}\sin\sqrt{\lambda} - k_3\cos\sqrt{\lambda} & \lambda^{\frac{3}{2}}\cosh\sqrt{\lambda} - k_3\sinh\sqrt{\lambda} & \lambda^{\frac{3}{2}}\sinh\sqrt{\lambda} - k_3\cosh\sqrt{\lambda} \\ -\sqrt{\lambda}\sin\sqrt{\lambda} + k_4\cos\sqrt{\lambda} & -\sqrt{\lambda}\cos\sqrt{\lambda} - k_4\sin\sqrt{\lambda} & \sqrt{\lambda}\sinh\sqrt{\lambda} + k_4\cosh\sqrt{\lambda} & \sqrt{\lambda}\cosh\sqrt{\lambda} + k_4\sinh\sqrt{\lambda} \end{vmatrix}$$

$$\begin{aligned} = {} & -k_3k_4\cos^2\sqrt{\lambda} - \lambda^2\cos^2\sqrt{\lambda} + 2k_3k_4\cos\sqrt{\lambda}\cosh\sqrt{\lambda} - 2\lambda^2\cos\sqrt{\lambda}\cosh\sqrt{\lambda} - k_3k_4\cosh^2\sqrt{\lambda} \\ & - \lambda^2\cosh^2\sqrt{\lambda} - 2k_3\sqrt{\lambda}\cosh\sqrt{\lambda}\sin\sqrt{\lambda} - 2k_4\lambda\sqrt{\lambda}\cosh\sqrt{\lambda}\sin\sqrt{\lambda} - k_3k_4\sin^2\sqrt{\lambda} - \lambda^2\sin^2\sqrt{\lambda} \\ & + 2k_3\sqrt{\lambda}\cos\sqrt{\lambda}\sinh\sqrt{\lambda} - 2k_4\lambda\sqrt{\lambda}\cos\sqrt{\lambda}\sinh\sqrt{\lambda} + k_3k_4\sinh^2\sqrt{\lambda} + \lambda^2\sinh^2\sqrt{\lambda} = 0 \end{aligned} \quad (13)$$

Substitution of k_3=1.22165×10^3, k_4=4.971 into Eq. (13) gives the following first three non-dimensional frequencies: λ_1=17.9996, λ_2=49.9913, λ_3=94.0085, which are extremely close to the measured ones.

5.2 **Non-Uniform Beam**

Consider a non-uniform beam with length L, Young's modulus E, the moment of inertia I and cross-sectional area A are varying proportionally along the axis ox_1 with I_1 and A_1 at one end and I_2 and A_2 at the other. Similar to the case of uniform beam, we visualize that only the first two nondimensional natural frequencies are measured, which again are given in Eq. (8). For the special case A_2=A_1/2=A/2, and I_2=I_1/2=I/2, the similar nondimensional stiffness intervals are

listed as follows

Table 2

step number	Interval for k_3	Interval k_4
1	$[0, 10]\times10^3$	[0, 100]
2	$[0,1.0]\times10^3$	[1,10]
3	$[0.55,0.65]\times10^3$	[2,3]
4	$[0.640,0.650]\times10^3$	[2.35,2.45]
5	$[0.6400,0.6410]\times10^3$	[2.410,2.420]

Thus, the final result is $k_3\in[0.6400, 0.6410]\times10^3$, $k_4\in[2.410, 2.420]$. The first three nondimensional natural frequencies corresponding to mid-intervals, i. e. to $k_3=0.6405\times10^3$, $k_4=2.415$, are $\lambda_1=17.9993$, $\lambda_2=50.0013$, $\lambda_3=94.3288$.

6. DISCUSSION

As one can expect, the availability of the information, namely of the number of the measured natural frequencies, will certainly have an effect on the identification process of the boundary conditions. It appears to be instructive to investigate the effect of adding the information of higher order frequencies to the criterion of frequency distance. The following two cases will be investigated. If the information on the third nondimensional frequency $\lambda_3=94.0$ is added to the criterion of frequency distance Eq.(6), i. e. for case of measured natural frequencies being equal to $\lambda_1=18.0$, $\lambda_2=50.0$, $\lambda_3=94.0$, the results of the identified intervals in various steps are listed in Table 3.

Table 3

step number	Interval for k_3	Interval k_4
1	$[0, 10]\times10^3$	[0, 100]
2	$[1.0,2.0]\times10^3$	[1,10]
3	$[1.15,1.25]\times10^3$	[4.5,5.5]
4	$[1.21,1.22]\times10^3$	[4.95,5.05]
5	$[1.215,1.216]\times10^3$	[4.975,4.985]
6	$[1.2153,1.2154]\times10^3$	[4.977,4.979]

where k_3 and k_4 are the nondimensional stiffnesses given by Eq. (12). For the mid-interval stiffnesses k_3=1.21535×10^3 and k_4=4.978, the first three theoretical nondimensional frequencies are λ_1=18.0000, λ_2=49.9834, λ_3=94.0001 respectively.

Let the third nondimensional frequency be taken as λ_3=94.0661, which is the "actual" nondimensional natural frequencies corresponding to the "identified" boundary stiffnesses k_3=1.22165×10^3, k_4=4.971. The results of the identified intervals in various steps are as follows:

Table 4

step number	Interval for k_3	Interval k_4
1	$[0, 10]\times10^3$	[0, 100]
2	$[1.0,2.0]\times10^3$	[1,10]
3	$[1.15,1.25]\times10^3$	[4.5,5.5]
4	$[1.215,1.225]\times10^3$	[4.95,5.05]
5	$[1.2210,1.2220]\times10^3$	[4.965,4.975]
6	$[1.2216,1.2217]\times10^3$	[4.970,4.971]

where k_3 and k_4 are the nondimensional stiffnesses given by Eq. (12). Thus the process converges to the same final interval as it should be.

Assume now that the measurement shows the same first two natural frequencies but with different third frequency, namely λ_3=95.0. This simulates the imprecision in the measurements. The results of the convex identification leads to intervals in various steps as follows:

Table 5

step number	Interval for k_3	Interval k_4
1	$[0, 10]\times10^3$	[0, 100]
2	$[1.0,2.0]\times10^3$	[1,10]
3	$[1.25,1.35]\times10^3$	[4.5,5.5]
4	$[1.31,1.32]\times10^3$	[4.8,4.9]
5	$[1.316,1.317]\times10^3$	[4.87,4.88]
6	$[1.3167,1.3168]\times10^3$	[4.875,4.876]

where k_3 and k_4 are the nondimensional stiffnesses given by Eq. (12). If one decides to let the "identified" frequency to be at the middle of the intervals, i.e. k_3=1.31675×10^3 and k_4=4.8755, the first three corresponding theoretical frequencies will be λ_1=18.0000, λ_2=50.2287, λ_3=95.0002. As is seen, the values of k_3 has changed by 8%, and values of k_4 has been changed by 2%, although the error in the third frequency constituted slightly above 1%. This shows that for accurate identification of the boundary conditions one needs much precision in the measured natural frequencies.

The above results show that the identified stiffnesses will change with the additional information on the measured higher order frequencies added to the criterion of the frequency distance Eq. (6).

To understand the present convex identification method, one may get some additional insight by contrasting it with the deterministic identification. By the finite element method, for

the known stiffnesses k_3 and k_4, one can always numerically obtain the corresponding nondimensional frequencies. Fig. 1 shows the variation of the first nondimensional frequency λ_1 for different values of k_3 and k_4. Similarly, we can obtain frequencies λ_2, λ_3, ···, λ_n for any n for different values of k_3 and k_4. By making cuts at λ_1=18 and λ_2=50 in the two three-dimensional figures for λ_1 and λ_2, we obtain two curves: curve (a) gives the combination of values k_3 and k_4 for which the first frequency λ_1 is constant, namely equals 18. Curve (b) is associated with the second frequency $\lambda_2(k_3, k_4)$=50. The intersection point of the two curves in Fig. 2 must identify the values of k_3 and k_4 if there are no errors in measurements. However, it is important to keep in mind that these two curves in Fig. 2 are not extremely accurate because in figures of λ_1 and λ_2 the nondimensional frequencies λ_1 and λ_2 are not continuously changing with k_3 and k_4, and some error is present. Furthermore, to reach high accuracy, extremely large amount of points are needed to obtain a collection of k_3 and k_4 for which λ_1=const. and λ_2=const., i.e. equal frequency curves. On the other hand, when higher order natural frequencies are measured, the deterministic identification method may be unapplicable. The reason is that the equal frequency curves obtained through higher order frequencies may not intersect at the same point where the curves λ_1=const. and λ_2=const. intersects due to the unavoidable measurement errors. However, the convex identification is still able to treat this effect. This is the advantage of convex modeling since it takes into account the uncertainty in the measurements.

7. CONCLUSION

In this problem, a special kind of convex model of boundary conditions of a beam is utilized to specify their possible realizations. The diagnostic process in fact implies identification of the interval to which the "true" boundary conditions belong. This process is realized by implementing the multi-hypothesis decision technique which is based on the minimum distance algorithm. The beams with one end clamped and the other end elastically supported are investigated. We assume that a certain number of natural frequencies of the beam were measured experimentally. The evaluation of the frequencies of a beam with specified boundary conditions is performed numerically by the finite element method. The final identified boundary stiffness intervals are checked by comparing the calculated natural frequencies with the measured ones.

It is found that they are extremely close to each other. The effect of the additional information, namely the number of the measured natural frequencies, on the identification results, is also investigated in this study. The present convex model identification based on multi-hypothesis decision can be utilized in identifying damaged regions in the boundary conditions in plates and shells. In addition to versatile finite element techniques, one can use some analytical techniques for uniform structures. Such a method of calculation of natural frequencies in rectangular plates with step-wise discontinuities in rotational stiffness along the edges was developed by Gorman (1993) at the suggestion of one of the present writers.

ACKNOWLEDGMENT

This study has been supported by the NASA Kennedy Space Center, through Cooperative Agreement No. NCC10-0005, S1 to the Florida Atlantic University; technical monitor: Mr. R. Caimi. Authors appreciate fruitful discussion with Professor Y. Ben-Haim of the Technion-Israel Institute of Technology.

REFERENCES

Baruch, M., 1982, "Correction of Stiffness Matrix Using Vibration Tests," *AIAA Journal*, Vol. 20, No. 3, pp441-442.

Baruh, H. and Meirovitch, L., 1985, "Parameter Identification on Distributed Systems," *Journal of Sound and Vibration*, Vol. 101, No. 4, pp551-564.

Baruh, H. and Boka, J.B., 1993, "Modeling and Identification of Boundary Conditions in Flexible Structures," *International Journal of Analytical and Experimental Modal Analysis*, Vol. 8, pp107-117.

Ben-Haim, Y. and Elishakoff, I., 1990, *Convex Models of Uncertainty in Applied Mechanics*, Elsevier Science Publishers, Amsterdam.

Ben-Haim, Y. and Natke, H.G., 1992, "Diagnosis of Changes in Elastic Boundary Conditions in Beams by Adaptive Vibration Testing," *Archives of Applied Mechanics*, Vol. 62, pp210-221.

Ben-Haim, Y. and Natke, H.G., 1993, "Sequential Adaptation in Estimating Elastic Boundary-Condition Influence Matrices," *Journal of Dynamic Systems, Measurements and Control*, Vol.115, No.3, pp370-378.

Cheung, Y.K., 1993, *Finite Element Methods in Dynamics*, Kluwer Academic Publications, Dordrecht.

Dong, X.Q., Cheng, Y. and Qi, J., 1991, "Identification of Structural Boundary Condition," *Proceeding of 9th International Conference of Modal Analysis*, Firenze (Florence), Italy, pp993-998.

Elishakoff, I. and Fang, J., "Diagnosis of Local Modifications in the Boundary Conditions of a Rectangular Plate," *Journal of Computer Methods in Applied Mechanics and Engineering*, (submitted).

Ewins, D.J. and Gleeson, P.T., 1982, "A Method for Modal Identification in Lightly Damped Structures," *Journal of Sound and Vibration*, Vol. 84, No. 1, pp57-59.

Gorman, D.J., 1975, *Free Vibration Analysis of Beams and Shafts*, Wiley, New York.

Gorman, D.J., 1993, "Free Vibration Analysis of Rectangular Plates with Step-Wise Discontinuities in Rotational Stiffness Along the Edges," *Journal of Sound and Vibration*, Vol.

166, pp397-408.

Ibrahim, S.R., 1983, "Computation of Normal Modes from Identified Complex Modes," *AIAA Journal*, Vol. 21, No. 3, pp446-451.

Juang, J.N. and Pappa, R.S., 1985, "An Eigensystem Realization Algorithm for Modal Parameter Identification and Model Reduction," *Journal of Guidance Control Dynamics*, Vol. 8, NO. 5, pp620-627.

Kabe, A.M., 1985, "Stiffness Matrix Adjustment Using Mode Data," *AIAA Journal*, Vol. 23, No. 9, pp1431-1436.

Leissa, 1969, A.W., "Vibrations of Plates," *NASA SP* 160, 1969.

Petyt, M., 1990, *Introduction to Finite Element Vibration Analysis*, Cambridge University Press.

Wald, A., 1947, *Sequential Analysis*, John Wiley. Re-issued by Dover Press, 1973.

Weaver, W., 1986, *Structural Dynamics by Finite Elements*, Englewood Cliffs, Prentice-Hall.

Weaver, W. Jr., Timoshenko, S.T. and Young, D.H., 1990, *Vibration Problems in Engineering*, John Wiley and Sons, New York.

APPENDIX A. VIBRATION OF ELASTICALLY SUPPORTED BEAMS BY FINITE ELEMENT METHOD

In order to perform the convex identification procedure, one needs to have an analytical or numerical algorithm for evaluation of natural frequencies of the structure under consideration. In our previous study (Elishakoff and Fang), devoted to elastically supported plates, the generalized Bolotin's dynamic edge effect method was utilized. For plates, one can use one of the numerous methods reviewed in the monograph by Leissa (1969), or employ the analytical approach based on the principle of superposition, by Gorman (1993). In this section the versatile finite element method will be discussed for vibration frequency evaluation. Whereas the finite element method for beams is exposed in several books, (Cheung, 1993; Petyt,1990; Weaver, 1986; Weaver, Timoshenko, and Young, 1990), none of them unfortunately deal with elastically supported beams. This gap is closed in this paper.

Strain energy of elastic deformations stored in an element of length $2a$ reads

$$U = \frac{1}{2}\int_{-a}^{a} E I_z \left(\frac{\partial^2 v}{\partial x^2}\right)^2 dx \tag{A.1}$$

where E is the modulus of elasticity, and I_z is the second moment of area of the cross-section about the z-axis. The kinetic energy of the element is

$$T = \frac{1}{2}\int_{-a}^{a} \rho A \dot{v}^2 dx \tag{A.2}$$

where ρ is the mass density, A is the cross-sectional area, dot denotes the derivative with respect to time. The element shown in the figure has a total of four degrees of freedom, displacements and rotations at each end of the beam (Petyt, 1990). The displacement function can thus be represented by a polynomial having four constants, namely

$$v = \alpha_1 + \alpha_2 \xi + \alpha_3 \xi^2 + \alpha_4 \xi^3, \quad \xi = x/a \tag{A.3}$$

This expression can be written in the following matrix form

$$v = [p(\xi)]^T \{\alpha\} \tag{A.4}$$

where

$$[p(\xi)]^T = [1 \quad \xi \quad \xi^2 \quad \xi^3]$$
$$[\alpha]^T = [\alpha_1 \quad \alpha_2 \quad \alpha_3 \quad \alpha_4] \tag{A.5}$$

Differentiating (A.3) yields

$$a\theta_z = a\frac{\partial v}{\partial x} = \frac{\partial v}{\partial \xi} = \alpha_2 + 2\alpha_3\xi + 3\alpha_4\xi^2 \tag{A.6}$$

Evaluating (A.3) and (A.6) at ξ=-1, and ξ=1 results in

$$\begin{bmatrix} v_1 \\ a\theta_{z_1} \\ v_2 \\ a\theta_{z_2} \end{bmatrix} = \begin{bmatrix} 1 & -1 & 1 & -1 \\ 0 & 1 & -2 & 3 \\ 1 & 1 & 1 & 1 \\ 0 & 1 & 2 & 3 \end{bmatrix} \begin{bmatrix} \alpha_1 \\ \alpha_2 \\ \alpha_3 \\ \alpha_4 \end{bmatrix} \tag{A.7}$$

where v_1=v(-1), θ_{z1}=θ(-1), v_2=v(1), θ_{z2}=θ(1), or, in matrix form

$$\{\overline{v}\} = [A]_e \{\alpha\} \tag{A.8}$$

where

$$\{\overline{v}\} = \{v_1, a\theta_{z_1}, v_2, a\theta_{z_2}\}^T \tag{A.9}$$

Solving $\{\alpha\}$ from Eq. (A.8) leads to

$$\{\alpha\} = [A]_e^{-1} \{\overline{v}\} \tag{A.10}$$

where

$$[A]_e^{-1} = \frac{1}{4}\begin{bmatrix} 2 & 1 & 2 & -1 \\ -3 & -1 & 3 & -1 \\ 0 & -1 & 0 & 1 \\ 1 & 1 & -1 & 1 \end{bmatrix} \tag{A.11}$$

Eq. (A.10) can be written in the different form

$$\{\alpha\} = [c]_e \{v\}_e \tag{A.12}$$

where

$$\{v\}_e^T = \begin{bmatrix} v_1 & \theta_{z_1} & v_2 & \theta_{z_2} \end{bmatrix} \tag{A.13}$$

and

$$[c]_e = \frac{1}{4}\begin{bmatrix} 2 & a & 2 & -a \\ -3 & -a & 3 & -a \\ 0 & -a & 0 & a \\ 1 & a & -1 & a \end{bmatrix} \tag{A.14}$$

Substituting (A.12) into (A.4) yields

$$v = [p(\xi)]^T [c]_e \{v\}_e \tag{A.15}$$

Eq. (A.15) can be expressed in the form

$$v = [N(\xi)] \{v\}_e \tag{A.16}$$

where

$$[N(\xi)] = [N_1(\xi) \quad aN_2(\xi) \quad N_3(\xi) \quad aN_4(\xi)] \tag{A.17}$$

The displacement functions in (A.17) are given by

$$
\begin{aligned}
N_1(\xi) &= \frac{1}{4}(2 - 3\xi + \xi^3) \\
N_2(\xi) &= \frac{1}{4}(1 - \xi - \xi^2 + \xi^3) \\
N_3(\xi) &= \frac{1}{4}(2 + 3\xi - \xi^3) \\
N_4(\xi) &= \frac{1}{4}(-1 - \xi + \xi^2 + \xi^3)
\end{aligned}
\tag{A.18}
$$

Substituting the displacement expression (A.16) into the kinetic energy (A.2) results in

$$
\begin{aligned}
T_e &= \frac{1}{2}\int_{-a}^{a} \rho A \dot{v}^2 \, dx = \frac{1}{2}\int_{-a}^{a} \rho A \dot{v}^2 \, a \, d\xi \\
&= \frac{1}{2}\{\dot{v}\}_e^T \rho a \int_{-1}^{1} A(\xi)\,[N(\xi)]^T [N(\xi)]\, d\xi \, \{\dot{v}\}_e \\
&= \frac{1}{2}\{\dot{v}\}_e^T [m]_e \{\dot{v}\}_e
\end{aligned}
\tag{A.19}
$$

Therefore, the element's inertia matrix is given by

$$
[m]_e = \rho a \int_{-1}^{1} A(\xi)\,[N(\xi)]^T [N(\xi)]\, d\xi \tag{A.20}
$$

Substitution of the displacement expression (A.16) into the strain energy (A.1) results in

$$
\begin{aligned}
U_e &= \frac{1}{2}\int_{-a}^{a} EI_z \left(\frac{\partial^2 v}{\partial x^2}\right)^2 dx = \frac{1}{2}\int_{-1}^{1} EI_z \frac{1}{a^4}\left(\frac{\partial^2 v}{\partial \xi^2}\right)^2 a \, d\xi \\
&= \frac{1}{2}\{v\}_e^T \frac{E}{a^3}\int_{-1}^{1} I_z(\xi)\,[N''(\xi)]^T [N''(\xi)]\, d\xi \, \{v\}_e \\
&= \frac{1}{2}\{v\}_e^T [k]_e \{v\}_e
\end{aligned}
\tag{A.21}
$$

The element stiffness matrix is

$$[k]_e = \frac{E}{a^3}\int_{-1}^{1} I_z(\xi)\,[N''(\xi)]^T[N''(\xi)]\,d\xi \tag{A.22}$$

For a uniform beam, the following element inertia matrix can be obtained from Eq.(20)

$$[m]_e = \frac{\rho A a}{105}\begin{bmatrix} 78 & 22a & 27 & -13a \\ 22a & 8a^2 & 13a & -6a^2 \\ 27 & 13a & 78 & -22a \\ -13a & -6a^2 & -22a & 8a^2 \end{bmatrix} \tag{A.23}$$

The element stiffness matrix is obtained from Eq. (22)

$$[k]_e = \frac{EI}{2a^3}\begin{bmatrix} 3 & 3a & -3 & 3a \\ 3a & 4a^2 & -3a & 2a^2 \\ -3 & -3a & 3 & -3a \\ 3a & 2a^2 & -3a & 4a^2 \end{bmatrix} \tag{A.24}$$

For a non-uniform beam with linearly changing cross-sectional area and inertia of moments, the element inertia matrix is obtained through the use of the computerized algebraic code MATHEMATICA

$$[m]_e = \frac{A_1+A_2}{2}\cdot\frac{\rho a}{105}\begin{bmatrix} 78 & 22a & 27 & -13a \\ 22a & 8a^2 & 13a & -6a^2 \\ 27 & 13a & 78 & -22a \\ -13a & -6a^2 & -22a & 8a^2 \end{bmatrix} + \frac{A_2-A_1}{2}\cdot\frac{\rho a}{105}\begin{bmatrix} -42 & -8a & 0 & a \\ -8a & -2a^2 & a & 0 \\ 0 & a & 42 & -8a \\ a & 0 & -8a & 2a^2 \end{bmatrix} \tag{A.25}$$

The element stiffness matrix is

$$[k]_e = \frac{I_1+I_2}{2}\cdot\frac{E}{2a^3}\begin{bmatrix} 3 & 3a & -3 & 3a \\ 3a & 4a^2 & -3a & 2a^2 \\ -3 & -3a & 3 & -3a \\ 3a & 2a^2 & -3a & 4a^2 \end{bmatrix} + \frac{I_2-I_1}{2}\cdot\frac{E}{2a^3}\begin{bmatrix} 0 & -a & 0 & a \\ -a & -2a & a & 0 \\ 0 & a & 0 & -a \\ a & 0 & -a & 2a^2 \end{bmatrix} \tag{A.26}$$

where A_1, A_2 and I_1, I_2 are cross-sectional areas and moments of inertia at the two ends of the element, respectively.

Let us consider the expression of the strain energy of the elastic supports. The whole beam is shown in Fig. 3. For element 1, the strain energy of the elastic support is

$$U_e^{(1)} = \frac{1}{2} k_1 v_1^2 + \frac{1}{2} k_2 \theta_{z_1}^2 \tag{A.27}$$

But

$$\begin{aligned} v_1 &= [1 \quad 0 \quad 0 \quad 0]\{v\}_e \\ \theta_{z_1} &= [0 \quad 1 \quad 0 \quad 0]\{v\}_e \end{aligned} \tag{A.28}$$

Therefore

$$v_1^2 = \{v\}_e^T \begin{bmatrix} 1 \\ 0 \\ 0 \\ 0 \end{bmatrix} [1 \; 0 \; 0 \; 0]\{v\}_e = \{v\}_e^T \begin{bmatrix} 1 & 0 & 0 & 0 \\ 0 & 0 & 0 & 0 \\ 0 & 0 & 0 & 0 \\ 0 & 0 & 0 & 0 \end{bmatrix} \{v\}_e \tag{A.29}$$

$$\theta_{z_1}^2 = \{v\}_e^T \begin{bmatrix} 0 \\ 1 \\ 0 \\ 0 \end{bmatrix} [0 \; 1 \; 0 \; 0]\{v\}_e = \{v\}_e^T \begin{bmatrix} 0 & 0 & 0 & 0 \\ 0 & 1 & 0 & 0 \\ 0 & 0 & 0 & 0 \\ 0 & 0 & 0 & 0 \end{bmatrix} \{v\}_e \tag{A.30}$$

Therefore the stiffness matrix of elastic support at end 1 is

$$[k]_e^{(1)} = \begin{bmatrix} k_1 & 0 & 0 & 0 \\ 0 & k_2 & 0 & 0 \\ 0 & 0 & 0 & 0 \\ 0 & 0 & 0 & 0 \end{bmatrix} \tag{A.31}$$

Similarly the stiffness matrix of elastic support at end 2 is

$$[k]_e^{(N+1)} = \begin{bmatrix} 0 & 0 & 0 & 0 \\ 0 & 0 & 0 & 0 \\ 0 & 0 & k_3 & 0 \\ 0 & 0 & 0 & k_4 \end{bmatrix} \tag{A.32}$$

Note that there are no support contribution at the elements 2 through N-1. Therefore the stiffness matrix at element 1 is

$$[k]_e^1 = [k]_e + [k]_e^{(1)} \tag{A.33}$$

and that at element N is

$$[k]_e^N = [k]_e + [k]_e^{(N+1)} \tag{A.34}$$

And for element 2 through N-1,

$$[k]_e^i = [k]_e, \qquad i = 2, 3, \cdots, N-1 \tag{A.35}$$

Following the general procedure of assembling the elemental mass and stiffness matrices into global mass and stiffness matrices, we can obtain $[M]$ and $[K]$. The eigenvalue problem is

$$[K - \omega^2 M]\{\Phi\} = 0 \tag{A.36}$$

where ω is the natural frequency of the beam. The nondimensional natural frequencies can be obtained by

$$\lambda_i = \omega_i L^2 \sqrt{\frac{\rho A}{EI}} \tag{A.37}$$

In the present study, subspace iteration method is applied to solve eigenvalue problem.

For the case of two element approximation, the mass matrix reads

$$[m]_e = \frac{\rho A a}{105}\begin{bmatrix} 78 & 22a & 27 & -13a & 0 & 0 \\ 22a & 8a^2 & 13a & -6a^2 & 0 & 0 \\ 27 & 13a & 156 & 0 & 27 & -13a \\ -13a & -6a^2 & 0 & 16a^2 & 13a & -6a^2 \\ 0 & 0 & 27 & 13a & 78 & -22a \\ 0 & 0 & -13a & -6a^2 & -22a & 8a^2 \end{bmatrix} \tag{A.38}$$

The element stiffness matrix is

$$[k]_e = \frac{EI}{2a^3}\begin{bmatrix} 3+k_1' & 3a & -3 & 3a & 0 & 0 \\ 3a & (4+k_2')a^2 & -3a & 2a^2 & 0 & 0 \\ -3 & -3a & 6 & 0 & -3 & 3a \\ 3a & 2a^2 & 0 & 8a^2 & -3a & 2a^2 \\ 0 & 0 & -3 & -3a & 3+k_3' & -3a \\ 0 & 0 & 3a & 2a^2 & -3a & (4+k_4')a^2 \end{bmatrix} \tag{A.39}$$

where k_1', k_2', k_3', k_4' are as follows

$$k_1' = k_1\frac{2a^3}{EI}, \quad k_2' = k_2\frac{2a}{EI}$$
$$k_3' = k_3\frac{2a^3}{EI}, \quad k_4' = k_4\frac{2a}{EI} \tag{A.40}$$

APPENDIX B. WEIGHTED RESIDUALS METHOD

The governing differential equation of a beam reads

$$\frac{\partial^2}{\partial x^2}\left(EI(x)\frac{\partial^2 w}{\partial x^2}\right)+\rho A(x)\frac{\partial^2 w}{\partial t^2}=0 \tag{B.1}$$

where E is Young's modulus, $I(x)$ is the moment of inertia, ρ is the material density, $A(x)$ is the cross-sectional area, $w(x,t)$ is the transverse displacement, x is the axial coordinate and t is time. The boundary conditions are

$$\begin{aligned}
&K_1 w+\gamma_1\frac{\partial}{\partial x}\left(EI(x)\frac{\partial^2 w}{\partial x^2}\right)=0 \qquad at \quad x=0\\
&K_2\frac{\partial w}{\partial x}-\gamma_2 EI(x)\frac{\partial^2 w}{\partial x^2}=0 \qquad at \quad x=0\\
&K_3 w-\gamma_3\frac{\partial}{\partial x}\left(EI(x)\frac{\partial^2 w}{\partial x^2}\right)=0 \qquad at \quad x=l\\
&K_4\frac{\partial w}{\partial x}+\gamma_4 EI(x)\frac{\partial^2 w}{\partial x^2}=0 \qquad at \quad x=l
\end{aligned} \tag{B.2}$$

Here, K_1 and K_3 are the stiffnesses of the translational springs, and K_2 and K_4 are the stiffnesses of the rotational springs. In addition, artificial parameters, γ_1, γ_2, γ_3, γ_4, taking value zero or unity, are introduced to model all possible idealized boundary conditions.

For a nonuniform beam with linearly changing cross-sectional area and inertia of moments, we have

$$\begin{aligned}
A(x) &= A_1\left[1+(\alpha-1)\frac{x}{L}\right]\\
I(x) &= I_1\left[1+(\alpha-1)\frac{x}{L}\right]
\end{aligned} \tag{B.3}$$

where

$$\alpha = \frac{A_2}{A_1} = \frac{I_2}{I_1} \tag{B.4}$$

Note that α=1 corresponds to the case of a uniform beam.

We introduce the nondimensional space coordinate ξ and time coordinate τ:

$$\xi = \frac{x}{L}, \quad \tau = at, \quad a = \frac{1}{L^2}\sqrt{\frac{EI_1}{\rho A_1}} \tag{B.5}$$

Therefore the differential equation (B.1) becomes

$$\frac{\partial^2}{\partial \xi^2}\{[1+(\alpha-1)\xi]\frac{\partial^2 w}{\partial \xi^2}\} + [1+(a-1)\xi]\frac{\partial^2 w}{\partial \tau^2} = 0 \tag{B.6}$$

Then the boundary conditions can be rewritten as

$$\begin{aligned}
&k_1 w + \gamma_1 \frac{\partial}{\partial \xi}\{[1+(\alpha-1)\xi]\frac{\partial^2 w}{\partial \xi^2}\} = 0 \qquad at \quad \xi = 0 \\
&k_2 \frac{\partial w}{\partial \xi} - \gamma_2 [1+(\alpha-1)\xi]\frac{\partial^2 w}{\partial \xi^2} = 0 \qquad at \quad \xi = 0 \\
&k_3 w - \gamma_3 \frac{\partial}{\partial \xi}\{[1+(\alpha-1)\xi]\frac{\partial^2 w}{\partial \xi^2}\} = 0 \qquad at \quad \xi = 1 \\
&k_4 \frac{\partial w}{\partial \xi} + \gamma_4 [1+(\alpha-1)\xi]\frac{\partial^2 w}{\partial \xi^2} = 0 \qquad at \quad \xi = 1
\end{aligned} \tag{B.7}$$

where the nondimensional stiffnesses are

$$k_1 = \frac{K_1 L^3}{EI_1}, \quad k_2 = \frac{K_2 L}{EI_1}, \quad k_3 = \frac{K_3 L^3}{EI_1}, \quad k_4 = \frac{K_4 L}{EI_1} \tag{B.8}$$

To obtain some insight into the problem, a single-term weighted residuals approximation associated with the computerized symbolic algebra is used in this study. We first construct a mode-shape function which satisfies both geometric and dynamic boundary conditions in the form

$$\Psi(\xi) = c_0 + c_1\xi + c_2\xi^2 + c_3\xi^3 + \xi^4 \tag{B.9}$$

Coefficients c_i's in the mode shape function, obtained through the use of the computerized symbolic algebraic code MATHEMATICA, are given as follows

$$c_0 = \frac{A_0}{A} \qquad c_1 = \frac{A_1}{A}$$
$$c_2 = \frac{A_2}{A} \qquad c_3 = \frac{A_3}{A} \tag{B.10}$$

where

$$\begin{aligned}
A_0 &= -(-24\gamma_1\gamma_3k_2 + 48\alpha\gamma_1\gamma_3k_2 - 24\alpha^2\gamma_1\gamma_3k_2 - 12\gamma_1\gamma_2k_3 - 8\gamma_1k_2k_3 + 2\alpha\gamma_1k_2k_3)(12\alpha\gamma_4 + 4k_4) \\
&\quad -(24\alpha\gamma_1\gamma_4k_2 - 12\alpha^2\gamma_1\gamma_4k_2 + 12\gamma_1\gamma_2k_4 + 18\gamma_1k_2k_4 - 6\alpha\gamma_1k_2k_4)(12\gamma_3 - 36\alpha\gamma_3 + k_3) \\
A_1 &= -(-12\gamma_2\gamma_3k_1 + 24\alpha\gamma_2\gamma_3k_1 + 12\gamma_1\gamma_2k_3 - 2\gamma_2k_1k_3)(12\alpha\gamma_4 + 4k_4) \\
&\quad -(12\gamma_3 - 36\alpha\gamma_3 + k_3)(12\alpha\gamma_2\gamma_4k_1 + 6\gamma_2k_1k_4) \\
A_2 &= -(-6\gamma_3k_1k_2 + 12\alpha\gamma_3k_1k_2 + 6\gamma_1k_2k_3 - k_1k_2k_3)(12\alpha\gamma_4 + 4k_4) - (12\gamma_3 - 36\alpha\gamma_3 + k_3)(6\alpha\gamma_4k_1k_2 + 3k_1k_2k_4) \\
A_3 &= -(2\gamma_3k_1k_2 - 2\alpha\gamma_3k_1k_2 + 2\gamma_2k_1k_3 + 2\gamma_1k_2k_3 - 2\alpha\gamma_1k_2k_3 + k_1k_2k_3)(12\alpha\gamma_4 + 4k_4) \\
&\quad -(12\gamma_3 - 36\alpha\gamma_3 + k_3)(-2\alpha\gamma_4k_1k_2 - 2\gamma_2k_1k_4 - 2k_1k_2k_4) \\
A &= 12\alpha^2\gamma_3\gamma_4k_1k_2 + 12\alpha\gamma_2\gamma_4k_1k_3 + 24\alpha\gamma_1\gamma_4k_2k_3 - 12a^2\gamma_1\gamma_4k_2k_3 + 4\alpha\gamma_4k_1k_2k_3 - 12\gamma_2\gamma_3k_1k_4 + 24\alpha\gamma_2\gamma_3k_1k_4 \\
&\quad -6\gamma_3k_1k_2k_4 + 18\alpha\gamma_3k_1k_2k_4 + 12\gamma_1\gamma_2k_3k_4 + 4\gamma_2k_1k_3k_4 + 18\gamma_1k_2k_3k_4 - 6\alpha\gamma_1k_2k_3k_4 + k_1k_2k_3k_4
\end{aligned} \tag{B.11}$$

For the case of uniform beam the coefficients A_j read

$$A_0 = 12\gamma_1\{[(5k_3 + 24\gamma_3)\gamma_4 + (k_3 + 24\gamma_3)k_4]k_2 + 3\gamma_2[(k_3 + 8\gamma_3)k_4 + 4\gamma_4 k_3]\}$$

$$A_1 = 2\gamma_2\{[(k_3 + 48\gamma_3)k_4 + 6(k_3 + 12\gamma_3)\gamma_4]k_1 - 24(k_4 + 3\gamma_4)\gamma_1 k_3\}$$

$$A_2 = \frac{k_2}{2}A_1 \tag{B.12}$$

$$A_3 = -2\{[(5k_3 + 24\gamma_3)\gamma_4 + (k_3 + 24\gamma_3)k_4]k_1k_2 + 3[(k_3 + 8\gamma_3)k_4 + 4\gamma_4 k_3]\gamma_2 k_1\}$$

$$A = \{[(k_3 + 12\gamma_3)k_4 + 4(k_3 + 3\gamma_3)\gamma_4]k_1 + 12(k_4 + \gamma_4)\gamma_1 k_3\}k_2$$
$$+ 4\{[(k_3 + 3\gamma_3)k_4 + 3\gamma_4 k_3]k_1 + 3\gamma_1 k_3 k_4\}\gamma_2$$

We seek a solution of Eq. (B.6) in the form

$$w(\xi, \tau) = W(\tau)\Psi(\xi) \tag{B.13}$$

Substituting Eq. (B.13) into Eq. (B.6), multiplying by $\Psi(\xi)$ and integrating over range $0 \le \xi \le 1$ yields

$$\left(\frac{d^4\Psi}{d\xi^4}, \Psi\right) W(\tau) + (\Psi, \Psi)\frac{d^2W}{d\tau^2} = (Q, \Psi) \tag{B.14}$$

where the inner product is denoted as

$$(\Psi_1, \Psi_2) \equiv \int_0^1 \Psi_1(\xi)\Psi_2(\xi)\,d\xi \tag{B.15}$$

Thus the fundamental natural frequency of the beam can be obtained as

$$\omega_n^2 = \left(\frac{d^4\Psi}{d\xi^4}, \Psi\right) / (\Psi, \Psi) = \frac{N}{D} \tag{B.16}$$

where

$$
\begin{aligned}
N = 504(&-36 + 60\alpha - 60c_0 + 180\alpha c_0 - 60c_1 + 120\alpha c_1 \\
&- 50c_2 + 90\alpha c_2 - 54c_3 + 84\alpha c_3 - 60c_0c_3 + 60\alpha c_0c_3 \\
&- 30c_1c_3 + 30\alpha c_1c_3 - 20c_2c_3 + 20\alpha c_2c_3 - 15c_3^2 + 15\alpha c_3^2)
\end{aligned}
$$

$$
\begin{aligned}
D = 28 &+ 252\alpha + 168c_0 + 840\alpha c_0 + 1260c_0^2 + 1260\alpha c_0^2 \\
&+ 120c_1 + 720\alpha c_1 + 840c_0c_1 + 1680\alpha c_0c_1 + 210c_1^2 + 630\alpha c_1^2 \\
&+ 90c_2 + 630\alpha c_2 + 420c_0c_2 + 1260\alpha c_0c_2 + 252c_1c_2 + 1008\alpha c_1c_2 \\
&+ 84c_2^2 + 420\alpha c_2^2 + 70c_3 + 560\alpha c_3 + 252c_0c_3 + 1008\alpha c_0c_3 \\
&+ 168c_1c_3 + 840\alpha c_1c_3 + 120c_2c_3 + 720\alpha c_2c_3 + 45c_3^2 + 315\alpha c_3^2
\end{aligned}
\qquad \text{(B.17)}
$$

For the uniform beam discussed in section 5.1, which is clamped at one end and elastically supported at the other, the corresponding control parameters are γ_1=0, γ_2=0, k_1=1, k_2=1, γ_3=1, γ_4=1. If we substitute the middle point value of the identified boundary stiffness interval, i.e. k_3=1221.65 and k_4=4.971, into Eq. (B.11), the coefficients c_i can be determined through Eq. (B.10) . Therefore, through Eq. (B.16), the nondimensional frequency by weighted residue method is obtained as λ_1=18.0637, which is associated with an error of 0.3539%. For the C-ES nonuniform beam, consider a special case α=0.5. For k_3=640.5 and k_4=2.415, Eq. (B.11) results in a set of coefficients c_i . Finally the weighted residues results in the following nondimensional frequency: λ_1=18.2561, which differs by 1.4228% from λ_1=18.

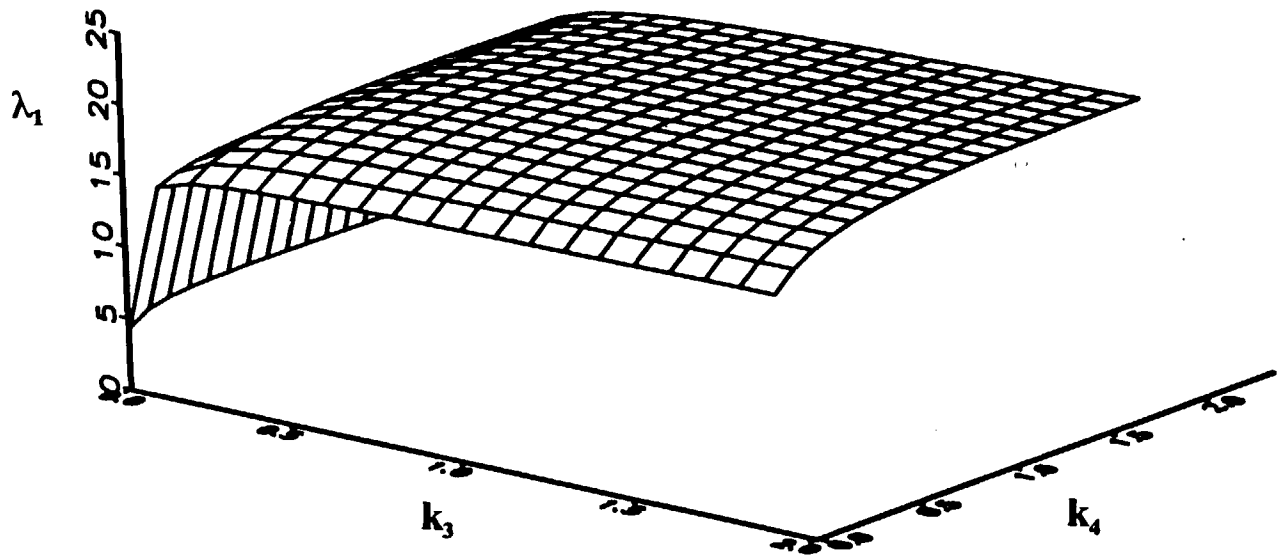

Fig. 1 The first nondimensional frequency λ_1 of the C-ES beam vs. the translational and rotational stiffnesses k_3 and k_4 at the elastically supported end

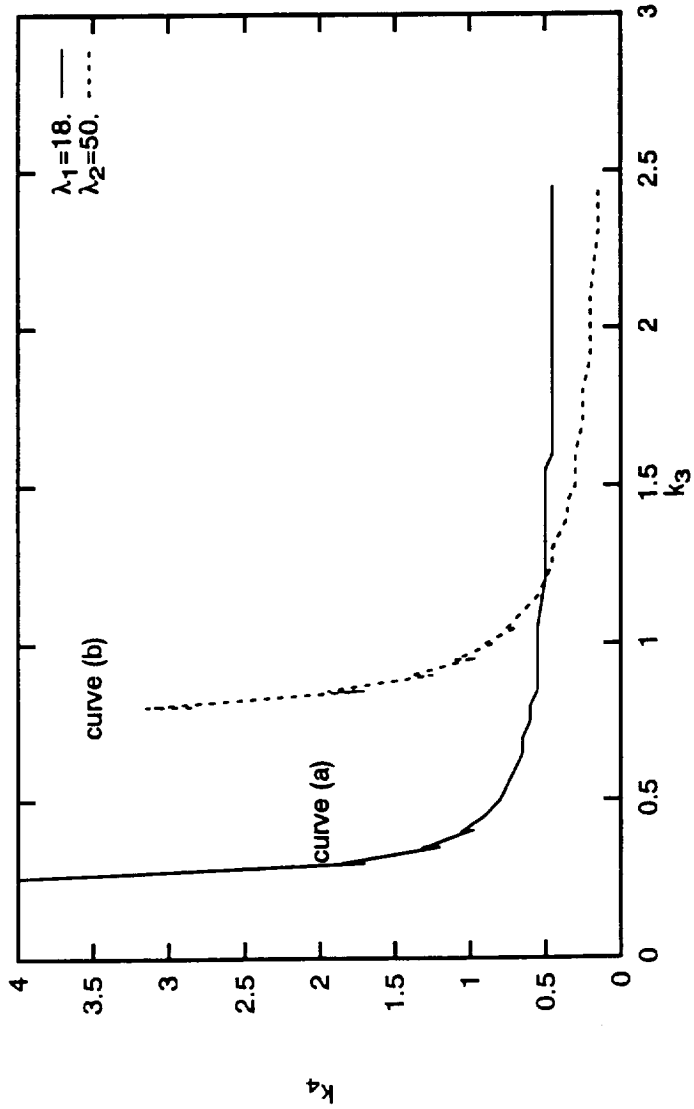

Fig. 2 The curves of k_3 and k_4 corresponding to λ_1=18. and λ_2=50.

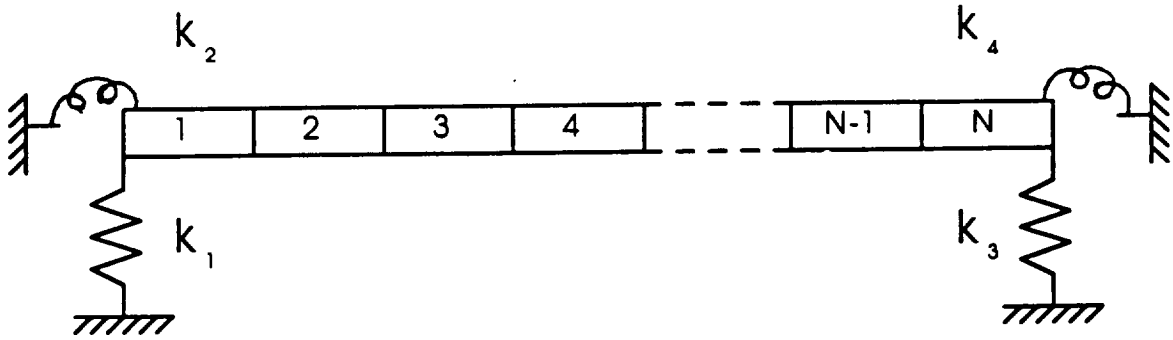

Fig. 3 The N-element beam which is elastically supported at both ends

CHAPTER # 3

Free and Forced Vibrations of

Periodic Multi-Span Beams

Free and Forced Vibrations of Periodic Multi-Span Beams

Liping Zhu, Isaac Elishakoff and Y. K. Lin

College of Engineering
Florida Atlantic University
Boca Raton, FL 33431-0991

Abstract

In this study, the following two topics are considered for multi-span beams of both finite and infinite lengths with rigid transversal constraint and elastic rotational constraint at each support: (a) free vibration and the associated frequencies and mode shapes; (b) forced vibration under a convected harmonic loading. The concept of wave propagation in periodic structures of Brillouin is utilized to investigate the wave motion at periodic supports of a multi-span beam. A dispersion equation and its asymptotic form is obtained to determine the natural frequencies. For the special case of zero rotational spring stiffness, an explicit asymptotic expression for the natural frequency is also given. New expressions for the mode shapes are obtained in the complex form for multi-span beams of both finite and infinite lengths. The orthoganolity conditions of the mode shapes for the two cases are formulated. The exact responses of both finite and infinite span beams under a convected harmonic loading are obtained. Thus, the position and the value of each peak in the harmonic response function can be determined precisely, as well as the occurrence of the so-called coincidence phenomenon, when the response is greatly enhanced.

Introduction

The model of a periodic multi-span beam with elastic supports is often utilized in engineering. For example, such a model is a reasonable approximation for a plate-like structure with parallel, regularly spaced stiffeners. The elastic supports may provide both the rotational and transversal restraints to the beam. Krein (1933) and Miles (1956) studied independently an N-span beam by using a finite difference approach, and established that the natural frequencies

fell into distinct bands with the same number of natural frequencies in each band as the number of spans. Lin (1962) generalized the finite difference approach to a multi-span beams with elastic supports. Abramovich and Elishakoff (1987) generalized Krein's and Miles's analyses to multi-span Timoshenko beams, taking into account shear deformation and rotary inertia. It was shown that the use of a finite difference approach might lead to computational difficulties and to inaccuracy in the determination of mode shapes of the system.

Lin and McDaniel (1969) also used a transfer matrix formulation which is more convenient for the imposition of constraints at the supports. However, numerical difficulty may still arise when the number of periodic units in a structure is large . To overcome this difficulty, Yong and Lin (1989), and Cai and Lin (1991) transformed the state vector of displacements and forces into a vector of incoming and outgoing waves, and correspondingly transformed the transfer matrix into the wave-scattering matrix. By so doing, the computational efficiency and accuracy are greatly improved, especially when obtaining the dynamic response due to point excitation, because the calculation can be channeled in the direction of wave propagation.

Mead (1970) made use of the concept of wave propagation in periodic structures originally due to Brillouin (1953) to analyze the free vibration of a multi-span beam of infinite length. Sen Gupta (1970) extended the analysis to finite multi-span beams and plates on rigid supports. In these studies, the wave propagation band and non-propagation band were studied in much detail. Sen Gupta (1970) also proposed a graphic method to determine the natural frequencies of the multi-span beams with rigid supports. In the framework of wave propagation, *non-harmonic* waves have to be decomposed into an infinite number of *harmonic* components in order to carry out the analysis of the forced vibration. This approach was used by Mead (1971) and Lin (1977) to obtain the response of an infinitely long multi-span beam to harmonic

excitation, as well as random boundary-layer pressure fields. In the actual calculation the infinite sum has to be truncated, and a large system of linear equations have to be solved to determine the unknown coefficients.

It should be noted that in the forced vibration analysis of a periodic multi-span beam of finite length, multiple peaks occur in each wave propagation band. The number of peaks in each band is equal to the number of the spans. The computational effort becomes excessive when the number of span is large. Furthermore, an accurate position of each peak and its value are difficult to obtain.

In order to circumvent the above difficulty, new expressions are proposed for the mode shapes of a periodic multi-span beam, based on the wave propagation concept, which can then be used in the forced vibration analysis. Since the transverse displacements within each span of the beam is related uniquely to the displacements at the two ends of the span, we may focus our attention only on the waves which propagate through each periodic support. Once these waves are determined, the motion of the beam between two neighboring supports can be computed if so desired. The dispersion equation which establishes the relationship between wave constant and frequency parameter is derived accordingly. The frequency parameters, wave constants and associated mode shapes for beams of both finite and infinite length can then be determined. The exact response of a multi-span beam to a convected loading is obtained for both the cases of finite total length and infinite total length. Furthermore, the locations of response peaks and their values can be precisely calculated, and the condition for the so-called *coincident phenomenon* can be predicted in exact terms.

Free Vibration Analysis

Basic equations

Consider an N-span beam with uniformly spaced supports. It is convenient to write the equation of motion in terms of the local nondimensional coordinate ξ as follows:

$$EI\, w_\beta^{(4)}(\xi,t) + \rho A L^4 \ddot{w}_\beta(\xi,t) = 0 , \quad (\beta = 1,2,...,N) \tag{1}$$

where $w_\beta(\xi,t)$ is the transverse displacement in the β-th span, and the local coordinate ξ is defined as

$$\xi = x/L - (\beta - 1) , \quad (\beta - 1)L \le x \le \beta L , \quad 0 \le \xi \le 1 \tag{2}$$

in which x is global coordinate and L is the individual span length. Assuming that the motion is harmonic

$$w_\beta(\xi,t) = W_\beta(\xi)\, e^{i\omega t} , \quad (\beta = 1,2,...,N) \tag{3}$$

where $W_\beta(\xi)$ is the mode shape function associated with the β-th span, Eq.(1) can be reduced to

$$W_\beta^{(4)}(\xi) - \lambda^4 W_\beta(\xi) = 0 \tag{4}$$

where

$$\lambda = \left(\frac{\rho A \omega^2 L^4}{EI} \right)^{1/4} \tag{5}$$

is a nondimensional frequency parameter, and ω is the sought angular frequency.

It is assumed that each interior support provides a rigid constraint against transverse motion, as well as an elastic constraint against rotation, with a spring constant k (see Fig. 1). Thus the continuity conditions at each interior support are as follows:

$$W_\beta(1) = W_{\beta+1}(0) = 0$$

$$W'_\beta(1) = W'_{\beta+1}(0) \qquad (6)$$

$$\nu W'_\beta(1) = W''_{\beta+1}(0) - W''_\beta(1) , \qquad (\beta = 1,2,...,N-1)$$

where $\nu=kL/EI$. The first two conditions in Eq.(6) represent, respectively, the continuity of vertical and angular displacements. The last condition in Eq.(6) is the requirement of moment equilibrium at each interior support. The conditions at the two end-supports for a multi-span beam of finite length will be specified later.

The mode shape that satisfies the first condition in Eq.(6) can be written as

$$W_\beta(\xi) = A_\beta f(\xi,\lambda) + B_\beta f(1-\xi,\lambda) , \quad (\beta = 1,2,...,N) \qquad (7)$$

where A_β and B_β are unknowns. Only the ratio A_β/B_β is of interest in the free vibration case. The function $f(\xi,\lambda)$ is defined as

$$f(\xi,\lambda) = \sin(\lambda\xi) - \frac{\sin(\lambda)}{\sinh(\lambda)} \sinh(\lambda\xi) . \qquad (8)$$

Harmonic waves and the associated wave constants

A simple wave of spatial sinusoidal variation cannot propagate along a multi-span beam, due to reflection at each support, giving rise to hyperbolic terms in the expression for the displacement. However, the concept of wave propagation can still be applied in the case of periodically supported beam, by focusing our attention on the waves which propagate through each support. The motion of a beam segment between two consecutive supports can then be determined from those of the two supports, if so desired. Since all the supports are assumed to

be transversely rigid, only the angular displacement at each support needs to be considered. Let $\theta_\beta(t)$ be the angular displacement at the β-th support, and let it be represented in the form of a harmonic wave propagating through the β-th support, i.e

$$\begin{aligned} \theta_\beta(t) &= C_\mu e^{i(\omega t - \mu\beta)} = \Theta_\beta e^{i\omega t} \\ \Theta_\beta &= C_\mu e^{-i\mu\beta} , \qquad (\beta = 0,1,...,N) \end{aligned} \tag{9}$$

where the nondimensional parameter μ is known as *wave constant*, and C_μ is the amplitude of the propagating wave associated with the wave constant μ. A positive μ corresponds to a wave propagating in the positive x-direction, whereas a negative μ corresponds to one propagating in the negative x-direction. The angular displacement function Θ_β is related to the mode shape function $W_\beta(\xi)$ as follows

$$\begin{aligned} W'_\beta(\xi)\,|_{\xi=0} &= \Theta_{\beta-1} L \\ W'_\beta(\xi)\,|_{\xi=1} &= \Theta_\beta L , \qquad (\beta = 1,2,...,N) \end{aligned} \tag{10}$$

obtained from the second condition in Eq.(6).

The ratio A_β/B_β in Eq.(7) will be determined for two special cases: The first case is associated with those mode shapes which are either symmetric or anti-symmetric with respect to the mid-point of each span. In such a case, the angular displacements at the two ends of a span are related as

$$\Theta_{\beta-1} = (-1)^s \Theta_\beta , \qquad s = \text{integer of } \left[\frac{\lambda}{\pi}\right] \tag{11}$$

where s=odd and s=even correspond to the symmetric and anti-symmetric mode shapes, respectively. In view of Eq.(9), the value of the wave constant for this case must be $\mu=m\pi$, implying a *non-propagating wave* or *standing wave*. The ratio A_β/B_β is obtained by substituting

Eqs.(7) and (11) into Eq.(10) to yield

$$\frac{A_\beta}{B_\beta} = (-1)^{s+1} \ . \tag{12}$$

The second case is associated with those mode shapes which are neither symmetric nor anti-symmetric with respect to the mid-point of each span. Therefore, the wave constant μ is not an integer multiple of π, i.e. $\mu \neq m\pi$. This implies that there is indeed wave propagation through each periodic support of multi-span beam. By applying Eqs.(7), (9) and (10), we find that A_β and B_β are given by

$$\begin{aligned} A_\beta &= \frac{L}{\Delta}[-f'(0,\lambda)\Theta_{\beta-1} + f'(1,\lambda)\Theta_\beta] \\ B_\beta &= \frac{L}{\Delta}[-f'(1,\lambda)\Theta_{\beta-1} + f'(0,\lambda)\Theta_\beta] \\ \Delta &= [f'(1,\lambda)]^2 - [f'(0,\lambda)]^2 \neq 0 \ . \end{aligned} \tag{13}$$

We note in passing that the first case corresponds precisely to $\Delta = 0$, associated with the same mode shape $W_\beta(\xi)$ as that of a single-span beam with either two simply supported or two fully clamped ends. Return now to the second case, and substitute Eq.(9) into Eq.(13) to obtain

$$\frac{A_\beta}{B_\beta} = -\frac{\eta}{\eta^* e^{-i\mu}} \ , \tag{14}$$

where

$$\eta = f'(1,\lambda)\, e^{-i\mu} - f'(0,\lambda) \ . \tag{15}$$

It is noted that the ratio A_β/B_β is independent of the span number β for both cases. This implies that one can choose a mode shape from any span as a reference, then the mode shape for the next span can be obtained by a phase shift. Thus, a general expression for the mode shape of a multi-

span beams may be written as follows

$$W_\beta(\xi,\mu,\lambda) = W_1(\xi,\mu,\lambda)\, e^{-i\mu(\beta-1)}$$
$$= [\, a f(\xi,\lambda) + b f(1-\xi,\lambda)\,]\, e^{-i\mu(\beta-1)}\,, \quad (\beta = 1,2,\ldots,N) \tag{16}$$

which is dependent on the span number β, the local coordinate ξ, the wave constant μ and frequency parameter λ. Here, a and b are obtained from Eqs.(12) and (14)

$$a = \begin{cases} \eta\,, & \mu \neq m\pi \\ 1\,, & \mu = m\pi \end{cases}; \qquad b = \begin{cases} -e^{-i\mu}\eta^*\,, & \mu \neq m\pi \\ (-1)^{s+1}\,, & \mu = m\pi \end{cases} \tag{17}$$

Coefficients a and b are generally complex, while function $f(\cdot)$ is real. Moreover, the span number β in Eq.(16) appears only in the exponential function. It will be shown later that this characteristic of mode shape is very useful, and it will be applied in the analysis of forced vibrations.

Substituting Eq.(16) into the last condition in Eq.(6), the bending moment equilibrium, we obtain a dispersion relationship between μ and λ as follows:

$$\cos(\mu) = F(\lambda)\,, \tag{18}$$

where

$$F(\lambda) = \frac{f'(1,\lambda)}{f'(0,\lambda)} + \nu \frac{f'^2(1,\lambda) - f'^2(0,\lambda)}{2f''(1,\lambda)f'(0,\lambda)}\,. \tag{19}$$

Eq.(18) shows that the values of μ and λ must satisfy a certain relationship for the wave propagation.

To examine the physical meaning of the dispersion equation, function $F(\lambda)$ is plotted in Figs. 2(a) and 2(b). It is seen that $F(\lambda)$ has an oscillatory character; thus, each μ value

corresponds to multiple values of λ. For the $F(\lambda)$ values between +1 and -1, the corresponding wave constants μ are real. This implies that there exists a non-zero phase difference between the motion in adjacent spans, and that the wave is propagating and the wave energy is being transferred from span to span without decay. The associated frequencies are grouped in distinctive bands, called the *propagation bands*. On the other hand, if the absolute values of $F(\lambda)$ are greater than 1, then μ is purely imaginary, indicating an exponential decay of wave motion from span to span. The corresponding frequencies are also grouped in distinctive bands, called the *non-propagation bands*.

As shown in Figs. 2(a) and 2(b), the wave constant μ corresponding to the bounding frequencies of a propagation band must be an integer multiples of π. At such a frequency , the motion of a multi-span beam reduces to a standing wave the same as that of a single-span beam with symmetric boundary conditions at the ends. The lower bounding frequency of the *s*-th propagation band is the same as the *s*-th natural frequency of a single-span beam with elastic rotational springs at the ends, whereas the upper bounding frequency coincides with the *s*-th natural frequency of a single span with fully clamped ends.

It should be noted that if μ is replaced by

$$\mu_m = \mu + 2\pi m , \qquad (m = \pm 1, \pm 2, \ldots) \tag{20}$$

the dispersion equation, Eq.(18), remains unchanged. Thus the state of vibration of the system corresponding to a wave constant μ will be identical to the state corresponding to the other wave constant, namely $\mu+2\pi m$. Therefore, if we want to have the one-to-one correspondence between the state of vibration of a system and the wave constant μ, the latter must be confined to a range of values of width 2π. The range of μ values satisfying

$$(m-1)\pi < \mu \le m\pi$$
$$-m\pi < \mu \le -(m-1)\pi\ , \quad (\ m\ =\ 1,2,3,\ldots\ ) \tag{21}$$

is known as the m-th Brillouin (1953) zone. For free vibration analysis, we may restrict to the first Brillouin zone (m=1) without loss of generality, i.e.

$$0 < \mu \le \pi\ ,$$
$$-\pi < \mu \le 0\ . \tag{22}$$

We reiterate that a positive μ corresponds to wave propagation in the positive x-direction and a negative μ corresponds to one in the negative x-direction.

Asymptotic dispersion relations and natural frequencies

As seen in Eq.(18), the frequency parameter λ is a multi-valued function of μ. Let $\lambda_s(\mu)$ denote the λ value in the s-th propagation band. For a large value of $\lambda_s(\mu)$, the following asymptotic approximation is sufficiently accurate

$$F(\lambda) \approx (\ 1\ +\ \frac{\nu}{2\lambda}\ )\cos(\lambda)\ -\ \sin(\lambda)\ , \quad \text{for}\ \ \lambda \ge \pi\ , \tag{23}$$

which is obtained from Eq.(19) by letting $\tanh(x)\approx 1$ and $\sinh^{-1}(x)\approx\cosh^{-1}(x)\approx 0$. This approximation is compatible with the dynamic edge effect method due to Bolotin(1961) and Elishakoff (1976), and is remarkably accurate as shown in Figs. 2(a) and 2(b). Moreover, as the rotational spring stiffness ν increases, the position of the lower bounding frequency of each propagation band moves toward the upper bounding frequency which is fixed. This implies that the multi-span beam structure becomes more rigid with larger ν, as expected. In the case of ν=0, the explicit asymptotic expression for the natural frequencies are obtained by combining Eq.(18)

and Eq.(23)

$$\lambda_s(\mu) = (s - \frac{1}{4})\pi + \cos^{-1}\left[(-1)^s \frac{\cos(\mu)}{\sqrt{2}}\right], \quad (s = 1,2,...,\infty) \tag{24}$$

where s denotes the serial number of the propagation band. Thus, the natural frequencies of a multi-span beam can be determined readily from a given wave constant μ which depends on the exterior boundary conditions of the entire system.

The mode shapes of a multi-span beam

It should be recalled that only the boundary conditions at the interior supports were used in obtaining an expression for $W_\beta(\xi,\mu,\lambda)$. This implies that the mode shape given in Eq.(16) is valid only for a multi-span beam of infinite total length. For a finitely long multi-span beam, wave reflections occur at two exterior boundaries. Therefore, wave propagating in both positive and negative directions should be included in the analysis. The total angular displacement at the β-th support is now given by

$$\begin{aligned} \bar{\Theta}_\beta(\mu) &= \Theta_\beta(\mu) + \Theta_\beta(-\mu) \\ &= C_\mu e^{-i\mu\beta} + C_{-\mu} e^{i\mu\beta}, \quad (\beta = 1,2,...,N) \end{aligned} \tag{25}$$

where the positive and negative subscripts denote the two directions of wave propagation. Hence, the associated mode shape for a finite multi-span beam becomes

$$\bar{W}_\beta(\xi,\mu,\lambda) = C'_\mu W_\beta(\xi,\mu,\lambda) + C'_{-\mu} W_\beta(\xi,-\mu,\lambda) \tag{26}$$

where the μ value will be chosen in the first Brillouin zone as defined by Eq.(22), and chosen to be positive without loss of generality.

For an infinitely long multi-span beam, the wave constant μ varies continuously over the

entire zone defined by Eq.(22). The associated frequency parameter λ also varies continuously over the entire propagation band. For a finitely long multi-span beam, however, the wave constant μ and the associated frequency parameter λ take on discrete values. The number of the discrete values for μ or λ in each propagation band is the same as the number of spans. These discrete wave constants are determined by imposing the boundary conditions at the exterior ends of the entire beam. Referring to Fig. 1, the boundary conditions at the exterior ends of the beam are

$$\begin{aligned} \nu_0 \bar{W}_1'(0,\mu,\lambda) &= \bar{W}_1''(0,\mu,\lambda) , \\ \nu_N \bar{W}_N'(1,\mu,\lambda) &= -\bar{W}_N''(1,\mu,\lambda) , \end{aligned} \qquad \nu_0 = \frac{k_0 L}{EI} , \quad \nu_N = \frac{k_N L}{EI} \tag{27}$$

where ν_0 and ν_N are the non-dimensionalized rotational spring constants at the left and right ends of the N multi-span beam, respectively. A vanishing ν corresponds to a simple support, and an infinite ν to a clamped support.

The mode shape of a finitely long multi-span beam can be rewritten in abbreviation as follows

$$\bar{W}_{\beta,j}(\xi) = \bar{W}_\beta(\xi,\mu_j,\lambda_j) = \bar{a}_{\beta,j} f_j(\xi) + \bar{b}_{\beta,j} f_j(1-\xi) , \tag{28}$$

where

$$\begin{aligned} \bar{a}_{\beta,j} &= \Lambda_j [a_j e^{-i\mu_j(\beta-1)} + \Gamma_j a_j^* e^{i\mu_j(\beta-1)}] , \\ \bar{b}_{\beta,j} &= \Lambda_j [b_j e^{-i\mu_j(\beta-1)} + \Gamma_j b_j^* e^{i\mu_j(\beta-1)}] . \end{aligned} \tag{29}$$

and where the subscript β denotes the β-th span, μ_j is the wave constant corresponding to λ_j, and Λ_j and Γ_j are the unknown constants to be determined by imposing the boundary conditions at the exterior ends.

Examples

The wave constant μ , frequency parameter λ and mode shapes for an N-span beam will be evaluated in detail for the following three cases.

(*a*) **Case $\nu_0=\nu_N=\nu/2$**

In this particular case the rotational spring constants at both ends of the multi-span beam are equal to one-half of those at the interior supports. The boundary conditions at the exterior ends are

$$\begin{aligned} \frac{\nu}{2}\bar{W}_1'(0,\mu,\lambda) &= \bar{W}_1''(0,\mu,\lambda) , \\ \frac{\nu}{2}\bar{W}_N'(1,\mu,\lambda) &= -\bar{W}_N''(1,\mu,\lambda) . \end{aligned} \tag{30}$$

Using Eqs.(18), (26) and (30), we obtain, after some algebra, an equation for μ as follows:

$$\sin(\mu N) = 0 . \tag{31}$$

The possible values of μ in the first Brillouin zone are

$$\mu_j = \frac{j}{N}\pi , \quad (j = 0,1,2,...,N) . \tag{32}$$

As seen in Fig. 2, the values μ=0 and μ=π are associated with the bounding frequencies of the propagation bands. In the case of an odd-numbered propagation band, μ is equal to zero at the upper bound and to π at the lower bound. The opposite is true for an even-numbered propagation band. Moreover, the lower and upper bound frequencies are the same as a single-span beam with elastic supports of rotational spring constant of value $\nu/2$, and with fully clamped supports, respectively. To incorporate the above features, Eq.(32) for μ is modified to read where the subscripts s and r denote, respectively, the s-th propagation band and the r-th

$$\mu_{j=(s-1)N+r} = \left\{ \frac{1}{2}[1-(-1)^s] + (-1)^s \frac{r-1}{N} \right\} \pi \ , \qquad (33)$$
$$(\ s = 1,2,...,\infty \ , \quad r = 1,2,...,N \ )$$

frequency within each band. Then the frequency parameters $\lambda_{j=(s-1)N+r}$ is numbered in an increasing order of j.

The mode shape $\bar{W}_{\beta,j}(\xi)$ should be taken as the real part of $W_\beta(\xi,\mu_j,\lambda_j)$, and the coefficients Λ_j and Γ_j in Eq.(29) should assume the values of

$$\Lambda_j = \frac{1}{2} \ , \qquad \Gamma_j = 1 \ . \qquad (34)$$

(*b*) **Case $\nu_0=\nu_N=\infty$**

In this case, the boundary conditions at the extreme ends are

$$\bar{W}_1'(0,\mu,\lambda) = \bar{\Theta}_0(\mu)L = 0 \ ,$$
$$\bar{W}_N'(1,\mu,\lambda) = \bar{\Theta}_N(\mu)L = 0 \ . \qquad (35)$$

Eq.(31) remains valid; however, the serialized version now reads

$$\mu_{j=(s-1)N+r} = \left\{ \frac{1}{2}[1-(-1)^s] + (-1)^s \frac{r}{N} \right\} \pi \ , \qquad (36)$$
$$(\ s = 1,2,...,\infty \ , \quad r = 1,2,...,N \ ) \ .$$

The wave constant $\mu=0$ and $\mu=\pi$ correspond to the upper bound of an odd-numbered and an even-numbered propagation bands, respectively, contrary to case (a). In this case the mode shape takes the imaginary part of $W_\beta(\xi,\mu_j,\lambda_j)$ and the coefficients in Eq.(29) are found to be

$$\Lambda_j = \begin{cases} 1/2 , & \mu_j = k\pi \\ -i/2 , & \mu_j \neq k\pi , \end{cases}$$

$$\Gamma_j = \begin{cases} 1 , & \mu_j = k\pi \\ -1 , & \mu_j \neq k\pi . \end{cases} \tag{37}$$

(*c*) **Case $\nu_0=\nu/2$ and $\nu_N=\infty$**

In this case, the left end of the multi-span beam is constrained by a rotational spring of stiffness constant $\nu/2$, while the right end is clamped. The corresponding boundary conditions read

$$\frac{\nu}{2}\bar{W}_1'(0,\mu,\lambda) = \bar{W}_1''(0,\mu,\lambda) ,$$

$$\bar{W}_N'(1,\mu,\lambda) = \bar{\Theta}_N(\mu)L = 0 . \tag{38}$$

Analogous to cases (a) and (b), the following equation for μ is obtained

$$\cos(\mu N) = 0 , \tag{39}$$

from which

$$\mu_{j=(s-1)N+r} = \left\{\frac{1}{2}[1-(-1)^s] + (-1)^s\frac{2r-1}{2N}\right\}\pi ,$$

$$(s = 1,2,...,\infty , \quad r = 1,2,...,N) . \tag{40}$$

Note that neither zero nor π is a solution of the above equation; thus a standing wave does not exist. The mode shape for this case is described by the real part of $W_\beta(\xi,\mu_j,\lambda_j)$ with coefficients specified in Eq.(34). If the left end of the multi-span beam is treated as being clamped ($\nu_0=\infty$), and the right end is treated as being elastically constrained by a rotational spring stiffness of $\nu/2$, then the mode shape is described by the imaginary part of $W_\beta(\xi,\mu_j,\lambda_j)$ with coefficients given in

Eq.(37); while Eqs.(39) and (40) remain unchanged.

Tables I-III list the frequency parameters in the first two bands of a six-span beam evaluated by using both the exact and asymptotic formulas for the three sets of boundary conditions at the extreme ends. It can be seen that the exact and asymptotic solutions differ by less than 0.4 % in the first band, and they are almost identical in the higher bands ($s \geq 2$).

The normal modes associated with the frequency parameters in the first band are illustrated in Figs. 3(*a*), 3(*b*) and 3(*c*), respectively. The solid and dash lines correspond to the cases of $\nu=0$ and $\nu=10$, respectively. Figs. 3(*a*) and 3(*b*) portray the mode shapes for the two sets of exterior supports, namely the set of $\nu_0=\nu_N=\nu/2$ and the set of $\nu_0=\nu_N=\infty$. In these two cases the mode shapes are either symmetric or anti-symmetric with respect to the mid-point of the multi-span beam due to symmetric boundary conditions at the two extreme ends. Fig. 3(*c*) illustrates the mode shapes for the case $\nu_0=\nu/2$ and $\nu_N=\infty$, and they are neither symmetric nor anti-symmetric, as expected.

Forced Vibration Analysis

In the preceding section, the frequency parameter λ, wave constant μ and the associated mode shape have been determined for a multi-span beam of finite or infinite total length. In this section, the exact analytic harmonic response of such a beam subjected to a convected harmonic loading is obtained using the normal mode approach. Furthermore, both the location and the magnitude of the peak response can be determined in advance. Thus, the important *coincident phenomenon* can be investigated in exact terms.

Orthogonality conditions of mode shapes

(a). Multi-span beam of finite total length

Consider two normal modes of a multi-span beam satisfying the following equations

$$\begin{aligned} \bar{W}^{(4)}_{\beta,j}(\xi) - \lambda_j^4 \bar{W}_{\beta,j}(\xi) &= 0 , \\ \bar{W}^{(4)}_{\beta,k}(\xi) - \lambda_k^4 \bar{W}_{\beta,k}(\xi) &= 0 , \end{aligned} \tag{41}$$

where the first subscript β denotes the β-th span, and the second subscript, j or k, corresponds to the serial number of a natural frequency. Multiplying the first equation in Eq.(41) by $\bar{W}_{\beta,k}(\xi)$ and the second by $\bar{W}_{\beta,j}(\xi)$, and integrating the difference between the two resulting expressions over the total length NL of the N-span beam, we obtain

$$\begin{aligned} \sum_{\beta=1}^{N} \{ \int_0^1 [\bar{W}_{\beta,k}(\xi) \bar{W}^{(4)}_{\beta,j}(\xi) - \bar{W}_{\beta,j}(\xi) \bar{W}^{(4)}_{\beta,k}(\xi)] d\xi \} \\ = (\lambda_j^4 - \lambda_k^4) \sum_{\beta=1}^{N} \int_0^1 \bar{W}_{\beta,j}(\xi) \bar{W}_{\beta,k}(\xi) d\xi . \end{aligned} \tag{42}$$

Integrating the product $\bar{W}_{\beta,k}(\xi) \bar{W}^{(4)}_{\beta,j}(\xi)$ by parts

$$\begin{aligned} \int_0^1 \bar{W}_{\beta,k}(\xi) \bar{W}^{(4)}_{\beta,j}(\xi) d\xi = [\bar{W}_{\beta,k}(\xi) \bar{W}'''_{\beta,j}(\xi) - \bar{W}'_{\beta,k}(\xi) \bar{W}''_{\beta,j}(\xi) + \bar{W}''_{\beta,k}(\xi) \bar{W}'_{\beta,j}(\xi) \\ - \bar{W}'''_{\beta,k}(\xi) \bar{W}_{\beta,j}(\xi)]_0^1 + \int_0^1 \bar{W}_{\beta,j}(\xi) \bar{W}^{(4)}_{\beta,k}(\xi) d\xi . \end{aligned} \tag{43}$$

Eqs.(42) and (43) can be combined to yield

$$\begin{aligned} \sum_{\beta=1}^{N} [\bar{W}_{\beta,k}(\xi) \bar{W}'''_{\beta,j}(\xi) - \bar{W}'_{\beta,k}(\xi) \bar{W}''_{\beta,j}(\xi) + \bar{W}''_{\beta,k}(\xi) \bar{W}'_{\beta,j}(\xi) - \bar{W}'''_{\beta,k}(\xi) \bar{W}_{\beta,j}(\xi)]_0^1 \\ = (\lambda_j^4 - \lambda_k^4) \sum_{\beta=1}^{N} \int_0^1 \bar{W}_{\beta,j}(\xi) \bar{W}_{\beta,k}(\xi) d\xi . \end{aligned} \tag{44}$$

Finally, taking into account the continuity conditions Eq.(6) at each interior support, we obtain

$$
\begin{aligned}
&[\,\bar{W}_{N,k}(1)\bar{W}'''_{N,j}(1) - \bar{W}'_{N,k}(1)\bar{W}''_{N,j}(1) + \bar{W}''_{N,k}(1)\bar{W}'_{N,j}(1) - \bar{W}'''_{N,k}(1)\bar{W}_{N,j}(1)\,] \\
&- [\,\bar{W}_{1,k}(0)\bar{W}'''_{1,j}(0) - \bar{W}'_{1,k}(0)\bar{W}''_{1,j}(0) + \bar{W}''_{1,k}(0)\bar{W}'_{1,j}(0) - \bar{W}'''_{1,k}(0)\bar{W}_{1,j}(0)\,] \\
&\qquad = (\lambda_j^4 - \lambda_k^4)\sum_{\beta=1}^{N}\int_0^1 \bar{W}_{\beta,j}(\xi)\bar{W}_{\beta,k}(\xi)\,d\xi\ .
\end{aligned}
\tag{45}
$$

It may be noted that the left-hand side of Eq.(45) vanishes for any set of homogeneous boundary conditions of the form

$$a\bar{W}(x) + b\bar{W}'''(x) = 0 \tag{46}$$

or

$$c\bar{W}'(x) + d\bar{W}''(x) = 0 \tag{47}$$

at the two ends, where *a, b, c, d* are constants. The idealized boundary conditions, such as clamped-free, simply-simply supports, and so on, are special cases. Eq.(46) corresponds to a transverse elastic support, and Eq.(47) to a rotational elastic support. Thus, we obtain an orthogonality condition for normal modes of an *N*-span beam as follows

$$\sum_{\beta=1}^{N}\int_0^1 \bar{W}_{\beta,j}(\xi)\bar{W}_{\beta,k}(\xi)\,d\xi = \gamma_j^2\,\delta_{jk}\ , \tag{48}$$

where δ_{jk} denotes the Kronecker delta and γ_j^2 is defined as follows:

$$\gamma_j^2 = \sum_{\beta=1}^{N}\int_0^1 \bar{W}_{\beta,j}^2(\xi)\,d\xi\ . \tag{49}$$

Note that the span serial number β and the local coordinate ξ are separable in the expression for the mode shape given in Eqs.(28) and (29). Indeed, β appears only in the

exponential functions not involving ξ. Therefore, integration over the entire length of a multi-span beam can be carried out with respect to the local coordinate ξ, and then summed over the span serial number β. It will be shown later that these properties can be used to advantage in reducing the computational efforts when evaluating the dynamic response of the system.

Eq.(49) may be rewritten as follows:

$$\gamma_j^2 = \sum_{\beta=1}^{N} \int_0^1 \bar{W}_{\beta,j}^2(\xi) d\xi = C_{jj}^{a} I_1(\lambda_j) + C_{jj}^{b} I_2(\lambda_j) , \tag{50}$$

where $I_1(\cdot)$ and $I_2(\cdot)$ are integrals defined as

$$\begin{aligned} I_1(\lambda) &= \int_0^1 f^2(\xi) d\xi \\ &= \frac{1}{2}\left\{1 + \frac{1}{2\lambda}\sin(2\lambda) - \frac{\sin^2(\lambda)}{\sinh^2(\lambda)}\left[1 + \frac{1}{2\lambda}\sinh(2\lambda)\right]\right\} , \end{aligned} \tag{51}$$

$$\begin{aligned} I_2(\lambda) &= \int_0^1 f(\xi) f(1-\xi) d\xi \\ &= \frac{1}{2}\left\{-\cos(\lambda) - \frac{1}{\lambda}\sin(\lambda) + \frac{\sin^2(\lambda)}{\sinh^2(\lambda)}\left[\cosh(\lambda) + \frac{1}{\lambda}\sinh(\lambda)\right]\right\} , \end{aligned} \tag{52}$$

and where C_{jj}^{a} and C_{jj}^{b} can be obtained from the following more general expressions

$$\begin{aligned} C_{jk}^{a} &= \sum_{\beta=1}^{N} (\bar{a}_{\beta,j} \bar{a}_{\beta,k} + \bar{b}_{\beta,j} \bar{b}_{\beta,k}) \\ &= \Lambda_j \Lambda_k \{ (a_j a_k + b_j b_k) S_N(\mu_j + \mu_k) + \Gamma_j \Gamma_k (a_j^* a_k^* + b_j^* b_k^*) S_N^*(\mu_j + \mu_k) \\ &\quad + \Gamma_j (a_j^* a_k + b_j^* b_k) S_N^*(\mu_j - \mu_k) + \Gamma_k (a_j a_k^* + b_j b_k^*) S_N(\mu_j - \mu_k) \} , \end{aligned} \tag{53}$$

In Eqs.(53) and (54), an asterisk denotes the complex conjugate. Γ's and Λ's are defined by

$$
\begin{aligned}
C_{jk}^{b} &= \sum_{\beta=1}^{N} \left(\bar{a}_{\beta,j} \bar{b}_{\beta,k} + \bar{a}_{\beta,k} \bar{b}_{\beta,j} \right) \\
&= \Lambda_j \Lambda_k \{ (a_j b_k + a_k b_j) S_N(\mu_j + \mu_k) + \Gamma_j \Gamma_k (a_j^* b_k^* + a_k^* b_j^*) S_N^*(\mu_j + \mu_k) \\
&\quad + \Gamma_k (a_j b_k^* + a_k b_j^*) S_N(\mu_j - \mu_k) + \Gamma_j (a_j^* b_k + a_k^* b_j) S_N^*(\mu_j - \mu_k) \}
\end{aligned}
\tag{54}
$$

$$
\Lambda = \begin{cases} 1/2 , & \bar{W}_\beta(\xi) = Re\{ W_\beta(\xi) \} \\ -i/2 , & \bar{W}_\beta(\xi) = Im\{ W_\beta(\xi) \} , \end{cases}
\qquad
\Gamma = \begin{cases} 1 , & \bar{W}_\beta(\xi) = Re\{ W_\beta(\xi) \} \\ -1 , & \bar{W}_\beta(\xi) = Im\{ W_\beta(\xi) \} . \end{cases}
\tag{55}
$$

and function $S_N(\mu)$ is given by

$$
S_N(\mu) = \sum_{\beta=1}^{N} e^{-i\mu(\beta-1)} = \begin{cases} \dfrac{1 - e^{-i\mu N}}{1 - e^{-i\mu}} & \mu \neq 2m\pi \\ N & \mu = 2m\pi . \end{cases}
\tag{56}
$$

(b). Multi-span beam of infinite length

In the case of a periodic beam of infinite length, the orthogonality condition of normal modes can also be derived by using a similar procedure. However, it is no longer necessary to impose any boundary conditions at the exterior supports. The mode shape $W_\beta[\xi,\mu,\lambda_s(\mu)]$ given in Eq.(16) is now applicable throughout the entire length. Eqs.(41) through (44) still hold, except that the finite sum is replaced by an infinite sum. By taking into account the continuity conditions, Eq.(6), at the interior supports, it is easy to show that the left-hand-side of Eq.(42) vanishes, i.e

$$2\pi\delta(\mu+\mu')\{(e^{i\mu}-e^{-i\mu})W_1''[0,\mu,\lambda_s(\mu)]W_1''[1,\mu',\lambda_{s'}(\mu')] + (e^{-i\mu}-e^{i\mu})W_1''[1,\mu,\lambda_s(\mu)]W_1''[0,\mu',\lambda_{s'}(\mu')]\} = 0 , \tag{57}$$

where $\delta(\cdot)$ is Dirac's delta function, and where use has been made of the identity

$$\sum_{\beta=-\infty}^{\infty} e^{-i\mu(\beta-1)} = 2\pi\,\delta(\mu) . \tag{58}$$

The orthogonality condition of the mode shapes for an infinitely long multi-span beam read

$$\sum_{\beta=-\infty}^{\infty}\int_0^1 W_\beta[\xi,\mu,\lambda_s(\mu)]\,W_\beta[\xi,\mu',\lambda_{s'}(\mu')]\,d\xi = \gamma_0^2[\mu,\lambda_s(\mu)]\,\delta(\mu+\mu')\,\delta_{ss'} , \tag{59}$$

where $\delta_{ss'}$ is the Kronecker delta, and $\gamma_0^2[\cdot]$ is defined as follows:

$$\gamma_0^2[\mu,\lambda_s(\mu)] = \int_0^1 |W_1[\xi,\mu,\lambda_s(\mu)]|^2\,d\xi = (|a|^2+|b|^2)\,I_1[\lambda_s(\mu)] + 2Re\{ab^*\}\,I_2[\lambda_s(\mu)] , \tag{60}$$

in which integrals $I_1(\cdot)$ and $I_2(\cdot)$ are given in Eqs.(51) and (52), respectively, and a, b are defined in Eq.(17).

Responses of multi-span beam under the convected loading

Let us consider the forced vibration of a multi-span beam with damping. The equation of motion in the local coordinate system is given by

$$EIL^{-4}\,y_\beta^{(4)}(\xi,t) + c\dot{y}_\beta(\xi,t) + \rho A\,\ddot{y}_\beta(\xi,t) = p_\beta(\xi,t) , \quad (\beta = N_-,\ldots,1,2,\ldots,N_+ ;\ \ 0 \le \xi \le 1) \tag{61}$$

where c = damping coefficient, $p_\beta(\xi,t)$= transverse pressure per unit length, and N_-=1 and N_+=N for a finitely long beam, whereas N_-=-∞ and N_+=∞ for an infinitely beam. Assuming that the

excitation and response are harmonic in time, we have

$$p_\beta(\xi,t) = P_\beta(\xi)\, e^{i\omega t} ,$$
$$y_\beta(\xi,t) = Y_\beta(\xi)\, e^{i\omega t} . \tag{62}$$

Function $Y_\beta(\xi)$ will be referred as the harmonic-response function in what follows. For a harmonic loading convected over the beam at a velocity $\omega L/\mu_f$

$$P_\beta(\xi) = P_0 e^{-i\mu_f(\xi+\beta-1)} , \quad (\beta = 1,2,...,N) \tag{63}$$

where P_0 is the amplitude, and μ_f is the wave constant of the loading.

(a) Multi-span beam of finite total length

First, let us consider the case of an N-span beam. We expand $Y_\beta(\xi)$ and $P_\beta(\xi)$ in terms of the normal modes of the system as follows

$$Y_\beta(\xi) = \sum_{j=1}^{\infty} c_j \bar{W}_{\beta,j}(\xi) ,$$
$$P_\beta(\xi) = \sum_{j=1}^{\infty} d_j \bar{W}_{\beta,j}(\xi) , \quad (\beta = 1,2,...,N) \tag{64}$$

The relationship between coefficients c_j and d_j can be found by substituting Eqs.(62) and (64) into Eq.(61) and using Eq.(41) to obtain

$$\sum_{j=1}^{\infty} (\lambda_j^4 - \lambda_f^4 + i\zeta\lambda_f^2)\, c_j \bar{W}_{\beta,j}(\xi) = \frac{L^4}{EI} \sum_{j=1}^{\infty} d_j \bar{W}_{\beta,j}(\xi) , \tag{65}$$

where $\lambda_f^4=\rho AL^4\omega^2/EI$ is a nondimensional loading frequency parameter, and $\zeta=cL^2/(\rho AEI)^{1/2}$ is a nondimensional damping parameter. Comparison of coefficients on the two sides of Eq.(65) yields

$$c_j = H(\lambda_j, \lambda_f) d_j \ , \tag{66}$$

where $H(\lambda_j,\lambda_f)$ is the frequency response function given by

$$H(\lambda_j, \lambda_f) = \frac{L^4}{EI}(\lambda_j^4 - \lambda_f^4 + i\zeta\lambda_f^2)^{-1} \ . \tag{67}$$

Hence, the harmonic response function is obtained in the following form

$$Y_\beta(\xi) = \sum_{j=1}^{\infty} d_j H(\lambda_j, \lambda_f) \bar{W}_{\beta,j}(\xi) \ , \quad (\beta = 1,2,...,N). \tag{68}$$

The coefficients d_j are obtained by applying the orthogonality condition for the mode shapes, namely Eq.(48), to the second equation in Eq.(64) to yield

$$\begin{aligned} d_j &= \frac{1}{\gamma_j^2} \sum_{\beta=1}^{N} \int_0^1 \bar{W}_{\beta,j}(\xi) P_\beta(\xi) \, d\xi \\ &= \frac{P_0}{\gamma_j^2} [\ E_j^{\ a} g(\lambda_j, \mu_f) + E_j^{\ b} e^{-i\mu_f} g^*(\lambda_j, \mu_f) \ ] \ , \end{aligned} \tag{69}$$

where

$$E_j^{\ a} = \Lambda_j [\ a_j S_N(\mu_j + \mu_f) + \Gamma_j a_j^* S_N(\mu_f - \mu_j) \ ] \ , \tag{70}$$

$$E_j^{\ b} = \Lambda_j [\ b_j S_N(\mu_j + \mu_f) + \Gamma_j b_j^* S_N(\mu_f - \mu_j) \ ] \ , \tag{71}$$

$$g(\lambda, \mu_f) = \int_0^1 f(\xi) e^{-i\mu_f \xi} d\xi = u - \frac{\sin(\lambda)}{\sinh(\lambda)} v \ , \tag{72}$$

$$v = \frac{1}{2(\mu_f^2 + \lambda^2)} [\ (\lambda - i\mu_f) e^{-(\lambda + i\mu_f)} + (\lambda + i\mu_f) e^{\lambda - i\mu_f} - 2\lambda \ ] \ , \tag{74}$$

in which $sgn(\cdot)$ denotes the sign function.

$$u = \begin{cases} \dfrac{1}{2(\mu_f^2 - \lambda^2)} \left[(\lambda + \mu_f)\, e^{i(\lambda - \mu_f)} + (\lambda - \mu_f)\, e^{-i(\lambda + \mu_f)} - 2\lambda \right], & |\mu_f| \neq \lambda \\ -\dfrac{i}{2} \operatorname{sgn}(\mu_f) + \dfrac{1}{2(\lambda + |\mu_f|)} \left\{ 1 - e^{-i[\lambda \operatorname{sgn}(\mu_f) + \mu_f]} \right\}, & |\mu_f| = \lambda \end{cases} \tag{73}$$

(b) Multi-span beam of infinite length

The dynamic response of an infinitely long multi-span beam subjected to a convected harmonic loading can also be evaluated in a similar way. Let us expand both the harmonic response and the loading function in the mode shapes of such a beam

$$\begin{aligned} Y_\beta(\xi) &= \sum_{s=1}^{\infty} \int_\mu c_s(\mu)\, W_\beta[\xi, \mu, \lambda_s(\mu)]\, d\mu , \\ P_\beta(\xi) &= \sum_{s=1}^{\infty} \int_\mu d_s(\mu)\, W_\beta[\xi, \mu, \lambda_s(\mu)]\, d\mu , \quad (\beta = 0, \pm 1, \pm 2, \ldots, \pm\infty) \end{aligned} \tag{75}$$

where s denotes the serial number of a propagation band. Multiplying both sides of the second equation in Eq.(75) by $W_\beta^*[\xi, \mu', \lambda_s(\mu')]$ and performing integration over the length of the entire beam, we obtain upon applying the orthogonality conditions, Eq.(59),

$$d_s(\mu) = \frac{1}{2\pi \gamma_0^2[\mu, \lambda_s(\mu)]} \sum_{\beta=-\infty}^{\infty} \int_0^1 P_\beta(\xi)\, W_\beta^*[\xi, \mu, \lambda_s(\mu)]\, d\xi . \tag{76}$$

For an external excitation in the form of Eq.(63), the numerator in Eq.(76) may be simplified to

$$\sum_{\beta=-\infty}^{\infty} \int_0^1 P_\beta(\xi)\, W_\beta^*[\xi,\mu,\lambda_s(\mu)]\, d\xi = 2\pi\, \delta(\mu_f-\mu)\, P_0\, D[\mu,\lambda_s(\mu),\mu_f] \ , \tag{77}$$

$$D[\mu,\lambda_s(\mu),\mu_f] = a^*[\mu,\lambda_s(\mu)]\, g[\lambda_s(\mu),\mu_f] + b^*[\mu,\lambda_s(\mu)]\, e^{-i\mu_f}\, g^*[\lambda_s(\mu),\mu_f] \ ,$$

in which $a(\cdot)$ and $b(\cdot)$ are defined in Eq.(17), and $g(\cdot)$ is given by Eq.(72). Eq.(66) is still valid for $c_s(\mu)$ and $d_s(\mu)$. Hence, $c_s(\mu)$ may be expressed as follows

$$c_s(\mu) = \frac{\delta(\mu_f-\mu)\, P_0}{\gamma_0^2[\mu,\lambda_s(\mu)]}\, D[\mu,\lambda_s(\mu),\mu_f]\, H[\lambda_s(\mu),\mu_f] \ . \tag{78}$$

The harmonic response function for the infinitely long multi-span beam can be obtained by substituting Eq.(78) into the first equation in Eq.(75) to yield

$$Y_\beta(\xi) = \sum_{s=1}^{\infty} \int_{\mu\in R} \frac{\delta(\mu_f-\mu)\, P_0}{\gamma_0^2[\mu,\lambda_s(\mu)]}\, D[\mu,\lambda_s(\mu),\mu_f]\, H[\lambda_s(\mu),\lambda_f]\, W_\beta[\xi,\mu,\lambda_s(\mu)]\, d\mu \ , \tag{79}$$

$$(\ \beta = 0,\pm1,\pm2,\ldots,\pm\infty\ ) \ .$$

Here, the integration range R must be chosen from the particular *Brillouin zone* defined in Eq.(21) which includes the loading wave constant μ_f. This is always possible since union of all Brillouin zones constitutes the entire one-dimensional space. Note the presence of a Dirac's delta function in Eq.(79) with an argument μ_f - μ. It implies that only a group of propagating waves associated with μ_f contributes to the response. Carrying out the integration in Eq.(79), we obtain

$$Y_\beta(\xi) = \sum_{s=1}^{\infty} \frac{P_0}{\gamma_0^2[\mu_f,\lambda_s(\mu_f)]}\, D[\mu_f,\lambda_s(\mu_f),\mu_f]\, H[\lambda_s(\mu_f),\lambda_f]\, W_\beta[\xi,\mu_f,\lambda_s(\mu_f)] \ , \tag{80}$$

$$(\ \beta = 0,\pm1,\pm2,\ldots,\pm\infty\ )$$

where $\gamma_0^2(\cdot)$, $D(\cdot)$, $H(\cdot)$ and $W_\beta(\cdot)$ are given by Eqs.(60), (77), (67) and (16), respectively.

Results and discussion

For a multi-span beam under harmonic excitation, large response is likely to occur if the excitation frequency is within a propagation frequency band. When the excitation is convected along the beam, the response can be further amplified due to the so-called *coincidence effect.* For an N-span beam the magnitude of the harmonic response function may have as many as N peaks in each propagation band. The possible location of a peak in a propagation band for $|Y_\beta(\xi)|$ can be determined from the condition

$$\lambda_f = \left(\lambda_j^4 - \frac{\zeta^2}{2}\right)^{\frac{1}{4}}, \quad (j = 1,2,\ldots), \tag{81}$$

when the denominator in expression (67) for $|H(\lambda_j,\lambda_f)|$ has a minimum magnitude, whereas the magnitude of harmonic response function $Y_\beta(\xi)$ is dominated by the term with $|H(\lambda_j,\lambda_f)|$. For an infinitely long multi-span beam, however, there is only one group of propagating waves, whose wave constant coincides with μ_f that contributes to the response, as it can be seen from Eq.(79). Therefore, there is only one peak at

$$\lambda_f = \left[\lambda_s(\mu_f)^4 - \frac{\zeta^2}{2}\right]^{\frac{1}{4}}, \quad (s = 1,2,\ldots) \tag{82}$$

appearing in each propagation band.

Fig. 4(a) portrays the harmonic response at the mid-point of the second span of a four-span beam. It shows that there are four peaks in the first propagation band. In contrast, there is only one peak in the first band for the infinite multi-span beam shown in Fig. 4(b), and the response is considerably magnified due to the coincidence effect.

The effects of damping on the harmonic responses are also shown in Fig. 5(a) and 5(b) for a four-span beam and an infinitely long multi-span beam, respectively. It can be seen that

the values of the peaks in each propagation band is reduced with a larger damping coefficient. Hence, the profile of each peak becomes flatter as damping increases.

The results obtained from the present approach and Mead's approach (1971) are compared in Figs. 6(a) and 6(b) for an infinitely long beam with an evenly spaced hinge supports (v=0). The dash line represents a 20-term approximation in Mead's formulation, whereas the solid curve represents a one-term approximation by the present approach in the first propagation band. The results are seen to be very close. The two results become indistinguishable in the first three propagation bands, when a twenty-term was used in the present approach, as shown in Fig.6(b). Most significantly, the present approach has the advantage in that the location of each possible peak in each propagation band can be determined; thus, the value of each peak can be evaluated precisely from Eq.(80).

Conclusions

The free and forced vibrations of periodically supported multi-span beams are studied in the this paper. Both the case of finite total length and the case of infinite total length are considered. The wave propagation concept is applied in the analysis of free vibration of the beam systems. The dispersion equation and its asymptotic form are derived from which the natural frequencies can be determined for a given wave constant. An explicit asymptotic expression for the natural frequencies is also proposed for the specific case of zero rotational spring stiffness. It is shown that the agreement between the asymptotic and the exact frequencies is excellent. The mode shapes of free vibration are obtained in the complex form. In these mode shapes the span serial number and the local spatial coordinate are separable; thus, an integration over the entire length is reduced to one within a single span, and a summation over the serial

numbers of the spans. It is shown that the use of these mode shape expressions can greatly reduce the computational efforts in the forced vibration analysis.

Acknowledgment

This study has been supported by the NASA Kennedy Space Center, through Cooperative Agreement No. NCC10-0005, S-1, Technical Monitor Mr. R. Caimi. This support is gratefully appreciated.

References

Abramovich, H., and Elishakoff, I., 1987, " Application of the Krein's method for determination of natural frequencies of periodically supported beam based on simplified Bresse-Timoshenko equations," *Acta Mechanica*, Vol. 66, 39-59.

Bolotin, V. V., "An asymptotic method for the study of the problem of eigenvalues for rectangular regions," in *Problems in Continum Mechanics*, 1961, SIAM, Philadelphia, 56-68.

Brillouin, L., 1953, *Wave propagation in periodic structures*, Dover, New York.

Cai, G. Q. and Lin, Y. K., 1991, " Wave propagation and scattering in structural networks," ASCE *J. Engrg. Mech.* Vol. 117, 1555-1575.

Elishakoff, I., 1976, "Bolotin's dynamic edge effect method," *The Shock and Vibration Digest*, Vol. 8(1), 95-104.

Krein, M. G., 1933, "Vibration theory of multi-span beams," (In Russian), *Vestnik Inzhenerov i Tekhnikov*, Vol. 4, 142-145.

Lin, Y. K., 1962, "Free vibration of a continuous beam on elastic supports," *International Journal of Mechanical Sciences*," Vol. 4, 409-423.

Lin, Y. K. and McDaniel, T. J., 1969, "Dynamics of beam type periodic structures," *Journal of Engineering for Industry*," Vol. 93, 1133-1141.

Lin, Y. K., Maekawa, S., Nijim, H. and Maestrello, L., "Response of periodic beam to supersonic boundary-layer pressure fluctuations," in *Stochastic Problems in Dynamics*, 1977, (Clarkson B.L., ed) Pitman, 468-485.

Mead, D. J., 1970, "Free wave propagation in periodically-supported infinite beams," *J. Sound and Vibration*. Vol. 11, 181-197.

Mead, D. J., 1971, "Space-harmonic analysis of periodically supported beams: Response to convected random loading," *J. Sound and Vibration*, Vol. 14, 525-541.

Miles, J. W., 1956, "Vibration of beams on many supports," ASCE *J. Engrg. Mech.*, Vol. 82, 1-9.

Sen Gupta, G., 1970, "Natural flexural wave and the normal modes of periodically-supported beams and plates," *J. Sound and Vibration*. Vol. 13, 89-101.

Yong, Y. and Lin, Y. K., 1989, "Propagation of decaying waves in periodic and piece-wise periodic structures of finite length," *J. Sound and Vibration*. Vol. 129, 99-118.

Table I. Frequency Parameters of Six-Span Beams with Rotational Spring Parameter ν (Case $\nu_0=\nu_N=\nu/2$)

$\nu=kL/EI$	0		2		200	
	Exact Eq.(18)	Asymp. Eq.(24)	Exact Eq.(18)	Asymp. Eq.(23)	Exact Eq.(18)	Asymp. Eq.(23)
Frequencies in the first band	π	π	3.398	3.397	4.641	4.624
	3.261	3.267	3.491	3.491	4.647	4.630
	3.556	3.566	3.729	3.730	4.663	4.646
	3.927	3.927	4.042	4.037	4.685	4.668
	4.298	4.288	4.362	4.351	4.707	4.699
	4.601	4.586	4.623	4.607	4.724	4.707
Frequencies in the second band	2π	2π	6.427	6.427	7.710	7.711
	6.410	6.410	6.536	6.536	7.720	7.720
	6.707	6.707	6.802	6.802	7.746	7.746
	7.069	7.069	7.134	7.134	7.781	7.782
	7.430	7.430	7.468	7.468	7.817	7.818
	7.727	7.728	7.740	7.741	7.844	7.844

Table II. Frequency Parameters of Six-Span Beams with Rotational Spring Parameter ν (Case $\nu_0=\nu_N=\infty$)

$\nu=kL/EI$	0		2		200	
	Exact Eq.(18)	Asymp. Eq.(24)	Exact Eq.(18)	Asymp. Eq.(23)	Exact Eq.(18)	Asymp. Eq.(23)
Frequencies in the first band	3.261	3.267	3.491	3.491	4.647	4.630
	3.556	3.566	3.729	3.730	4.663	4.646
	3.927	3.927	4.042	4.037	4.685	4.668
	4.298	4.288	4.362	4.351	4.724	4.690
	4.601	4.586	4.623	4.607	4.724	4.706
	4.730	4.712	4.730	4.712	4.730	4.713
Frequencies in the second band	6.410	6.410	6.536	6.536	7.720	7.720
	6.708	6.707	6.802	6.802	7.746	7.746
	7.069	7.069	7.134	7.134	7.781	7.782
	7.430	7.430	7.468	7.468	7.817	7.818
	7.727	7.728	7.740	7.741	7.843	7.844
	7.853	7.854	7.853	7.854	7.853	7.854

Table III. Frequency Parameters of Six-Span Beams with Rotational Spring Parameter ν (Case $\nu_0=\nu/2$, $\nu_N=\infty$)

$\nu=kL/EI$	0		2		200	
	Exact Eq.(18)	Asymp. Eq.(24)	Exact Eq.(18)	Asymp. Eq.(23)	Exact Eq.(18)	Asymp. Eq.(23)
Frequencies in the first band	3.173	3.175	3.422	3.421	4.643	4.626
	3.393	3.403	3.596	3.598	4.654	4.637
	3.738	3.743	3.881	3.879	4.674	4.656
	4.116	4.111	4.205	4.196	4.697	4.679
	4.463	4.451	4.505	4.491	4.717	4.699
	4.696	4.679	4.702	4.685	4.728	4.711
Frequencies in the second band	6.317	6.317	6.456	6.456	7.713	7.713
	6.545	6.545	6.656	6.656	7.731	7.732
	6.885	6.885	6.964	6.964	7.763	7.763
	7.252	7.253	7.304	7.304	7.800	7.800
	7.592	7.592	7.617	7.618	7.832	7.833
	7.820	7.820	7.823	7.824	7.851	7.852

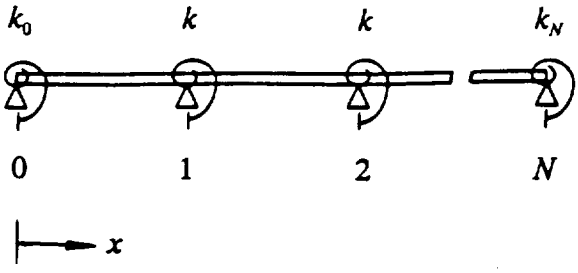

1(a). Finite length

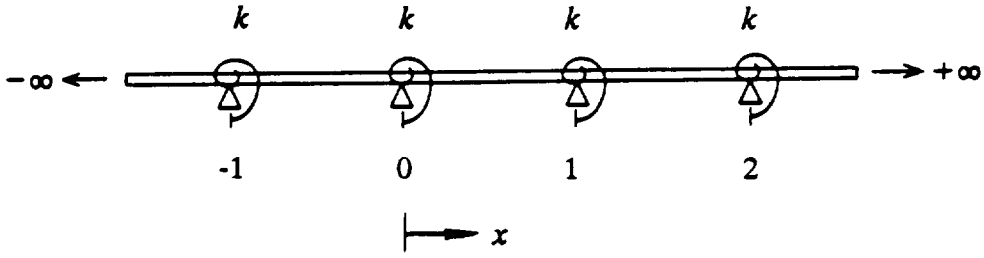

1(b). Infinite length

Fig. 1. Multi-span beams with elastic rotational spring at each support

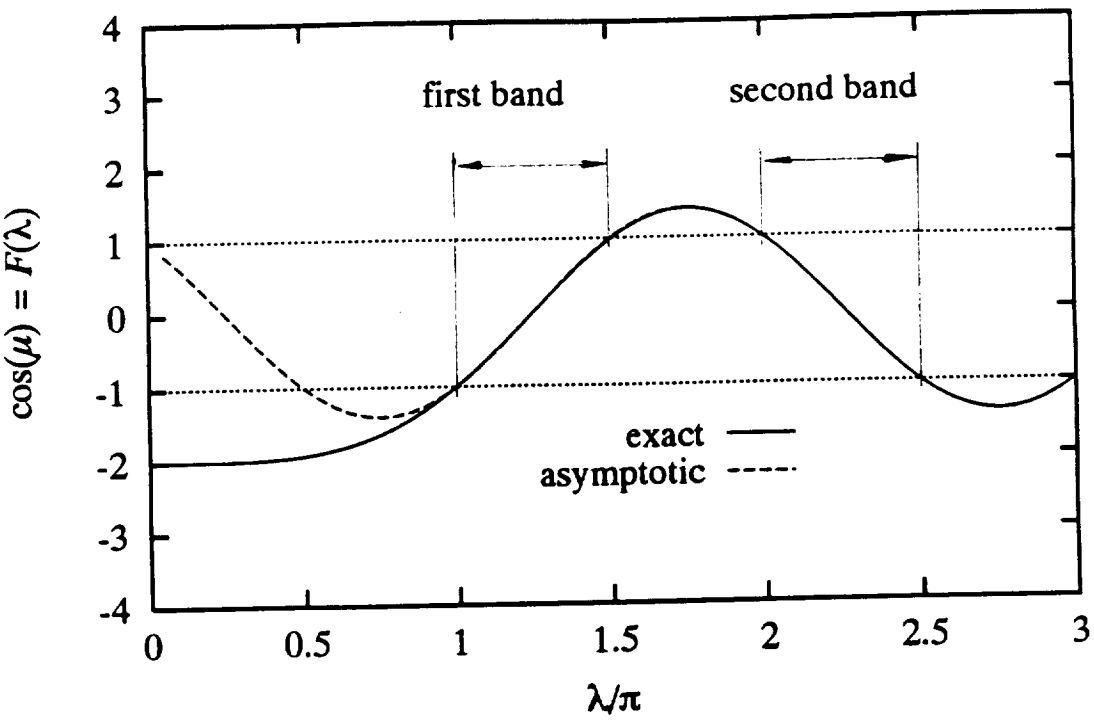

2(a). $\nu = 0$

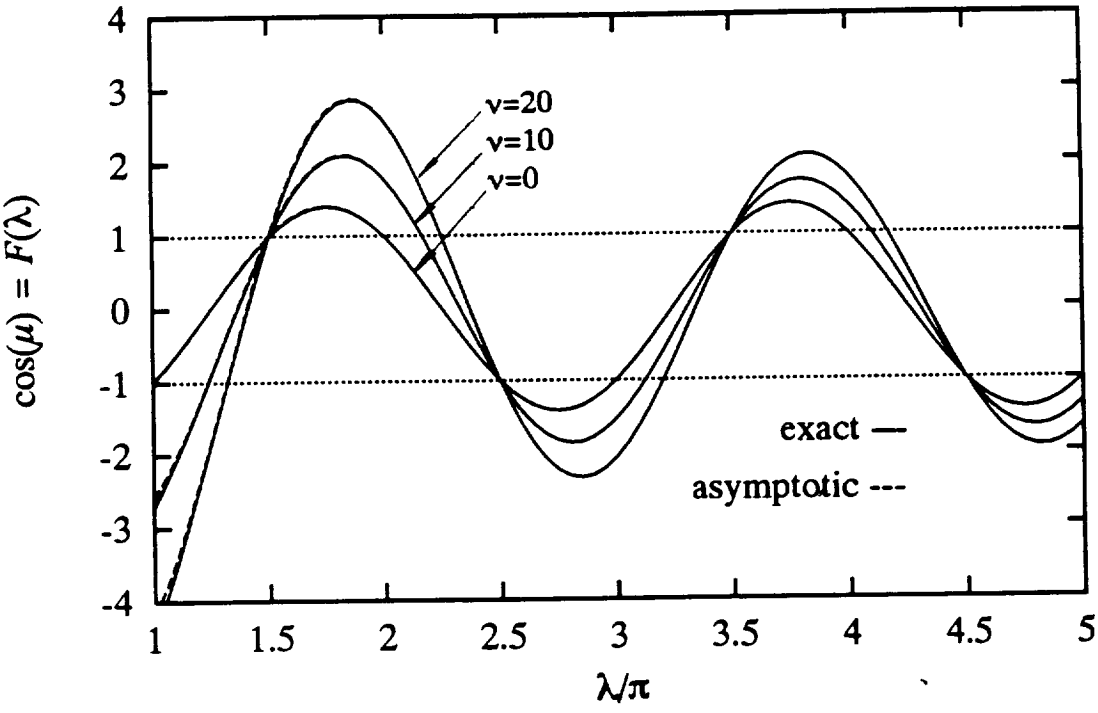

2(b). $\nu = 0, 10, 20$

Fig. 2. Dispersion relationships

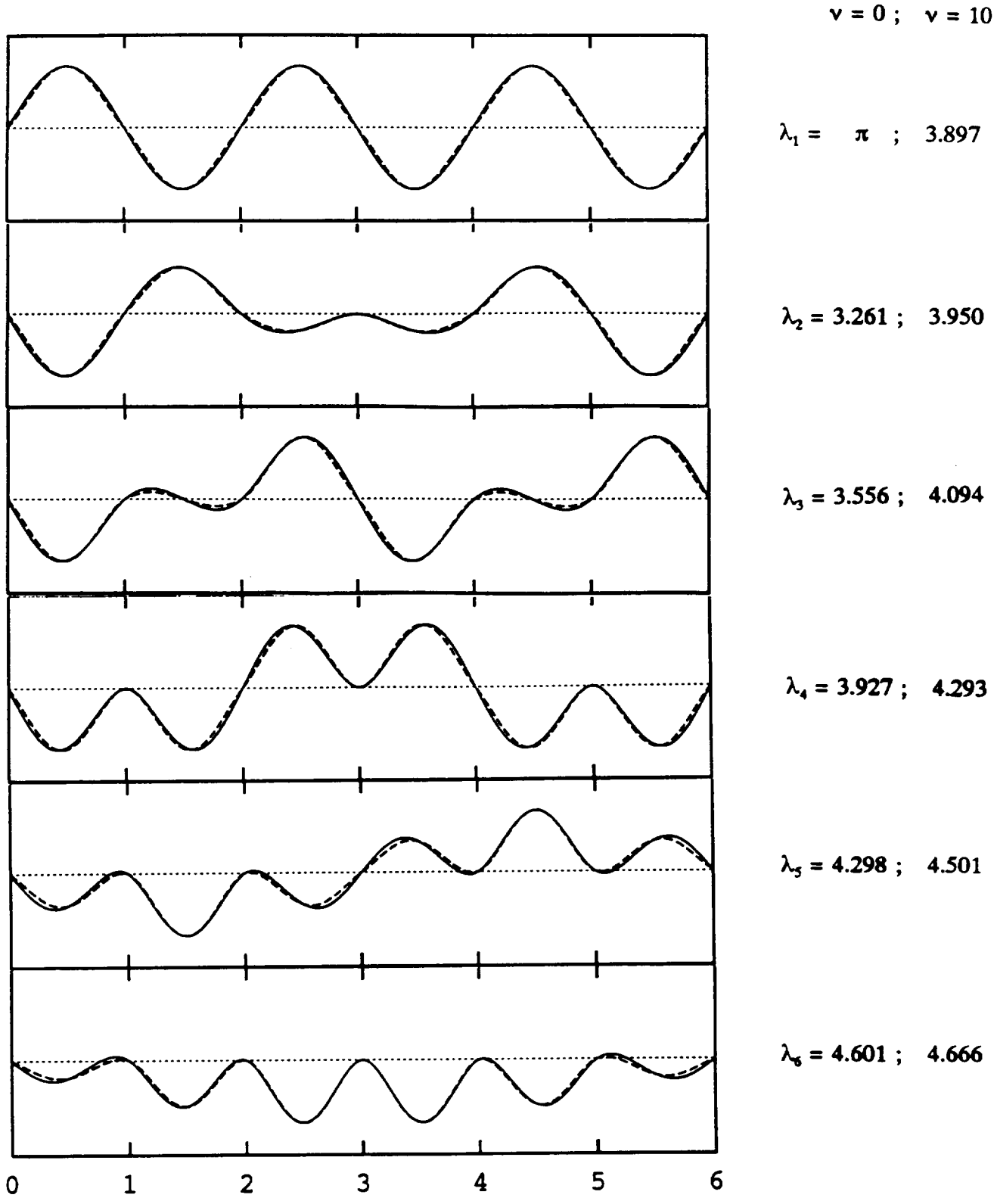

3(a). $\nu_0=\nu/2$ and $\nu_N=\nu/2$

Fig. 3. Normal modes in the first band of a six-span beam (— for ν=0; --- for ν=10)

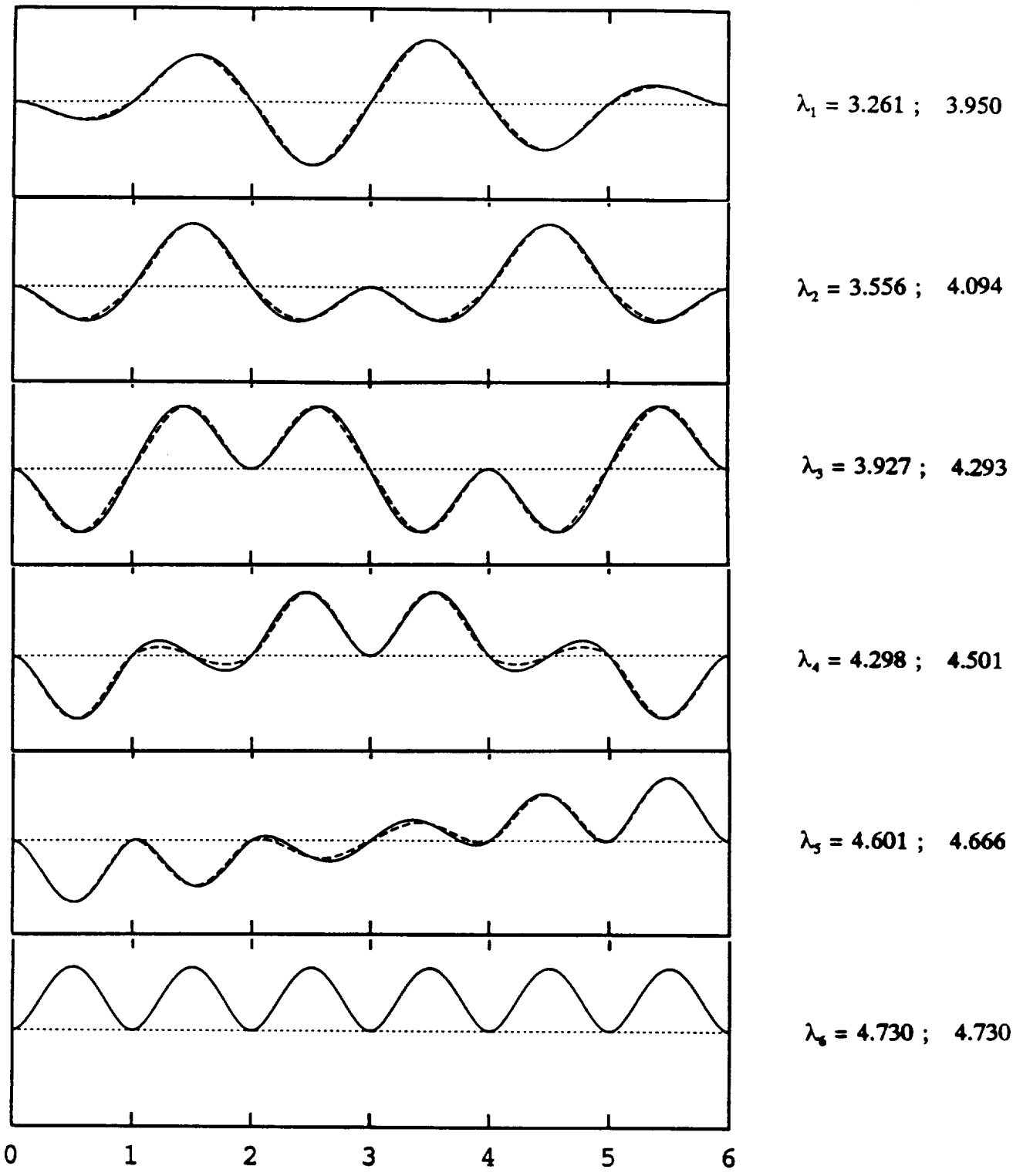

3(b). $\nu_0=\infty$ and $\nu_N=\infty$

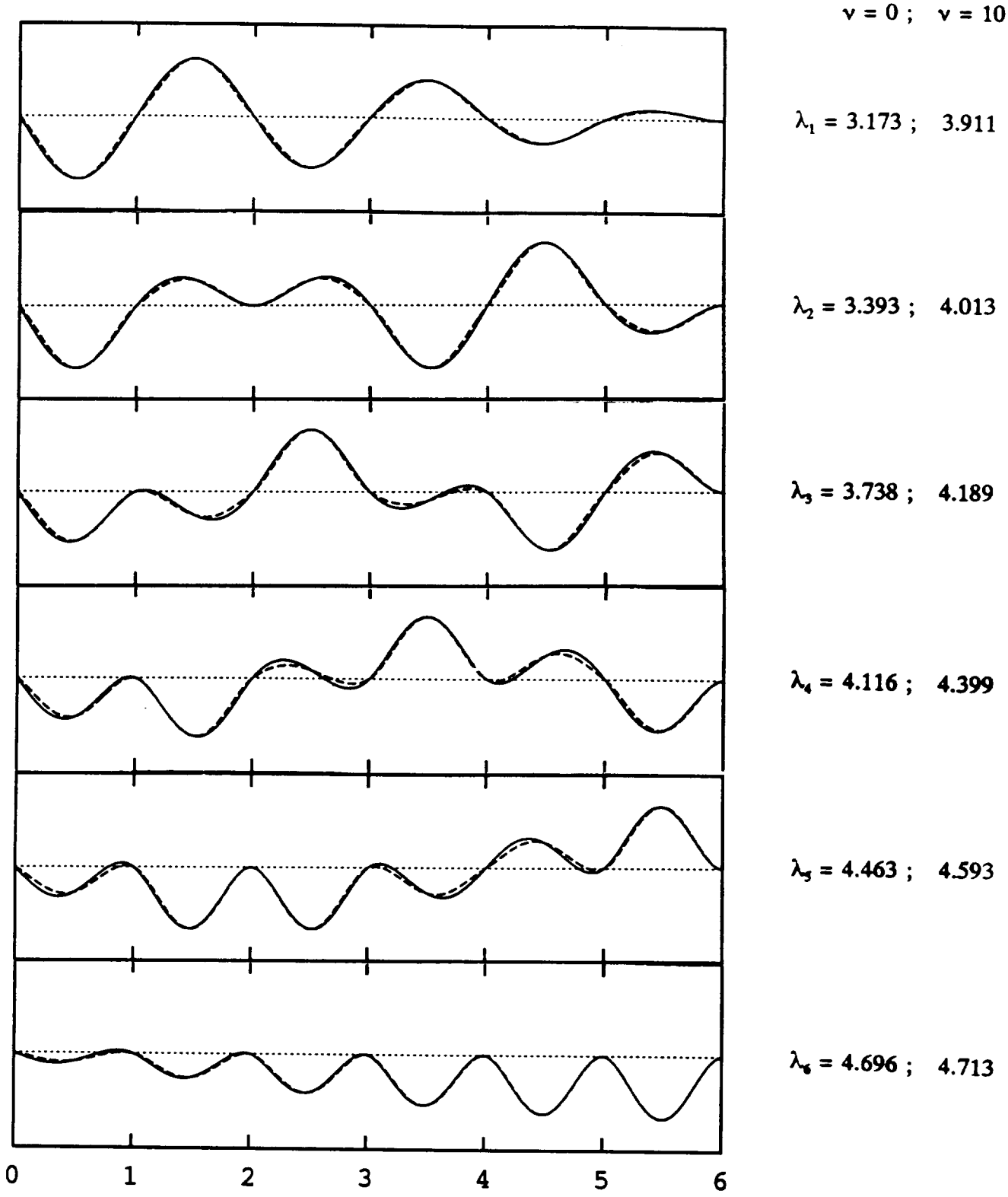

3(c). $\nu_0=\nu/2$ and $\nu_N=\infty$

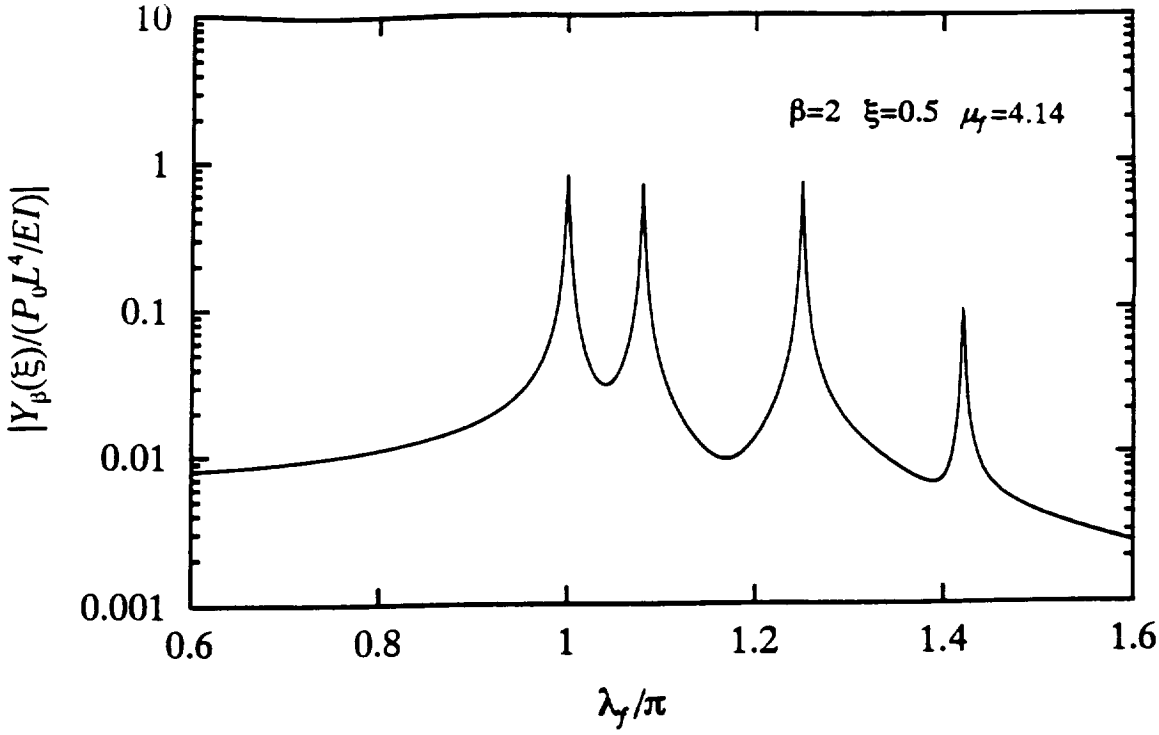

Fig. 4(a). Nondimensional harmonic response of a four-span beam vs loading frequency parameter λ_f (— Using normal modes of the first band; --- Using normal modes of the first two bands)

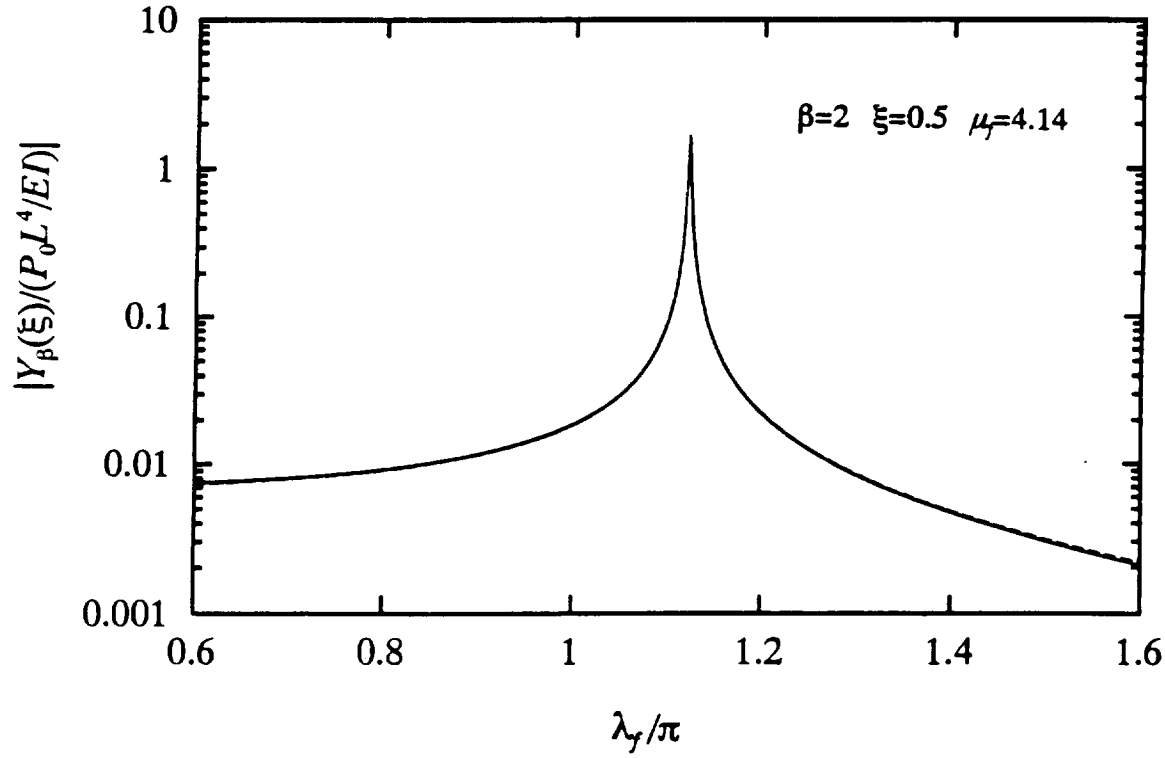

Fig. 4(b). Nondimensional harmonic response of an infinitely long multi-span beams vs loading frequency parameter λ_f (— Using normal modes of the first band; --- Using normal modes of the first two bands)

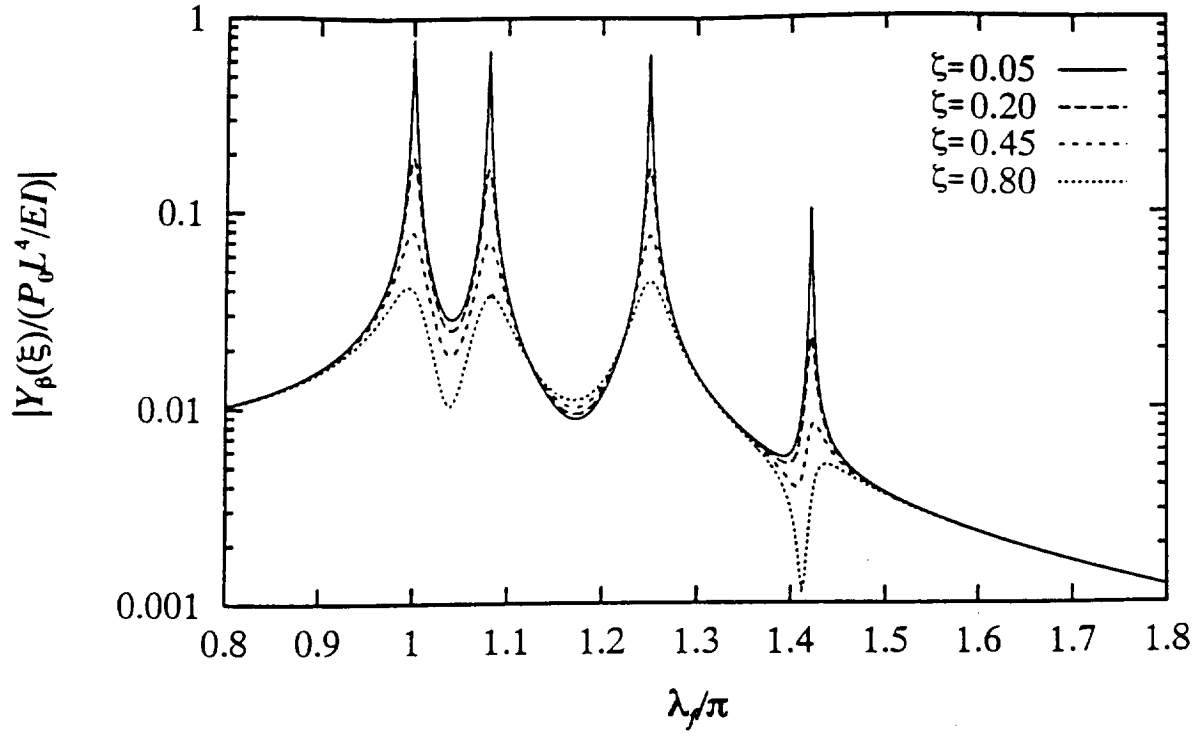

Fig. 5(a). Nondimensional harmonic response of a four-span beam vs loading frequency parameter λ_f with different damping coefficients (β=2, ξ=0.5, μ_f=4.14)

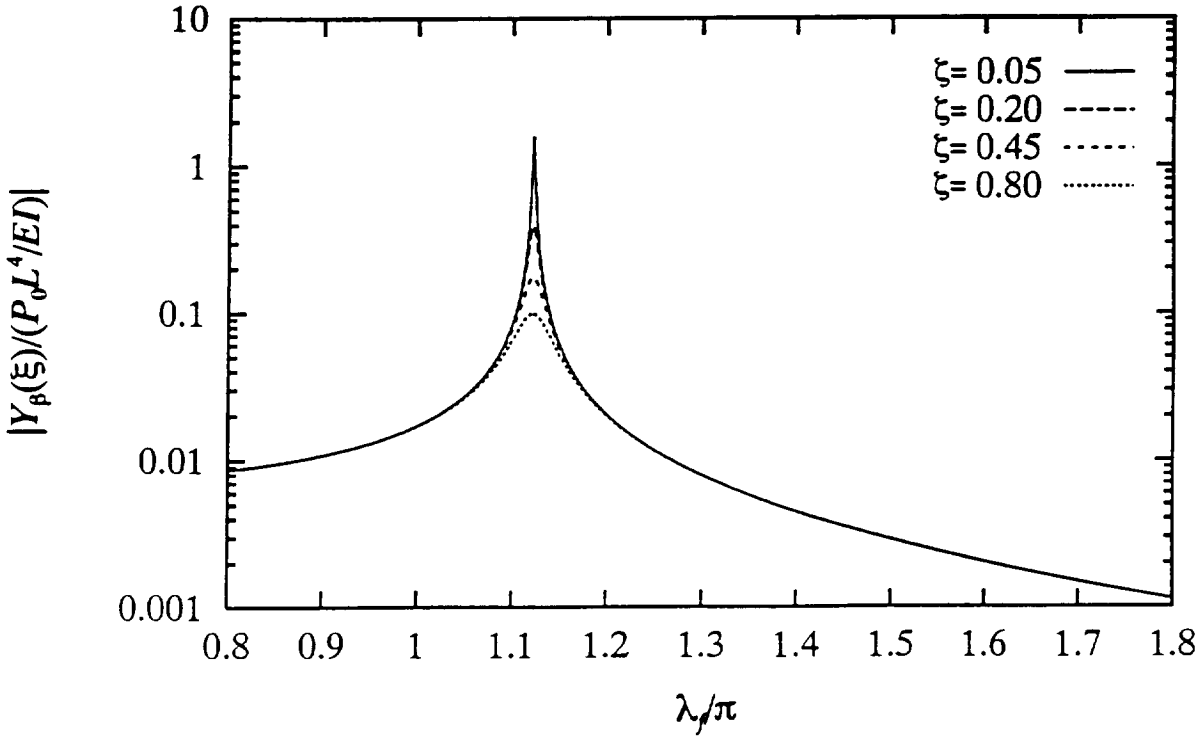

Fig. 5(b). Nondimensional harmonic response of an infinite long multi-span beam vs loading frequency parameter λ_f with different damping coefficients (β=2, ξ=0.5, μ_f=4.14)

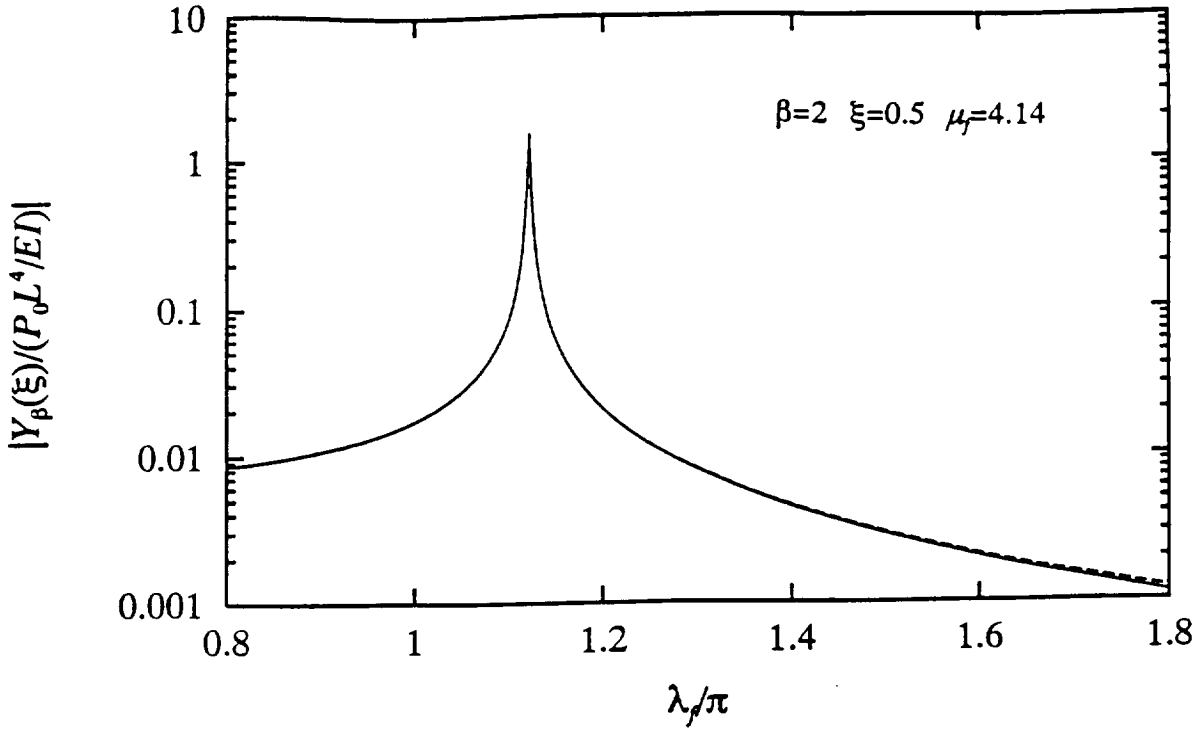

Fig. 6(a) Nondimensional harmonic response of an infinitely long multi-span beam in the first band (— by present approach; --- by Mead's approach)

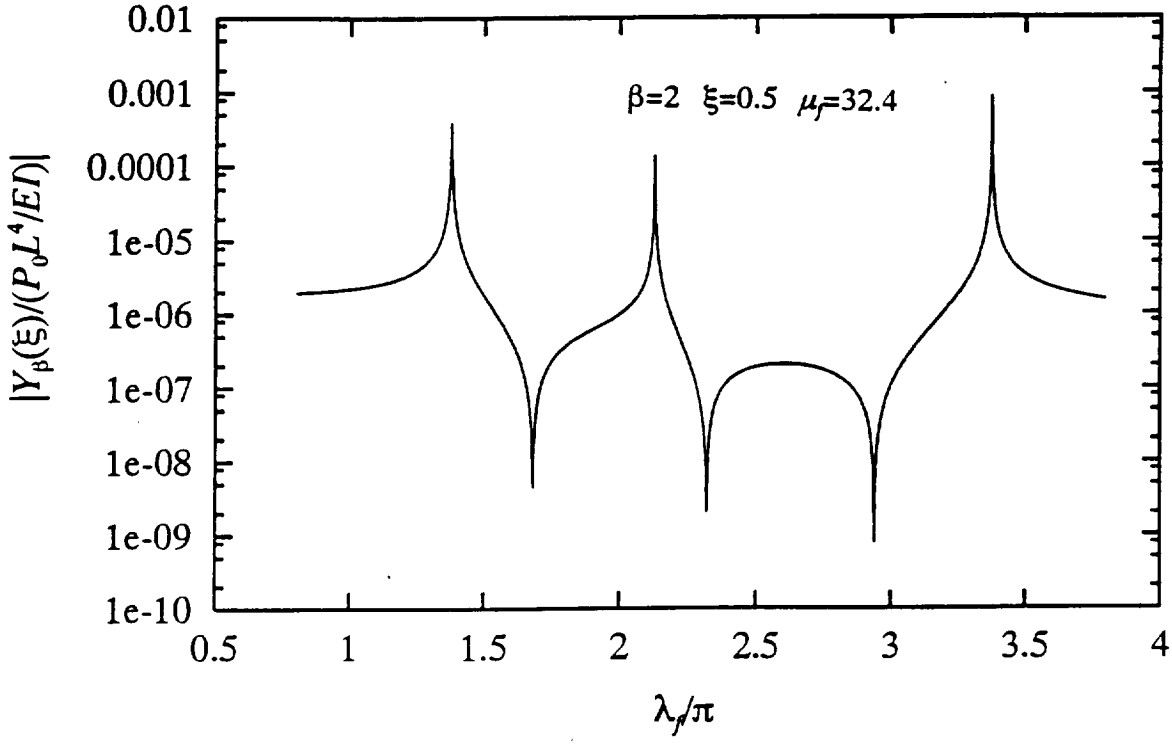

Fig. 6(b) Nondimensional harmonic response of an infinitely long multi-span beam in the first three bands (— by present approach; --- by Mead's approach)

CHAPTER # 4

Vibration of Two-Dimensional Grillage

VIBRATION OF TWO-DIMENSIONAL GRILLAGE

L. P. Zhu, Y. K. Lin and I. Elishakoff

Center for Applied Stochastics Research and Department of Mechanical Engineering, Florida Atlantic University, Boca Raton, FL 33432

Abstract

In this paper, an exact solution for free vibration of a two dimensional periodic grillage structure is obtained by using wave propagation concept. Each periodic node (or support) of such a grillage structure is constrained by a rigid transverse support, and two elastic rotational springs in two orthogonal directions. The rotational springs in each direction are identical. The four boundary edges of the grillage as a whole are either simply supported or clamped. The wave motions at all periodic nodes are investigated and the associated dispersion equation relating the natural frequency and wave constant is derived. It is shown that there exist both bending and torsional motions in a grillage structure, which are coupled between members in two perpendicular directions. General expressions of the synchronous mode shapes and non-synchronous deflection shapes are obtained for both bending and torsional motions in two directions. These can then be applied in formulating forced vibrations of the grillage structure. An example of a grillage with four-spans in each direction is given for illustration.

1. Introduction

A grillage consists of two sets of mutually orthogonal beams rigidly connected at the intersections where additional elastic constraints may be imposed in rotational and/or transverse directions. The properties and spacing of the beams, and the constraining springs in each direction are spatially periodic; however, they may differ in two different directions.

Grillages find wide applications in many forms of construction. A steel or concrete deck is often placed on a grillage to transfer the imposed loads. There are several methods for the analysis of a linear elastic grillage. The general method of statically indeterminate structures is applicable in the case of static loading, but it is extremely tedious except when the number of intersections is small. If the space between two neighboring beams is small then approximation of the overall grillage by an orthotropic plate is reasonable, for which the appropriate differential equation can be found (e.g. Timoshenko 1959). Ellington and McCallion (1957) proposed a more accurate method to obtain deflection under static loads by using a finite difference formulation, but they assumed that the beams did not resist torsion.

There have been rather few papers on the vibration of grillages. In their pioneering work, Ellington and McCallion (1959) assumed that the mass of the beams was concentrated at the nodes (intersections) of the grillage. Again, by neglecting the torsional stiffness of the beams, and using a finite difference equation approach, they obtained a frequency equation for a grillage with various boundary conditions. Wah (1963) improved this method by considering the torsional stiffness of the beams with both

distributed and lumped masses. It was noted in his work that the derivation of the frequency equation required an admissible transverse displacement at each node which satisfies the boundary conditions. Unfortunately, such an expression is not easily determinable except for the case of a rectangular grillage simply supported on all four exterior edges. For other support conditions, only the case of zero torsional stiffness was discussed in his paper. Recently, Dinkevich (1993) considered a grillage with a transverse spring at each support. A frequency equation was obtained for the case of simply supported edges and negligible torsional stiffness.

In this paper, both wave propagation in a periodic grillage of infinite size and free vibration of a grillage of finite size are investigated. Exact solutions for both cases are obtained by using the wave propagation concept. Every periodic node (or support) is constrained by a rigid transverse support and two elastic rotational springs in two orthogonal directions. The rotational springs are identical in the same direction, but they may be different in different directions. In the case of a grillage of finite size, the four boundary edges are assumed to be either simply supported or fully clamped. Both bending and torsional motions of each beam are taken into account in the analysis. The bending motions of the beams in one direction are coupled with the torsional motions of the beams in the other direction. The wave motions at all periodic nodes are investigated, and a dispersion equation that relates the natural frequency and the wave constant is derived. The general expressions of the mode shapes for both bending and torsional motions are obtained, which can be applied in the analysis of forced vibrations. An example of a grillage with four-spans in each direction is given for illustration.

2. Wave Propagation in an Infinite-Size Grillage

2.1 Basic Equations

Consider a two-dimensional grillage structure of an infinite size, composed of two sets of multi-span beams in two perpendicular directions. It is assumed that each support provides a rigid constraint against transverse motion, as well as elastic constraints against rotations about two axes, with elastic constants k_x and k_y, respectively, as shown in Figs. 1(a) and 1(b). Although the transverse and torsional motions are uncoupled for a prismatic beam in one direction, they may be coupled in two sets of beams in the perpendicular directions. Let us focus our attention on node/support (α,β) as shown in Fig. 1(a). The displacements in the four beams sharing the same support (α,β) are denoted by the symbols as shown in Fig. 1(b). The equations for the bending motions of the beams in the x and y directions are, respectively,

$$D_x \frac{\partial^4 X_{\alpha\beta}(\xi,t)}{\partial \xi^4} + m_x L_x^4 \frac{\partial^2 X_{\alpha\beta}(\xi,t)}{\partial t^2} = 0 \tag{1}$$

$$D_y \frac{\partial^4 Y_{\alpha\beta}(\zeta,t)}{\partial \zeta^4} + m_y L_y^4 \frac{\partial^2 Y_{\alpha\beta}(\zeta,t)}{\partial t^2} = 0 \tag{2}$$

where $X_{\alpha\beta}$, $Y_{\alpha\beta}$ = transverse displacements, m_x, m_y = masses per unit length, L_x, L_y = span lengths and D_x, D_y = bending rigidities of the two beams in the x and y directions, respectively.

The equations of the torsional motions are

$$C_y \frac{\partial^2 \theta_{\alpha\beta}(\zeta,t)}{\partial \zeta^2} - n_y L_y^2 \frac{\partial^2 \theta_{\alpha\beta}(\zeta,t)}{\partial t^2} = 0 \tag{3}$$

$$C_x \frac{\partial^2 \psi_{\alpha\beta}(\xi,t)}{\partial \xi^2} - n_x L_x^2 \frac{\partial^2 \psi_{\alpha\beta}(\xi,t)}{\partial t^2} = 0 \tag{4}$$

Here, ψ and θ are, respectively, the torsional displacements of the beams in the x and y directions, n_x, n_y = polar mass-moments of inertia per unit length, and C_x, C_y = torsional rigidities. The effect of warping of a cross-section due to non-uniform torsion is neglected. The positive directions of ψ and θ are determined by the usual right-hand rule. The local coordinates ξ and ζ in the two directions are defined as follows:

$$\begin{aligned} \xi &= x/L_x - (\alpha - 1) ; \quad (\alpha - 1)L_x \le x \le \alpha L_x ; \quad 0 \le \xi \le 1 \\ \zeta &= y/L_y - (\beta - 1) ; \quad (\beta - 1)L_y \le y \le \beta L_y ; \quad 0 \le \zeta \le 1 \end{aligned} \tag{5}$$

For an infinitely large grillage, there are no exterior supports. Continuity conditions must be met at each support. For the transverse motion of the beam, they require that

$$\begin{aligned} & X_{\alpha\beta}(\xi,t)\,|_{\xi=1} = X_{\alpha+1\beta}(\xi,t)\,|_{\xi=0} = 0 \\ & X'_{\alpha\beta}(\xi,t)\,|_{\xi=1} = X'_{\alpha+1\beta}(\xi,t)\,|_{\xi=0} = \Theta_{\alpha\beta}(t)L_x \\ & D_x\left[X''_{\alpha+1\beta}(\xi,t)\,|_{\xi=0} - X''_{\alpha\beta}(\xi,t)\,|_{\xi=1}\right] \\ & \quad + C_y\left[\theta'_{\alpha\beta+1}(\zeta,t)\,|_{\zeta=0} - \theta'_{\alpha\beta}(\zeta,t)\,|_{\zeta=1}\right] = k_x \Theta_{\alpha\beta}(t) \end{aligned} \tag{6}$$

and

$$
\begin{aligned}
&Y_{\alpha\beta}(\zeta,t)\,|_{\zeta=1} = Y_{\alpha\beta+1}(\zeta,t)\,|_{\zeta=0} = 0 \\
&Y'_{\alpha\beta}(\zeta,t)\,|_{\zeta=1} = Y'_{\alpha\beta+1}(\zeta,t)\,|_{\zeta=0} = -\Psi_{\alpha\beta}(t)\,L_y \\
&D_y\left[Y''_{\alpha\beta+1}(\zeta,t)\,|_{\zeta=0} - Y''_{\alpha\beta}(\zeta,t)\,|_{\zeta=1}\right] \\
&\quad - C_x\left[\psi'_{\alpha+1\beta}(\xi,t)\,|_{\xi=0} - \psi'_{\alpha\beta}(\xi,t)\,|_{\xi=1}\right] = k_y\Psi_{\alpha\beta}(t)
\end{aligned}
\tag{7}
$$

where a prime denotes differentiation with respect to ξ or ζ. For the torsional motion, the boundary conditions read

$$
\theta_{\alpha\beta}(\zeta,t)\,|_{\zeta=0} = \Theta_{\alpha-1\beta}(t)\ , \quad \theta_{\alpha\beta}(\zeta,t)\,|_{\zeta=1} = \Theta_{\alpha\beta}(t) \tag{8}
$$

$$
\psi_{\alpha\beta}(\xi,t)\,|_{\xi=0} = \Psi_{\alpha\beta-1}(t)\ , \quad \psi_{\alpha\beta}(\xi,t)\,|_{\xi=1} = \Psi_{\alpha\beta}(t) \tag{9}
$$

in which $\Theta_{\alpha\beta}(t)$ and $\Psi_{\alpha\beta}(t)$ are, respectively, the rotations at the (α,β)th support about two horizontal axes as shown in Fig. 1(b).

As seen from Eqs. (1) through (9), the $\Theta(t)$ motion is related to the bending motion of the beams in the x direction and the torsional motion of the beams in the y direction, whereas, the $\Psi(t)$ motion is related to the bending motion of the beams in the y direction and the torsional motion of the beams in the x direction. It is, therefore, possible that the vibration of a grillage structure can be decomposed into two uncoupled states in terms of the Θ'*s* and Ψ'*s*, respectively. In what follows, we shall discuss the Θ motion only. The Ψ motion is similar. Assume that the motions is harmonic

$$X_{\alpha\beta}(\xi,t) = \bar{X}_{\alpha\beta}(\xi)\, e^{i\omega t} \tag{10}$$

$$\theta_{\alpha\beta}(\zeta,t) = \bar{\theta}_{\alpha\beta}(\zeta)\, e^{i\omega t} \tag{11}$$

$$\Theta_{\alpha\beta}(t) = \bar{\Theta}_{\alpha\beta}\, e^{i\omega t} \tag{12}$$

Then, Eqs. (1) and (3) become

$$\bar{X}''''_{\alpha\beta}(\xi) - \lambda_\Theta^4 \bar{X}_{\alpha\beta}(\xi) = 0 \tag{13}$$

$$\bar{\theta}''_{\alpha\beta}(\zeta) + \eta_\Theta^2 \bar{\theta}_{\alpha\beta}(\zeta) = 0 \tag{14}$$

where λ_Θ and η_Θ are nondimensional frequency parameters given by

$$\lambda_\Theta = \left(\frac{m_x L_x^4}{D_x}\omega^2\right)^{\frac{1}{4}}, \quad \eta_\Theta = \left(\frac{n_y L_y^2}{C_y}\omega^2\right)^{\frac{1}{2}}, \quad \eta_\Theta = \kappa_x \lambda_\Theta^2 \tag{15}$$

Solutions of Eqs. (13) and (14) are obtained as

$$\bar{X}_{\alpha\beta}(\xi) = A_{\alpha\beta} f_{\lambda_\Theta}(\xi) + B_{\alpha\beta} f_{\lambda_\Theta}(1-\xi) \tag{16}$$

$$\bar{\theta}_{\alpha\beta}(\zeta) = C_{\alpha\beta} \sin\eta_\Theta\zeta + D_{\alpha\beta} \sin\eta_\Theta(1-\zeta) \tag{17}$$

where function $f_\lambda(\cdot)$ is given by

$$f_\lambda(\xi) = \sin\lambda\xi - \frac{\sin\lambda}{\sinh\lambda}\sinh\lambda\xi \tag{18}$$

By applying the continuity condition at the node (α,β), the coefficients in Eqs. (16) and (17) are determined in terms of the angular displacements at the nodes (α-1,β), (α,β-1) and (α,β) as follows:

$$A_{\alpha\beta} = \frac{L_x}{\Delta(\lambda_\Theta)}[\, f'_{\lambda_\Theta}(1)\bar{\Theta}_{\alpha\beta} - f'_{\lambda_\Theta}(0)\bar{\Theta}_{\alpha-1\beta}\,]$$

$$B_{\alpha\beta} = \frac{L_x}{\Delta(\lambda_\Theta)}[\, f'_{\lambda_\Theta}(0)\bar{\Theta}_{\alpha\beta} - f'_{\lambda_\Theta}(1)\bar{\Theta}_{\alpha-1\beta}\,] \qquad (19)$$

$$C_{\alpha\beta} = \frac{\bar{\Theta}_{\alpha\beta}}{\sin\eta_\Theta}\ ; \qquad D_{\alpha\beta} = \frac{\bar{\Theta}_{\alpha\beta-1}}{\sin\eta_\Theta} \qquad (20)$$

where $\Delta(\cdot)$ is given by

$$\Delta(\lambda_\Theta) = 2\lambda_\Theta^2 \frac{\sin\lambda_\Theta}{\sinh\lambda_\Theta}(\,1 - \cos\lambda_\Theta \cosh\lambda_\Theta\,) \qquad (21)$$

It can be seen from Eq. (17) that $\sin\eta_\Theta = 0$ corresponds to a single span beam with clamped supports for the torsional motion.

2.2 Wave Motions and Dispersion Relation

Similar to the case of one-dimensional multi-span beam discussed in previous paper[9], only the motions at the periodic supports (nodes) of the structure are to be investigated. Note that the motions at all periodic nodes (supports) of the grillage are not independent, but they may belong to that of a two-dimensional harmonic wave, which may propagate through all the nodes of the grillage.

For the grillage structure presently considered, only rotational displacements are possible at the supports due to the transversely rigid constraint. Let $\Theta_{\alpha\beta}(t)$ be the angular displacement at node (α,β) shown in Fig. 1(b), which can be represented by a two dimensional harmonic wave propagating through node (or support) (α,β) as

$$\Theta_{\alpha\beta}(t) = C_\Theta e^{i[\omega t - (\mu_{\Theta,x}\alpha + \mu_{\Theta,y}\beta)]}, \quad \text{or}$$
$$\bar{\Theta}_{\alpha\beta} = C_\Theta e^{-i(\mu_{\Theta,x}\alpha + \mu_{\Theta,y}\beta)} \tag{22}$$

in which $\mu_{\Theta,x}$ and $\mu_{\Theta,y}$ are the components of a wave constant vector in the x and y directions, and C_Θ is the amplitude of the wave motion.

If this two dimensional harmonic wave can propagate through the periodic nodes of the grillage, the frequency parameters λ_Θ and η_Θ, which are functions of natural frequency ω and wave constants ($\mu_{\Theta,x}$, $\mu_{\Theta,y}$), must be related in a *dispersion equation* as follows

$$2\gamma_x\lambda_\Theta \frac{\sinh\lambda_\Theta(\cos\lambda_\Theta - \cos\mu_{\Theta,x}) - \sin\lambda_\Theta(\cosh\lambda_\Theta - \cos\mu_{\Theta,x})}{\cos\lambda_\Theta\cosh\lambda_\Theta - 1}$$
$$+ 2\sqrt{1-\gamma_x^2}\,\eta_\Theta \frac{\cos\eta_\Theta - \cos\mu_{\Theta,y}}{\sin\eta_\Theta} + \nu_x = 0 \tag{23}$$

where ν_x and γ_x are nondimensional parameters given by

$$\nu_x = k_x\left(\frac{D_x^2}{L_x^2} + \frac{C_y^2}{L_y^2}\right)^{-\frac{1}{2}}; \quad \gamma_x = \frac{D_x}{L_x}\left(\frac{D_x^2}{L_x^2} + \frac{C_y^2}{L_y^2}\right)^{-\frac{1}{2}}; \quad 0 \le \gamma_x \le 1 \tag{24}$$

The dispersion equation is obtained by substituting Eqs. (16) through (20) into the third condition in Eq. (6). The first and second terms in Eq. (23) indicate, respectively, the contributions from the bending motion of the beams in the x direction and the torsional motion of the beams in the y direction, and the last term is attributable to the external rotational spring k_x. When $\gamma_x = 0$ (or $D_x = 0$), the problem reduces to a purely torsional vibration of a multi-span beam with periodic elastic rotational constraints in the y-

direction. On the other hand, when $\gamma_x = 1$ (or $C_y = 0$), the problem becomes a purely bending vibration of a multi-span beam in the x-direction that has been discussed in the previous paper[9].

It should be noted that if the wave components $(\mu_{\theta,x}, \mu_{\theta,y})$ are replaced by

$$\begin{aligned} \mu_{\theta,x}^{(j_x)} &= \mu_{\theta,x} + 2j_x\pi \\ \mu_{\theta,y}^{(j_y)} &= \mu_{\theta,y} + 2j_y\pi \ , \quad (\ j_x, j_y = \pm 1, \pm 2, \ldots\ ) \end{aligned} \tag{25}$$

the dispersion equation, Eq. (23), remains unchanged. For free vibration analysis, we may, without loss of generality, choose $\mu_{\theta,x}$ and $\mu_{\theta,y}$ as follows

$$\begin{aligned} -\pi < \mu_{\theta,x} \leq \pi \ ; \\ -\pi < \mu_{\theta,y} \leq \pi \ . \end{aligned} \tag{26}$$

The range of $\mu_{\theta,x}$ and $\mu_{\theta,y}$ specified in Eq. (26) is known as the first *Brillouin zone* (Brillouin 1953) in the case of two dimensional periodic structure. A positive $\mu_{\theta,x}$ corresponds to a wave propagation in the positive x-direction, and a negative $\mu_{\theta,x}$ corresponds to that in the negative x-direction. The meaning of $\mu_{\theta,y}$ is analogous, except that it pertains to the y direction.

The natural frequencies of the grillage can be readily determined from the dispersion equation (23), given the values of wave constants $(\mu_{\theta,x}, \mu_{\theta,y})$, where λ_θ and η_θ are both functions of ω as seen from Eq. (15). Analogous to the one dimensional case, it can be seen from the dispersion equation that the natural frequency of the grillage is a multi-valued function of the wave constant. The relationship between λ_θ (or η_θ) and $(\mu_{\theta,x}, \mu_{\theta,y})$ in the propagating bands may be represented by a set of frequency surfaces as

shown in Fig. 2. Among four edges of each surface, the edge along which the value of λ_Θ (or η_Θ) is a constant as well as a maximum corresponds to an *upper-bound frequency*. These upper-bound frequencies can also be determined from one of the conditions, each of which is obtained by letting a denominator in the dispersion equation be zero, namely,

$$\begin{aligned} 1 - \cosh\lambda_\Theta \cos\lambda_\Theta &= 0 \\ \sin\eta_\Theta &= 0 \end{aligned} \tag{27}$$

The upper-bound frequencies along the edges $\mu_{\Theta,x} = 0$ and π, determined from the first condition in (27), correspond to a single span beam with clamped ends for bending motion. The upper-bound frequencies along the edges of $\mu_{\Theta,y} = 0$ are π, given by the second condition of Eq. (27), correspond to a single span beam with clamped ends for torsional motion. It is interesting to note that the propagation band (or frequency surface) between 1.5π and 2π for the grillage structure is a *non-propagating band* for a one-dimensional periodic multi-span beam, as shown in [9]. The range of a *non-propagating band* for the grillage structure becomes narrower due to the contribution of the torsional motion in the beams.

Analogously, the dispersion equation for the wave motion of $\Psi(t)$ has the same form as Eq. (23). It may be obtained easily from Eq. (23) by formally replacing the subscripts x and Θ by y and Ψ, respectively, to yield

$$2\gamma_y\lambda_\Psi \frac{\sinh\lambda_\Psi(\cos\lambda_\Psi - \cos\mu_{\Psi,y}) - \sin\lambda_\Psi(\cosh\lambda_\Psi - \cos\mu_{\Psi,y})}{\cos\lambda_\Psi\cosh\lambda_\Psi - 1}$$

$$+ 2\sqrt{1-\gamma_y^2}\,\eta_\Psi \frac{\cos\eta_\Psi - \cos\mu_{\Psi,x}}{\sin\eta_\Psi} + \nu_y = 0 \tag{28}$$

where

$$\lambda_\Psi = \left(\frac{m_y L_y^4}{D_y}\omega^2\right)^{\frac{1}{4}}; \quad \eta_\Psi = \left(\frac{n_x L_x^2}{C_x}\omega^2\right)^{\frac{1}{2}}, \quad \eta_\Psi = \kappa_y\lambda_\Psi^2 \tag{29}$$

$$\nu_y = k_y\left(\frac{D_y^2}{L_y^2} + \frac{C_x^2}{L_x^2}\right)^{-\frac{1}{2}}; \quad \gamma_y = \frac{D_y}{L_y}\left(\frac{D_y^2}{L_y^2} + \frac{C_x^2}{L_x^2}\right)^{-\frac{1}{2}}; \quad 0 \le \gamma_y \le 1 \tag{30}$$

2.3 Deflections of Bending and Torsional Motions

The bending and torsional deflections of the beams in the x and the y directions within an individual span can readily be obtained by substituting Eqs. (19) and (20) into Eqs. (16) and (17), where $\bar{\Theta}_{\alpha\beta}$ is given by Eq. (21). It is noted from Eqs. (19), (20) and (22) that the ratios $A_{\alpha\beta}/B_{\alpha\beta}$ and $C_{\alpha\beta}/D_{\alpha\beta}$ are independent of the span numbers α and β. This implies that deflections in two neighboring spans differ only by a phase shift. Thus, the deflections of bending and torsional motions of the entire structure can be represented as follows:

$$\bar{X}_{\alpha\beta}(\xi) = \bar{X}_{10}(\xi)\, e^{-i[\mu_{\bullet,x}(\alpha-1)+\mu_{\bullet,y}\beta]}, \quad (\alpha, \beta = 0, \pm1, \pm2, \ldots \pm\infty) \tag{31}$$

$$\bar{\theta}_{\alpha\beta}(\zeta) = \bar{\theta}_{01}(\zeta)\, e^{-i[\mu_{\Theta,x}\alpha + \mu_{\Theta,y}(\beta-1)]}, \quad (\alpha, \beta = 0, \pm 1, \pm 2, \ldots \pm\infty) \tag{32}$$

where

$$\bar{X}_{10}(\xi) = A_{10} f_{\lambda_\Theta}(\xi) + B_{10} f_{\lambda_\Theta}(1-\xi) \tag{33}$$

$$\bar{\theta}_{01}(\zeta) = C_{01} \sin\eta_\Theta \zeta + D_{01} \sin\eta_\Theta (1-\zeta) \tag{34}$$

and where $f_\lambda(\cdot)$ is defined in Eq. (18), and coefficients A_{10}, B_{10}, C_{01} and D_{01} are given for several cases as follows:

***Case a*: $\mu_{\Theta,x} \neq j_x\pi$ and $\mu_{\Theta,y} \neq j_y\pi$**

In this case, the wave motions of $\Theta_{\alpha\beta}(t)$ propagate in four directions, as shown in Fig. 3. The coefficients A_{10}, B_{10} and C_{01} and D_{01} are obtained from Eqs. (19) to (22)

$$\begin{aligned} A_{10} &= C\,[f'_{\lambda_\Theta}(1)\, e^{-i\mu_{\Theta,x}} - f'_{\lambda_\Theta}(0)], \\ B_{10} &= C\,[f'_{\lambda_\Theta}(0)\, e^{-i\mu_{\Theta,x}} - f'_{\lambda_\Theta}(1)] \end{aligned} \tag{35}$$

$$C_{01} = e^{-i\mu_{\Theta,y}}, \qquad D_{01} = 1 \tag{36}$$

where C is determined by using the continuity condition of angular displacement at the support (α,β), that is

$$L_x^{-1} \bar{X}'_{\alpha\beta}(\xi)\,|_{\xi=1} = \bar{\theta}_{\alpha\beta}(\zeta)\,|_{\zeta=1} = \bar{\Theta}_{\alpha\beta} \tag{37}$$

Eq. (37) is solved to yield

$$C = \frac{L_x \sin\eta_\Theta}{\Delta(\lambda_\Theta)} \tag{38}$$

where $\Delta(\cdot)$ is defined in Eq. (20).

Case b: $\mu_{\Theta,x} = j_x\pi$ **and** $\mu_{\Theta,y} \neq j_y\pi$

It should be noted that when $\mu_{\Theta,x} = j_x\pi$ the harmonic wave in the x direction has the appearance of a standing wave. As discussed in [9], the deflection in each span in the x direction coincides with a mode shape of single span beam with either idealized supported or fully clamped ends. The ratio between two angular displacements at two ends of a span in the x direction is

$$\frac{\bar{\Theta}_{\alpha\beta}}{\bar{\Theta}_{\alpha-1\beta}} = (-1)^{s_B}, \qquad s_B = \text{integer of } [\frac{\lambda_\Theta}{\pi}] \tag{39}$$

It follows from substituting Eq. (39) into Eq. (19) that

$$\frac{A_{\alpha\beta}}{B_{\alpha\beta}} = (-1)^{s_B+1} \tag{40}$$

Thus, the coefficients in Eqs. (33) and (34) are

$$A_{10} = 1, \qquad B_{10} = (-1)^{s_B+1} \tag{41}$$

$$C_{01} = C e^{-i\mu_{\Theta,y}}, \qquad D_{01} = C \tag{42}$$

where C may be determined from Eq. (37) to yield

$$C = (-1)^{j_x} \frac{f'_{\lambda_\Theta}(1) - (-1)^{s_B+1} f'_{\lambda_\Theta}(0)}{L_x \sin\eta_\Theta} \tag{43}$$

Case c: $\mu_{\Theta,x} \neq j_x\pi$ **and** $\mu_{\Theta,y} = j_y\pi$

Contrary to case b, the wave motion in the y direction has a standing wave appearance. The torsional motion in the y direction in each span has the same form as

that of a single span beam with either simply supported or fully clamped ends. The corresponding angular displacements at the two ends of a span in the y direction are related as

$$\frac{\bar{\Theta}_{\alpha\beta}}{\bar{\Theta}_{\alpha\beta-1}} = (-1)^{s_T+1}, \qquad s_T = \text{integer part of } [\frac{\eta_\Theta}{\pi}] \tag{44}$$

which is based on the fact that the odd-numbered (even-numbered) mode shapes of a single span beam for torsional motions are symmetric (anti-symmetric) with respect to the mid-point of the span for either simply supported or fully clamped ends. Hence, the coefficients in Eqs. (33) and (34) are obtained as

$$\begin{aligned} A_{10} &= C\,[f'_{\lambda_\Theta}(1)\,e^{-i\mu_{\Theta x}} - f'_{\lambda_\Theta}(0)]\,, \\ B_{10} &= C\,[f'_{\lambda_\Theta}(0)\,e^{-i\mu_{\Theta x}} - f'_{\lambda_\Theta}(1)] \end{aligned} \tag{45}$$

$$C_{01} = 1\,, \qquad D_{01} = (-1)^{s_T+1} \tag{46}$$

in which

$$C = (-1)^{j_y}\frac{L_x \sin\eta_\Theta}{\Delta(\lambda_\Theta)} \tag{47}$$

***Case d*: $\mu_{\Theta x} = j_x\pi$ and $\mu_{\Theta y} = j_y\pi$**

In this specific case, the motion has the form of a standing wave in both the x and y directions. Combining the cases b and c, we have

$$A_{10} = L_x \sin\eta_\Theta\,(-1)^{j_x}\,, \qquad B_{10} = A_{10}(-1)^{s_\beta+1} \tag{48}$$

$$C_{01} = \left[f'_{\lambda_0}(1) - (-1)^{s_r+1} f'_{\lambda_0}(0) \right](-1)^{j_y}, \quad D_{01} = C_{01}(-1)^{s_r+1} \tag{49}$$

3. Free Vibration of a Finite-Size Grillage

3.1 Boundary Conditions along the Exterior Edges

For a grillage of finite size, having N_x spans in the x direction and N_y spans in the y direction, the boundary conditions along the four exterior edges should be imposed. These four edges are identified as $\alpha = 0$, $\alpha = N_x$, $\beta = 0$ and $\beta = N_y$. Each boundary is treated as an edge-beam, with one-half the elastic and inertia properties of an interior beam. The boundary conditions at each node along each edge may be expressed in the following general form

$$\begin{aligned} k_{\alpha\beta}\Theta_{\alpha\beta}(t) = D_x\left(1 - \frac{1}{2}\delta_{0\beta} - \frac{1}{2}\delta_{N_y\beta}\right)\left[(1-\delta_{\alpha N_x})X''_{\alpha+1\beta}(0,t) - (1-\delta_{\alpha 0})X''_{\alpha\beta}(1,t)\right] \\ + C_y\left(1 - \frac{1}{2}\delta_{\alpha 0} - \frac{1}{2}\delta_{\alpha N_x}\right)\left[(1-\delta_{N_y\beta})\,\theta'_{\alpha\beta+1}(0,t) - (1-\delta_{0\beta})\,\theta'_{\alpha\beta}(1,t)\right] \end{aligned} \tag{50}$$

where δ_{ij} is the Kronecker delta. The case $k_{\alpha\beta} = \infty$ represents a clamped edge, for which the boundary condition (50) reduces to $\Theta_{\alpha\beta}(t) = 0$ (or $\bar{\Theta}_{\alpha\beta} = 0$). The case

$$k_{\alpha\beta} = \frac{1}{2}\left(1 - \frac{1}{2}\sum_{r=0,N_x}\sum_{s=0,N_y}\delta_{\alpha r}\delta_{s\beta}\right)k_x \tag{51}$$

will be referred to as an *ideally supported* edge.

3.2 Mode Shapes of Bending and Torsional Motions

For a grillage of finite size there generally exist four wave motions in different

directions, as shown in Fig. 3, sharing the same frequency ω, due to reflections at the boundaries. By taking into account these four wave motions, the angular displacement function at node (α,β) becomes

$$\bar{\Theta}_{\alpha\beta} = c_1 e^{-i(\mu_{\Theta,x}\alpha + \mu_{\Theta,y}\beta)} + c_2 e^{i(\mu_{\Theta,x}\alpha + \mu_{\Theta,y}\beta)} + c_3 e^{-i(\mu_{\Theta,x}\alpha - \mu_{\Theta,y}\beta)} + c_4 e^{i(\mu_{\Theta,x}\alpha - \mu_{\Theta,y}\beta)} \tag{52}$$

where c_k {k=1,2,3,4} are constants to be determined by imposing the boundary conditions. In view of Eqs. (16) through (20), the mode shapes of such a grillage can be obtained by combining the above four wave motions. Analogous to the case of a grillage of infinite size, these mode shapes are formulated for the following four cases:

Case *a*: $\mu_{\Theta,x} \neq j_x\pi$ **and** $\mu_{\Theta,y} \neq j_y\pi$

In this case, four wave motions in (50) propagate in directions not parallel to the x or the y axis shown in Fig. 3. Once the value of $\bar{\Theta}_{\alpha\beta}$ is determined, the mode shapes for the bending and torsional motions are obtained from Eqs. (16) and (17) with the coefficients given in Eqs. (19) and (20), respectively.

The case of a grillage with clamped edges along the four edges is selected as an illustrative example. The other cases are listed in Table 1. Upon imposing the boundary conditions along the edges of α = 0 and β = 0, i.e.

$$\begin{aligned} \bar{\Theta}_{0\beta} &= 0 , \quad (\beta = 0,1,2,\ldots,N_y) \\ \bar{\Theta}_{\alpha 0} &= 0 , \quad (\alpha = 0,1,2,\ldots,N_x) \end{aligned} \tag{53}$$

we obtain $C_1 = C_2 = -C_3 = -C_4 = -C$. Thus, Eq. (52) reduces to

$$\bar{\Theta}_{\alpha,\beta} = 4C \sin\mu_{\Theta,x}\alpha \sin\mu_{\Theta,y}\beta \tag{54}$$

By imposing on equation (54) the other two boundary conditions along the edges $\alpha = N_x$ and $\beta = N_y$

$$\begin{aligned} \bar{\Theta}_{N_x,\beta} &= 0 , \quad (\beta = 0,1,2,\ldots,N_y) \\ \bar{\Theta}_{\alpha N_y} &= 0 , \quad (\alpha = 0,1,2,\ldots,N_x) \end{aligned} \tag{55}$$

we then have

$$\sin\mu_{\Theta,x}N_x = 0 ; \quad \sin\mu_{\Theta,y}N_y = 0 \tag{56}$$

Therefore,

$$\begin{aligned} \mu_{\Theta,x} &= \frac{j}{N_x}\pi , \quad (j = 1,2,\ldots,N_x-1) \\ \mu_{\Theta,y} &= \frac{k}{N_y}\pi , \quad (k = 1,2,\ldots,N_y-1) \end{aligned} \tag{57}$$

Table 1 lists the angular displacement functions $\bar{\Theta}_{\alpha\beta}$ and the equations for obtaining the wave constants $\mu_{\Theta x}$ and $\mu_{\Theta y}$ for all sixteen sets of boundary conditions.

It is seen from the Table 1 that when a pair of opposite edges of a grillage are either *ideally supported* or clamped, the associated wave constants in that direction can also be an integer multiple of π. These cases are discussed in detail in the following sections.

Case *b*: $\mu_{\Theta,x} = j_x\pi$ **or** $\mu_{\Theta,y} \neq j_y\pi$

In this case, a pair of opposite boundary edges parallel to the y direction can be either *ideally supported* or clamped. Then the $\Theta_{\alpha\beta}(t)$ motion can be represented by two

waves propagating in the positive and negative y-direction. In view of Eqs. (31) and (32), the mode shapes for the bending and torsional motions may be written as follows

$$\bar{X}_{\alpha\beta}(\xi) = \bar{X}_{10}(\xi)(-1)^{j_x(\alpha-1)}(c_1 e^{-i\mu_{\Theta,y}\beta} + c_2 e^{i\mu_{\Theta,y}\beta}) \tag{58}$$

$$\bar{\theta}_{\alpha\beta}(\zeta) = \left\{c_1\bar{\theta}_{01}(\zeta)e^{-i\mu_{\Theta,y}(\beta-1)} + c_2\bar{\theta}^*_{01}(\zeta)e^{i\mu_{\Theta,y}(\beta-1)}\right\}(-1)^{j_x\alpha} \tag{59}$$

where asterisk denotes the complex conjugate and $\bar{X}_{10}(\xi)$ and $\bar{\theta}_{01}(\zeta)$ are given in Eqs. (33) and (34) with the coefficients specified by Eqs. (41) through (43). The coefficients c_1 and c_2 in Eqs. (58) and (59) are determined by using the boundary condition along edge $\beta = 0$ for the following two cases, namely, the *ideally supported* and the clamped edges.

Consider first the case in which the boundary along $\beta = 0$ is clamped, i.e. $\bar{\Theta}_{\alpha 0} = \bar{\theta}_{\alpha 0}(1) = 0$. The opposite boundary along $\beta = N_y$ could be either the *ideally supported* or clamped. Imposing the boundary condition $\bar{\Theta}_{\alpha 0} = 0$ on Eq. (59) results in $c_1 = -c_2$. Thus, the mode shapes for the bending and torsional motions reduce to

$$\bar{X}_{\alpha\beta}(\xi) = \bar{X}_{10}(\xi)(-1)^{j_x(\alpha-1)}\sin\mu_{\Theta,y}\beta \tag{60}$$

$$\bar{\theta}_{\alpha\beta}(\zeta) = Im\left\{\bar{\theta}^*_{01}(\zeta)e^{i\mu_{\Theta,y}(\beta-1)}\right\}(-1)^{j_x\alpha} \tag{61}$$

where $Im\{\cdot\}$ denotes the imaginary part of a complex expression, and the common factor $2ic_2$ has been omitted.

Consider next the case of *ideally supported* edge along $\beta = 0$. The opposite boundary along $\beta = N_y$ may be either the *ideally supported* or the clamped edges. The boundary condition along $\beta = 0$ obtained from (50) has the form of

$$\frac{1}{2}k_x\bar{\Theta}_{\alpha 0} = \frac{1}{2}D_x[\,\bar{X}''_{\alpha+1\,0}(0) - \bar{X}''_{\alpha 0}(1)\,] + C_y\,\bar{\theta}'_{\alpha 1}(0)\,, \qquad (\alpha = 1,2,\ldots,N_x-1) \tag{62}$$

Substituting Eqs. (58) and (59) into Eq. (62), we conclude that if $c_1 = c_2$. Then Eq.(62) is equivalent to the dispersion equation Eq. (23) in the special case of $\mu_{\Theta,x} = j_x\pi$. It follows from Eqs. (58) and (59) that the mode shapes for the bending and torsional motions are

$$\bar{X}_{\alpha\beta}(\xi) = \bar{X}_{1\,0}(\xi)\,(-1)^{j_x(\alpha-1)}\cos\mu_{\Theta,y}\beta \tag{63}$$

$$\bar{\theta}_{\alpha\beta}(\zeta) = Re\left\{\bar{\theta}_{0\,1}(\zeta)\,e^{-i\mu_{\Theta,y}(\beta-1)}\right\}(-1)^{j_x\alpha} \tag{64}$$

where $Re\{\cdot\}$ denotes the real part of a complex expression.

Of course, Eqs. (63) and (64) are equivalent to Eqs. (60) and (61) when one edge is *ideally supported* and the opposite edge is clamped.

Case *c*: $\mu_{\Theta,x} \neq j_x\pi$ and $\mu_{\Theta,y} = j_y\pi$

Analogous to Case b, the motion can be represented by two waves propagating in the positive and the negative x-direction. Two opposite edges parallel to the x direction can be either clamped or *ideally supported.* The following mode shapes of the bending and torsional motions are obtained from Eqs. (31) through (34), with the coefficients given by Eqs. (45), (46) and (47)

$$\bar{X}_{\alpha\beta}(\xi) = \left[\, c_1\bar{X}_{1\,0}(\xi)\,e^{-i\mu_{\Theta,x}(\alpha-1)} + c_2\bar{X}^{*}_{1\,0}(\xi)\,e^{i\mu_{\Theta,x}(\alpha-1)}\,\right](-1)^{j_y\beta} \tag{65}$$

$$\bar{\theta}_{\alpha\beta}(\zeta) = \bar{\theta}_{01}(\zeta)(-1)^{j_y(\beta-1)}\left[c_1 e^{-i\mu_{\theta,x}\alpha} + c_2 e^{i\mu_{\theta,x}\alpha}\right] \tag{66}$$

Let the edge along $\alpha = 0$ be clamped; i.e. $\bar{\Theta}_{0\beta} = 0$, where $\beta = 1,2,...,N_y-1$. The opposite edge along $\alpha = N_x$ may be either clamped or *ideally supported.* By imposing the boundary condition along $\alpha = 0$ on Eq. (66), we find $c_1 = -c_2$. Thus, the expressions for mode shapes Eqs. (65) and (66) reduce to -

$$\bar{X}_{\alpha\beta}(\xi) = Im\left\{\bar{X}^{*}_{10}(\xi) e^{i\mu_{\theta,x}(\alpha-1)}\right\}(-1)^{j_y\beta} \tag{67}$$

$$\bar{\theta}_{\alpha\beta}(\zeta) = \bar{\theta}_{01}(\zeta)(-1)^{j_y(\beta-1)}\sin\mu_{\theta,x}\alpha \tag{68}$$

If the edge along $\alpha = 0$ is *ideally supported,* then the boundary condition may be obtained from Eq. (50) as follows

$$\frac{1}{2}k_x\bar{\Theta}_{0\beta} = D_x\bar{X}''_{1\beta}(0) + \frac{1}{2}C_y[\,\bar{\theta}'_{0\beta+1}(0) - \bar{\theta}'_{0\beta}(1)\,] \qquad (\beta = 1,2,...,N_y-1) \tag{69}$$

The edge along $\alpha = N_x$ may be either ideally supported or clamped. Substitution of Eqs. (65) and (66) into the boundary condition Eq. (69), and use of dispersion equation (23) result in $c_1 = c_2$. Hence, the mode shapes in this case become

$$\bar{X}_{\alpha\beta}(\xi) = Re\left\{\bar{X}_{10}(\xi) e^{-i\mu_{\theta,x}(\alpha-1)}\right\}(-1)^{j_y\beta} \tag{70}$$

$$\bar{\theta}_{\alpha\beta}(\zeta) = \bar{\theta}_{01}(\zeta)(-1)^{j_y(\beta-1)}\cos\mu_{\theta,x}\alpha \tag{71}$$

Case *d*: $\mu_{\theta,x} = j_x\pi$ **and** $\mu_{\theta,y} = j_y\pi$

In this case, each pair of opposite edges must be both clamped or both *ideally*

supported, and the mode shapes coincide with the deflection shapes of a grillage of infinite size. These mode shapes may be expressed as follows:

$$\bar{X}_{\alpha\beta}(\xi) = \bar{X}_{10}(\xi)(-1)^{j_x(\alpha-1)+j_y\beta} \tag{72}$$

$$\bar{\theta}_{\alpha\beta}(\zeta) = \bar{\theta}_{01}(\zeta)(-1)^{j_x\alpha+j_y(\beta-1)} \tag{73}$$

where $\bar{X}_{10}(\xi)$ and $\bar{\theta}_{01}(\zeta)$ are given by Eqs. (33) and (34), and the associated coefficients are specified by Eqs. (48) and (49).

3.3 Example and Discussion

As an example, a grillage of finite size, consisting of four spans each in the x and y directions (N_x = 4 and N_y = 4) with all clamped edges is investigated. The nondimensional parameters are chosen as $\nu_x = 0$, $\gamma_x = 0.5$, $\kappa_x = 0.08$.

The wave constants and the associated frequencies obtained from the first and second frequency surfaces are listed in Table 2. It is seen from Figs. 2(a) and 2(b) that the first upper-bound frequency occurs at $\mu_{\Theta,x} = 0$, whereas the second upper-bound frequency appears at $\mu_{\Theta,y} = \pi$. Note that the first upper-bound frequency corresponds to a bending motion of the beams in the x- direction, whereas the second upper-bound frequency corresponds to a torsional motion of the beams in the y-direction. For emphasis, each of these is marked by an asterisk in Table 2.

The mode shapes in the spans in the x- and y-directions are shown in Figs. 3(a)-3(m) for both bending and torsional motions, where the parameters are fixed at $\nu_x = 0.5$, $\gamma_x = 0.5$, $\kappa_x = 0.08$. It is seen that the mode shapes of the bending and torsional motions

for all spans are related, since they must be consistent at the nodes. Moreover, the mode shapes must be either symmetric or anti-symmetric since the boundary conditions on opposite edges are symmetric in this case. The mode shape corresponding to each upper-bound frequency in the first column in Table 2 is devoid of torsional motion. In contrast, the mode shapes corresponding to each upper-bound frequency in the second column is devoid of bending motion.

4. Conclusions

Exact solutions have been obtained for wave propagation in a periodic grillage of infinite size, and for free vibration of one of finite size. Attention is focused on the motion at the periodic supports, thus by-passing the complicated motion between two neighboring supports. It is shown that the non-propagation frequency bands are narrower for a two-dimensional grillage structure than that of a one-dimensional periodic multi-span beam. The mode shapes of free vibration for both bending and torsional motions obtained herein may be used in a forced vibration analysis using the normal mode approach. One implicit assumption in the present analysis is that wave propagation in the x and y directions are synchronized such that they appear as components of a "plane" wave propagating in an oblique direction. The possibility of a "curvilinear" wave front will not be considered at this time.

Table 1. Angular displacement and wave constants of grillage of finite size with various boundary conditions.

Boundary conditions	$\bar{\Theta}_{\alpha,\beta}$ ($\mu_{\theta,x} \neq m_x\pi$, $\mu_{\theta,y} \neq m_y\pi$)	Equations for $\mu_{\theta,x}$ and $\mu_{\theta,y}$
C_x-C_x and C_y-C_y	$\sin\mu_{\theta,x}\alpha \sin\mu_{\theta,y}\beta$	$\sin\mu_{\theta,x}N_x=0$; $\sin\mu_{\theta,y}N_y=0$
S_x-S_x and C_y-C_y	$\cos\mu_{\theta,x}\alpha \sin\mu_{\theta,y}\beta$	$\sin\mu_{\theta,x}N_x=0$; $\sin\mu_{\theta,y}N_y=0$
S_x-C_x and C_y-C_y	$\cos\mu_{\theta,x}\alpha \sin\mu_{\theta,y}\beta$	$\cos\mu_{\theta,x}N_x=0$; $\sin\mu_{\theta,y}N_y=0$
C_x-S_x and C_y-C_y	$\sin\mu_{\theta,x}\alpha \sin\mu_{\theta,y}\beta$	$\cos\mu_{\theta,x}N_x=0$; $\sin\mu_{\theta,y}N_y=0$
C_x-C_x and S_y-S_y	$\sin\mu_{\theta,x}\alpha \cos\mu_{\theta,y}\beta$	$\sin\mu_{\theta,x}N_x=0$; $\sin\mu_{\theta,y}N_y=0$
C_x-S_x and S_y-S_y	$\sin\mu_{\theta,x}\alpha \cos\mu_{\theta,y}\beta$	$\cos\mu_{\theta,x}N_x=0$; $\sin\mu_{\theta,y}N_y=0$
S_x-C_x and S_y-S_y	$\cos\mu_{\theta,x}\alpha \cos\mu_{\theta,y}\beta$	$\cos\mu_{\theta,x}N_x=0$; $\sin\mu_{\theta,y}N_y=0$
S_x-S_x and S_y-S_y	$\cos\mu_{\theta,x}\alpha \cos\mu_{\theta,y}\beta$	$\sin\mu_{\theta,x}N_x=0$; $\sin\mu_{\theta,y}N_y=0$
C_x-C_x and C_y-S_y	$\sin\mu_{\theta,x}\alpha \sin\mu_{\theta,y}\beta$	$\sin\mu_{\theta,x}N_x=0$; $\cos\mu_{\theta,y}N_y=0$
C_x-C_x and S_y-C_y	$\sin\mu_{\theta,x}\alpha \cos\mu_{\theta,y}\beta$	$\sin\mu_{\theta,x}N_x=0$; $\cos\mu_{\theta,y}N_y=0$
C_x-S_x and C_y-S_y	$\sin\mu_{\theta,x}\alpha \sin\mu_{\theta,y}\beta$	$\cos\mu_{\theta,x}N_x=0$; $\cos\mu_{\theta,y}N_y=0$
C_x-S_x and S_y-C_y	$\sin\mu_{\theta,x}\alpha \cos\mu_{\theta,y}\beta$	$\cos\mu_{\theta,x}N_x=0$; $\cos\mu_{\theta,y}N_y=0$
S_x-S_x and C_y-S_y	$\cos\mu_{\theta,x}\alpha \sin\mu_{\theta,y}\beta$	$\sin\mu_{\theta,x}N_x=0$; $\cos\mu_{\theta,y}N_y=0$
S_x-S_x and S_y-C_y	$\cos\mu_{\theta,x}\alpha \cos\mu_{\theta,y}\beta$	$\sin\mu_{\theta,x}N_x=0$; $\cos\mu_{\theta,y}N_y=0$
S_x-C_x and C_y-S_y	$\cos\mu_{\theta,x}\alpha \sin\mu_{\theta,y}\beta$	$\cos\mu_{\theta,x}N_x=0$; $\cos\mu_{\theta,y}N_y=0$
S_x-C_x and S_y-C_y	$\cos\mu_{\theta,x}\alpha \cos\mu_{\theta,y}\beta$	$\cos\mu_{\theta,x}N_x=0$; $\cos\mu_{\theta,y}N_y=0$

Note: C_x, C_y = clamped support; S_x, S_y = ideal support; subscripts indicate direction. N_x = number of spans in the x-direction; N_y = number of spans in the y-direction.

Table 2. The first two groups of frequencies of a finite-size grillage(N_x=4, N_y=4) with all edges clamped (ν_x=0, γ_x=0.5, η_x=0.08)

$\mu_{\theta,x}=\frac{i\pi}{N_x}$ i	$\mu_{\theta,y}=\frac{j\pi}{N_y}$ j	$\frac{\lambda_\theta^{(1)}}{\pi}$	$\frac{\lambda_\theta^{(2)}}{\pi}$
0	1	1.5056*	—
0	2	1.5056*	—
0	3	1.5056*	—
0	4	—	—
1	1	1.3829	1.6852
1	2	1.4198	1.7664
1	3	1.4422	1.8882
1	4	—	1.9947* ($\eta_\theta=\pi$)
2	1	1.2162	1.7729
2	2	1.2752	1.8386
2	3	1.3185	1.9332
2	4	—	1.9947* ($\eta_\theta=\pi$)
3	1	1.0666	1.8207
3	2	1.1478	1.8775
3	3	1.2076	1.9531
3	4	—	1.9947* ($\eta_\theta=\pi$)

Note: An asterisk denotes an upper-bound frequency.

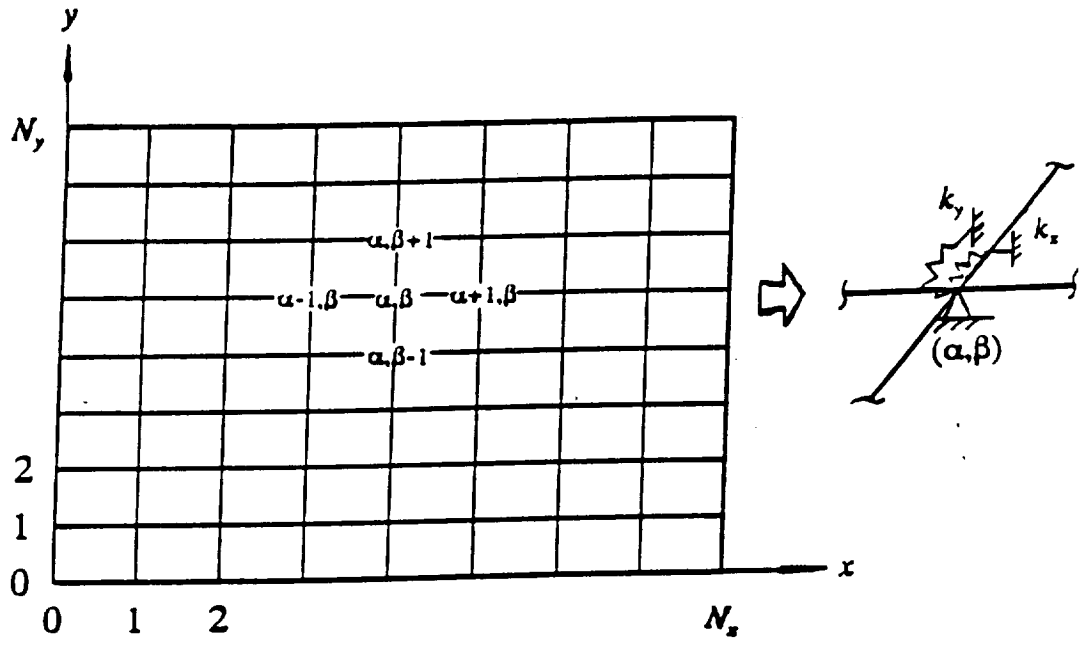

Fig. 1(a) Periodic grillage with rotational constraints at each node

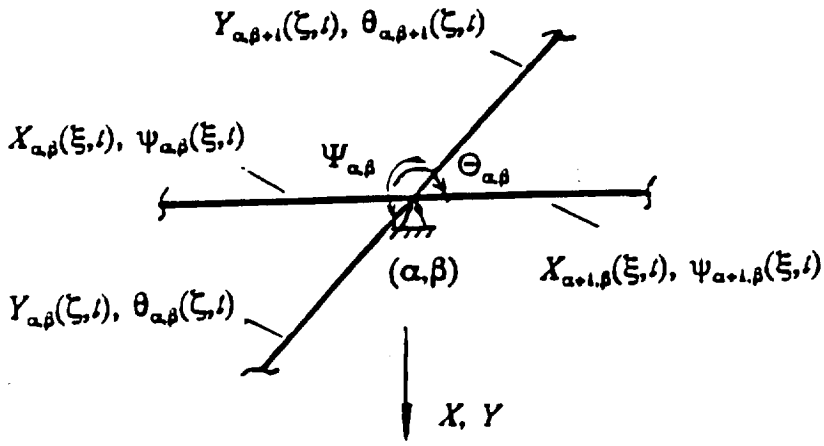

Fig. 1(b) Notations for displacements at node (α,β)

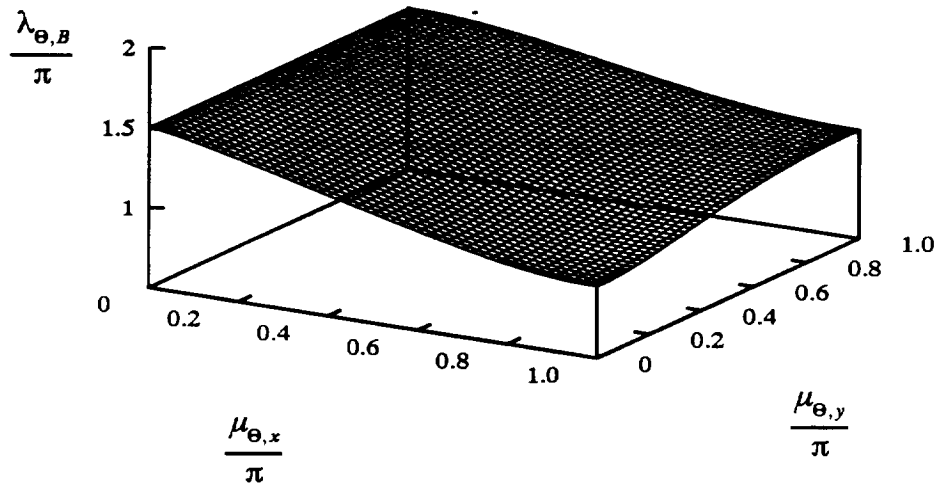

(a). The first frequency surface

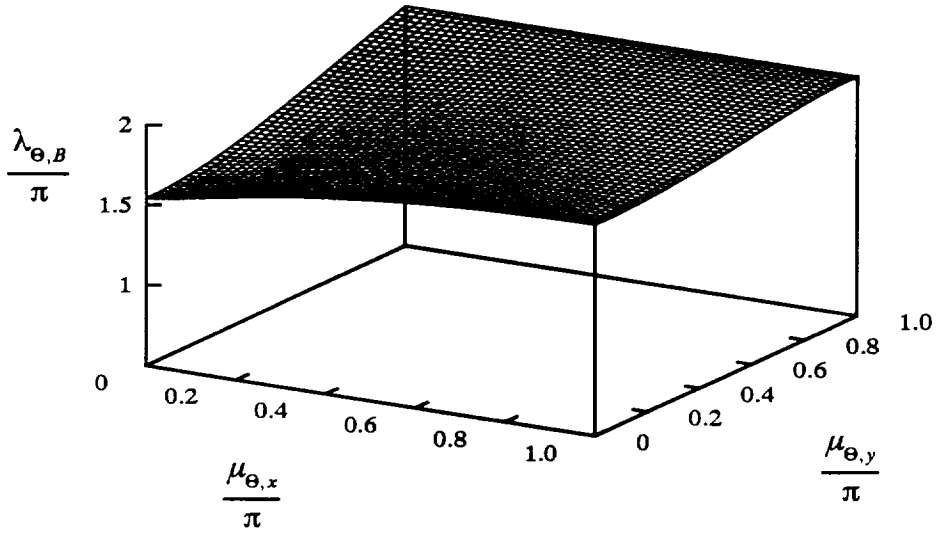

(b). The second frequency surface

Fig. 2 Dispersion relationship of wave motion in a grillage

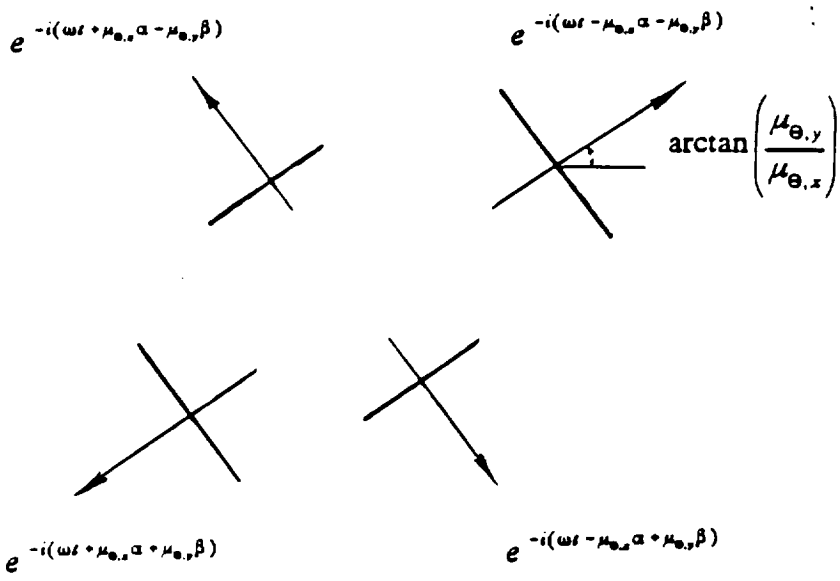

Fig. 3 Wave propagation in four directions in a grillage of finite size

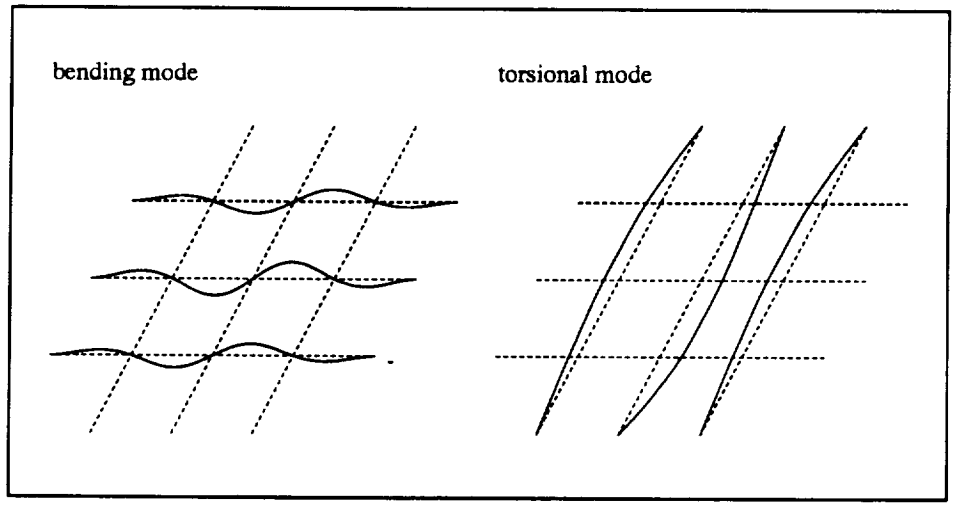

4(a). $\mu_{\Theta,x} = 3\pi/4$, $\mu_{\Theta,y} = \pi/4$; $\lambda_{\Theta} = 1.0981\pi$

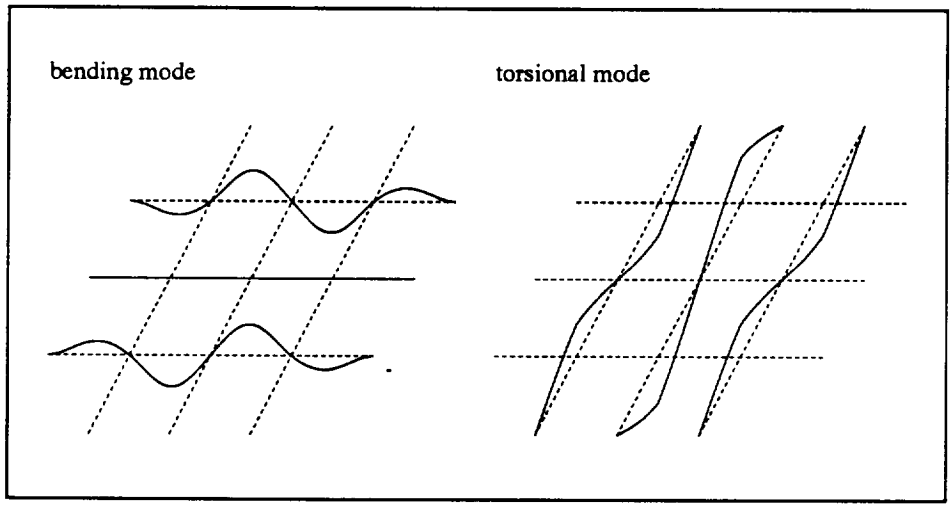

4(b) $\mu_{\Theta,x} = 3\pi/4$, $\mu_{\Theta,y} = 2\pi/4$; $\lambda_{\Theta} = 1.1696\pi$

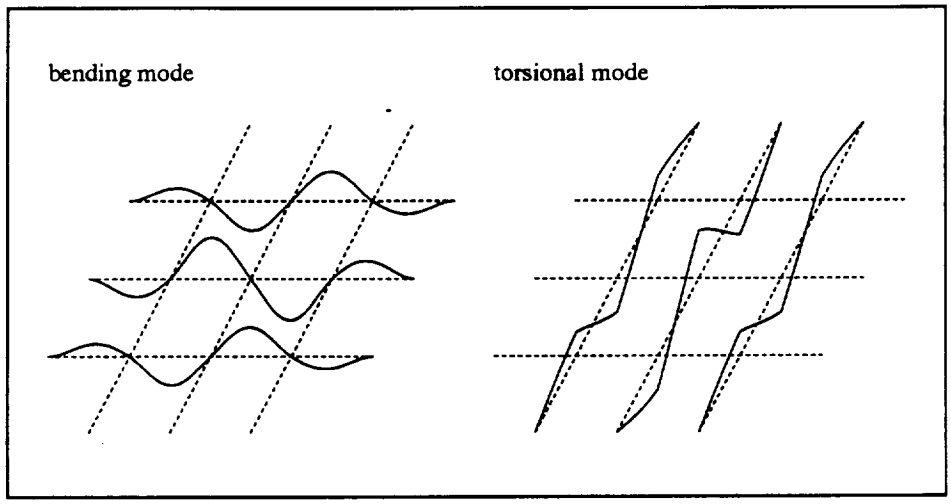

4(c). $\mu_{\Theta,x} = 3\pi/4$, $\mu_{\Theta,y} = 3\pi/4$; $\lambda_{\Theta} = 1.22351\pi$

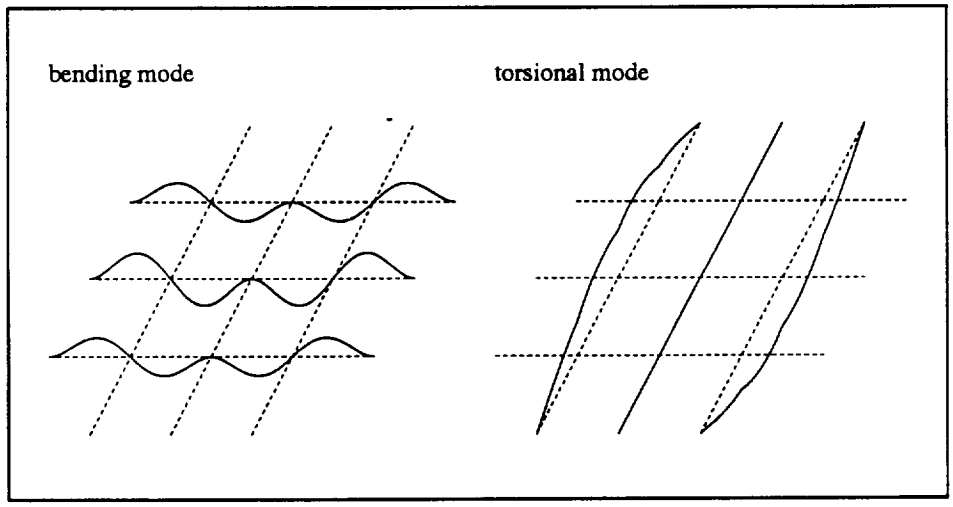

4(d) $\mu_{\Theta,x} = 2\pi/4$, $\mu_{\Theta,y} = \pi/4$; $\lambda_{\Theta} = 1.2369\pi$

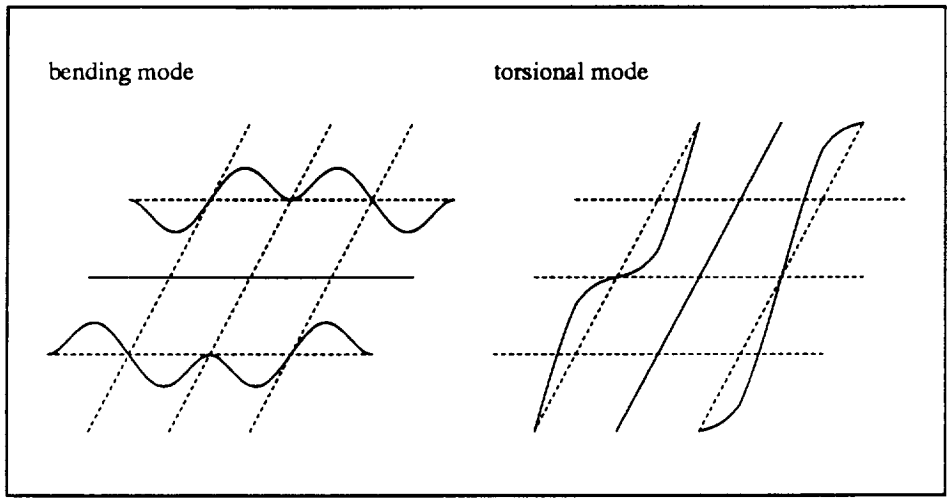

4(e) $\mu_{\Theta,x} = 2\pi/4$, $\mu_{\Theta,y} = 2\pi/4$; $\lambda_{\Theta} = 1.2896\pi$

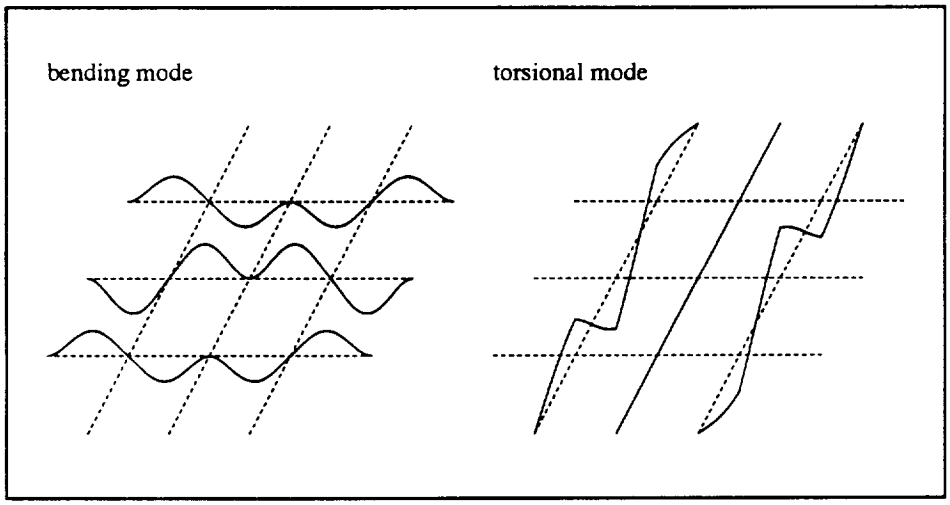

4(f). $\mu_{\Theta,x} = 2\pi/4$, $\mu_{\Theta,y} = 3\pi/4$; $\lambda_{\Theta} = 1.3288\pi$

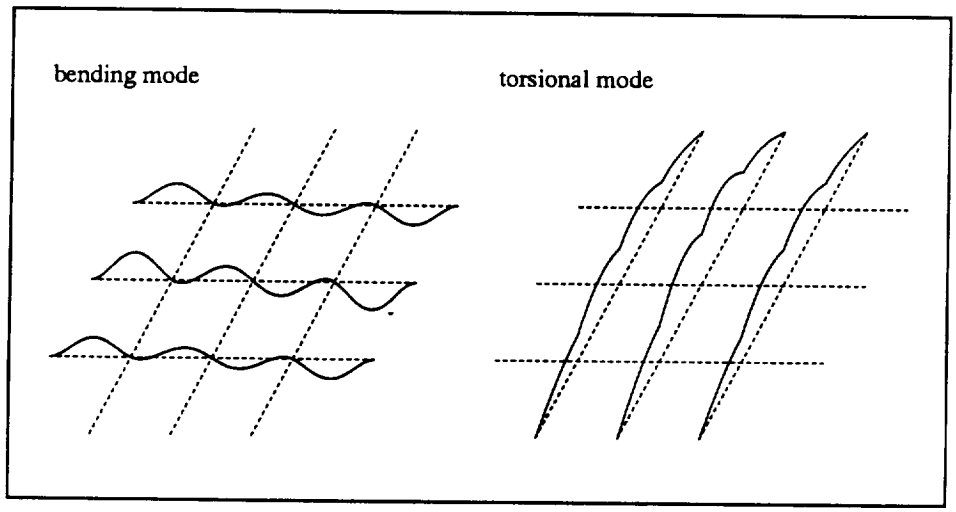

4(g). $\mu_{\Theta,x} = \pi/4$, $\mu_{\Theta,y} = \pi/4$; $\lambda_{\Theta} = 1.3946\pi$

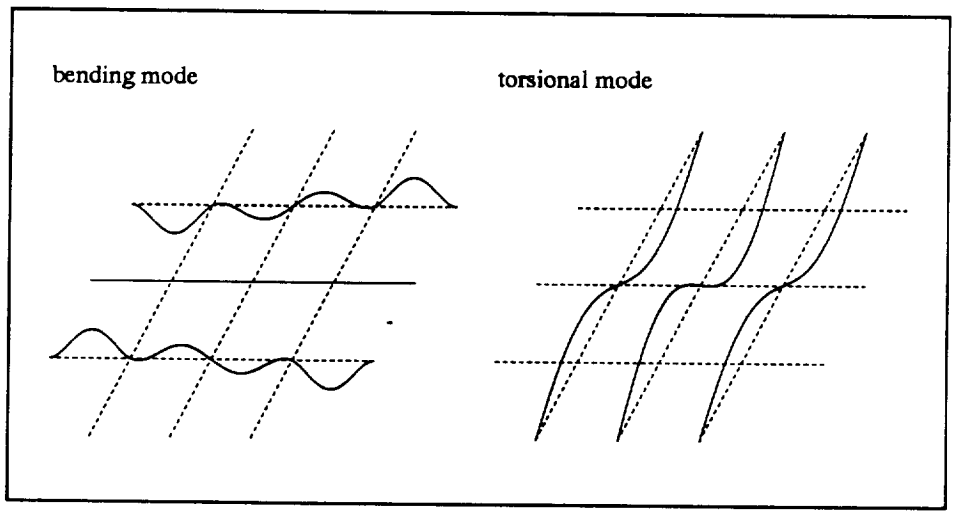

4(h). $\mu_{\Theta,x} = \pi/4$, $\mu_{\Theta,y} = 2\pi/4$; $\lambda_{\Theta} = 1.4266\pi$

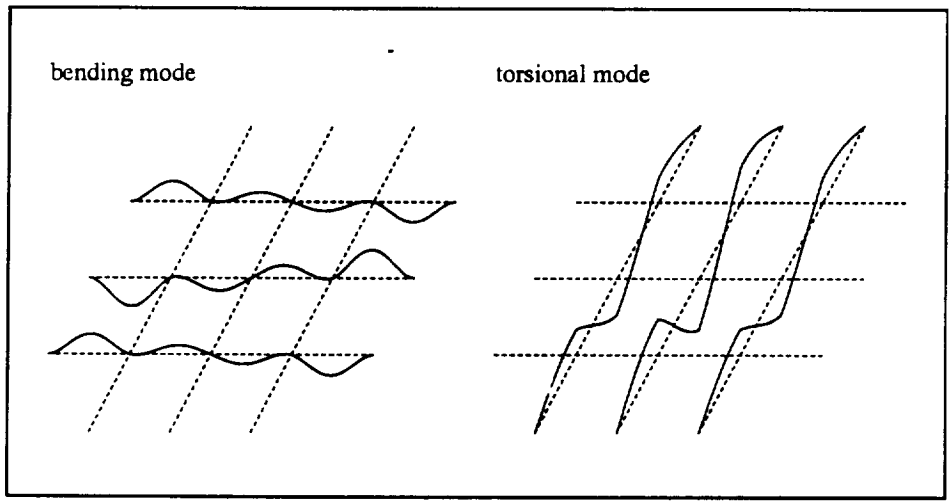

4(i). $\mu_{\Theta,x} = \pi/4$, $\mu_{\Theta,y} = 3\pi/4$; $\lambda_{\Theta} = 1.4462\pi$

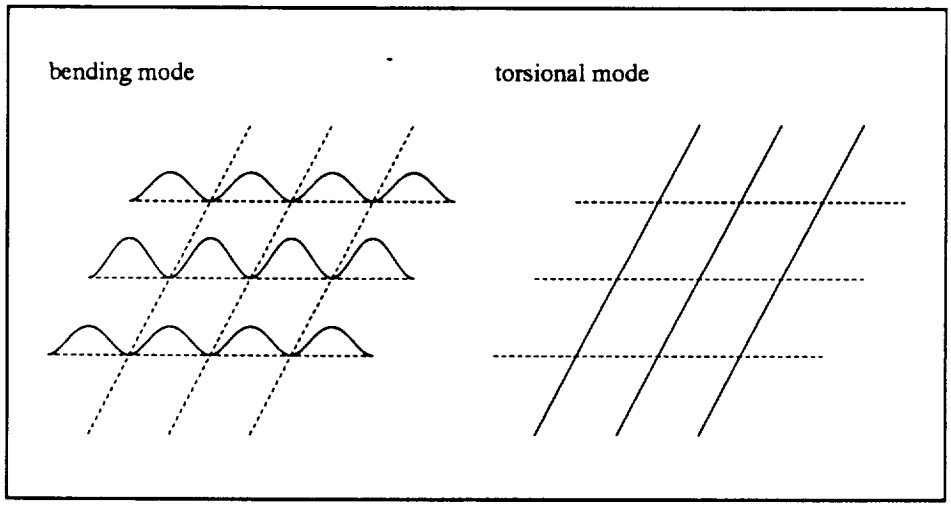

4(j). $\mu_{\Theta,x} = 0$, $\mu_{\Theta,y} = \pi/4$; $\lambda_{\Theta} = 1.5056\pi$

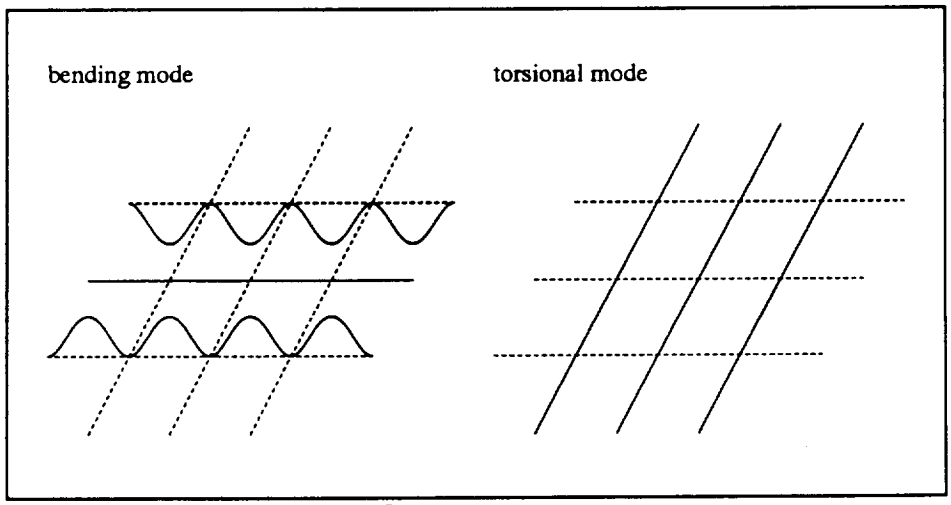

4(k). $\mu_{\theta,x} = 0,\ \mu_{\theta,y} = 2\pi/4;\ \lambda_\theta = 1.5056\pi$

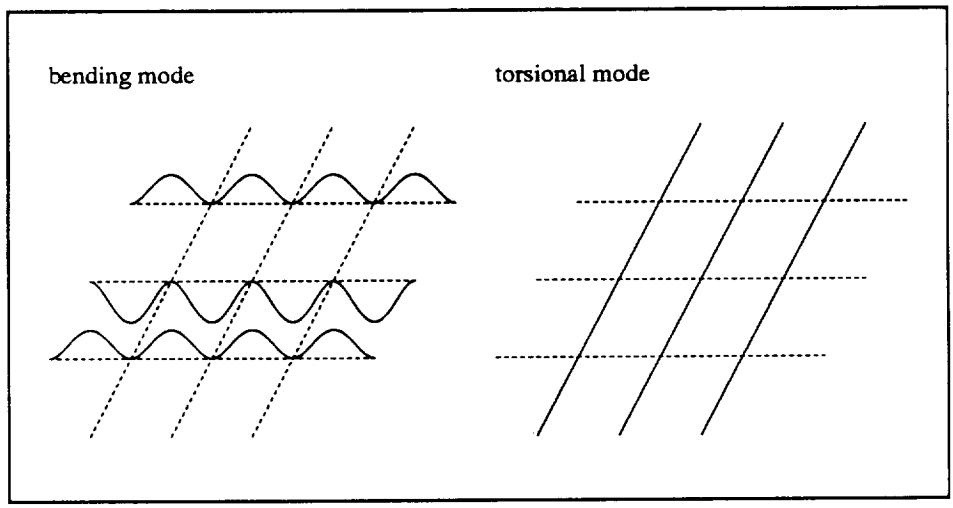

4(l). $\mu_{\theta,x} = 0,\ \mu_{\theta,y} = 3\pi/4;\ \lambda_\theta = 1.5056\pi$

Fig. 4 Mode shapes of grillage with clamped edges ($\nu_x = \gamma_x = 0.5;\ \kappa_x = 0.08$)

REFERENCES

1. Brillouin, L., Wave Propagation in Periodic Structures, Dover, New York, 1953.

2. Dinkevich, S., "Vibration of grillage", Private communication to Dr. I. Elishakoff, 1993.

3. Ellington, J. P., and McCallion, H., "Moments and deflections of a simply supported beam grillage," Aeronautical Quarterly, Vol. 8, 360-370, 1957.

4. Ellington, J. P., and McCallion, H., "The free vibrations of grillages," Journal of Applied Mechanics, Vol. 26, 603-610, 1959.

5. Timoshenko, S., and Woinowsky-Krieger, S., Theory of Plate and Shells, pp. 190, 392, New York, McGraw-Hill Book Company, Inc, 1959.

6. Wah, T., "Natural frequencies of uniform grillages," Journal of Applied Mechanics, Vol. 30, 571-580, 1963.

7. Wah, T. and Calcote, L., Structural Analysis by Finite Difference Calculus, New York, Van Nostrand Reinhold Company, 1970.

8. Wah, T., "Free lateral oscillations of a supported Grillage," Journal of the Franklin Institute, Vol. 277, 349-355, 1964.

9. Zhu, L. P., Elishakoff, I. and Lin, Y. K., "Free and Forced Vibrations of Periodic Multi-Span Beams," Shock and Vibration, Vol. 1(3), 217-232, 1994.

CHAPTER # 5

Random Vibration of Space Shuttle

Weather Protection Systems

RANDOM VIBRATION OF SPACE SHUTTLE WEATHER PROTECTION SYSTEMS

by

Isaac Elishakoff[1], Menahem Baruch[2], Liping Zhu[1] and Raoul Caimi[3]

[1] Center for Applied Stochastics Research
Florida Atlantic University
Boca Raton, Fl 33431-0991, U.S.A.

[2] Faculty of Aerospace Engineering
Technion-Israel Institute of Technology
Haifa 32000, Israel

[3] NASA Kennedy Space Center
Titusville, FL 32899, U.S.A.

Abstract

The paper deals with random vibrations of the space shuttle weather protection systems. It is shown that the Timoshenko beam theory must be utilized to describe the structural behavior of the system. Use of the simple Bernoulli-Euler theory may result in an error of about 50% in determining the mean-square value of the bending moment in the weather protection system.

Introduction

This study deals with the random vibrations of space shuttle weather protection systems modeled as Timoshenko beams. The experimentally determined excitation, rather than assumed expression of its cross-spectral density will be utilized. Random vibrations of Timoshenko beams

under simplest, "rain-under-roof" excitation, namely with both time-wise and space-wise white noise, was considered previously. Samuels and Eringen [1] were the first authors to study random vibrations of Timoshenko beams. They concluded, for the above excitation, that the results produced by using either the Timoshenko or Bernoulli-Euler theory differed by less than five percent. Crandall and Yildiz [2] studied effects of both the dynamical models utilized and of the postulated damping mechanism. They considered, as an excitation, the time-wise band-limited white noise and investigated the growth pattern of the response characteristics with the increase of the cut-off frequency. Banerjee and Kennedy (1985) investigated the effect of axial compression, whereas Singh and Abdelnaser (1993), studied the effect of boundary conditions. The latter study is in agreement with the paper by Samuels and Eringen (1957) in the sense that for the length-to-depth ration L/d above nine, the percentage-wise difference between results produced on one hand, by the Timoshenko theory and, on the other hand by the Bernoulli-Euler theory is less than five percent. Therefore, one may conclude that for this case of the length-to-depth ratio one should utilize a simpler Bernoulli-Euler theory.

However the above studies were concentrating on the excitation whose spectral density is constant. As a result, within the modal analysis approach, only the low end of the frequency spectrum is contributing significantly to the response. However, the shear deformation and rotary inertia are affecting considerably only the higher frequencies. Since the contribution of jth mode is inverse proportional to ω_j^4 for the viscously-damped beam, the significantly affected frequencies contributed very little in formulation of the response. This is the reason of uncovering a small numerical difference between the Bernoulli-Euler and Timoshenko beams.

However, the situation must not be such in the general case of excitation, as was first demonstrated by Elishakoff and Lubliner (1985). They considered the band-limited white nose excitation with two out-off frequencies, namely, the lower one $\omega_{c,1}$ and the upper one $\omega_{c,2}$, i.e. the spectral density was taken constant for frequency ranges $-\omega_{c,2} \le \omega \le -\omega_{c,1}$ and $\omega_{c,1} \le \omega \le \omega_{c,2}$. Such a band limited white noise tends to ideal white noise when $\omega_{c,1}$ tends to zero and $\omega_{c,2}$ tends to infinity. It was demonstrated that when $\omega_{c,1}$ is zero or close to zero, both the Timoshenko theory and the Bernoulli-Euler theory produce similar results. However, when $\omega_{c,1}$ increases, the higher modes become more important. Since the higher natural frequencies are reduced by the effects of shear deformation and rotary inertia, the response predicted by Timoshenko theory is in excess of that predicted by the Bernoulli-Euler theory. In such circumstances one must utilize Timoshenko beam theory. In several example cases Lubliner and Elishakoff (1985) demonstrated that the application of the Bernoulli-Euler theory would yield up error of order of 50% or more.

In this study we consider the response of weather protection systems to random excitations. The set of consistent differential equation, as discussed by Elishakoff and Lubliner (1985) is utilized. Namely, the fourth order derivative of the displacement with respect to time, appearing in the original Timoshenko equation is neglected as discussed by Love (1927), Tseitlin (1961), Egle (1969), Elishakoff and Abramovich (1992).

The typical weather protection systems for launch vehicles are made of thin corrugated metal sheets (see Fig. 1), with a much larger bending stiffness in the direction perpendicular to the corrugation, namely, $I_z >> I_y$;. These sheets are supported by thin beams parallel to the O_z direction. Such a weather protection system is susceptible to excessive shear deformation. It is

therefore reasonable to model such a system as a Timoshenko beam.

Equivalent Timoshenko Beam

For the sake of analysis, a typical segment of the corrugated sheet may be substituted by an equivalent *I* beam as shown in (Fig. 2). We equate an infinitesimal element of the web of the corrugated beam with its equivalent part on the *I* beam, (Fig.2).

$$y = \eta \cos\alpha \tag{1}$$

$$t_1 dy = t d\eta \; ; \qquad t_1 = \frac{t}{\cos\alpha} \tag{2}$$

Furthermore, the shear flow in the two elements must be equal,

$$\tau t = \tau_1 t_1 \tag{3}$$

where τ and τ_1 are the shear stresses in the corrugated sheet and the *I* beams, respectively. Hence

$$\tau_1 = \tau \cos\alpha \tag{4}$$

The shear strains are given by

$$\gamma = \frac{\tau}{G} \; ; \qquad \gamma_1 = \frac{\tau_1}{G_1} \tag{5}$$

where G is the shear modulus of the material in the corrugated beam, and G_1 is the equivalent shear modulus in the *I* beam.

Now, for the *I* beam web to have the same shear stiffness, the displacement u in the

longitudinal direction must be the same as that of the corrugated web,

$$du = \gamma d\eta = \gamma_1 dy \tag{6}$$

Hence

$$\gamma_1 = \frac{\gamma}{\cos\alpha} \tag{7}$$

and

$$\frac{\tau_1}{G_1} = \frac{\tau\cos\alpha}{G_1} = \frac{\tau}{G\cos\alpha} \tag{8}$$

From Eq.(8), one obtains the equivalent shear modulus

$$G_1 = G\cos^2\alpha \tag{9}$$

one can show that shear stress energies are equal in the two models

$$dU = \frac{1}{2}\frac{\tau_1^2}{G_1} t_1 dy = \frac{1}{2}\frac{\tau^2\cos^2\alpha}{G\cos^2\alpha} t d\eta = \frac{1}{2}\frac{\tau^2}{G} t d\eta \tag{10}$$

Free Vibration of Timoshenko Beam

The equation of motion for a Timoshenko beam may be written as follows (Elishakoff and Lubliner 1985),

$$EI\frac{\partial^4 w}{\partial x^4} + \rho A\frac{\partial^2 w}{\partial t^2} - \rho I\left(1+\frac{E}{k'G_1}\right)\frac{\partial^4 w}{\partial x^2 \partial t^2}$$
$$+\rho A\beta_0\frac{\partial w}{\partial t} - \frac{\rho IE}{k'G_1}\frac{\partial^3 w}{\partial x^2 \partial t} = q(x,t) + \frac{1}{k'G_1 A}\left(-EI\frac{\partial^2 q}{\partial x^2} + \rho I\frac{\partial^2 q}{\partial t^2}\right) \tag{11}$$

where β_0 is the transverse viscous damping coefficient $\beta_0 = c/\rho A$. The natural frequencies of the structure are found by letting $\beta_0 = 0$, $q(x,t) = 0$ and

$$w(x,t) = \psi(x)e^{i\omega t} \tag{12}$$

For a simply supported beam, the mode shape can be chosen as

$$\psi_j(x) = \sin\frac{j\pi x}{L} \tag{13}$$

where j is the number of half sine waves in the x direction. The natural frequencies are computed from

$$\omega_j^2 = \frac{EI}{\rho A}\left(\frac{j\pi}{L}\right)^4\left[1 + \frac{I}{A}\left(\frac{j\pi}{L}\right)^2\left(1 + \frac{E}{k'G_1}\right)\right]^{-1} \tag{14}$$

The shear correction factor k' is given by (Cowper, 1966)

$$k' = 10(1+\nu)\ (1+3m)^2/B \tag{15}$$

where ν is Poisson's ratio, and B is defined as

$$B = 12 + 72m + 150m^2 + 90m^3 + \nu(11 + 66m + 135m^2 + 90m^3)$$
$$+ 30n^2(m + m^2) + 5\nu n^2(8m + 9m^2) \tag{16}$$

$$m = \frac{2bt_f}{ht_w}, \quad t_f = t_w = t_1, \quad b = \frac{a}{2}, \quad n = \frac{b}{h} \tag{17}$$

Random Vibration of Timoshenko Beam

Consider a random acoustic excitation field characterized by a cross-spectral density

$$\Phi_q(x_1,x_2;\omega) = S_q(\omega)\exp\left[-\alpha(\omega)|x_1 - x_2| - i\gamma(\omega)(x_1 - x_2)\right] \tag{18}$$

where $S_q(\omega)$ is the spectral density at the reference point $x_1 = x_2 = x$; $\alpha(\omega)$ and $\gamma(\omega)$ are, respectively, the decay and phase functions of ω. They are determined from experimental data and are given in the Appendix . Assuming that the beam has reached the state of probabilistic stationarity, the cross-spectral densities of response for displacement and moment are respectively found as follows (Lin 1976; Elishakoff 1983):

$$\Phi_{DD}(x_1,x_2;\omega) = b^2\int_0^L\int_0^L \Phi_q(y_1,y_2;\omega)H_D(x_1,y_1;\omega)H_D^*(x_2,y_2;\omega)dy_1dy_2 \tag{19}$$

$$\Phi_{MM}(x_1,x_2;\omega) = b^2\int_0^L\int_0^L \Phi_q(y_1,y_2;\omega)H_M(x_1,y_1;\omega)H_M^*(x_2,y_2;\omega)dy_1dy_2 \tag{20}$$

where H_D and H_M are the frequency response functions of displacement and bending moment, respectively, L is the length of the beam, b is the width of the beam.

In order to derive the function H_D , let the harmonic point loading be imposed at location y:

$$q(x,t) = \delta(x - y)e^{i\omega t} \tag{21}$$

Thus, the responses of displacement and moment at location of x will be

$$w(x,t) = H_D(x,y;\omega)e^{i\omega t} \tag{22}$$

$$M(x,t) = H_M(x,y;\omega)e^{i\omega t} \tag{23}$$

Substituting Eq.(22) into Eq.(11) and expending H_D in the series in terms of the mode shapes $\psi_j(x)$, we obtain the following expression for $H_D(x,y;\omega)$

$$H_D(x,y;\omega) = \sum_{j=1}^{\infty} \frac{1}{\nu_j^2} H_j(\omega)\psi_j(x)\psi_j(y) \tag{24}$$

with ν_j^2 being the norm of *jth* mode namely,

$$\nu_j^2 = \int_0^L \psi_j^2(x)dx = \frac{L}{2} \tag{25}$$

The modal frequency response function in the j-th mode $H_j(\omega)$, is derived as

$$H_j(\omega) = \frac{1+\alpha\lambda_1\lambda_2[(j\pi)^2 - \rho L^2/E\omega^2]}{\rho A\left[1+\alpha\lambda_2(1+\lambda_1)(j\pi)^2\right]}\left[\omega_j^2 - \omega^2 + i\omega\beta_0\frac{1+\alpha\lambda_1\lambda_2(j\pi)^2}{1+\alpha\lambda_2(1+\lambda_1)(j\pi)^2}\right]^{-1} \tag{26}$$

with two nondimensional parameters

$$\lambda_1 = \frac{E}{kG}, \quad \lambda_2 = \frac{I}{AL^2} \tag{27}$$

Moreover, α is an artificial parameter, with $\alpha = 1$ corresponding to the Bresse-Timoshenko

theory and $\alpha = 0$ associated with the Bernoulli-Euler theory.

Note that the relationship between the bending moment $M(x,t)$ and displacement $w(x,t)$ is

$$\begin{aligned} M(x,t) &= -EI\left[w''(x,t) - \frac{\alpha}{k'GA}V'_y(x,t)\right] \\ &= -EI\left[w''(x,t) - \frac{\alpha}{k'GA}[c_0\dot{w}(x,t) + \rho A\ddot{w}(x,t) - q(y,t)\right] \end{aligned} \tag{28}$$

Substituting Eqs.(21)-(23) into equation Eq.(28), we obtain H_M as follows

$$H_M(x,y,\omega) = -EI\left\{H_D''(x,y,\omega) + \frac{\alpha\rho}{k'}G[(\omega^2 - i\omega\beta_0)H_D(x,y,\omega) + \frac{1}{\rho A}\delta(x-y)\right\} \tag{29}$$

The cross-spectral densities for displacement and moment can be rewritten by substituting Eqs. (24) (29) into Eqs. (19), (20) as follows

$$\Phi_{DD}(x_1,x_2;\omega) = b^2\sum_{j=1}^{\infty}\sum_{k=1}^{\infty}H_j(\omega)H_k^*(\omega)\psi_j(x_1)\psi_k(x_2)I_{jk}(\omega) \tag{30}$$

$$\Phi_{MM}(x_1,x_2;\omega) = b^2(EI)^2\Bigg\{\sum_{j=1}^{\infty}\sum_{k=1}^{\infty}\Big[\psi_j''(x_1)\psi_k''(x_2) + \eta^2(\omega^4 + \omega^2\beta_0^2)\psi_j(x_1)\psi_k(x_2)$$

$$+\eta(\omega^2 + i\omega\beta_0)\psi_j''(x_1)\psi_k(x_2) + \eta(\omega_2 - i\omega\beta_0)\psi_k''(x_2)\psi_j(x_1)\Big]H_j(\omega)H_k^*(\omega)I_{jk}(\omega)$$

$$+ \frac{\eta}{\rho A}\sum_{k}^{\infty}[\eta(\omega^2 + i\omega\beta_0)\psi_k(x_2) + \psi_k''(x_2)]H_k^*(\omega)J_k^*(x_1;\omega) \tag{31}$$

$$+ \frac{\eta}{\rho A}\sum_{j}\Big[\eta(\omega^2 - i\omega\beta_0)\psi_j(x_1) + \psi''_j(x_1)\Big]H_j(\omega)J_j(x_2;\omega)$$

$$+ \left(\frac{\eta}{\rho A}\right)^2\Phi_q(x_1,x_2;\omega)\Bigg\}; \qquad \eta = \frac{\alpha\rho}{kG}$$

where two integrals of I_{jk} and J_j are defined as follows:

$$I_{jk}(\omega) = \frac{1}{\nu_j^2\nu_k^2}\int_0^L\int_0^L\Phi_q(y_1,y_2;\omega)\psi_j(y_1)\psi_k(y_2)dy_1dy_2 \tag{32}$$

and

$$J_j(x) = \frac{1}{\nu_j^2}\int_0^L\Phi_q(y,x,\omega)\psi_j(y)dy \tag{33}$$

Note that the integral of $I_{jk}(\omega)$ possesses the Hermitian property,

$$\begin{aligned} I_{jk}(\omega) &= I_{kj}^*(\omega) \\ I_{jk}(-\omega) &= I_{jk}^*(\omega) \end{aligned} \tag{34}$$

Hence, the mean square values of both displacement and moment can be obtained by integration of both two spectral densities defined by Eqs (28),(29) over positive range of frequencies only, i.e.

$$E[w^2(x,t)] = 2\int_0^\infty \Phi_{DD}(x,x,\omega)\,d\omega \tag{35}$$

$$E[M^2(x,t)] = 2\int_0^\infty \Phi_{MM}(x,x,\omega)\,d\omega \tag{36}$$

in which, the integrals I_{jk} and J_j can be replaced by their respective real parts and are evaluated in the exact form as follows:

$$I_{jk}(\omega) = \frac{1}{\nu_j^2\nu_k^2}\int_0^L\int_0^L Re\{\Phi_q(y_1,y_2;\omega)\}\psi_j(y_1)\psi_k(y_2)dy_1dy_2$$

$$= 4S_q(\omega)jk\pi^2\left[2Re\left\{\frac{1+\exp[-(\bar{\alpha}+i\bar{\gamma})]}{[(\bar{\alpha}+i\bar{\gamma})^2+(k\pi)^2][\bar{\alpha}+i\bar{\gamma})^2+(j\pi)^2]}\right\}\right. \tag{37}$$

$$\left.+\bar{\alpha}\delta_{jk}\frac{1+[\bar{\alpha}^2+\bar{\gamma}^2](jk\pi^2)^{-1}}{[(\bar{\alpha}+i\bar{\gamma})^2+(j\pi)^2][(\bar{\alpha}-i\bar{\gamma})^2+(k\pi)^2]}\right]$$

$$J_j(x,\omega) = \frac{1}{\nu_j^2}\int_0^L Re\{\Phi_q(y,x;\omega)\}\psi_j(y)dy$$

$$= 2S_q(\omega)Re\left\{\frac{1}{(\bar{\alpha}-i\bar{\gamma})^2+(j\pi)^2}\left[(\bar{\alpha}-i\bar{\gamma})\sin(j\pi\xi) - j\pi\cos(j\pi\xi) + j\pi e^{-(\bar{\alpha}-i\bar{\gamma})\xi}\right]\right. \tag{38}$$

$$\left.+\frac{1}{(\bar{\alpha}+i\bar{\gamma})^2+(j\pi)^2}\left[(\bar{\alpha}+i\bar{\gamma})\sin(j\pi\xi) + j\pi\cos(j\pi\xi) + (-1)j\pi e^{(\bar{\alpha}+\bar{\gamma})(\xi-1)}\right]\right\},$$

where nondimensional parameters $\bar{\alpha}$ and $\bar{\gamma}$ are defined as follows:

$$\bar{\alpha} = \alpha(\omega)L\ ; \qquad \bar{\gamma} = \gamma(\omega)L\ ; \qquad \xi = x/L \tag{39}$$

Numerical Example and Discussion

A thin corrugated metal sheet-the typical weather protection system for launch vehicles, (Fig.1) is chosen as an example for application. We chose an element of a sheet (Fig. 2) and modeled it as an equivalent *I*-beam, with properties $I = 0.0247$ in^4, $A = 0.264$ in^2, $b = 1.1$ in. Thus, two nondimensional parameters in Eq.(27), become $\lambda_1 = 8.852$; $\lambda_2 = 3.3 \times 10^5$.

Table 1 lists the natural frequencies of the beam within both the Timoshenko theory, and the Bernoulli-Euler theory approximations. It can be seen, as expected, that the values of natural frequencies of the Timoshenko beam are less than those of the Bernoulli beam , and for the higher order modes there is a bigger difference between two approximations.

Fig. 4 and Fig. 5 portray the exact spectral densities of the displacement and the moment at the mid-section of the beam. The solid curve presents results associated with the Bernoulli-Euler theory while the dashed one denotes the results obtained using the Timoshenko beam theory. Only odd-numbered modes contribute to the response, due to sinusoidal mode shapes. It is shown that within the same range of frequencies (0 to 1000 Hz), the spectral density of response for the Timoshenko beam has more peaks than that for the Bernoulli-Euler beam. In other words, for the Timoshenko beam there are generally more modal contributions to the response of the structure due to the increased modal density of natural frequencies. For the spectral density of displacement (Fig. 4) the first peak is the largest within both beam theories. The difference of values of the first peak for two beams is very small. Hence the value of areas under the spectral density curves, or the mean square values of displacement are very close, with attendant difference constituting about 1.2%.

However, for the spectral density of moment (Fig. 5), the higher order modes dominate in formulating the response of the structure. This is because there is a high peak around 585 Hz in the loading spectral density $S_q(\omega)$ (Fig. 3), and in addition there appears a factor j^2k^2 in

the expression for H_M. Therefore the contribution of higher modes is significant. The difference between the values of spectral densities calculated via the Timoshenko and the Bernoulli-Euler theories, and their associated contribution to the mean square value of moment is remarkable.

The value of mean square for the Timoshenko beam is almost twice that for the Bernoulli beam. This implies that choosing Bernoulli-Euler beam model may not be on the safe side, for the design of the weather protection systems. As a result the refined Timoshenko beam model rather than simple Bernoulli-Euler theory should be chosen for the space shuttle weather protection structure under the acoustic loading.

Acknowledgment

This study has been supported by the NASA Kennedy Space Center, through Cooperative Agreement No. NCC10-0005, S1 to the Florida Atlantic University. This support is gratefully appreciated.

References

Banerjee, J.R. and Kennedy, D. (1985). Response of Axially Loaded Timoshenko Beam to Random Loads, *Journal of Sound and Vibration*, **104**, 481-487.

Crandall, S.H. and Yildiz, A. (1962). Random Vibrations of Beams, *Journal of Applied Mechanics*, **31**, 267-275.

Crandall, S.H. et al, (1978). *An Introduction to the Mechanics of Solids*, McGraw Hill Kogakusha, Tokyo, p. 435.

Cowper, C.R., (1966). The Shear Coefficient in Timoshenko Beam Theory, *Journal of Applied Mechanics*, **35**, 335-340.

Egle, D.M., (1969). An Approximate Theory for Transverse Shear Deformation and Rotary Effects in Vibrating Beams, *NASA CR-1317*.

Elishakoff,I. (1983). *Probabilistic Methods in the Theory of Structures*, Wiley-Interscience, New York.

Elishakoff, I and Lubliner, E. (1985). Random Vibration of a Structure via Classical and Nonclassical Theories, in *Probabilistic Methods in the Mechanics of Solids and Structures* (S.Eggwertz and N. C. Lind, eds), Springer Verlag, Berlin, 455-467.

Elishakoff, I. and Livshits, D., (1989). Some Closed-Form Solutions in Random Vibration of Bresse-Timoshenko Beams, *Probabilistic Engineering Mechanics*, **4**, 49-54.

Elishakoff, I. and Abramovich, H., (1992). A Note on Dynamic Response of Large space Structures, *Journal of Sound and Vibration*, **156**, 178-184.

Filin, A.P. (1978). *Applied Mechanics of Solid Deformable Body*, "Nauka" Publishing House, Moscow, **2**, 196 (in Russian).

Lin, Y.K. (1967). *Probabilistic Theory of Structural Dynamics* McGraw-Hill, New York.

Love, M.A., (1927). *A Treatise on the Mathematical Theory of Elasticity*, (4th edition), Dover, New York, pp. 430-431.

Samuels, J.C., and Eringen, A.C. (1957). Response of Beams and Plates to Random Loads, Journal of Applied Mechanics, **24**, 46-52.

Singh, M.P. and Abdelnaser, A.S., (1993). Random Vibrations of Externally Damped Viscoelastic Timoshenko Beams with General Boundary Conditions, *Journal of Applied Mechanics*, **60**, 149-156.

Tseitlin, A.I., (1961). On the Effect of Shear Deformation and Rotary Inertia in Vibrations of Beams on Elastic Foundation, *PMM-Journal of Applied Mathematics and Mechanics*, **25**, 531-535.

Table 1. Natural Frequencies of the Weather Protection System Modeled as Bernoulli Euler-Beam or Timoshenko-Beam

i	Natural Frequencies, f_i [Hz]	
	Timoshenko-Beam	Bernoulli Euler-Beam
1	1.739829	1.742619
2	6.926167	6.970474
3	15.46189	15.68357
4	27.19260	27.88190
5	41.91663	43.56546
6	59.39734	62.73426
7	79.37590	85.38831
8	101.5836	111.5276
9	125.7528	141.1521
10	151.6251	174.2619
11	178.9584	210.8569
12	207.5304	250.9370
13	237.1413	294.5025
14	267.6140	341.5533
15	298.7939	392.0891
16	330.5479	446.1104
17	362.7619	503.6167
18	395.3398	564.6084
19	428.2004	629.0853
20	461.2764	697.0474
21	494.5116	768.4949
22	527.8599	843.4274
23	561.2834	921.8451
24	594.7518	1003.748
25	628.2399	1089.137
26	661.7276	1178.010
27	695.1992	1270.369
28	728.6419	1366.213
29	762.0460	1465.542
30	795.4041	1568.356
31	828.7104	1674.656
32	861.9608	1784.441
33	895.1523	1897.712
34	929.2831	2014.467
35	961.3519	2134.708
36	994.3586	2258.434
37	1027.303	2385.645
38	1060.186	2516.341
39	1093.008	2650.523
40	1125.770	2788.190

Appendix

The model of cross-spectral density for acoustic loading utilized in this study is given by Eq. (18) where the spectral density $S_q(\omega)$ is approximated by the following expression

$$S_q(\omega) = \sum_{j=1}^{3} a_j \left| \frac{\omega}{\omega_j} \right| \exp\left[-\frac{b_j^2 - (1 - c_j)^2}{2\,(1 - c_j)} \right] ; \quad \omega_j = 2\pi f_j \quad ; \quad b_j = \left(\frac{\omega}{\omega_j} - c_j \right) \tag{40}$$

with parameters listed in the Table:

j	1	2	3
a_j [(psi)^2/(r/s)]	1.1×10^{-2}	4.5×10^{-3}	1.9×10^{-2}
f_j [Hz]	105	290	585
c_j	0.8	-1.0	0.995

Decay function $\alpha(\omega)$ is defined as

$$\alpha(\omega) = 0.03 + 5.0 \times 10^{-5} \frac{\omega}{2\pi} \left(\left| \frac{\omega}{2\pi} - 22 \right| \right) \tag{41}$$

and has a width dimension of [1/ft]. Phase function $\gamma(\omega)$reads

$$\gamma(\omega) = 0.77 \sin\,(0.14 \frac{\omega}{2\pi}) + 0.045 \frac{\omega}{2\pi} \quad , \tag{42}$$

having a dimension [degree/ft].

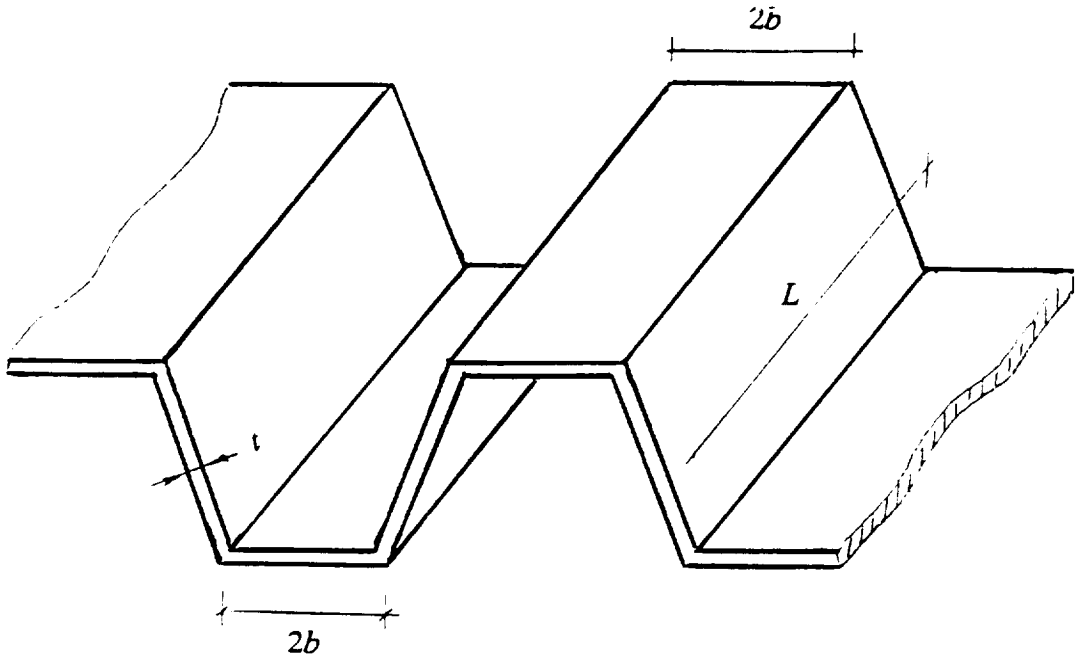

Fig. 1 A corrugated metal sheet

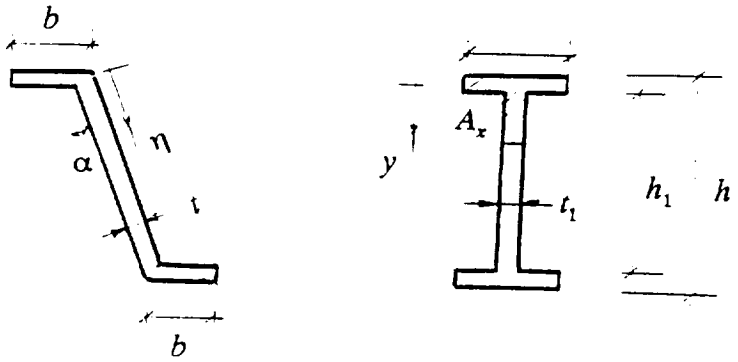

Fig. 2 A typical segment of the corrugated sheet and the equivalent I beam

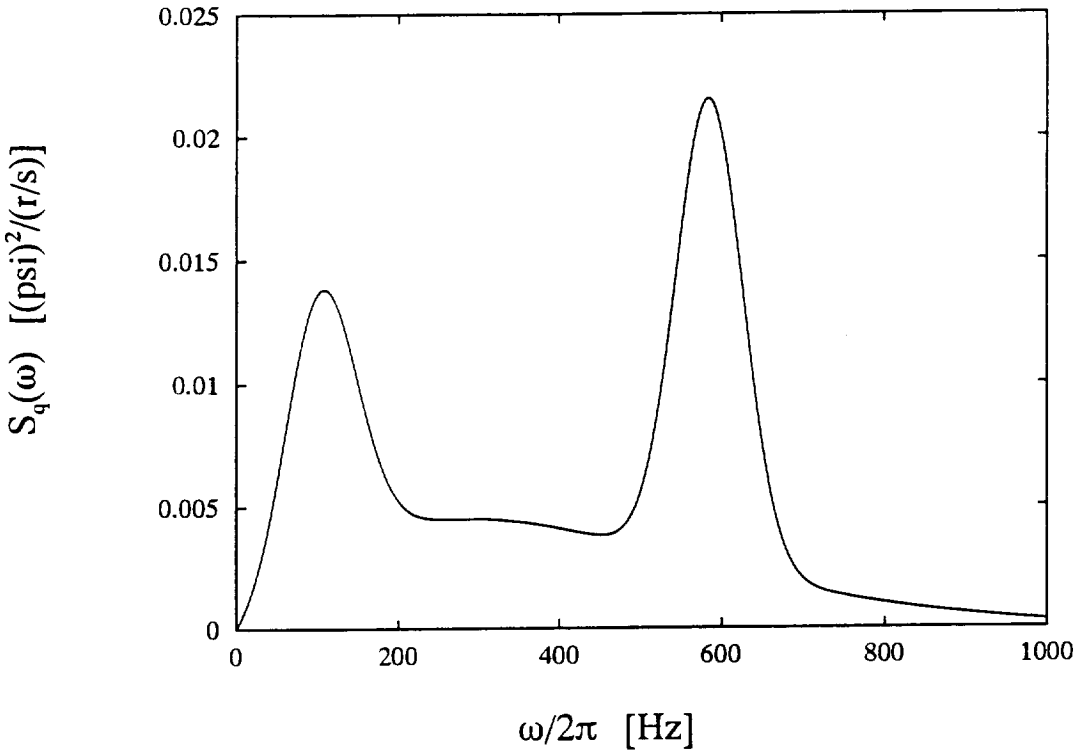

Fig. 3a Spectral density of acoustic loading

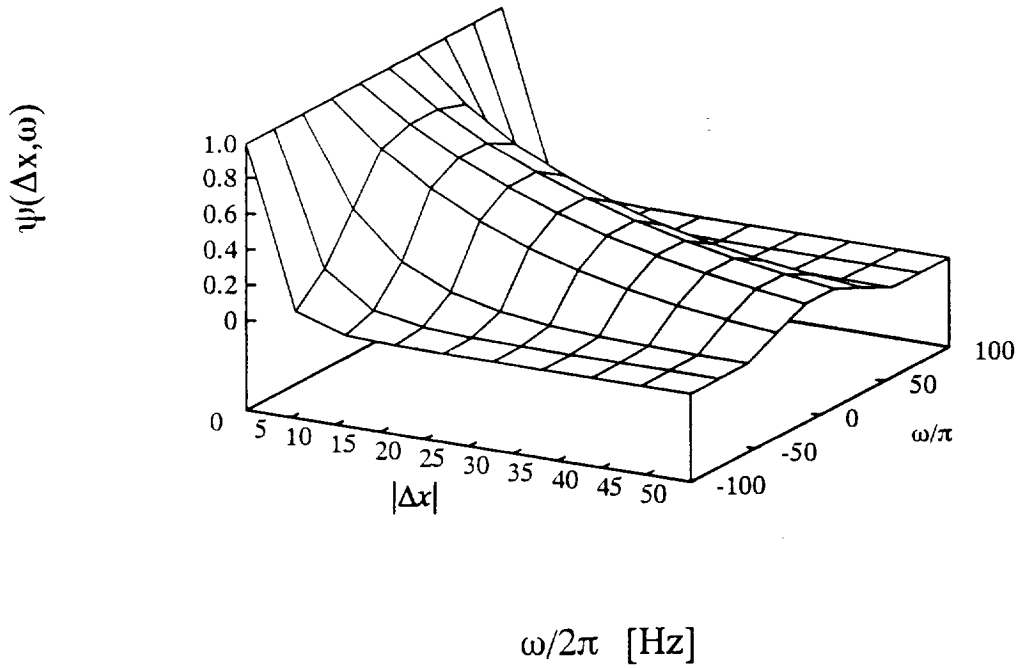

Fig. 3b Variation of the decay function $\psi(\Delta x,\omega) = e^{-\alpha(\omega)|\Delta x|}$

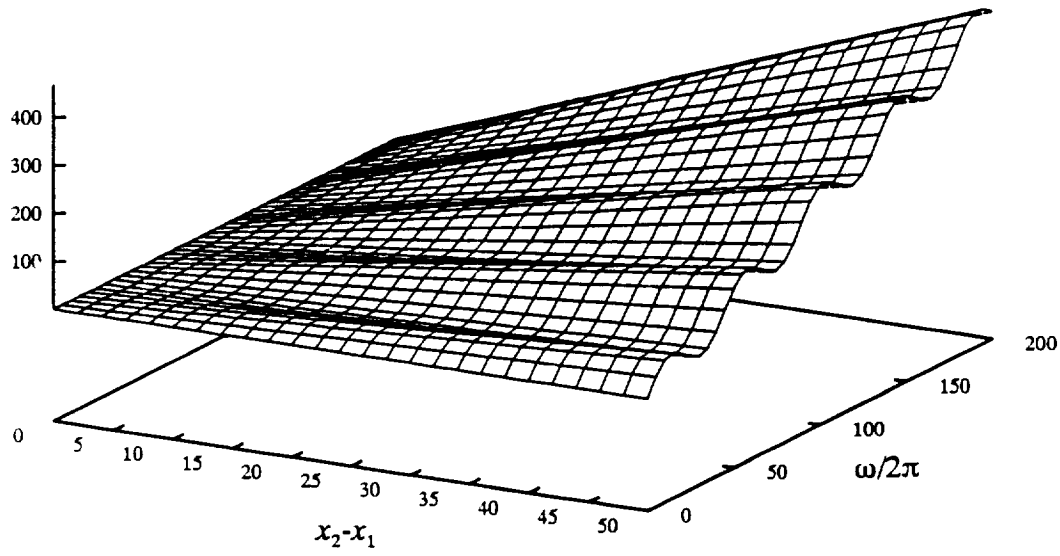

Fig. 3c Phase function $\gamma(\omega)(x_2-x_1)$

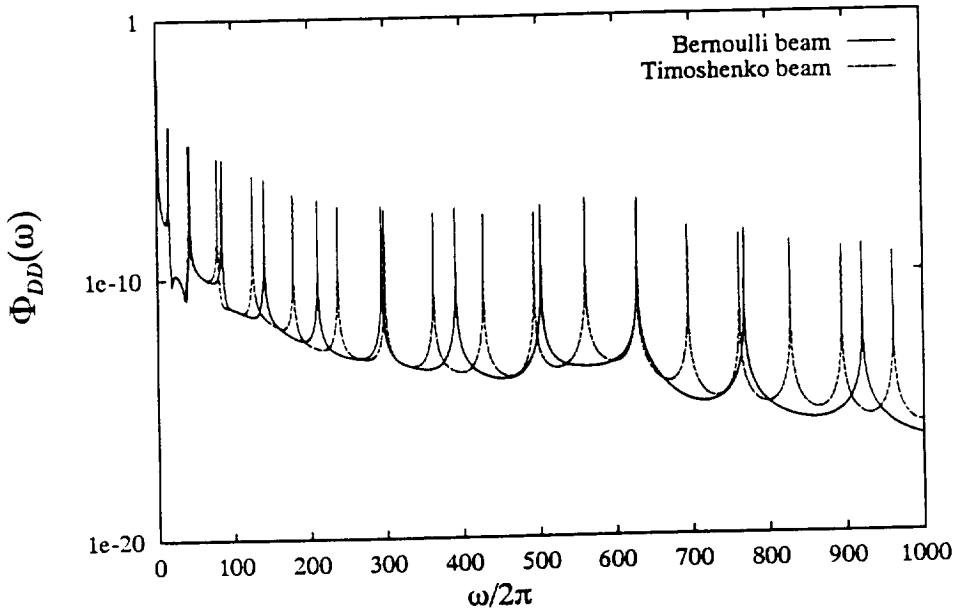

Fig. 4 Spectral densities of the displacement at the mid-point of the beam

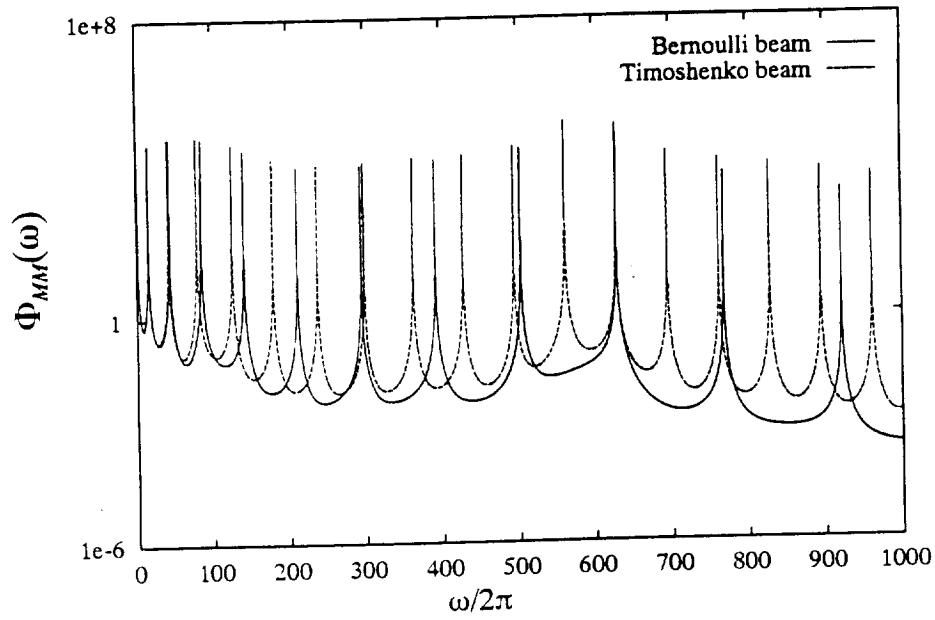

Fig. 5 Spectral densities of the bending moment at the mid-point of the beam

CHAPTER # 6

A New Stochastic Linearization Technique and Its Application to Discrete Nonlinear Systems

A New Stochastic Linearization Technique and Its Application to Discrete Nonlinear Systems

Isaac Elishakoff
Center for Applied Stochastics Research
and Department of Mechanical Engineering, Florida Atlantic University
Boca Raton, 33431-0991, U.S.A.

ABSTRACT

Several recent developments in the stochastic linearization technique are summarized in this review paper. The nonlinear oscillator subjected to colored noise is examined; the case of the nonlinear damping is discussed; the "true" stochastic linearization technique is described. The results of the latter match the exact mean square responses of the nonlinear structure. The combination of the stochastic linearization with the Monte Carlo method is outlined. In addition, the accuracy of a new linearization technique in contrast with the classical linearization scheme is examined for a Duffing oscillator subjected to white or colored noise excitations. The results obtained by the two linearization schemes are compared in terms of percentage-wise error in reference with the exact solution or numerical results obtained through Monte Carlo simulation. These applications confirm a superior performance of new linearization technique in comparison with the classical one, in several examples considered. Under some circumstances however, namely for some nonlinear softening oscillators, the conventional linearization may yield more accurate results. The method of weighing functions improves the accuracy of both the conventional and new stochastic linearization methods.

The developments which are described in this review mostly took place after excellent accounts on the classical version of the stochastic linearization technique, the monograph by Roberts and Spanos (1990), and the review article by Socha and Soong (1991), have been published recently.

INTRODUCTION

Stochastic linearization technique is the most versatile method for analysis of general non-linear systems and structures under random excitation. In almost thirty years since it was proposed for the first time by Booton (1953) and Kazakov (1954) it has been widely applied for the study of various non-linear systems which are not amenable to exact solutions. For example, the monograph by Roberts and Spanos (1990), and the recent review paper by Socha and Soong (1991) give comprehensive accounts of some of these developments. The fundamental idea of the method lies in replacing the original non-linear system by a linearized one in such a way that the difference between two systems is minimal in some probabilistic sense. Following the classical approach, the linearized system parameters are determined in the manner that the difference between the nonlinear force and the force in the linearized system is minimal in the mean square value. In some recent papers by Falsone (1992.a,1992.b) it has been demonstrated that, when parametric excitations are present, it is more suitable to measure the difference on the coefficients of the Itô differential rule. It is remarkable that, when only purely external excitations are present, Falsone's approach coincides with the classical stochastic linearization.

Recently, for the case of purely external excitations, some new stochastic linearization techniques have been suggested (Wang and Zhang, 1985; Zhang, 1989; Zhang, Elishakoff,Zhang, 1991; Elishakoff, 1991; Elishakoff and Zhang, 1992.a; Elishakoff and Zhang, 1992.b) in which the differences between the nonlinear original system and the linearized one are considered in terms of potential energy. In particular, Elishakoff (1991) investigated a Duffing oscillator subjected to a white noise excitation; it has been shown that the best results are obtained when the linearized system parameters are obtained through minimizing the mean square error between the potential energies of the original non-linear and the replacing linear system. The exact solution for the stationary probability density of Duffing oscillator is readily available and approximate solutions are not needed for this problem; therefore the validity of the modified stochastic linearization technique is easily checked for this case. Moreover, the results furnished by the stochastic linearization technique are compared with those yielded by the Monte Carlo simulations when the exact solutions are unavailable.

It has demonstrated, (Elishakoff, 1991) that for some combinations of the parameters of the Duffing oscillator the proposed linearization criteria may yield results in perfect agreement with exact solution. For other sets of parameters, the proposed linearization yields results which are slightly greater than the exact probabilistic responses, whereas the conventional linearization yields responses which are below the exact values. Since generally engineers utilize the notion of safety factors, the structures designed through use of conventional stochastic linearization, may turn out to be "over-designed." When the Duffing oscillator is extremely weakly nonlinear, the conventional stochastic linearization may exhibit less error, than the energy-wise stochastic linearization. However, for these almost linear systems the percentage-wise error is under two percent for either stochastic linearization criteria. Therefore, for the Duffing oscillator, the energy-wise stochastic linearization is almost always preferable.

The aim of this paper is to give a brief account of some recent developments, as well as to investigate the accuracy of this new linearization technique in the case of colored noise excitation. The results obtained in this way have been compared with those obtained by means of the Monte Carlo simulation.

The combined use of concept of potential energy and energy dissipation function is discussed for nonlinearly damped structures with nonlinear restoring force. Finally, the combined use of the stochastic linearization and Monte Carlo method is discussed.

NEW VERSUS CLASSICAL LINEARIZATION TECHNIQUES

Let us consider the single-degree-of-freedom system governed by the following equation of motion

$$m\ddot{X} + c\dot{X} + f(X) = W(t) \tag{1}$$

where m is the mass, c is the damping, $f(\cdot)$ is the restoring force, which is considered here as a non-linear function of the displacement X, $W(t)$ is a random, stationary, Gaussian excitation upper dots denote time derivatives . The basic idea of any stochastic linearization technique consists in the replacement of the original non-linear equation (1) by such a linear equation that

the difference between the two systems is minimal in some probabilistic sense. According to the classical linearization technique (Booton, 1953; Kazakov, 1954; Roberts and Spanos, 1990; Socha and Soong, 1991), equation (1) is replaced by the following linear one:

$$m\ddot{X} + c\dot{X} + k_{eq}^{(1)}X = W(t) \tag{2}$$

in which $k_{eq}^{(1)}$ is the spring coefficient, chosen in such a way that the difference between equation (2) and equation (1) attains a minimum in mean square sense, that is

$$E\left[\left\{f(X) - k_{eq}^{(1)}X\right\}^2\right] = \min \tag{3}$$

where $E[\cdot]$ means mathematical expectation of $(\cdot)$. Following this approach one finds the well-known relationship for $k_{eq}^{(1)}$, namely (booton, 1953; Kazakov, 1954)

$$k_{eq}^{(1)} = \frac{E[f(X)X]}{E[X^2]} \tag{4}$$

where $E[f(X)X]$ is evaluated taking into account that the replacing system is linear; so that, since the input is Gaussian, the response is assumed to be likewise Gaussian.

An alternative criterion was suggested by Kazakov (1954) in his pioneering paper. This criterion requires that the mean square values of the nonlinear restoring force $f(X)$ and the equivalent, linear restoring force $k_{eq}^{(2)}X$ be equal

$$E[f^2(X)] = E\left[\left(k_{eq}^{(2)}X\right)^2\right] \tag{5}$$

which leads to expression

$$k_{eq}^{(2)} = \sqrt{\frac{E[f^2(X)]}{E(X^2)}} \tag{6}$$

It is interesting to note that the Booton-Kazakov criterion (3) is almost universally utilized in the literature. To the best of author's knowledge, the Kazakov criterion (5) has been elucidated only in the book by Popov and Paltov (1960). They have observed that for numerous cases, mean-square values of the response, furnished by the Booton-Kazakov criterion constituted a larger value than the result delivered by the Kazakov criterion. Hence they suggested to utilize the arithmetic mean of these two results to obtain an approximation which would be closer to the exact mean square, than the ones delivered by either Booton-Kazakov (1953) or Kazakov (1954) criteria.

Bolotin (1984) demonstrated on the particular example of a half-degree-of-freedom system (the simple oscillator with negligible mass, for which an exact solution was constructed by Caughey and Dienes, 1961) that the exact mean-square displacement may be in access of results

furnished by either Booton-Kazakov or Kazakov criteria. Therefore the approximation suggested by Popov and Paltov (1960) is not necessarily more exact than those given by either criteria (3) or (5).

Recently, a new stochastic linearization technique has been suggested (Wang and Zhang, 1985; Zhang, 1989; Zhang, Elishakoff, Zhang, 1991; Elishakoff, 1991; Elishakoff and Zhang, 1992), based on the concept of potential energy.

Following this technique, equation (1) is replaced by the following linear one:

$$m\ddot{X} + c\dot{X} + k_{eq}^{(2)}X = W(t) \ , \tag{7}$$

in which the new stiffness spring $k_{eq}^{(2)}$ is chosen in such a way that the mean square deviation between the potential energies possessed by the original non-linear system (1) and by its linear counterpart in Eq.(5), attains its minimum, that is:

$$E\left[\left\{U(X) - k_{eq}^{(3)}X^2/2\right\}^2\right] = \min \tag{8}$$

resulting in:

$$k_{eq}^{(3)} = 2\,\frac{E[U(X)X^2]}{E[X^4]} \tag{9}$$

In equations (8) and (9) the expression $U(X)$ represents the potential energy of the original non-linear system. Elishakoff (1991) applied this new technique to a Duffing oscillator subjected to a white noise excitation, and performed a systematic comparison with an exact solution. It was shown that the new technique exhibits a "better" performance than the classical linearization; namely, for particular values of parameters, the new linearization may yield the *exact* response. In the next section the classical and new linearization techniques are applied to Duffing oscillator to illustrate the superiority of the new stochastic linearization technique.

In analogy with Kazakov's (1954) criterion, given in Eq. (5), Elishakoff and Zhang (1992) suggested to use the fourth criterion, based on the requirement that the mean-square values of the potential energy of the original system and its linear counterpart be equal:

$$E\left\{\left[U(X)\right]^2\right\} = E\left\{\left[k_{eq}^{(4)}X^2/2\right]^2\right\} \tag{10}$$

yielding

$$k_{eq}^{(4)} = \sqrt[2]{\frac{E\left\{\left[U(X)\right]^2\right\}}{E(X^4)}} \tag{11}$$

Criteria (3), (4), (8) and (10) are applicable to systems with linear damping characteristics. For the nonlinearly damped system these four criteria are directly generalized. The conventional stochastic linearization technique demands that the mean square difference between the nonlinear damping force $\varphi(\dot{X})$ and its linear counterpart $c_{eq}^{(1)}\dot{X}$ be minimal:

$$E\left[\left\{\varphi(\dot{X}) - c_{eq}^{(1)}\dot{X}\right\}^2\right] = \min \tag{12}$$

yielding

$$c_{eq}^{(1)} = \frac{E[\varphi(\dot{X})\dot{X}]}{E(\dot{X}^2)} \tag{13}$$

In full analogy with the Kazakov's criterion (5), applicable for the system with nonlinear restoring force, we can also require that the mean-square values of the dissipation force and its linear equivalent be equal, i.e.

$$E\left[\varphi^2(\dot{X})\right] = E\left[\left(c_{eq}^{(2)}\dot{X}\right)^2\right] \tag{14}$$

which results in

$$c_{eq}^{(2)} = \sqrt{\frac{E\left[\varphi^2(\dot{X})\right]}{E(\dot{X}^2)}} \tag{15}$$

To the best of our knowledge this criterion is formulated here for the first time. The third possible criterion of equivalence between the nonlinearly damped system and the one with linear damping was formulated by Wang and Zhang (1985) and Elishakoff and Zhang (1992.b). They required that the mean-square difference between the energy dissipation function $\Phi(\dot{X})$ of the original nonlinear system and that of the equivalent linear system $c_{eq}^{(2)}\dot{X}^2/2$ should be minimal

$$E\left[\Phi(\dot{X}) - c_{eq}^{(3)}\dot{X}^2/2\right]^2 = \min \tag{16}$$

resulting in the equivalent damping coefficient

$$c_{eq}^{(3)} = \frac{2E\left[\Phi(\dot{X})\dot{X}^2\right]}{E(\dot{X}^4)} \tag{17}$$

The fourth criterion was suggested by Elishakoff and Zhang (1992.b). It is based on requirement of equality of mean squares of $\Phi(\dot{X})$ and $c^{(4)}\dot{X}^2/2$, namely

$$E\left[\Phi^2(\dot{X})\right] = E\left[\left(c_{eq}^{(4)}\dot{X}^2/2\right)^2\right] \tag{18}$$

with attendant value of $c_{eq}^{(4)}$

$$c_{eq}^{(4)} = 2\sqrt{\frac{E\left[\Phi^2(\dot{X})\right]}{E(\dot{X}^4)}} \tag{19}$$

We will evaluate several examples to illustrate the performance of the proposed stochastic linearization criteria.

DUFFING OSCILLATOR UNDER WHITE NOISE

Consider Duffing oscillator subjected to ideal white noise excitation

$$\ddot{X} + \beta\dot{X} + \alpha X + \varepsilon X^3 = W(t) \tag{20}$$

The mean-square displacement for the system with $\varepsilon = 0$ reads

$$E(X^2)\big|_{\varepsilon=0} = \pi S/\alpha\beta = e_0^2 \tag{21}$$

where S is the value of the spectral density of excitation $W(t)$. The exact probability density of X is uniformly available in the literature and will allow a comparison between the conventional and the new stochastic linearization methods:

$$p_X(x) = C_2 \exp\left[-\frac{\pi S}{\alpha\beta}\left(\frac{1}{2}x^2 + \frac{1}{4}\frac{\varepsilon}{\alpha}x^4\right)\right] \tag{22}$$

where C_2 is a normalization constant. In view of Eq.(21), Eq.(22) can be rewritten as

$$p_X(x) = C_2 \exp\left[-\frac{1}{e_0^2}\left(\frac{1}{2}x^2 + \frac{1}{4}\frac{\varepsilon}{\alpha}x^4\right)\right] \tag{23}$$

We introduce new variables

$$x = p\tau, \qquad p = \left(\frac{4\alpha e_0^2}{\varepsilon}\right)^{1/4} \qquad y = \frac{1}{4e_0}\left(\frac{\alpha}{\varepsilon}\right)^{1/2} \tag{24}$$

The normalization condition

$$C_2 \int_{-\infty}^{\infty} \exp\left[-\frac{1}{e_0^2}\left(\frac{1}{2}x^2 + \frac{1}{4}\frac{\varepsilon}{\alpha}x^4\right)\right]dx = 1 \tag{25}$$

yields

$$C_2 = [pZ_1(y)]^{-1} \tag{26}$$

where

$$Z_1(y) = 2\int_0^{\infty} \exp(-\tau^4 - 4y^2\tau^2)d\tau \tag{27}$$

Mean square displacement

$$E(X^2) = \int_{-\infty}^{\infty} x^2 p_X(x)dx \tag{28}$$

reads

$$E(X^2) = \frac{p^2 Z_2(y)}{Z_1(y)} = 2e_0\frac{Z_2(y)}{Z_1(y)}\left(\frac{\alpha}{\varepsilon}\right)^{1/2} \tag{29}$$

where

$$Z_2(y) = 2\int_0^{\infty} \tau^2 \exp(-\tau^4 - 4y^2\tau^2)dx \tag{30}$$

Functions $Z_1(y)$ and $Z_2(y)$ are defined and tabulated for certain values of y by Stratonovich (1961). Note that these functions can also be reduced to cylindrical functions of a fractional order (Bolotin; 1984, Piszczek and Niziol, 1984; Constantinou, 1985). Consider a particular case

$$e_0^2 = 0.54\ , \quad \alpha/\varepsilon = 1 \tag{31}$$

In these circumstances,

$$y = 0.34021 , \quad Z_1(y) = 1.26368 , \quad Z_2(y) = 0.26310 \tag{32}$$

The exact mean square value becomes

$$E(X^2) = 0.306 \tag{33}$$

Let us now contrast the performance of the conventional and new stochastic linearization techniques. Conventional stochastic linearization yields

$$k_{eq}^{(1)} = \alpha + 3\varepsilon E(X^2) \tag{34}$$

Substitution into expression for the mean-square value

$$E(X^2) = \pi S / k_{eq}^{(1)} \beta \tag{35}$$

yields

$$E(X^2) = \pi S / \beta [\alpha + 3\varepsilon E(X^2)] \tag{36}$$

or, in view of Eq.(34)

$$E(X^2) = e_0^2 / [1 + 3(\varepsilon/\alpha) E(X^2)] \tag{37}$$

resulting in a quadratic

$$3(\varepsilon/\alpha)[E(X^2)]^2 + E(X^2) - e_0^2 = 0 \tag{38}$$

For numerical values adopted in Eq.(44), we have, instead of Eq.(38)

$$3[E(X^2)]^2 + E(X^2) - 0.54 = 0 \tag{39}$$

with attendant mean-square value

$$E(X^2) = 0.289 \tag{40}$$

which constitutes a difference of 6.47% with the exact solution.

Consider now the energy based stochastic linearization method. Eq.(6) yields

$$k_{eq}^{(3)} = \alpha + 2.5\varepsilon E(X^2) \tag{41}$$

Substitution $k_{eq}^{(2)}$ instead of $k_{eq}^{(1)}$ in Eq.(35) yields

$$E(X^2) = \pi S/\beta[\alpha + 2.5\varepsilon E(X^2)] \tag{42}$$

or in view of Eq.(21)

$$E(X^2) = e_0^2/[1 + 2.5(\varepsilon/\alpha)E(X^2)] \tag{43}$$

This results in a quadratic

$$2.5(\varepsilon/\alpha)\ [E(X^2)]^2 + E(X^2) - e_0^2 = 0 \tag{44}$$

For the values in Eq.(44), we get an equation

$$2.5[E(X^2)]^2 + E(X^2) - 0.54 = 0 \tag{45}$$

with attendant mean-square value $E(X^2) = 0.306$ which *coincides* with the exact value given in Eq.(33). For value of e_0^2 in vicinity of 0.54 and ratio ε/α in vicinity of unity, the relative error furnished by a new stochastic linearization technique may constitute about one percent, much smaller than the one produced by the conventional stochastic linearization technique.

The discovered coincidence of the stochastic linearization result with exact solution suggests that for specific set of parameters (namely for $e_0^2 \approx 0.54$) the new version of stochastic linearization constitutes a "*true*" linearization, in terminology of Kozin (1987).

DUFFING OSCILLATOR UNDER COLORED NOISE

For the Duffing oscillator subjected to Gaussian white noise the problem is amenable to exact solution. Consider now the case where the exact solution is absent. Indeed, the power of the stochastic linearization lies in its applicability when all other analytical methods may fail. Consider a Duffing oscillator subjected to a colored noise (Falsone and Elishakoff, 1992). The motion of the system is governed by the differential Eq.(20), where, under new circumstances, $Q(t)$ is a filtered noise; in particular, we assume that $Q(t)$ is the response of the following first order filter equation

$$\dot{Q} = -\gamma Q + \gamma W(t) \tag{46}$$

$W(t)$ being a white noise with constant spectral density S. In equation (46) the parameter γ gives the measure of the filtering. In fact, it is easy to verify that the spectral density function $S_Q(\omega)$ of $Q(t)$ is given by

$$S_Q(\omega) = \frac{\gamma^2}{\gamma^2 + \omega^2} S \tag{47}$$

and, for large values of γ, $S_Q(\omega)$ tends to S.

According to the classical linearization technique, Eq.(46) is replaced by the linearized one in which the linearized spring $k_{eq}^{(1)}$ is given by Eq.(34). In this way, the stationary mean square value response of the linearized system reads

$$E[X^2] = \frac{\gamma(\gamma + \beta)}{k_{eq}^{(1)}\beta(k_{eq}^{(1)} + \beta\gamma + \gamma^2)}\pi S \tag{48}$$

It is worth noting that, for large values of γ, this quantity tends to the mean square response of the linear system subjected to the white noise $W(t)$.

According to the new linearization technique, specified in Eq.(11), the linearized spring $k_{eq}^{(3)}$ is given by Eq. (41). The stationary mean-square response is given in Eq.(48) where $k_{eq}^{(1)}$ is replaced by $k_{eq}^{(3)}$.

The two linearization techniques have been first applied to the Duffing oscillator by varying the filter parameter γ and fixing the system parameters at values utilized by (Elishakoff, 1991):

$$\pi S/\alpha\beta = 0.54; \quad \varepsilon/\alpha = 1.00 \tag{49}$$

These values are the same ones for which the new linearization technique yielded the exact stationary solution, when the input is a white noise (Elishakoff, 1991). Falsone and Elishakoff (1992) evaluated the percentage-wise error between the results obtained by means of each of the two linearization schemes, and the results obtained by means of Monte Carlo simulation. The superior accuracy of the new linearization approach than that of the classical one was evident for each value of the filter parameter γ examined. Moreover, it is worth noting that, for $\gamma = 10$, the percentage error of the results obtained by the new technique is practically zero, confirming the previous result obtained by Elishakoff (1991). In the paper by Falsone and Elishakoff (1992) the percentage error for $\gamma = 1$, $\pi S/\alpha\beta = 0.54$ and varying the ε/α was studied. The preferable accuracy of the new approach established even for high level of non-linearity; indeed for $\varepsilon/\alpha = 2$ the classical linearization yielded an error of 12% whereas the error within the new method was under two percent.

These results confirm that, in the case of a Duffing oscillator, the linearization with respect to the potential energy yields much more accurate results than the classical linearization approach, even when the input is a colored noise and the level of non-linearity is high.

Let us elucidate now the proposed criteria on an example which was studied earlier in the literature via the perturbation method (Khabbaz, 1964). Namely, the system governed by the following differential equation

$$m\ddot{X} + c_0\dot{X}(1+b_2\dot{X}^2 + b_4\dot{X}^4) + k_0X(1+a_2X^2 + a_4X^4) = W(t) \tag{50}$$

is investigated. In Eq. (11) m is the mass, c_0 and k_0 are coefficients modelling the damping and spring stiffness of the linear system which is obtained by a formal substitution: $a_2 = b_2 = a_4 = b_4 = 0$. Here coefficients a_2, b_2, a_4 and b_4 are assumed to be positive and specified, $W(t)$ is a stationary Gaussian white noise. The exact solution of Eq. (50) is unavailable. We derive approximate solutions through various stochastic linearization criteria. The results are compared both with those yielded by the perturbation method and by the Monte Carlo simulation.

We first consider the analysis through conventional stochastic linearization. Conditions (4) and (13) yield respectively,

$$k_{eq}^{(1)} = k_0\left[E(X^2) + a_2E(X^4) + a_4E(X^6)\right]/E(X^2) \tag{51}$$

$$c_{eq}^{(1)} = c_0\left[E(\dot{X}^2) + b_2E(\dot{X}^4) + b_4E(\dot{X}^6)\right]/E(\dot{X}^2) \tag{52}$$

The mean square displacement of the linear system (with $a_2 = b_2 = a_4 = b_4 = 0$) equals

$$\sigma_{X_0^2} = \pi S/c_0k_0 \tag{53}$$

where S is the spectral density of $W(t)$. For the equivalent linear system the mean-square displacement is

$$\sigma_X^2 = \pi S/c_{eq}k_{eq} \tag{54}$$

Moreover, the mean-square velocity equals

$$\sigma_{\dot{X}}^2 = k_{eq}\sigma_X^2/m = \pi S/c_{eq}m \tag{55}$$

Utilizing the postulated jointly normal probability density of the displacement and velocity for evaluation of Eqs. (51) and (52), results in

$$k_{eq}^{(1)} = k_0(1+3a_2\sigma_X^2 + 15a_4\sigma_X^4) \tag{56}$$

$$c_{eq}^{(1)} = c_0\Big[1 + 3b_2(k_o/m)(1 + 3a_2\sigma_X^2 + 15a_4\sigma_X^4)\sigma_X^2 + 15b_4(k_0^2/m^2)(1 + 3a_2\sigma_X^2 + 15a_4\sigma_X^4)^2\sigma_X^4\Big] \tag{57}$$

Substitution of Eqs. (56) and (57) into Eq. (54) yields a polynomial equation

$$\sum_{i=0}^{9} A_i(\sigma_X^2)^i = 0 \tag{58}$$

where coefficients A_i read

$$A_0 = -\sigma_{X_0}^2, \qquad A_1 = 1, \qquad A_2 = 3(a_2m+k_0b_2)/m$$

$$A_3 = 3(5a_4m^2+6mk_0a_2b_2+5k_0^2b_4)/m^2$$

$$A_4 = 9k_0(3ma_2^2b_2+10ma_4b_2+15k_0a_2b_4)/m^2$$

$$A_5 = 135k_0(2ma_2a_4b_2+3k_0a_2^2b_4+5k_0a_4b_4)/m^2 \tag{59}$$

$$A_6 = 135k_0(5ma_4^2b_2+3k_0a_2^3b_4+30k_0a_2a_4b_4)/m^2$$

$$A_7 = 2025k_0^2a_4b_4(3a_2^2+5a_4)/m^2$$

$$A_8 = 30375k_0^2a_2a_4^2b_4/m^2, \qquad A_9 = 50625k_0^2a_4^3b_4/m^2$$

Here $\sigma_{X_0}^2$ is the mean-square response of the corresponding linear system. According to the Descartes' rule of signs, the polynomial Eq.(58) has a single positive root for σ_X^2, since the sequence of coefficients in Eq.(18) has only one change in sign. The evaluation of the mean-square displacement should be performed numerically.

Let us now utilize the criteria (8) and (16). The potential energy of the system reads

$$U(X) = k_0\left\{(1/2)X^2 + (1/4)a_2X^4 + (1/6)a_4X^6\right\} \tag{60}$$

For the energy dissipation function we obtain

$$\Phi(\dot{X}) = \int_0^{\dot{X}} c_0 \dot{u}(1 + b_2\dot{u}^2 + b_4\dot{u}^4)d\dot{u}$$
$$= c_0\left\{(1/2)\dot{X}^2 + (1/4)b_2\dot{X}^4 + (1/6)b_4\dot{X}^6\right\} \tag{61}$$

The expression for $k_{eq}^{(3)}$ reads

$$k_{eq}^{(3)} = 2k_0 K_{eq}^{(2)} \tag{62}$$

where

$$K_{eq}^{(2)} = (1/2) + (5/4)a_2\sigma_x^2 + (35/6)a_4\sigma_x^4 \tag{63}$$

The expression for the equivalent linear damping reads

$$c_{eq}^{(2)} = 2c_0\left[(1/2) + (5/4)b_2\sigma_{\dot{X}}^2 + (35/6)b_4\sigma_{\dot{X}}^4\right] = 2c_0 C_{eq}^{(2)} \tag{64}$$

where

$$C_{eq}^{(2)} = \frac{1}{2} + \frac{5}{4}b_2\frac{2k_0}{m}\left(\frac{1}{2} + \frac{5}{4}a_2\sigma_x^2 + \frac{35}{6}a_4\sigma_x^4\right)\sigma_x^2$$
$$+ \frac{35}{6}b_4\frac{4k_0^2}{m^2}\left(\frac{1}{2} + \frac{5}{4}a_2\sigma_x^2 + \frac{35}{6}a_4\sigma_x^4\right)^2\sigma_x^4 \tag{65}$$

The mean-square displacement equals

$$\sigma_X^2 = \frac{\pi S}{c_{eq}^{(2)}k_{eq}^{(2)}} = \frac{\sigma_{X_0}^2}{4C_{eq}^{(2)}K_{eq}^{(2)}} \tag{66}$$

Substitution of Eqs.(63) and (64) into Eq.(66) leaves us with a polynomial equation

$$\sum_{i=0}^{9} B_i(\sigma_X^2)^i = 0 \tag{67}$$

where the coefficients B_i are defined as

$$B_0 = -\sigma_{X_0}^2, \qquad B_1 = 1, \qquad B_2 = 5(a_2 m + k_0 b_2)/2m$$

$$B_3 = 5(14a_4 m^2 + 15mk_0 a_2 b_2 + 14k_0^2 b_4)6m^2$$

$$B_4 = 25\ k_0\ (15a_2^2 b_2 m + 56a_4 b_2 m + 84k_0 a_2 b_4)/24m^2$$

$$B_5 = 175\ k_0\ (10a_2 a_4 b_2 m + 15k_0 a_2^2 b_4 + 28k_0 a_4 b_4)/12m^2 \tag{68}$$

$$B_6 = 875\ k_0\ (28a_4^2 b_2 m + 15k_0 a_2^3 b_4 + 168k_0 a_2 a_4 b_4)/72m^2$$

$$B_7 = 6125\ k_0^2 a_4 b_4 (15a_2^2 + 28a_4)/36m^2$$

$$B_8 = 214375 k_0^2 a_2 a_4^2 b_4/18m^2, \qquad B_9 = 1500625 k_0^2 a_4^3 b_4/81m^2$$

Again, Eq.(67), like Eq.(58) has a single positive root. Combined utilization of criteria (10) and (18) yields

$$k_{eq}^{(3)} = 2k_0 K_{eq}^{(3)} \tag{69}$$

where

$$K_{eq}^{(3)} = \left[\frac{1}{4} + \frac{5}{4}a_2\sigma_X^2 + 35\left(\frac{1}{16}a_2 + \frac{1}{6}a^4\right)\sigma_X^4 + \frac{105}{4}a_2 a_4 \sigma_X^6 + 105 a_4 \sigma_X^8\right]^{1/2} \tag{70}$$

Also

$$C_{eq}^{(3)} = 2c_0 C_{eq}^{(3)} \tag{71}$$

where

$$C_{eq}^{(3)} = \left\{\frac{1}{4} + \frac{5}{4}\frac{b_2 k_{eq}^{(3)}}{m}\sigma_X^2 + 35\left(\frac{1}{16}b_2 + \frac{1}{6}b_4\right)\left[\frac{k_{eq}^{(3)}}{m}\right]^2 \sigma_X^4 + \frac{105}{4}b_2 b_4\left[\frac{k_{eq}^{(3)}}{m}\right]^3 \sigma_X^6 + 105 b_4\left[\frac{k_{eq}^{(3)}}{m}\right]^4 \sigma_X^8\right\}^{1/2} \tag{72}$$

Substitution of expressions for equivalent spring stiffness and equivalent damping coefficient into Eq.(54) yields an equation for σ_X^2:

$$\sigma_X^2 - \frac{\pi S}{c_{eq}^{(3)} k_{eq}^{(3)}} \equiv \sigma_X^2 - \frac{\sigma_{\dot{X}_0}^2}{4K_{eq}^{(3)} C_{eq}^{(3)}} = 0 \tag{73}$$

The explicit form of the resulting polynomial equation in terms of σ_X^2 is cumbersome and is not reproduced here. One can show, however, that the resulting equation also possesses a single root, as in previous cases.

The numerical results for Eq.(58)~(67) have been obtained by Elishakoff and Zhang (1992.b). Comparison with the results of Monte Carlo method (see Fig. 1 in the above paper) demonstrated that the conventional stochastic linearization technique results in the largest error. For small values of the parameter ε criteria 3 and 4 yielded values which were extremely close to the simulated mean-square responses. For intermediate values of ε, namely $\varepsilon \sim 1$, the fourth criterion performed the best, whereas for larger values, namely for $\varepsilon \sim 2$, the third criterion yielded results in close vicinity to those of the Monte Carlo method. Elishakoff and Zhang (1992.b) considered also a softening system:

$$m\ddot{X} + c\dot{X} + (k_0/\varepsilon) sgn(X)(1 - e^{-\varepsilon|X|}) = W(t)$$

For values of ε up to unity the criterion of equal energy variances yielded results in best agreement with the simulation. In the range $1 \leq \varepsilon \leq 2$ the energy wise minimum mean square criterion turned out to be superior to other criteria.

HYBRID WEIGHTED STOCHASTIC LINEARIZATION-MONTE CARLO METHOD

The motivating considerations for developing a hybrid stochastic linearization-Monte Carlo Method are as follows.

The fraction of problems amenable to exact solutions is very small. For most problems the exact solutions are unavailable. In these circumstances either purely numerical approximate techniques are utilized, or the Monte Carlo method is applied. Amount of computations within the Monte Carlo solution of the problem may be enormous for a large system. One still may want some analytical method combined with small scale simulation. One can significantly reduce the amount of calculations by the proposed method. To do this we choose the following form of the weighting functions (Elishakoff and Colombi, 1993)

$$w(X) = \left(1 + \sum_{i=1}^{n} \alpha_i U^i\right)^{1/2} \tag{75}$$

where coefficients α_i and β_i should be determined from the numerical experiments by the Monte Carlo method; n signifies the number of series of Monte Carlo simulations. Note that weighting functions have also been considered, although in totally different contexts by Wang and Zhang (1985), Yu and Cao (1988), Izumi et al (1989), Fang and Fang (1991), Elishakoff and Zhang

(1991.a) and Zhang (1992).

In other respects however, the proposed method is that of stochastic linearization. The four alternative criteria are replaced by their equivalents utilizing the weighting functions. For example, the third, criterion is replaced by

$$E\left\{w(X)\left[U(X) - k_{eq}^{(3)}X^2/2\right]\right\}^2 = \min \tag{76}$$

yielding

$$k_{eq}^{(3)} = \frac{2E\{w^2(X)U(X)X^2\}}{E\{w^2(X)X^4\}} \tag{77}$$

Each simulation series should be conducted for specified sets of parameters of the system. Thus for n specified sets of parameters the results of Monte Carlo simulations will numerically coincide with the results of the stochastic linearization technique. It is expected that for other sets of parameters the accuracy of the results yielded by the stochastic linearization technique with weighting function will be quite satisfactory.

Consider, for illustration purposes, a system governed by the following differential equation

$$m\ddot{X} + c\dot{X} + k_1X + k_2X^5 = W(t) \tag{78}$$

where m, c, k_1 and k_2 are positive constants, $W(t)$ is an ideal white noise with zero mean. The system (82) is amenable of exact solution. It has been chosen in order to elucidate the errors associated with approximate techniques. It was shown by Zhang, Elishakoff and Zhang (1991) that energy based linearization technique, even without recourse to the weighting functions reduces the errors in determining the mean-square displacement of the system, by about 50%.

We will illustrate the application of the energy based stochastic linearization technique with weighing function. The potential energy of the nonlinear system in Eq.(83) reads

$$U(X) = (1/2)k_1X^2 + (1/6)k_2X^6 \tag{79}$$

We perform a single series of Monte Carlo simulations. Hence, in Eq.(79), n is fixed at unity, with

$$w(X) = \left(1 + \alpha_1 U\right)^{1/2} \tag{80}$$

Substitution of Eq.(112) in Eq.(77), in view of Eq.(111) results in

$$k_{eq} = k_1 + 2k_2\frac{E[6X^8 + 3\alpha k_1X^{10} + \alpha k_2X^{14}]}{E[36X^4 + 18\alpha k_1X^6 + 6\alpha k_2X^{10}]} \tag{81}$$

The spectral analysis, yields the following mean-square displacement

$$\sigma_X^2 = \frac{\pi S}{c k_{eq}} = \frac{\sigma_{X_0}^2}{1 + A} \tag{82}$$

where $\sigma_{X_0}^2$ is defined as

$$\sigma_{X_0}^2 = \pi s / c k_1 \tag{83}$$

The "corrective" term A reads

$$A = 2\frac{k_2}{k_1}\frac{E[6X^8 + 3\alpha k_1 X^{10} + \alpha k_2 X^{14}]}{E[36X^4 + 12\alpha k_1 X^6 + 6\alpha X^{10}]} \tag{84}$$

To calculate $E[X^{2j}]$ we use the usual approximation that X has a normal probability density with zero mean Eq.(88) becomes:

$$\begin{aligned} &15015\alpha k_2^2\sigma_X^{12} + 630\alpha k_2\sigma_X^8 + \left(70k_2 - 315\alpha k_2 k_1\sigma_{X_0}\right)\sigma_X^6 \\ &+ 15\alpha k_1^2\sigma_X^4 + \left(6k_1 - 15\alpha k_1^2\sigma_{X_0}\sigma_X^2\right)\sigma_X^2 - 6k_1\sigma_{X_0} = 0 \end{aligned} \tag{85}$$

In the latter equation the parameter α is not known. In order to determine it, we first solve an auxiliary problem of evaluation the mean square displacement σ_X^2 for specified set of parameters, by the Monte Carlo method, say for

$$m = m^{(1)} \quad , \quad k_1 = k_1^{(1)} \quad , \quad c = c^{(1)}, \quad k_2 = k_2^{(1)} \tag{86}$$

The result of simulation is denoted by $\hat{\sigma}_X^2$. This allows one to determine the value of $\alpha = \hat{\alpha}$ corresponding the simulation results

$$\hat{\alpha} = \frac{-2\left(35k_2\hat{\sigma}_X^6 - 3k_1\hat{\sigma}_X^2 + 3k_1\hat{\sigma}_{X_0}\right)}{15\hat{\sigma}_X\left(1001k_2^2\hat{\sigma}_X^{12} + 42k_2k_1\hat{\sigma}_X^8 - 21k_2k_1\hat{\sigma}_X^6\hat{\sigma}_{X_0} + k_1^2\hat{\sigma}_X^4 - k_1^2\hat{\sigma}_{X_0}\sigma_X^4\right)} \tag{87}$$

We fix α at the value $\hat{\alpha}$ determined from this equation, and use it in Eq.(85) for values of parameters, other than those listed in Eq.(86). Once $\hat{\alpha}$ is substituted, Eq.(85) becomes a polynomial equation with respect to σ_X^2:

$$35035k_2^3\sigma_X^{15} - 35035k_2^3\sigma_X^{14} + 4473k_1k_2^2\sigma_X^{11} + 3003k_1k_2^2\sigma_X^{10}$$

$$- 1470k_2^2\sigma_X^{10} - 3738k_1k_2^2\sigma_{X_0}\sigma_X^9 - 2268k_1k_2^2\sigma_{X_0}\sigma_X^8 - 35k_1^2k_2\sigma_{X_0}\sigma_X^7$$

$$+ 161k_1^2k_2\sigma_X^7 + 35k_1^2k_2\sigma_{X_0}\sigma_X^6 - 35k_1^2k_2\sigma_X^6 + 126k_1k_2\sigma_X^6 - 189k_1^2k_2\sigma_{X_0}\sigma_X^5 \quad (88)$$

$$- 63k_1^2k_2\sigma_{X_0}\sigma_X^4 - 126k_1k_2\sigma_{X_0}\sigma_X^4 + 63k_1^2k_2\sigma_{X_0}^2\sigma_X^3 - 3k_1^3\sigma_{X_0}\sigma_X^3$$

$$+ 3k_1^3\sigma_X^3 + 63k_1^2k_2\sigma_{X_0}^2\sigma_X^2 - 3k_1^3\sigma_{X_0}\sigma_X^2 + 3k_1^3\sigma_X^2 + 3k_1^3\sigma_{X_0}^2\sigma_X$$

$$- 3k_1^3\sigma_{X_0}\sigma_X + 3k_1^3\sigma_{X_0}^2 - 3k_1^3\sigma_{X_0} = 0$$

To gain some insight, let us consider some numerical results. Let $m^{(1)} = 1$, $c^{(1)} = 0.1$, $k_1^{(1)} = 10$, $k_2^{(1)} = 15$. Simulation results are in close vicinity with exact solution. Calculations yield $\hat{\sigma}_X^2 = 0.687$. The conventional linearization yields for this set of parameters $\sigma_X^2 = 0.5043$, or 23.44% off the exact solution, and about 20% off the simulation for a sample of 10^6 simulating systems. The energy based stochastic linearization without weighting function results in an estimate $\sigma_X^2 = 0.5456$, or 17% off the exact value.

The value of $\hat{\alpha}$, matching the results of the Monte Carlo method and stochastic linearization equals $\hat{\alpha} = -0.000607$. As noted above, at $k_1^{(1)}=10$ the stochastic linearization technique yields results coincident with those furnished by the Monte Carlo Method. At value $k_1^{(2)} = 11$, the conventional stochastic linearization is off the solution predicted by the Monte Carlo method by 22.77%. The energy based criterion without weighting function results in 17% of error. The proposed combination of the energy-wise linearization with the Monte Carlo method yields an error under 5%, which corresponds to the reduction of error associated with the conventional stochastic linearization, by the factor of 4.6. In the closer vicinity to the parameters for which Monte Carlo analysis was performed error may be significantly smaller. For example, for $k_1^{(3)} = 10.5$, the proposed method yields an error of only 3.85%.

CONCLUSION

The results of the application have confirmed a superior performance of the new linearization techniques, for various cases, including both "hard" and "soft" oscillators. It appears that additional studies will prove useful to study the applicability of the proposed new stochastic linearization criteria in civil, mechanical, aeronautical, aerospace and naval engineering contexts.

ACKNOWLEDGEMENT

This study has been supported by the NASA Kennedy Space Center, through Cooperative Agreement No. NCC 10-0005, 51 to Florida Atlantic University. This support is gratefully appreciated.

REFERENCES

Anh, N.D., Krause, R., and Schiehlen, W., 1992, "Statistical Linearization and Large Excitation of Nonlinear Stochastic Mechanical Systems," *Nonlinear Stochastic Mechanics*, eds. N. Bellomo and F. Casciati, Springer Verlag, Berlin, pp. 1-12.

Atalik, T.S., and Utku S., 1976, "Stochastic Linearization of Multi-Degree-of-Freedom Non-Linear Systems," *Earthquake Engineering and Structural Dynamics*, Vol. 4, pp. 411-420.

Beaman, J.J., 1980, "Accuracy of Statistical Linearization," *New Approaches to Nonlinear Problems in Dynamics*, ed. P. J. Holmes, SIAM, Philadelphia, pp. 195-207.

Beaman, J.J., and Hedrick J.K., 1981, "Improved Statistical Linearization for Analysis and Control of Nonlinear Stochastic Systems," *Journal of Dynamical Systems, Measurement, and Control*, Vol. 103, pp. 22-27.

Bernard, P., 1992, "About Stochastic Linearization," *Nonlinear Stochastic Mechanics*, eds. N. Bellomo and F. Casciati, Springer Verlag, Berlin, pp. 61-70.

Bolotin, V.V., 1984, *Random Vibrations of Elastic Systems*, Martinus Nijhoff Publishers, The Hague, pp. 240-292.

Booton, R.C., 1953, "The Analysis of Nonlinear Control Systems with Random Inputs," *Proceedings Symposium on Nonlinear Circuit Analysis*, Vol. 2, pp. 341-344.

Busby, H.R., Jr., and Weingarten, V.I., 1973, "Response of Nonlinear Beam to Random Excitation," *Journal of Engineering Mechanics Division*, Vol. 99, pp. 55-68.

Caughey, T.K., 1963, "Equivalent Linearization Techniques," *Journal of Acoustical society of America*, Vol. 35 (11), pp. 1706-1711.

Caughey, T.K., and Dienes, J.K., 1961, "Analysis Nonlinear First-Order System with a White Noise Input," *Journal of Applied Physics*, Vol. 23, pp. 2476-2479.

Chang, R.J., 1990, "Non-Gaussian Linearization Method for Stochastic Parametrically and Externally Excited Nonlinear Systems," ASME Paper 90-WA/DSC-16, Presented at the ASME Winter Annual Meeting, Dallas, TX, Nov. 25-30, 1990.

Chang, R.J., and Young, G.E., 1989, "Methods and Gaussian Criterion for Statistical Linearization of Stochastic Parametrically and Externally Excited Nonlinear Systems," *Journal of Applied Mechanics*, Vol. 56, pp. 179-185.

Crandall, S.H., 1974, "Nonlinearities in Structural Dynamics," *The Shock and Vibration*

Digest, Vol. 6(8), pp. 1-13.

Crandall, S.H., 1977, " On Statistical Linearization for Nonlinear Oscillators," *Problems of the Asymptotic Theory of Nonlinear Oscillators*, Academy of Sciences of the Ukrainian SSR, Naukova Dumka, pp. 115-122. Reprinted, 1980, *Nonlinear System Analysis and Synthesis*, Vol. 2, *Techniques and Applications*, eds. R.V. Ramnath, J.K. Hedrick and H.M. Paynter, ASME, New York, pp. 199-209.

Constantinou, M.C., and I.G. Tadjbakhsh, 1984, "Response of a Sliding Structure to Filtered Random Excitation," *Journal of Structural Mechanics*, Vol. 12, pp. 401-418.

Constantinou, M.C., 1985, "Vibration Statistics of the Duffing Oscillator," *Soil Dynamics and Earthquake Engineering*, Vol. 4, pp. 221-223.

Donley, M.G., and Spanos, P.D., 1990, *Dynamic Analysis of Non-Linear Structures by the Method of Statistical Quadratization*, Springer Verlag, New York.

Donley, M.G., and Spanos, P.D., 1992, "Equivalent Statistical Quadratization for Multi-Degree-of-Freedom Nonlinear Systems," *Nonlinear Stochastic Mechanics*, eds. N. Bellomo and F. Casciati, Springer Verlag, Berling, pp. 185-200.

Elishakoff, I., 1991, "Method of Stochastic Linearization Revisited and Improved," *Computational Stochastic Mechanics*, eds. P.D. Spanos and C.A. Brebbia, Computational Mechanics Publications, Southampton, pp. 101-111.

Elishakoff, I., and Colombi, P., 1993, "Successful Combination of the Stochastic Linearization and Monte-Carlo Methods," *Journal of Sound and Vibration*, 160 (3), pp. 554-558.

Elishakoff, I., and Zhang, X.T., 1992.a, "An Appraisal of Different Stochastic Linearization Techniques," *Journal of Sound and Vibration*, Vol. 153, pp.370-375.

Elishakoff, I., and Zhang, R., 1992.b, "Comparison of the New Energy-Based Versions of the Stochastic Linearization Technique," *Nonlinear Stochastic Mechanics* , eds. N. Bellomo and F. Casciati, Springer Verlag, Berlin, pp. 201-212.

Falsone, G., 1992.a, "Stochastic Linearization for the Response of MDOF Systems Subjected to External and Parametric Gaussian Excitations," *Computational Stochastic Mechanics*" eds. P.D. Spanos and C.A. Brebbia, Computational Mechanics Publications, Southampton.

Falsone, G., 1992.b, "Stochastic Linearization of MDOF Systems under Parametric Excitations," *International Journal of Non-Linear Mechanics*, Vol. 27, pp. 1025-1037.

Falsone, G., and Elishakoff, I., 1992, "Modified Stochastic Linearization Technique for Colored Noise Excitation of Duffing Oscillator," *International Journal of Non-Linear Mechanics*, submitted for publication.

Fan, F.-G., and Ahmadi, G., 1990, "On Loss of Accuracy and Non-Uniqueness of

Solutions Generated by Equivalent Linearization and Cumulant-Neglect Methods," *Journal of Sound and Vibration*, Vol. 137, pp. 385-401.

Fang, J., and Fang, T.S., 1991, " A Weighted Equivalent Linearization Method in Random Vibration," *Chinese Journal of Applied Mechanics*, Vol. 8(3), pp. 114-120, (in Chinese).

Fang, T., Zhang, T. S. and Fang, J., 1991, "Nonstationary Response of Nonlinear Systems Under Random Excitation," *Proceedings, Third National Conference on Random Vibrations,* Taian, pp. 147-155, (in Chinese).

Iwan, W.D., and Mason, A.B., Jr., 1980, "Equivalent Linearization for Systems Subjected to Non-Stationary Random Excitation," *International Journal of Non-Linear Mechanics*, Vol. 15, pp. 71-82.

Izumi, M., Zaiming, L., and Kimuza, M., 1989, "A Stochastic Linearization Technique and Its Application to Response Analysis of Nonlinear Systems Based on Weighted Leas-Square Minimization," *Journal of Structural and Construction Engineering, Transaction of AIJ*, Vol. 395, pp. 72-81.

Kazakov, I.E., 1954, "An Approximate Method for the Statistical Investigation for Nonlinear Systems," *Trudi Voenno-Vozdushnoi Inzhenernoi Akademii imeni Prof. N.E. Zhukovskogo*, Vol. 399,(in Russian).

Khabbaz, G.R., 1964 "Power Spectral Density of the Response of a Nonlinear System to Random Excitation," *Journal of Acoustical Society of America*, Vol. 38, pp. 847-850.

Kolovskii, M.Z., 1966, "Estimating the Accuracy of Solutions Obtained by the Method of Statistical Linearization," *Automation and Remote Control*, Vol. 27, pp. 1692-1701.

Kozin, F., 1965, "Comments Upon the Technique of Statistical Linearization," *Proceedings Japan, Association of Automatic Control Engineers*, Annual Convention, pp. 15.1-15.10.

Kozin, F., 1987, "The Method of Statistical Linearization for Non-Linear Stochastic Vibrations," *Nonlinear Stochastic Dynamic Engineering Systems*, eds. F. Ziegler and G.I. Schuëller, Springer, Berlin, pp. 45-56.

Langley, R.S., 1988, "An Investigation of Multiple Solutions Yielded by the Equivalent Linearization Method, *Journal of Sound and Vibration*, Vol. 127, pp. 271-281.

Lee, X.X., and Chen, J.Q., 1992, "A Linearization Technique for Random Vibrations of Nonlinear Systems," *Mechanics Research Communications*, Vol. 19, pp. 1-6.

Mei, C., and Wentz, K. R. 1982, "Large Amplitude Random Response of Angle Ply Laminated Composite Plates," *AIAA Journal*, Vol. 20, pp. 1450-1458.

Mei, C., and Wolfe, H.F., 1986, "On Large Deflection Analysis in Acoustic Fatigue

Design," *Random Vibration-Status and Recent Developments*, eds. I. Elishakoff and R.H. Lyon, Elsevier, Amsterdam, pp. 279-302.

Mochio, T., Samaras, E. and Shinozuka, M., 1985, "Stochastic Linearization in a Finite Element Based Reliability Analysis," *Proceedings, Fourth International Conference on Structural Safety and Reliability*, eds. I. Konishi, A.H. S. Ang and M. Shinozuka, pp. 1375-1384.

Noori, M., and Davoodi, H., 1990, "Comparison between Equivalent Linearization and Gaussian Closure for Random Vibration Analysis of Several Nonlinear Systems," *International Journal of Engineering Sciences*, Vol. 28, pp. 897-905.

Piszczek, K., and Niziol, J., 1984, *Random Vibration of Mechanical Systems*, Ellis Horwood, Chichester, pp. 173-175.

Pradlwarter, H.J., 1991, "Non-Gaussian Linearization an Efficient Tool to Analyse Nonlinear MDOF-Systems," *Nuclear Engineering and Design*, Vol. 128, pp. 175-192.

Pradlwarter, H.J., and Schüeller, G.I., 1988, "Accuracy and Limitations of the Method of Equivalent Linearization for Hysterectic Multi-Storey Structures," *Nonlinear Stochastic Dynamic Engineering Systems*, eds. F. Ziegler and G. I. Schüeller, Springer Verlag, Berlin, pp. 3-21.

Pradlwarter, H. J., and Schüeller, G.I., 1992, "A Practical Approach to Predict the Stochastic Response of Many-DOF Systems Modeled by Finite Elements," *Nonlinear Stochastic Mechanics*, eds. N. Bellomo and F. Casciati, Springer Verlag, Berlin. pp. 427-437.

Popov, E.P., and Paltov, I. N., 1960, *Approximate Methods of Investigation of Nonlinear Automatic Systems*, "Fizmatgiz" Publishers, Moscow (in Russian).

Roberts, J.B., 1989, "Response of Nonlinear Mechanical Systems to Random Excitation, Part 2: Equivalent Linearization and Other Methods," *The Shock and Vibration Digest*, Vol. 13, No. 5, pp. 15-29.

Roberts, J.B., 1990, "Statistical Linearization: Multiple Solutions and Their Physical Significance," *Structural Dynamics*, eds. W.B. Krätzig et al, Balkema Publishers, Rottterdam, pp. 671-681.

Roberts, J.B., and Spanos, P.D., 1991, *Random Vibration and Statistical Linearization*, John Wiley and Sons, Chichester.

Seide, P., 1975, "Nonlinear Stresses and Deflections of Beams Subjected to Random Time Dependent Uniform Pressure," *Israel Journal of Technology*, Vol. 13, pp. 143-151.

Seide, P., 1976, "Nonlinear Stresses and Deflections of Beams Subjected to Random Time Dependent Uniform Pressure," *Journal of Engineering for Industry*, Vol. 98, pp. 1014-1020.

Shinozuka, M., 1972, "Monte Carlo Solution in Structural Dynamics," *Computers and*

Structures, Vol. 2, pp. 855-874.

Shinozuka, M., and Deodatis, G., 1991, "Simulation of Stochastic Process by Spectral Decomposition," *Applied Mechanics Reviews*, Vol. 44, pp. 191-203.

Sinitsin, I.N., 1974, "Methods of Statistical Linearization (Survey)", *Automation and Remote Control*, Vol. 35, pp. 765-8776.

Socha, L., and Soong, T. T., 1991, "Linearization in Analysis of Nonlinear Stochastic Systems," *Applied Mechanics Reviews*, Vol. 44, No. 1, 399-422.

Spanos, P.D., 1980, "Formulation of Stochastic Linearization for Symmetric or Asymmetric M.D.O.F. Nonlinear Systems," *Journal of Applied Mechanics*, Vol. 47, pp. 209-211.

Stratonovich, R.L., 1961, *Selected Problems of Theory of Fluctuation in Radiotechnics*, "Sovetskoe Radio" Publishers, Moscow, pp. 368 and 545 (in Russian).

To, C.W.S., 1984, "The Response of Nonlinear Structures to Random Excitation," *The Shock and Vibration Digest*, Vol. 16, pp. 13-33.

Zhang, X.T., 1989, "Equivalent Potential Technique for Deterministic and Random Response Analysis of Nonlinear Systems," *Applied Mechanics*, pp. 236-241, (in Chinese).

Zhang, X.T., Elishakoff, I., and Zhang, R.Ch., 1991, "A Stochastic Linearization Technique Based on Minimum Mean Square Deviation of Potential Energies", *Stochastic Structural Dynamics - New Theoretical Developments*, eds. Y. K. Lin and I. Elishakoff, Springer Verlag, Berlin, pp. 327-338.

Zhang, R. Ch., Elishakoff, I., and Shinozuka, M., 1992, "Analysis of Nonlinear Sliding Structures by Modified Stochastic Linearization Methods," *Probabilistic Mechanics and Structural and Geotechnical Reliability*", ed. Y.K.Lin, ASCE Press, New York, pp. 196-199. Extended version, *International Journal of Nonlinear Dynamics*, to appear.

Zhang, X., 1992, "Study of Weighted Energy Technique in Analysis of Nonlinear RAndom Vibration," *Nonlinear Vibration and Chaos*, Tianjin University Press, pp. 139-144.

Wang, C., and Zhang, X.T., 1985, "An Improved Equivalent Linearization Technique in Nonlinear Random Vibration," *Proceedings, International Conference on Nonlinear Mechanics*, pp. 959-964.

Wentz, K.R., Paul D.B., and Mei, C., 1982, "Large Deflection Random Response of Symmetric Laminated Composite Plates," *Shock and Vibration Bulletin*, Vol. 52, pp. 99-111.

Yu, Z.D., and Gao, G.A., 1988, *Theory of Random Vibration with Applications*, Tongji University Press (in Chinese).

CHAPTER # 7

Random Vibration of Beams with Nonlinear Stiffness: Comparison between Approximate and Exact Solutions

Random Vibration of Beams with Nonlinear Stiffness: Comparison between Approximate and Exact Solutions

I. Elishakoff[1], J. Fang[1] and R. Caimi[2]

[1]Center for Applied Stochastics Research

and Department of Mechanical Engineering

Florida Atlantic University

Boca Raton, FL 33431-0991

[2]NASA Kennedy Space Center, FL 32899

Abstract--A new stochastic linearization technique is employed to investigate the large amplitude random vibrations of a simply-supported or a clamped beam on elastic foundation under a stochastic loading which is space-wise either (a) white-noise or (b) uniformly distributed load and time-wise white noise. The new version of the stochastic linearization method is based on the requirement that mean square deviation of the strain energy of the nonlinearly deformed beam, and the strain energy of the equivalent beam in a linear state, should be minimal. As a result, the modal mean square displacements are expressed as solutions of a set of nonlinear algebraic equations. Results obtained by conventional equivalent linearization method and by the new technique are compared with the numerical results obtained from integration of the exact probability density function (when exact solution is available) or with the result of the Monte Carlo simulations (when the exact solution is unavailable). It is shown that the new stochastic linearization technique yields much more accurate estimate of the mean square displacement than the classical linearization method, which has attracted in the past interest of about 400 investigators in variety of nonlinear random vibration problems.

INTRODUCTION

Since it was first proposed by Booton [1] and Kazakov [2] four decades ago, the stochastic linearization method has been applied in numerous engineering fields. Application of this method to mechanical systems was performed by Caughey [3-5]. The excellent reviews of these studies have been given by Roberts and Spanos [6] and Socha and Soong [7]. Several authors recently have studied the various new versions of the improved stochastic linearization technique [8-10], which can be classified into two main categories: energy-based versions [8] and weighting function based versions [9-10]. Review of these developments was recently presented by Elishakoff and Falsone [11]. In the recent study [12] by the present authors, the beam under the time-wise and space-wise white noise loading was studied by the conventional and the new version of stochastic linearization technique, which is based on the criterion of minimum mean square deviation of potential energies. Comparison was performed with the exact solution available in that case. In the present study, the same energy-based method is employed to investigate the beam under general time dependent stationary random excitation, when exact solution is *unavailable*. The beam is resting on an elastic foundation and simply supported at both ends, and loaded by a stationary random excitation. As a result of moderately large vibrations, the different modes are coupled with each other, whose effect has been shown quite significant in Ref. [13-14]. Numerical simulations are carried out to compare their results with those yielded by the new and conventional linearization techniques. It is found that the new version of the stochastic linearization technique yields considerably more accurate results for the mean square response of the beam than the conventional stochastic linearization technique, especially in the case of large nonlinearity.

PROBLEM FORMULATION

Consider a beam resting on an elastic foundation, restrained at its ends, and loaded with spacewise distributed time dependent loading $p(x,t)$. The equation governing moderately large vibrations reads [8]

$$EI\frac{\partial^4 w}{\partial x^4} - N\frac{\partial^2 w}{\partial x^2} + \rho A\frac{\partial^2 w}{\partial t^2} + \beta\frac{\partial w}{\partial t} + K_f w = p(x,t) \tag{1}$$

where the axial force is given by

$$N = \frac{EA}{2L}\int_0^L \left(\frac{\partial w}{\partial x}\right)^2 dx \tag{2}$$

and E is the elastic modulus, I=moment of inertia of the cross section, ρ=mass density, A=cross sectional area, L=length of beam, K_f=stiffness of the elastic foundation, $p(x,t)$=time dependent stationary and ergodic random distributed loading acting on the beam. Moreover, for the load we will make an assumption of the multiplicative representation, i.e.

$$p(x,t) = r(x)\,q(t) \tag{3}$$

where $r(x)$ is the deterministic function of the axial coordinate only and $q(t)$ is the random function of the time alone. Also the autocorrelation function of the loading, which is considered to be weakly stationary in time, is known. According to the Wiener-Khintchine relationship

$$E[q(t_1)q(t_2)] = R(t_2 - t_1) = \int_{-\infty}^{\infty} S(\omega)\,e^{i\omega(t_2 - t_1)}\,d\omega \tag{4}$$

where $S(\omega)$ is the spectral function of $q(t)$.

Let the beam deflection function be expanded in terms of appropriate *orthonormal* set of mode shapes in vacuum $\phi_n(x)$ of the associated linear structure as

$$w = \sum_{n=1}^{\infty} W_n(t)\,\phi_n(x) \tag{5}$$

where $\phi_n(x)$ satisfy the following relationships

$$\begin{aligned} EI\frac{d^4\phi_n}{dx^4} &= \rho A\,\omega_n^2\phi_n \\ \int_0^1 \phi_m\phi_n\,d\xi &= \delta_{mn} \qquad \xi = x/l \end{aligned} \tag{6}$$

Then the expression for the axial force becomes

$$\begin{aligned} N &= \frac{EA}{2L}\int_0^L \sum_{m=1}^{\infty}\sum_{n=1}^{\infty} W_m W_n \frac{d\phi_m}{dx}\frac{d\phi_n}{dx}\,dx \\ &= \frac{EA}{2L^2}\sum_{m=1}^{\infty}\sum_{n=1}^{\infty} D_{mn} W_m W_n \end{aligned} \tag{7}$$

where

$$D_{mn} = \int_0^1 \frac{d\phi_m}{d\xi}\frac{d\phi_n}{d\xi}\,d\xi = D_{nm} \tag{8}$$

In view of Eq.(6), the governing equation (1) takes the following form

$$\sum_{n=1}^{\infty}\left[(\ddot{W}_n + \frac{\beta}{\rho A}\dot{W}_n + \omega_n^2 W_n + \frac{K_f}{\rho A}W_n)\phi_n - \frac{E}{2\rho L^4}\sum_{i=1}^{\infty}\sum_{j=1}^{\infty}D_{ij}W_iW_jW_n\frac{d^2\phi_n}{d\xi^2}\right] = \frac{r(x)q(t)}{\rho A} \quad (9)$$

Multiplication of Eq.(9) by ϕ_m, integration over the length of the beam and the use of orthogonality conditions given in Eq.(6) yield a set of coupled nonlinear differential equations for the modal amplitudes $W_m(t)$

$$\ddot{W}_m + \frac{\beta}{\rho A}\dot{W}_m + \omega_m^2 W_m + \frac{K_f}{\rho A}W_m + \frac{E}{2\rho L^4}\sum_{i=1}^{\infty}\sum_{j=1}^{\infty}\sum_{n=1}^{\infty}D_{ij}R_{mn}W_iW_jW_n = \frac{Q_m}{\rho A}q(t) \quad (10)$$

where

$$Q_m = L\int_0^1 \phi_m(\xi)\, r(\xi)\, d\xi$$
$$R_{mn} = \int_0^1 \phi_m \frac{d^2\phi_n}{d\xi^2}\, d\xi \quad (11)$$

By either conventional or the new version of the stochastic linearization technique, Eq.(10) is replaced by a linear one

$$\ddot{W}_m + \frac{\beta}{\rho A}\dot{W}_m + k_{m,eq}\omega_m^2 W_m = \frac{Q_m}{\rho A}q(t) \quad (12)$$

where $k_{m,eq}$ is the nondimensional equivalent stiffness. The problem consists in evaluating $k_{m,eq}$ through two versions of stochastic linearization technique and comparing the results for response with those obtained from the Monte Carlo simulations.

ANALYSIS

The potential energy of the system, represented by Eq.(10) reads, in conjunction with Eq. (9)

$$U = \sum_{m=1}^{\infty} \frac{1}{2}(\omega_m^2 + \frac{K_f}{\rho A})W_m^2 + \sum_{m=1}^{\infty} \frac{E}{2\rho L^4} \int_0^{W_m} (\sum_{i=1}^{\infty} \sum_{j=1}^{\infty} \sum_{n=1}^{\infty} D_{ij} R_{mn} W_i W_j W_n) dW_m \tag{13}$$

The main idea of the modified method consists in the requirement that the mean square difference between the potential energy, associated with the original nonlinear equation, Eq.(10), and its equivalent linear counterpart Eq.(12), to be minimal. That is

$$E\left\{\left[U - \sum_{n=1}^{\infty} \frac{1}{2} k_{n,eq} \omega_n^2 W_n^2\right]^2\right\} = \min \tag{14}$$

which is achieved by demanding

$$\frac{d}{d(k_{m,eq}\omega_m^2)} \left\{E\left[U - \sum_{n=1}^{\infty} \frac{1}{2} k_{n,eq} \omega_n^2 W_n^2\right]^2\right\} = 0 \tag{15}$$

$$(m = 1, 2, \cdots)$$

The conditions (15) are equivalent to

$$E\left\{\left[U - \sum_{n=1}^{\infty} \frac{1}{2} k_{n,eq} \omega_n^2 W_n^2\right] W_m^2\right\} = 0 \tag{16}$$

$$(m = 1, 2, \cdots)$$

Thus, if only first N normal modes are included, Eq.(16) can be written as

$$[A]\{k_{eq}\} = 2\{B\} \tag{17}$$

where

$$[A] = \begin{bmatrix} E[W_1^2W_1^2] & E[W_1^2W_2^2] & \cdots & E[W_1^2W_N^2] \\ E[W_2^2W_1^2] & E[W_2^2W_2^2] & \cdots & E[W_2^2W_N^2] \\ & & \cdots & \\ E[W_N^2W_1^2] & E[W_N^2W_2^2] & \cdots & E[W_N^2W_N^2] \end{bmatrix} \tag{18}$$

$$\{k_{eq}\}^T = \{k_{1,eq}, \quad k_{2,eq}, \quad \cdots \quad , \quad k_{N,eq}\}$$

$$\{B\}^T = \{E[W_1^2U] \quad E[W_2^2U] \quad \cdots \quad E[W_N^2U]\}$$

The solution can be written as

$$\{k_{1,eq}\omega_1^2, k_{2,eq}\omega_2^2, \cdots, k_{N,eq}\omega_N^2\}^T = 2[A]^{-1}\{B\} \tag{19}$$

For the Gaussian random processes with zero mean, we have [14]

$$E[z_1z_2\ldots z_{2m}] = \sum_{\text{all independent pairs}} \left[\prod_{j\neq k} E[z_jz_k]\right] \tag{20}$$

where the number of independent pairs is equal to $(2m)!/2^m m!$. In view of the representation of the potential energy by Eq.(13), the following terms will appear in {B}

$$E[W_m^2 W_n^2] = E[W_m^2]\,E[W_n^2] + 2(E[W_m W_n])^2$$

$$E[W_l^2 W_m^2 W_n^2] = E[W_l^2]\,E[W_m^2 W_n^2] + 2E[W_l W_m]\,E[W_l W_m W_n^2]$$

$$+ 2E[W_l W_n]\,E[W_l W_m^2 W_n] \qquad (21)$$

$$= E[W_l^2]E[W_m^2 W_n^2] + 2(E[W_l W_m])^2\,E[W_n^2]$$

$$+ 2(E[W_l W_n])^2\,E[W_m^2] + 8E[W_l W_m]\,E[W_l W_n]\,E[W_m W_n]$$

The moments $E[W_m W_n]$ are related with the spectra of the system in the following way

$$E[W_m W_n] = \frac{Q_m Q_n}{(\rho A)^2} \int_{-\infty}^{\infty}\int_{-\infty}^{\infty} h_m(t-t_1)\,h_n(t-t_2)\,E[q(t_1)q(t_2)]\,dt_1\,dt_2 \qquad (22)$$

where the function $h_m(t)$ is the response of the SDOF system represented by each of equations (12) to a unit impulse. The Fourier transform of $h_m(t)$

$$h_m(t) = \frac{1}{2\pi}\int_{-\infty}^{\infty} e^{i\omega t} H_m(\omega)\,d\omega$$

$$H_m(\omega) = \int_{-\infty}^{\infty} e^{-i\omega t} h_m(t)\,dt \qquad (23)$$

is given by

$$H_m(\omega) = \frac{1}{k_{m,eq}\omega_m^2 - \omega^2 + i\dfrac{\beta}{\rho A}\omega_m} \qquad (24)$$

For stationary random excitations

$$E[q_1(t)q_2(t)] = R(t_2 - t_1) = \int_{-\infty}^{\infty} S(\omega)\,e^{i\omega(t_2 - t_1)}\,d\omega \qquad (25)$$

With the use of Eq. (23), the double integral in Eq. (22) becomes

$$S_{mn} = \int_{-\infty}^{\infty}\int_{-\infty}^{\infty} h_m(t-t_1)\, h_n(t-t_2)\, E[q(t_1)q(t_2)]\, dt_1\, dt_2$$
$$= \int_{-\infty}^{\infty} H_m(-\omega)\, H_n(\omega)\, S(\omega) d\omega \tag{26}$$

For the white noise excitation, S_{mn} can be evaluated through frequency response function of system (12) by means of residue theorem to yield

$$S_{mn} = \frac{4\pi S_0 \frac{\beta}{\rho A}}{(k_{m,eq}\omega_m^2 - k_{n,eq}\omega_n^2)^2 + 2(\frac{\beta}{\rho A})^2 (k_{m,eq}\omega_m^2 + k_{n,eq}\omega_n^2)} \tag{27}$$

where S_0 is a constant value of the spectral density $S(\omega)$. As a result, S_{mn} is expressed through the sought parameters $k_{m,eq}$. After substituting Eq.(27) to Eq.(22), and the result into Eqs.(21), (19), (18), we obtain a set of nonlinear algebraic equations, i.e, Eq.(17) in terms of $k_{m,eq}$, which must be solved numerically to obtain $k_{m,eq}$.

From the conventional stochastic linearization technique, we have

$$\bar{k}_{m,eq} = 1 + \frac{K_f}{\rho A \omega_m^2} + \frac{E}{2\rho L^4 \omega_m^2 Q_m} (\frac{1}{\rho A})^2 \sum_{i=1}^{\infty}\sum_{j=1}^{\infty}\sum_{n=1}^{\infty} D_{ij} R_{mn} Q_i Q_j Q_n \frac{(S_{ij}S_{mn} + 2S_{im}S_{jn})}{S_{mn}} \tag{28}$$

The overbar denotes the association with the conventional stochastic linearization. Note that in obtaining the latter expression for $\bar{k}_{m,eq}$, we utilized the same procedure as Seide [15]; indeed when K_f=0, Eq.(28) coincides with Eq.(22) of Ref. [15]. In the same fashion as for the new stochastic linearization, we have arrived at a set of nonlinear algebraic equations which must be

solved numerically.

A particular case of the beam simply supported at both ends under a spacewise uniform random excitation is numerically evaluated:

$$\phi_m(\xi) = \sqrt{2}\sin m\pi\xi$$

$$Q_m = \begin{cases} 0 & \text{if } m \text{ is even} \\ \dfrac{2\sqrt{2}}{m\pi} & \text{if } m \text{ is odd} \end{cases}$$

$$D_{mn} = \begin{cases} 0 & \text{if } m = n \\ m^2\pi^2 & \text{if } m = n \end{cases} \tag{29}$$

$$R_{mn} = D_{mn}$$

$$\omega_m^2 = \frac{EI}{\rho AL^4} m^4\pi^4$$

Then accordance with Eq.(13) the potential energy reads

$$U = \frac{\omega_0^2}{2}\left[\sum_{m=1}^{N} m^4 W_m^2 + \alpha\sum_{m=1}^{N} W_m^2 + \frac{1}{4R^2}\left(\sum_{m=1}^{N} m^2 W_m^2\right)^2\right] \tag{30}$$

where

$$\alpha = \frac{K_f}{\rho A\omega_0^2}\ , \qquad \omega_0^2 = \frac{\pi^4 EI}{\rho AL^4}$$

$$\omega_m^2 = \omega_0^2 m^4\ , \qquad R = \sqrt{\frac{I}{A}} \tag{31}$$

Therefore Eq. (19) becomes

$$\left\{k_{1,eq}, 16k_{2,eq}, \cdots, N^4 k_{N,eq}\right\}^T = \frac{2}{\omega_0^2}[A]^{-1}\left\{E[W_1^2 U], E[W_2^2 U], \cdots, E[W_n^2 U]\right\}^T \tag{32}$$

This set represents a set of nonlinear algebraic equations since $E[W_j^2 U]$ themselves contain $k_{j,eq}$.

For the simply supported beam with elastic foundation, the motion of equation (10) becomes

$$\ddot{W}_m + \frac{\beta}{\rho A}\dot{W}_m + \omega_m^2\left(1 + \frac{\alpha}{m^4} + \frac{1}{2R^2 m^2}\sum_{n=1}^{\infty} n^2 W_n^2\right)W_m = \frac{q(t)}{\rho A}Q_m \tag{33}$$

As a result, the equivalent coefficients in Eq.(28) by the conventional stochastic linearization technique become

$$\bar{k}_{m,eq} = 1 + \frac{\alpha}{m^4} + \frac{1}{2R^2 m^2}\sum_{n=1}^{\infty} n^2 \frac{Q_n^2}{(\rho A)^2}\frac{(S_{mm}S_{nn} + 2S_{mn}^2)}{S_{mm}} \tag{34}$$

For $R \to \infty$ the contribution of nonlinear terms disappears. Therefore, R in actuality is a nonlinearity parameter. We will be interested in evaluating the effect of this parameter on the mean square response.

NUMERICAL RESULTS AND DISCUSSION

Calculations are performed to compute the mean square responses by the new and conventional stochastic linearization techniques. Since no exact solution is available for the beam under spacewise excitation, the numerical simulation is also carried out for all the cases of parameters listed at the figures.

In carrying out the numerical computations, the following material parameters have been

assumed through out the present work, $\omega_0^2=1.0$, and $\beta_0=\beta/(\rho A)=0.1$. Three normal modes are considered in the numerical evaluation, but only the first mode response is plotted in the figures since the first mode response dominates the mean square displacements of the beam. In Fig. 1, the mean square responses by conventional and new linearization and Monte Carlo simulation versus the nonlinearity coefficient R are shown for the case of $S_0=1.0$, $\alpha=0.0$, $\beta=0.1$. Fig. 2 also shows the three results obtained both through conventional and new stochastic linearization techniques, and Monte Carlo simulation for another set of parameters with $S_0=5.0$, $\alpha=1.0$, $\beta=0.1$. It can be seen that the new version of stochastic linearization method exhibits a superior performance over the conventional one at all ranges of variation of R. Fig. 3 displays the influence of the stiffness of the elastic foundation on the mean square response of the system for the case $S_0=0.1$, $\beta=0.1$, $R=1.0$. These results clearly indicate that the present method yields results in closer vicinity with the simulation results than the conventional linearization technique.

ACKNOWLEDGEMENT

This study has been supported by the NASA Kennedy Space Center, through Cooperative Agreement No. NCC 10-0005, S1 to Florida Atlantic University. This support is gratefully appreciated.

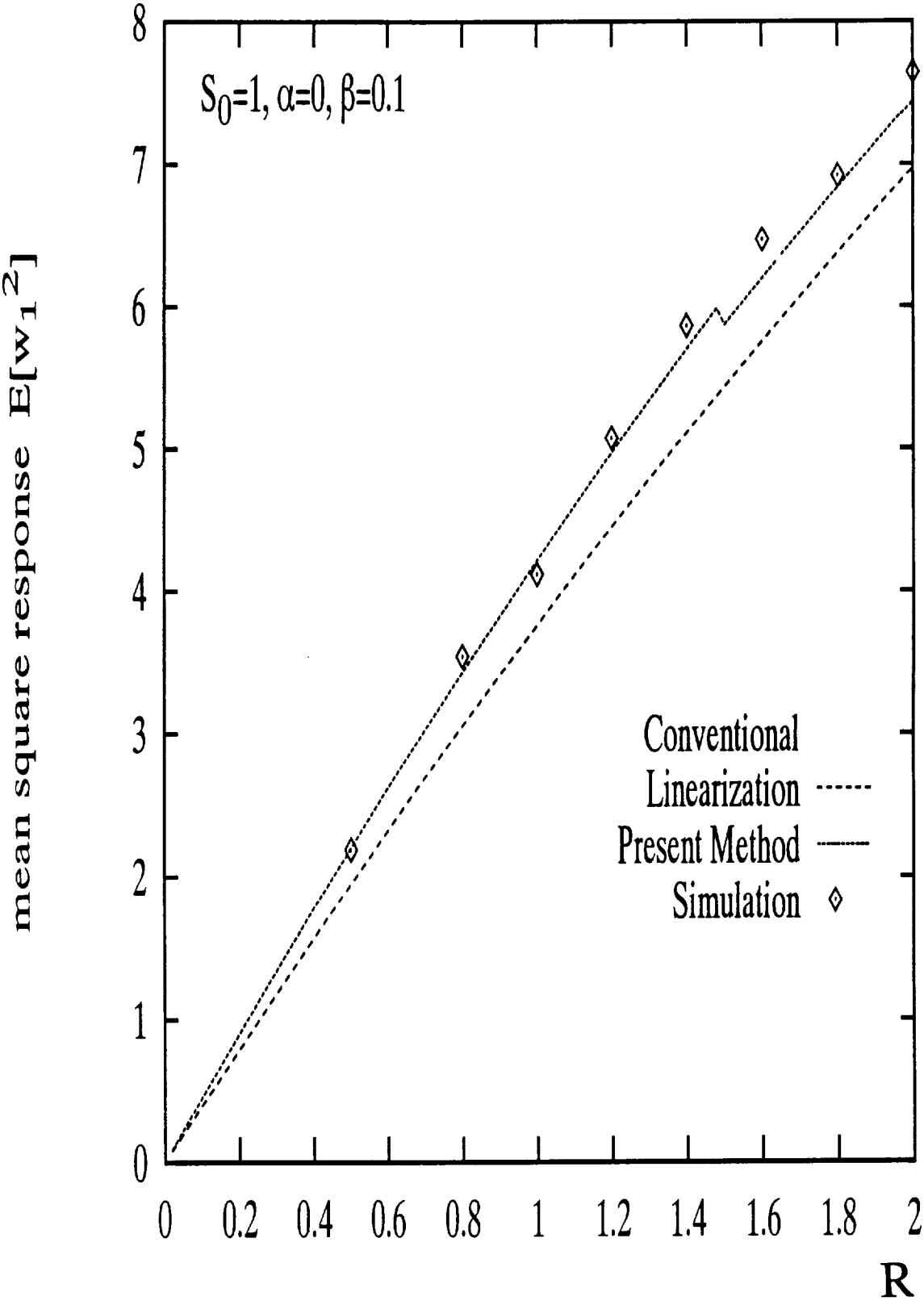
S_0=1, α=0, β=0.1
mean square response $E[w_1^2]$
R
Conventional
Linearization
Present Method
Simulation
0
1
2
3
4
5
6
7
8
0
0.2
0.4
0.6
0.8
1
1.2
1.4
1.6
1.8
2

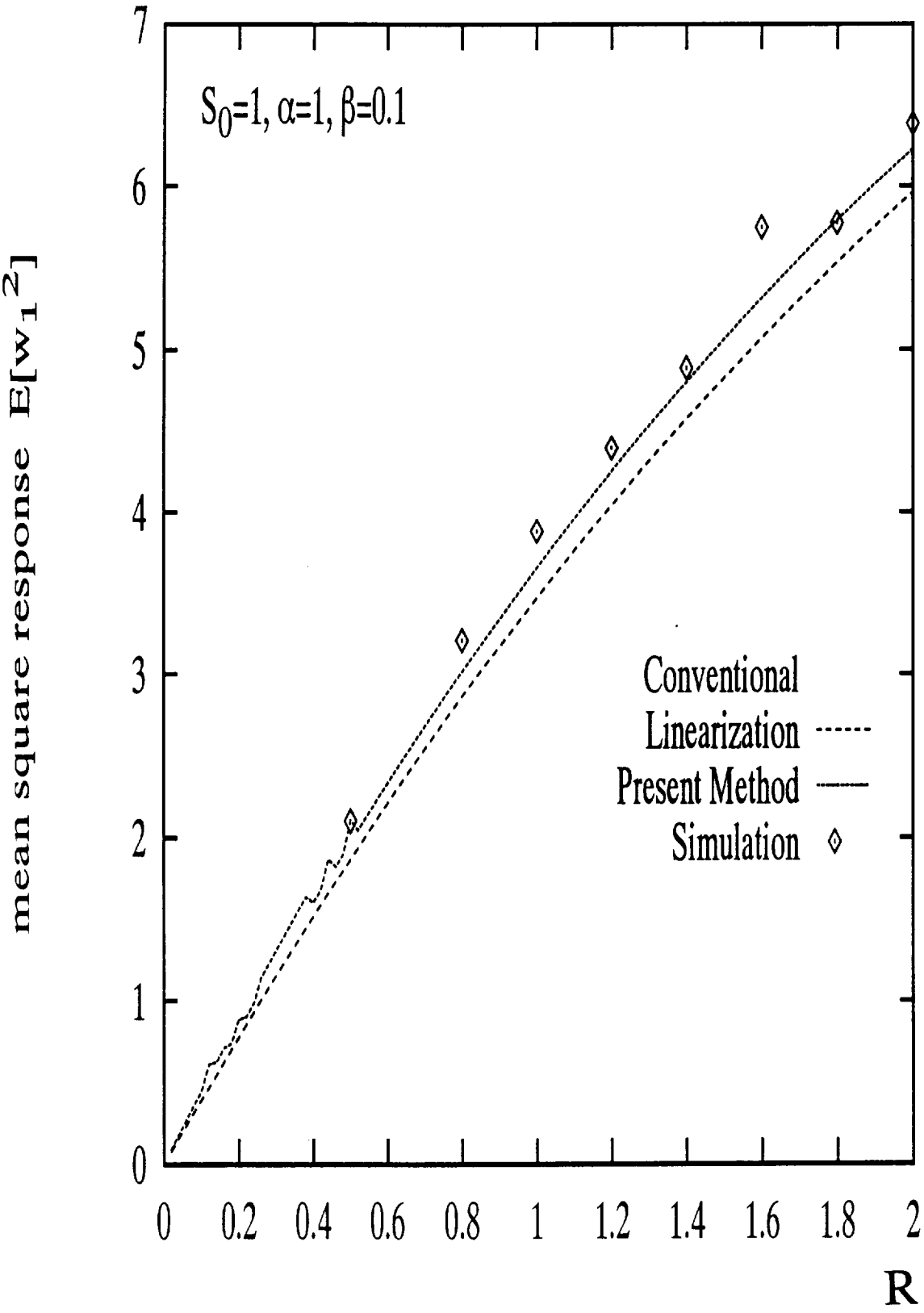
S_0=1, α=1, β=0.1
mean square response $E[w_1^2]$
R
Conventional
Linearization
Present Method
Simulation
0
1
2
3
4
5
6
7
0
0.2
0.4
0.6
0.8
1
1.2
1.4
1.6
1.8
2

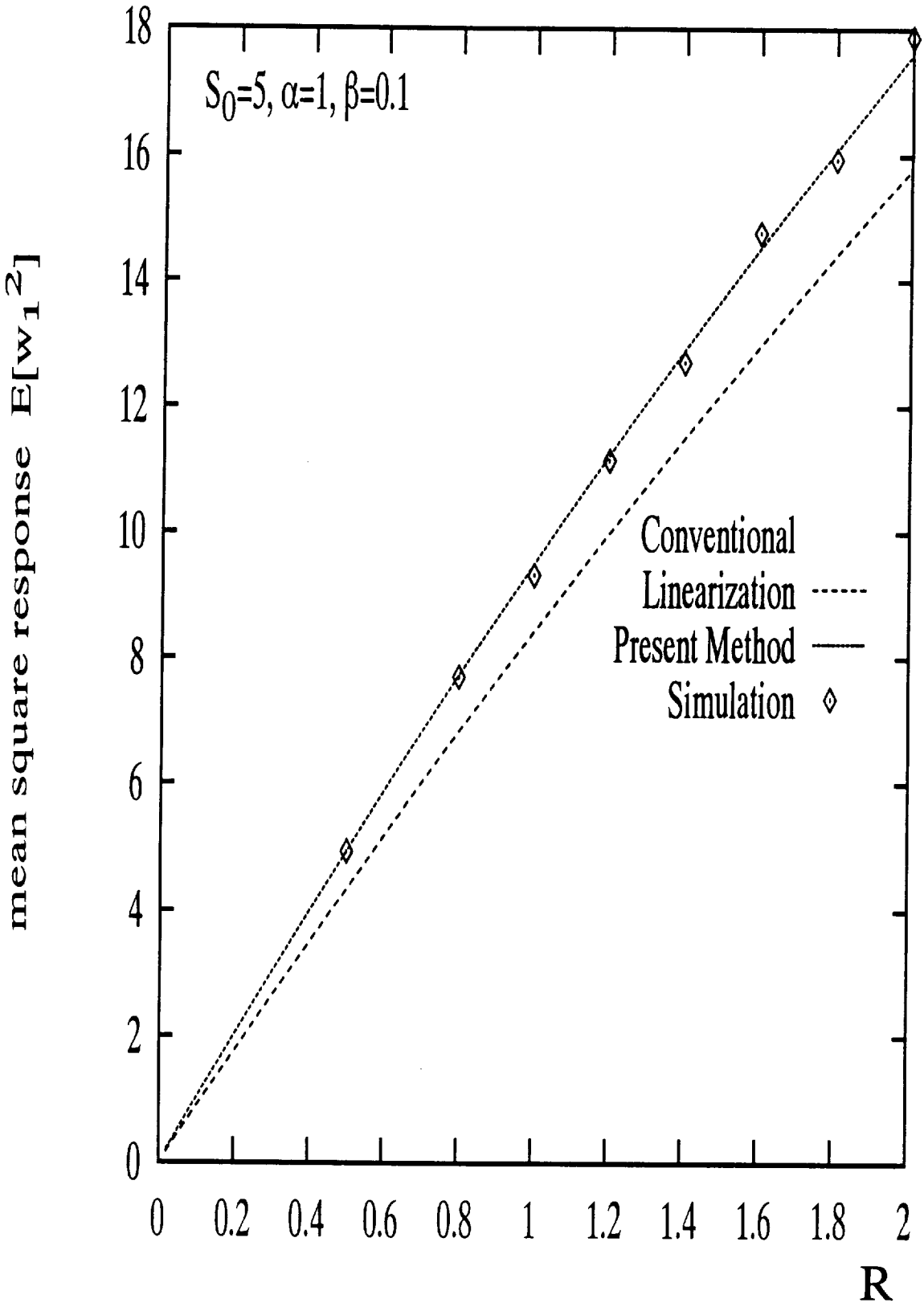
S_0=5, α=1, β=0.1
mean square response E[w_1^2]
Conventional
Linearization
Present Method
Simulation
0
2
4
6
8
10
12
14
16
18
0
0.2
0.4
0.6
0.8
1
1.2
1.4
1.6
1.8
2
R

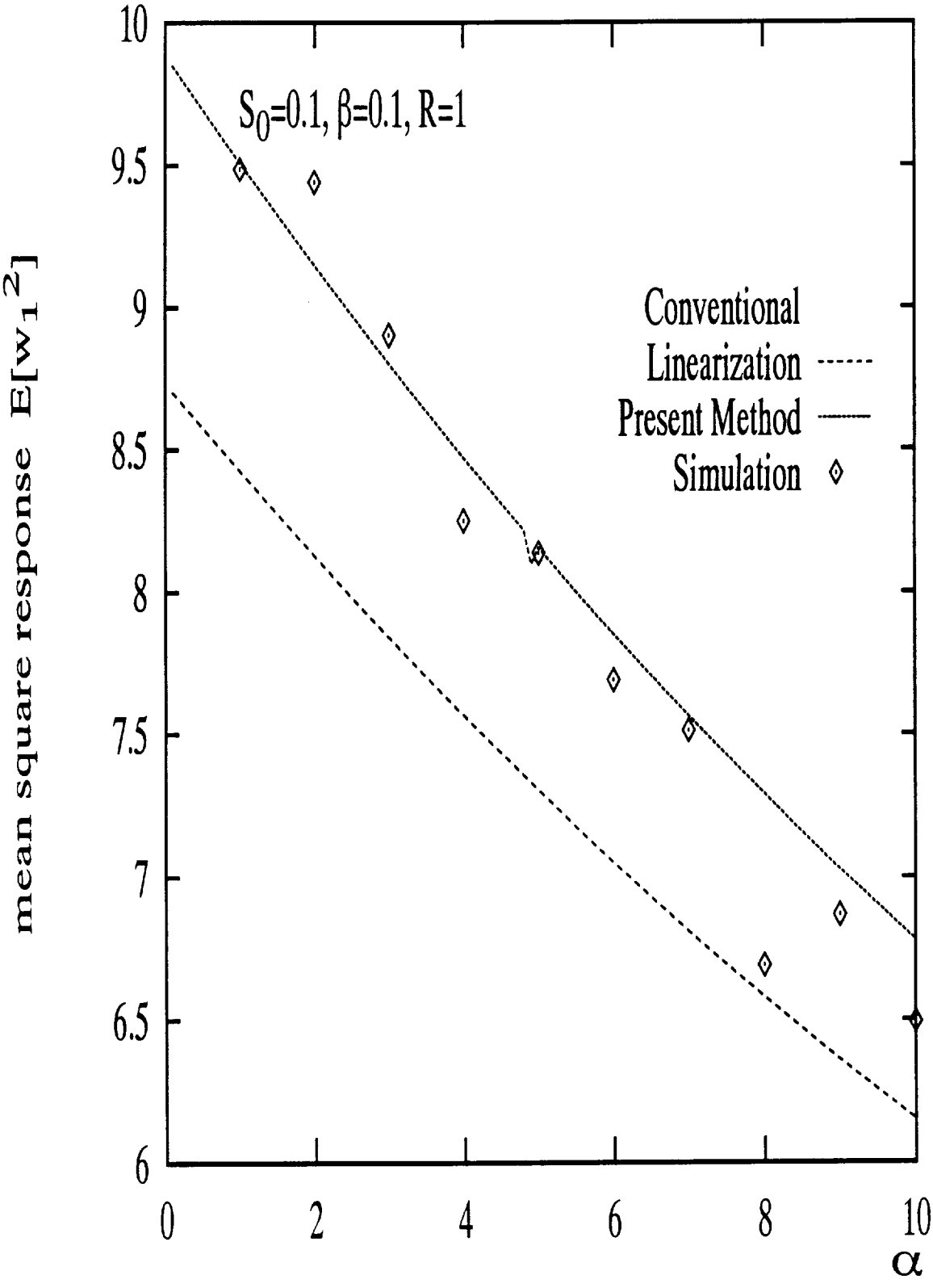
S_0=0.1, β=0.1, R=1
Conventional Linearization
Present Method
Simulation
mean square response $E[w_1^2]$
α
10
9.5
9
8.5
8
7.5
7
6.5
6
0
2
4
6
8
10

REFERENCES

1. Booton, R. C., Nonlinear Control Systems with Random Inputs, *IRE Transactions, Circuit Theory*, CT-1, 1954, **1**, 9-19.

2. Kazakov, I. E., An Approximate Method for the Statistical Investigation for Nonlinear Systems, *Trudy Voenno Vozdushnoi Akademii Imeni Professora N.E. Zhukovskogo, (Proceedings of the Military Air Force Academy Named after Prof. N. E. Zhukovskii)*, 1954, p394.

3. Caughey, T. K., Response of a Nonlinear String to Random Loading, *J. Appl. Mech.*, 1959, **26**, 341-344.

4. Caughey, T. K., Response of Van del Pol's Oscillator to Random Excitations, *J. Appl. Mech.*, 1959, **26**, 345-348.

5. Caughey, T. K., Equivalent Linearization Techniques, *J. Acoust. Soc. Am*, 1963, **35**, 1706-1711.

6. Roberts, J. B. and Spanos, P. D., *Random Vibration and Statistical Linearization*. John Wiley, Chichester, UK, 1990.

7. Socha, L. and Soong, T. T., Linearization in Analysis of Nonlinear Stochastic Systems, *Appl. Mech. Reviews*, 1991, **44**, 399-422.

8. Zhang, X. T., Elishakoff, I. and Zhang, R. C., A Stochastic Linearization Technique Based on Minimum Mean Square Deviation of Potential Energies, *Stochastic Structural Dynamics-1* (Y. K. Lin and I. Elishakoff, eds.), Springer, Berlin, 1990, 327-338.

9. Izumi, M., Zaiming, L. and Kimura, M., A Stochastic Linearization Technique and Its Application to Response Analysis of Nonlinear System Based on Weighted Least Square Minimization, *J. Structural and Construction Engineering*, Trans., AJJ, 1989, **395**, 72-81.

10. Fang, J. and Fang, T., A New Equivalent Linearization Method in Random Vibration, *Chinese J. Appl. Mech.*, 1991, **8**, 114-120 (in Chinese).

11. Elishakoff, I. and Falsone, G., Some Recent Developments in Stochastic Linearization Technique, *Computational Stochastic Mechanics*, (A. H-D Cheng and C. Y. Yang, eds.), Computational Mechanics Publications, Southampton, 1993, 175-194.

12. Elishakoff, I. and Fang, J., Random Vibration of a Nonlinearly Deformed Beam by a New Stochastic Linearization Technique, submitted for publication in *Int. J. Solids Structures*.

13. Herbert, R. E., Random Vibrations of a Nonlinear Elastic Beam, *J. Acoust. Soc. Am*, 1964, **36**, 2090-2094.

14. Herbert, R. E., On the Stresses in a Nonlinear Beam subject to Random Excitation, *Int. J. Solids Structures*, 1965, **1**, 235-242.

15. Seide, P., Nonlinear Stresses and Deflections of Beams Subjected to Random Time Dependent Uniform pressure, *J. of Engng. for Industry*, paper No. 75-DET-23, 1975.

Fig. 1 The mean square response of the first mode $E[W_1^2]$ calculated in the three mode approximation (N=3) vs. the nonlinearity coefficient R (S_0=1, α=0, β=0.1).

Fig. 2 The mean square response of the first mode $E[W_1^2]$ calculated in the three mode approximation (N=3) vs. the nonlinearity coefficient R (S_0=1, α=1, β=0.1).

Fig. 3 The mean square response of the first mode $E[W_1^2]$ calculated in the three mode approximation (N=3) vs. the nonlinearity coefficient R (S_0=5, α=1, β=0.1).

Fig. 4 The influence of the stiffness of the elastic foundation α on the mean square response of the system (S_0=0.1, β=0.1, R=1).

CHAPTER # 8

Nonlinear Response of a Beam under Stationary Random Excitation: Comparison between Approximate and Monte Carlo Solutions

Nonlinear Response of a Beam Under Stationary Random Excitation: Comparison between Approximate and Monte Carlo Solutions

Jianjie Fang[1], Isaac Elishakoff[1] and Raoul Caimi[2]

[1]Center for Applied Stochastics Research

and Department of Mechanical Engineering

Florida Atlantic University

Boca Raton, FL 33431-0991

[2]NASA Kennedy Space Center

FL 32899

Abstract: The new stochastic linearization technique is employed to investigate the nonlinear mean square response of a beam with arbitrary boundary conditions under time dependent stationary random excitation. To demonstrate the accuracy of this new method, mean square response is obtained through both the new and conventional versions of the stochastic linearization technique. An example of a beam with both ends simply supported, is presented, for the case of white noise excitation, to illustrate the present method. Numerical simulations are performed to check the accuracy of the modified technique. It is shown that the modified version can yield more accurate results for the mean square response of the beam than the conventional stochastic linearization technique, especially when there exists a large nonlinearity.

Keywords: conventional and new stochastic linearization, nonlinear beam, mean square response, Monte-Carlo simulation

1. INTRODUCTION

The random vibrations of beams in linear and nonlinear settings have been investigated by several authors. Linear random vibrations have been investigated by Eringen (1957), Bogdanoff and Goldberg (1960), Crandall and Yildiz (1962), Elishakoff and Livshits (1984) and Elishakoff (1987), by employing the normal mode method. Eringen (1957), Elishakoff (1987) and Elishakoff and Livshits (1984) were able to sum up the infinite series of modal contributions and derive closed-form solutions for simply supported beams subjected to loading which is both time-wise and space-wise white noise. For this particular excitation, Herbert (1964, 1965) succeeded to obtain an exact, although not a closed-form solution, for probability density function of modal displacements. For the general case of excitation, when dealing with the nonlinear stochastic boundary-value problems, most investigators have employed approximate techniques: either the classical perturbation method or the stochastic linearization technique. The latter method has attracted numerous investigators. Indeed the only monograph in this subject, that by Roberts and Spanos (1990) lists approximately 250 papers utilizing the stochastic linearization technique. The review by Sinitsin (1974) lists about 120 studies predominantly performed in Russia. The review paper by Socha and Soong (1991) lists numerous publications written in both West and East. Thus presently there are approximately 400 studies based on the classical stochastic linearization technique. Unfortunately, these methods have severe limitations: the perturbation method usually only leads to results of acceptable accuracy for the case of small nonlinearity; stochastic linearization technique can yield an error as large as 20% in the estimate of the mean-square response for some cases of nonlinearity and excitation. It should be born in mind that even an exact solution by the Fokker-Planck equation method may involve a large

amount of multiple integrations to evaluate the mean square responses if many modes need to be included. The latter difficulty is of purely numerical nature whereas the approximate methods have their inherent difficulties. Furthermore the fact that the (numerically cumbersome) exact solution is available for extremely specific cases of excitations rules out its general application. The above disadvantages of the approximate methods and absence of the exact solution for the general loading case encouraged the present authors to seek for alternative approximate technique. Improved stochastic linearization method seems to be an attractive method in this respect due to the fact that it not only retains the advantages of the conventional stochastic linearization method such as simplicity and straightforward manner of derivations, but also may greatly improve the accuracy. Several authors recently studied the various versions of the improved stochastic linearization technique (Elishakoff and Zhang, 1991; Elishakoff, 1991; Zhang, Elishakoff and Zhang 1990; Fang and Fang, 1991). In this study a new stochastic linearization technique, as discussed in several references (Elishakoff and Zhang, 1991; Elishakoff,1991; Zhang, Elishakoff and Zhang, 1990), is extended to treat random vibrations of the nonlinearly deformed beam. The main idea of the new method consists in the requirement that the mean square value of the difference of potential energies of deformation, associated with the original nonlinear equation and its equivalent linear counterpart, should be minimal. It is instructive to first elucidate the basic idea on the example of the single-degree-of-freedom system, governed by the following differential equation

$$m\ddot{x} + c\dot{x} + g(x) = F(t) \tag{1}$$

where $F(t)$ is a random excitation resulting in stochastic response $x(t)$; $g(x)$ is a nonlinear deterministic function of displacement x. Within the stochastic linearization scheme, this

differential equation is replaced by the "equivalent" linear equation

$$m\ddot{x} + c\dot{x} + k_{eq}x = F(t) \tag{2}$$

where the coefficient k_{eq} is determined through some suitable criterion of equivalence. In the linearization scheme utilized by Elishakoff and Zhang (1991), the equivalence criterion is chosen as follows

$$E\left\{[U(x) - \frac{1}{2}k_{eq}x^2]^2\right\} = \min \tag{3}$$

where $U(x)$ is the potential energy of deformation of the original nonlinear structure, i.e.

$$U(x) = \int_0^x g(\alpha)d\alpha \tag{4}$$

This is accomplished by requiring

$$\frac{d}{dk_{eq}}E\left\{[U(x) - \frac{1}{2}k_{eq}x^2]^2\right\} = 0 \tag{5}$$

Eq.(5) results in the following expression for the equivalent spring stiffness

$$k_{eq} = \frac{2E[x^2U(x)]}{E(x^4)} \tag{6}$$

In recent studies (Elishakoff and Zhang, 1991; Elishakoff, 1991; Zhang, Elishakoff and Zhang, 1990), the authors have demonstrated the accuracy of this linearization technique by comparing the computed mean square displacements from different stochastic linearization methods with some known exact solutions. In present study, the authors extend the above technique to the continuous structures. The main idea is same as the one described for the single-degree-of-freedom system, except that the original continuous nonlinear structure is replaced by a multi-

degree-of-freedom linear system, and a set of equivalent spring stiffnesses are expressed by equations analogous to Eq.(6) with x now corresponding to different modal displacements. The procedure will be elucidated in detail for random vibrations of the nonlinearly deformed beam.

In this paper we consider beams simply supported or damped at their ends. Two loading conditions are considered: (a) the space-wise and time-wise white noise, in which case the exact solution is also obtained, (b) the space-wise uniformly distributed load and time-wise white noise, in which case no exact solution is available and the Monte Carlo simulations should be performed. In all cases and wide variety of levels of excitation the proposed method turns out to be superior to the classical stochastic linearization method.

2. FORMULATION OF THE PROBLEM

Consider a beam on elastic foundation with pin-ended supports that are restrained from axial motion (Fig. 1).

The beam is under a loading $q(x,t)$ which is space-wise and time-wise white noise with the following auto-correlation function

$$R_{qq}(x_1, t_1; x_2, t_2) = 2\pi S_0 \delta(x_2 - x_1)\delta(t_2 - t_1) \tag{7}$$

The deflection is represented by the Fourier series in terms of mode shapes of the undamped beam

$$w(x, t) = \sum_{n=1}^{N} w_n(t) \sin\frac{n\pi x}{L} \tag{8}$$

$w_n(t)$ is the modal contribution corresponding to nth mode. It is assumed that only the first N

modes of the beam are significantly contributing to formulating the response. However, it should be born in mind that the assumption that the power spectral density of the load is that of white noise implies that all the modes are excited and contribute to the response of the beam; N is determined by the required accuracy in evaluation of the specific response characteristic, such as mean-square displacement or mean-square stress. Crandall and Yildiz (1962) have shown that for the linearly deformed beam under white noise excitation, if the infinite series representing quantities such as mean square displacement, mean square stress, etc., converge, then the results can be made as accurate as desired by taking sufficiently large N. It is reasonable to expect similar results for the nonlinear problem. We consider a Bernoulli-Euler beam with transverse damping. Due to the fact that the equivalence criterion will utilize the concept of energy, we first formulate appropriate energies of the beam. Kinetic energy of the beam is given by, with Eq.(8) taken into account

$$T = \frac{\rho A}{2}\int_0^L \left(\frac{\partial w}{\partial t}\right)^2 dx = \frac{\rho A L}{4}\sum_{n=1}^{N}(\dot{w}_n)^2 \tag{9}$$

the potential energy of bending deformation reads

$$V_b = \frac{EI}{2}\int_0^L \left(\frac{\partial^2 w}{\partial x^2}\right)^2 dx = \frac{\pi^4 EI}{4L^3}\sum_{n=1}^{N} n^4 w_n^2 \tag{10}$$

Potential energy of stretching is given by

$$V_s = \frac{AE}{2L}\left[\frac{1}{2}\int_0^L \left(\frac{\partial w}{\partial x}\right)^2 dx\right]^2 = \frac{\pi^4 AE}{32L^3}\left[\sum_{n=1}^{N} n^2 w_n^2\right]^2 \tag{11}$$

whereas the potential energy of the deformation due to elastic foundation is

$$V_e = \int_0^L \frac{1}{2} k_f w^2 dx = \frac{1}{4} k_f L \sum_{n=1}^{N} w_n^2 \tag{12}$$

where k_f is the translational stiffness of Winkler foundation. Potential function of the load is

$$V_l = -\int_0^L q(x,t)\, w(x,t)\, dx \tag{13}$$

We expand the load in the series analogous to Eq.(8)

$$q(x,t) = \sum_{n=1}^{N} q_n(t) \sin \frac{n\pi x}{L} \tag{14}$$

where again N terms have been retained. Then V_l becomes

$$V_l = -\frac{L}{2} \sum_{n=1}^{N} q_n w_n \tag{15}$$

The Lagrangian $\mathcal{L}=T-V$, where $V=V_b+V_s+V_e+V_b$ may now be written as

$$\begin{aligned} \mathcal{L} = {} & \frac{\rho A L}{4} \sum_{n=1}^{N} (\dot{w}_n)^2 - \frac{\pi^4 EI}{4L^3} \sum_{n=1}^{N} n^4 w_n^2 \\ & - \frac{\pi^4 EA}{32L^3} \left[\sum_{n=1}^{N} n^2 w_n^2 \right]^2 - \frac{1}{4} k_f L \sum_{n=1}^{N} w_n^2 + \frac{L}{2} \sum_{n=1}^{N} q_n w_n \end{aligned} \tag{16}$$

The equations of motion are

$$\frac{d}{dt}\left(\frac{\partial \mathcal{L}}{\partial \dot{w}_n} \right) - \frac{\partial \mathcal{L}}{\partial w_n} = 0 \qquad (n = 1, 2, \cdots, N) \tag{17}$$

where w_n are considered as generalized coordinates. Substitution of Eq.(16) into (17) yields the following N equations in terms of the modal amplitudes $w_n(t)$

$$\ddot{w}_n + \frac{\beta}{\rho A}\dot{w}_n + \omega_0^2 n^4 \left[1 + \frac{\alpha}{n^4} + \frac{1}{4R^2 n^2}\sum_{m=1}^{N} m^2 w_m^2\right] w_n = f_n \qquad (n = 1, 2, \cdots, N) \tag{18}$$

where β is an introduced linear viscous-damping term. In addition, following notations have been utilized

$$\omega_0^2 = \frac{\pi^4 EI}{\rho A L^4}, \qquad \alpha = \frac{k_f}{\rho A \omega_0^2}, \qquad R = \sqrt{\frac{I}{A}}, \qquad f_n = \frac{q_n}{\rho A} \tag{19}$$

Eq.(18) is a nonlinear stochastic differential equation. We seek the mean square response of the modal amplitudes. In this study, a new stochastic linearization technique described in the preceding section for the single-degree-of-freedom system, is generalized to investigate the continuous structure at hand. The nonlinear system (18) is replaced by the following equivalent linear one

$$\ddot{w}_n + \frac{\beta}{\rho A}\dot{w}_n + k_{eq}^{(n)} w_n = f_n(x) \qquad (n = 1, 2, \cdots, N) \tag{20}$$

In Eq.(20), it is assumed that the replacing linear system is a decoupled one. The question of the decoupling will be addressed in detail in Appendix.

In our problem, the total potential energy of the system (18) is

$$U(w_1, \cdots, w_N) = \frac{\pi^4 EI}{2\rho AL^4}\sum_{n=1}^{N} n^4 w_n^2 + \frac{k_f}{2\rho A}\sum_{n=1}^{N} w_n^2 + \frac{\pi^4 E}{16\rho L^4}\left[\sum_{n=1}^{N} n^2 w_n^2\right]^2$$
$$= \frac{\omega_0^2}{2}\sum_{n=1}^{N} n^4 w_n^2 + \frac{\alpha\omega_0^2}{2}\sum_{n=1}^{N} w_n^2 + \frac{\omega_0^2}{16R^2}\left[\sum_{n=1}^{N} n^2 w_n^2\right]^2 \tag{21}$$

We generalize the requirement of Eq.(3) valid for the single-degree-of-freedom system, for continuous beam by requiring

$$E\left\{\left[U(w_1, w_2, \cdots, w_N) - \sum_{n=1}^{N}\frac{1}{2}k_{eq}^{(n)} w_n^2\right]^2\right\} = \min \tag{22}$$

which is achieved by using conditions

$$\frac{d}{dk_{eq}^{(m)}}\left\{E\left[U(w_1, w_2, \cdots, w_N) - \sum_{n=1}^{N}\frac{1}{2}k_{eq}^{(n)} w_n^2\right]^2\right\} = 0 \tag{23}$$
$$(m = 1, 2, \cdots, N)$$

The conditions (23) are equivalent to

$$E\left\{\left[U(w_1, w_2, \cdots, w_N) - \sum_{n=1}^{N}\frac{1}{2}k_{eq}^{(n)} w_n^2\right] w_m^2\right\} = 0 \tag{24}$$
$$(m = 1, 2, \cdots, N)$$

After some algebra, we arrive at the following expression for nonlinear spring constants

$$\{k_{eq}\} = 2[A]^{-1}\{B\} \tag{25}$$

where

$$\{k_{eq}\}^T = \left\{k_{eq}^{(1)} \quad k_{eq}^{(2)} \quad \cdots \quad k_{eq}^{(N)}\right\}$$

$$\{B\}^T = \left\{E[w_1^2 U] \quad E[w_2^2 U] \quad \cdots \quad E[w_N^2 U]\right\}$$

$$[A] = \begin{bmatrix} E[w_1^2 w_1^2] & E[w_1^2 w_2^2] & \cdots & E[w_1^2 w_N^2] \\ E[w_2^2 w_1^2] & E[w_2^2 w_2^2] & \cdots & E[w_2^2 w_N^2] \\ & \cdots \ \cdots \ \cdots & & \\ E[w_N^2 w_1^2] & E[w_N^2 w_2^2] & \cdots & E[w_N^2 w_N^2] \end{bmatrix} \tag{26}$$

We denote

$$y_i = E[w_i^2] \tag{27}$$

Gaussian assumption for distribution of w_i and the subsequent conclusion that the equivalent system is decoupled (see Appendix), leads to the independence between different modal amplitudes w_i and w_j $(i \neq j)$. Therefore

$$\begin{aligned} E[w_i^4] &= 3y_i^2 \\ E[w_i^2 w_j^2] &= y_i y_j \qquad i \neq j \end{aligned} \tag{28}$$

For simplicity, let us investigate the particular case $N=3$. We have

$$[A]^{-1} = \frac{1}{10 y_1 y_2 y_3} \begin{bmatrix} \dfrac{4y_2y_3}{y_1} & -y_3 & -y_2 \\ -y_3 & \dfrac{4y_1y_3}{y_2} & -y_1 \\ -y_2 & -y_1 & \dfrac{4y_1y_2}{y_3} \end{bmatrix} \tag{29}$$

Consequently we obtain

$$E[w_n^2 U] = \frac{\omega_0^2}{2} E[w_n^2 \sum_{m=1}^{3} m^4 w_m^2] + \frac{\alpha\omega_0^2}{2} E[w_n^2 \sum_{m=1}^{3} w_m^2] + \frac{\omega_0^2}{16R^2} E[w_n^2 (\sum_{m=1}^{3} m^2 w_m^2)^2] \quad (30)$$

Under the assumption that the system is driven by zero mean Gaussian white noise q_n with spectral density S_0, i.e. f_n with spectral density $S_0/(\rho A)^2$, we obtain from Eq.(20)

$$k_{eq}^{(n)} = \sigma_0^2 \omega_0^2 / y_n \quad (31)$$

or

$$\{k_{eq}\} = \sigma_0^2 \omega_0^2 \{ 1/y_1 \quad 1/y_2 \quad \cdots \quad 1/y_n \}^T \quad (32)$$

where

$$\sigma_0^2 = \frac{L^4 S_0}{\pi^3 \beta E I} \quad (33)$$

Substituting $k_{eq}^{(n)}$ in Eq.(32) into Eq.(25) and noting the fact that w_n is Gaussian yields

$$\begin{Bmatrix} \sigma_0^2 \\ \sigma_0^2 \\ \sigma_0^2 \end{Bmatrix} = \left(\frac{2}{\omega_0^2}\right)\left(\frac{1}{10 y_1 y_2 y_3}\right) \begin{bmatrix} 4y_2y_3 & -y_1y_3 & -y_1y_2 \\ -y_2y_3 & 4y_1y_3 & -y_1y_2 \\ -y_2y_3 & -y_1y_3 & 4y_1y_2 \end{bmatrix} \begin{Bmatrix} E[w_1^2 U] \\ E[w_2^2 U] \\ E[w_3^2 U] \end{Bmatrix} \quad (34)$$

where

$$E[w_1^2 U] = \frac{\omega_0^2}{2} y_1 \{(3y_1 + 16y_2 + 81y_3) + \alpha(3y_1 + y_2 + y_3) + \frac{1}{8R^2}(15y_1^2 + 48y_2^2 + 243y_3^2 + 24y_1y_2 + 72y_2y_3 + 54y_1y_3)\}$$

$$E[w_2^2 U] = \frac{\omega_0^2}{2} y_2 \{(y_1 + 48y_2 + 81y_3) + \alpha(y_1 + 3y_2 + y_3) + \frac{1}{8R^2}(3y_1^2 + 240y_2^2 + 243y_3^2 + 24y_1y_2 + 216y_2y_3 + 18y_1y_3)\} \quad (35)$$

$$E[w_3^2 U] = \frac{\omega_0^2}{2} y_3 \{(y_1 + 16y_2 + 243y_3) + \alpha(y_1 + y_2 + 3y_3) + \frac{1}{8R^2}(3y_1^2 + 48y_2^2 + 1215y_3^2 + 8y_1y_2 + 216y_2y_3 + 54y_1y_3)\}$$

Substitution of Eq. (35) into Eq.(34) results in a set of algebraic nonlinear equations for y_1, y_2, and y_3. For different excitation levels characterized by σ_0, the foundation modulus α and various radii of gyration R, Eq.(34) can be solved numerically. In our study, the standard Levenberg-Marquardt algorithm is implemented.

With $y_i = E[w_i^2]$ obtained, we arrive at the mean square response of the beam as

$$E[w^2(x,t)] = \sum_{n=1}^{3}\sum_{m=1}^{3} E(w_m w_n) \sin\frac{m\pi x}{L} \sin\frac{n\pi x}{L} \quad (36)$$

However, the modal amplitudes w_m are uncorrelated. Therefore, while the membrane stress causes the modal amplitudes to become statistically dependent, it still leaves them uncorrelated. Eq.(36) then reduces to

$$E[w^2(x,t)] = \sum_{m=1}^{3} y_m \sin^2 \frac{m\pi x}{L} \tag{37}$$

3. COMPARISON WITH OTHER METHODS

(1) Fokker-Planck equation method.

From the solution of Fokker-Planck equation, the exact expression of the probability density function is obtained as

$$p(w_1, w_2, \cdots, w_N) = \frac{1}{c}\exp\left\{-\frac{1}{2\sigma_0^2}\left[\sum_{n=1}^{N} n^4 w_n^2 + \frac{1}{8R^2}\sum_{n=1}^{N}\sum_{m=1}^{N} m^2 n^2 w_m^2 w_n^2 + \alpha\sum_{n=1}^{N} w_n^2\right]\right\} \tag{38}$$

where c is the normalization factor, i.e.

$$c = \int_{-\infty}^{\infty} dw_1 \cdots \int_{-\infty}^{\infty} \exp\left\{-\frac{1}{2\sigma_0^2}\left[\sum_{n=1}^{N} n^4 w_n^2 + \frac{1}{8R^2}\sum_{n=1}^{N}\sum_{m=1}^{N} m^2 n^2 w_m^2 w_n^2 + \alpha\sum_{n=1}^{N} w_n^2\right]\right\} dw_N \tag{39}$$

Eq.(38) coincides with that of Herbert (1964) except that we have introduced an additional term associated with the elastic foundation. Hence, the modal mean square responses are obtained by integration

$$E[w_m^2] = \frac{1}{c}\int_{-\infty}^{\infty} dw_1 \cdots \int_{-\infty}^{\infty} w_m^2 \exp\left\{-\frac{1}{2\sigma_0^2}\left[\sum_{n=1}^{N} n^4 w_n^2 + \frac{1}{8R^2}\sum_{r=1}^{N}\sum_{n=1}^{N} n^2 r^2 w_n^2 w_r^2 + \alpha\sum_{n=1}^{N} w_n^2\right]\right\} dw_N \tag{40}$$

Eq.(40) must be evaluated by numerical integration.

(2) Conventional Stochastic linearization Technique.

By the conventional equivalent linearization method, we obtain

$$k_{eq}^{(n)} = n^4\omega_0^2 + \alpha\omega_0^2 + \frac{\omega_0^2 n^2}{4R^2}\frac{E[w_n^2\sum_{m=1}^{N} m^2 w_m^2]}{E[w_n^2]} \tag{41}$$

From the equivalent linear system (20), we have Eq.(31).

Substituting $k_{eq}^{(n)}$ in Eq.(42) into Eq.(31) yields

$$\sigma_0^2 = (n^4+\alpha)E[w_n^2] + \frac{n^2}{4R^2}E[w_n^2\sum_{m=1}^{N} m^2 w_m^2] \tag{42}$$

$$(n = 1, \cdots, N)$$

If only the first three modes are considered, in view of Eq.(27), we obtain

$$\begin{aligned}
\sigma_0^2 &= (1+\alpha)y_1 + \frac{1}{4R^2}(3y_1^2 + 4y_1y_2 + 9y_1y_3) \\
\sigma_0^2 &= (16+\alpha)y_2 + \frac{1}{R^2}(y_1y_2 + 12y_2^2 + 9y_2y_3) \\
\sigma_0^2 &= (81+\alpha)y_3 + \frac{9}{4R^2}(y_1y_3 + 4y_2y_3 + 27y_3^2)
\end{aligned} \tag{43}$$

For specific values of σ_0^2, α and R, one can evaluate $E[w_1^2]$, $E[w_2^2]$ and $E[w_3^2]$ through solving the set of nonlinear equations Eq.(43).

4. RESULTS AND DISCUSSION

Numerical computations have been performed for the mean square deflection at the midspan of the beam for various values of three parameters σ_0^2, α and R. The results from the three methods are presented in Figs. 2 through 5. As pointed out by Seide (1975) and as is confirmed in equation (37), accurate values of the mean square deflections can be obtained by using a three-term approximation, while the number of terms required for accurate stress values may be much larger. In the present study, only the first three modal displacements are considered, with the emphasis on demonstrating the effectiveness of the new stochastic linearization technique.

As is seen from the differential equation (18), when formally R tends to infinity the effect of the nonlinearity disappears. Therefore, magnitude of $1/R$ can be viewed as the parameter related with the magnitude of nonlinearity. The effect of the foundation stiffness on mean square maximum deflection at the midspan of beam is shown in Fig. 2 for one set of levels of excitation and nonlinearity. It can be seen that the new equivalent linearization method yields more accurate results than the conventional technique. Also, it is shown that the new method usually gives greater values of mean square deflection than the exact solution, while the conventional method yields values below the exact one. Furthermore, when the stiffness of the foundation k_f becomes larger (and consequently the parameter α is larger too), both methods tend to produce equally accurate results. This conclusion should have been anticipated in view of the fact that the system is "more" linear in this case, due to linearity of the Winkler foundation model. However, when α is small, the new stochastic linearization method achieves much better estimate of the mean square deflection than the conventional technique. The mean square

deflections vs parameter R are shown in Figs. 3 and 4; the new method performs much better than the conventional stochastic linearization technique for the relatively high nonlinearity of the system, i.e. R is from 0 to 1. The effect of strength of excitation on the accuracy of the two methods is shown in Fig. 5, where the vertical axis denotes the percentage error of the mean square deflection at the midspan of the beam either between the conventional linearization method or the new linearization method, and the exact solution; the new approach achieves more accurate results than the conventional technique for all the excitation levels.

To get additional insight into the performance of the proposed method the other set of boundary conditions was investigated. Namely, the beam clamped at both ends under the both space-wise and time-wise white noise was considered. Fig. 6 portrays the mean square displacement calculated by the proposed stochastic linearization method, conventional stochastic linearization method and exact solution. An exact solution follows the derivation given in Eqs. (14)-(32) except that instead of the sinusoidal mode shape in Eq. (8), the following mode shape is utilized

$$\psi_j(x) = \cosh \gamma_j x - \cos\gamma_j x - \alpha_j(\sinh \gamma_j x - \sin\gamma_j x) \tag{44}$$

where

$$\alpha_j = \begin{cases} \tanh\frac{1}{2}\gamma_j & \text{if } m \text{ is odd} \\ \coth\frac{1}{2}\gamma_j & \text{if } m \text{ is even} \end{cases} \tag{45}$$

and the values of γ_j are the consecutive solutions of the transcendental equation

$$\cosh \gamma_j \cos \gamma_j = 1 \tag{46}$$

As is seen from Fig. 6 for the clamped beam too, the proposed method results in the mean square response which is much closer to the exact solution, than the classical linearization method.

In both cases of the beams considered the exact solutions were also obtained. The natural question arises: How does the proposed method perform when exact solution is not available? To answer this question, the additional loading condition was also investigated. Namely, the load $q(x,t)$ was represented as a product $r(x)q(t)$. Whereas $q(t)$ was assumed to be weakly stationary Gaussian random process namely white noise, $r(x)$ was taken as a deterministic function. Specifically $r(x)$ was taken as a constant, representing space-wise uniformly distributed load. This representation is valid for the members of relatively short length when the correlation length of the excitation is much greater than the length of the beam. For such a loading condition an exact solution is unavailable and instead, Monte Carlo simulations should be conducted to check the accuracy of the proposed stochastic linearization. Fig. 7 depicts results of such a comparison for the simply supported beam. As is clearly seen, the proposed method again exhibits much higher accuracy than the conventional linearization technique.

To sum up, for different boundary conditions and the loading patterns, the suggested method is superior to the classical stochastic linearization technique, especially in the important high nonlinearity range of the parameters.

5. ACKNOWLEDGEMENT

This study has been supported by the NASA Kennedy Space Center, through Cooperative Agreement No. NCC 10-0005, S1 to Florida Atlantic University. This support is gratefully appreciated.

REFERENCES

Bogdanoff, J. L. and Goldberg, J. E. (1960). On the Bernoulli-Euler Beam Theory with Random Excitation. *J. Aero/space Sci.*, **27**, 371-376.

Busby, H.R. and Weingarten, V.I. (1973). Response of Nonlinear Beam to Random Vibration. *J. Engng. Mech. Div.*, ASCE, **99**, 55-68.

Crandall S. H. and Yildiz A. (1962). Random Vibrations of Beams. *J. Appl. Mech.*, **29**, 267-275.

Elishakoff, I. (1987). Generalized Eringen Problem: Influence of Axial Force on Random Vibration Response of Simply Supported Beam. *J. Struct. Safety*, **4**, 255-265.

Elishakoff, I. (1991). Method of Stochastic Linearization Revised and Improved. *Computational stochastic Mechanics* (edited by P. D. Spanos and C. A. Brebbia), Computational Mechanics Publications and Elsevier Applied Science, 101-111.

Elishakoff, I and Livshits, D. (1984). Some Closed-Form Solutions in Random Vibration of Bernoulli-Euler Beams. *Int. J. Engng. Sci.*, **22**, 1291-1302.

Elishakoff, I. and Zhang, R. C. (1991). Comparison of the New Energy-Based Versions of the Stochastic Linearization Technique. *Nonlinear Stochastic Mechanics* (edited by N. Bellomo and F. Casciati), Springer, Berlin, 201-212.

Eringen, A. C. (1957). Response of Beams and Plates to Random Loads. *J. Appl. Mech.*, **24**, 46-52.

Fang, J. and Fang, T. (1991). A New Equivalent Method in Random Vibration. *Chinese J. Appl. Mech.*, **8**, 114-120 (in Chinese).

FORTRAN Subroutines for Mathematical Applications. (1989). IMSL MATH/LIBRARY, 776-783.

Herbert, R.E. (1964). Random Vibrations of a Nonlinear Elastic Beam. *J. Acoust. Soc. Am.*, **36**, 2090-2094.

Herbert, R.E. (1965). On the Stresses in a Nonlinear Beam Subject to Random Excitation. *Int. J. Solids Structures*, **1**, 235-242.

Roberts, J. B. and Spanos, P. D. (1990). *Random Vibration and Statistical Linearization*, John Wiley & Sons.

Seide, P. (1975). Nonlinear Stress and Deflections of Beams Subjected to Random Time Dependent Uniform Pressure. *Design Engng Technical Conf.*, ASME, paper No. 75-DET-23.

Sinitsin, I. N. (1974). Methods of Statistical Linearization (Survey). *Automation and Remote Control*, **35**, 765-786.

Socha, L. and Soong, T. T. (1991). Linearization of Nonlinear Stochastic Systems. *Appl. Mech. Rev.*, **44**, 399-422.

Zhang, X. T., Elishakoff, I. and Zhang, R. C. (1990). A Stochastic Linearization Technique Based on Minimum Mean Square Deviation of Potential Energies. *Stochastic Structural Dynamics 1* (edited by Y. K. Lin and I. Elishakoff), Springer, Berlin, 327-338.

APPENDIX

Uncoupledness of Equivalent Linear System

Under the assumption that the modal displacements are Normally distributed, one can show that the equivalent linear system is uncoupled. Indeed, suppose that the equivalent linear system is governed by the vector equation

$$M\ddot{w} + C\dot{w} + Kw = f \tag{A·1}$$

where M and C are diagonal mass and damping matrices, and K is non-diagonal stiffness matrix, and f's are independent white noises. New equivalence criterion requires

$$E\left\{\left[U(w) - \frac{1}{2}w^T K w\right]^2\right\} = \min \tag{A·2}$$

where

$$w = \{w_1 \quad w_2 \quad \cdots \quad w_N\}^T \tag{A·3}$$
$$K = [k_{ij}]$$

The condition that the derivatives of (A.2) with respect to k_{ij} equal zero leads to

$$E[ww^T K ww^T] = 2E[wU(w)w^T] \tag{A·4}$$

For simplicity, let us consider the two-degree-of-freedom system. Suppose

$$K = \begin{bmatrix} k_{11} & k_{12} \\ k_{12} & k_{22} \end{bmatrix} \tag{A·5}$$

Then

$$ww^T K ww^T = \begin{bmatrix} w_1^4 k_{11} + 2w_1^3 w_2 k_{12} + w_1^2 w_2^2 k_{22} & w_1^3 w_2 k_{11} + 2w_1^2 w_2^2 k_{12} + w_1 w_2^3 k_{22} \\ w_1^3 w_2 k_{11} + 2w_1^2 w_2^2 k_{12} + w_1 w_2^3 k_{22} & w_1^2 w_2^2 k_{11} + 2w_1 w_2^3 k_{12} + w_2^4 k_{22} \end{bmatrix}$$

$$E[wU(w)w^T] = \begin{bmatrix} w_1^2 U & w_1 w_2 U \\ w_1 w_2 U & w_2^2 U \end{bmatrix} \tag{A·6}$$

Therefore Eq. (A·4) becomes

$$[A_1]\{k_1\} = 2\{B_1\} \tag{A·7}$$

where

$$[A_1] = \begin{bmatrix} E[w_1^4] & 2E[w_1^3 w_2] & E[w_1^2 w_2^2] \\ E[w_1^3 w_2] & 2E[w_1^2 w_2^2] & E[w_1 w_2^3] \\ E[w_1^2 w_2^2] & 2E[w_1 w_2^3] & E[w_2^4] \end{bmatrix} \tag{A·8}$$

$$\{k_1\} = \{k_{11} \quad k_{12} \quad k_{22}\}^T$$

$$\{B_1\} = \left\{E[w_1^2 U] \quad E[w_1 w_2 U] \quad E[w_2^2 U]\right\}^T$$

The assumption of zero-mean Gaussian distribution of the modes w_n implies

$$E[w_1^3 w_2] = 0$$
$$E[w_1 w_2^3] = 0 \tag{A·9}$$

In view of Eq. (21), we also have

$$E[w_1 w_2 U] = 0 \tag{A·10}$$

As a result, A_1 and B_1 turn out to be

$$[A_1] = \begin{bmatrix} E[w_1^4] & 0 & E[w_1^2 w_2^2] \\ 0 & 2E[w_1^2 w_2^2] & 0 \\ E[w_1^2 w_2^2] & 0 & E[w_2^4] \end{bmatrix} \tag{A·11}$$

$$\{B_1\} = \{E[w_1^2 U] \quad 0 \quad E[w_2^2 U]\}^T$$

Substituting $[A_1]$, $\{B_1\}$ in Eq. (A·11) into Eq. (A·7), one obtains

$$k_{12} = 0 \tag{A·12}$$

This illustrates the uncoupledness of the equivalent linear system in the two-degree-of-freedom setting. Analogous proof holds for $N > 2$.

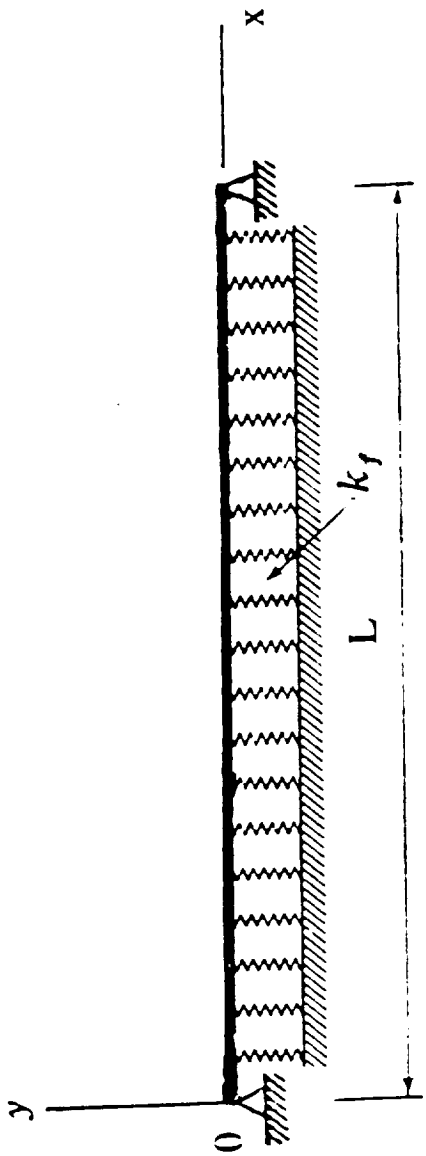

Fig. 1 Nonlinear beam on elastic foundation

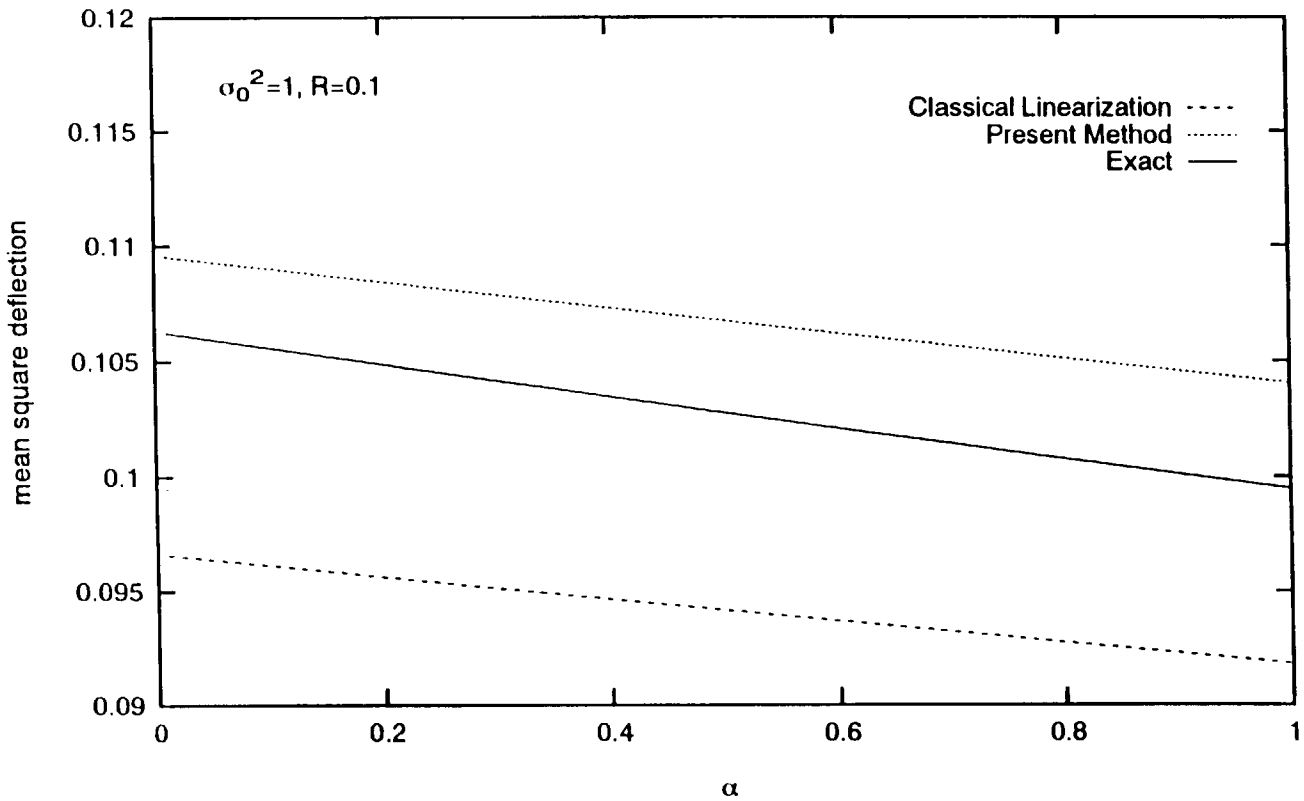

Fig. 2 Effect of foundation stiffness (α) on mean square deflection at the midspan of the simply supported beam (space-wise white noise loading).

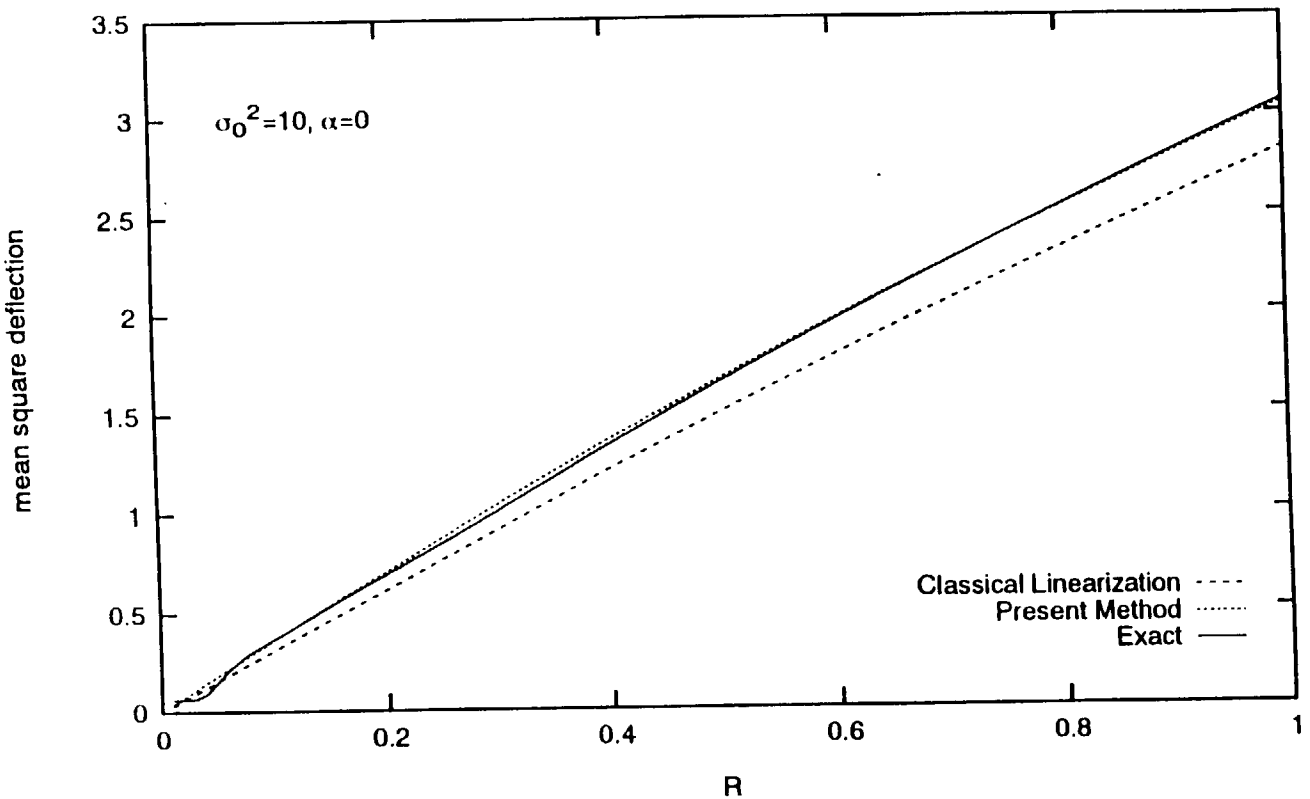

Fig. 3 Effect of nonlinearity (R) on mean square deflection at the midspan of the simply supported beam ($\sigma_0^2 = 10,\ \alpha = 0$) (space-wise white noise loading).

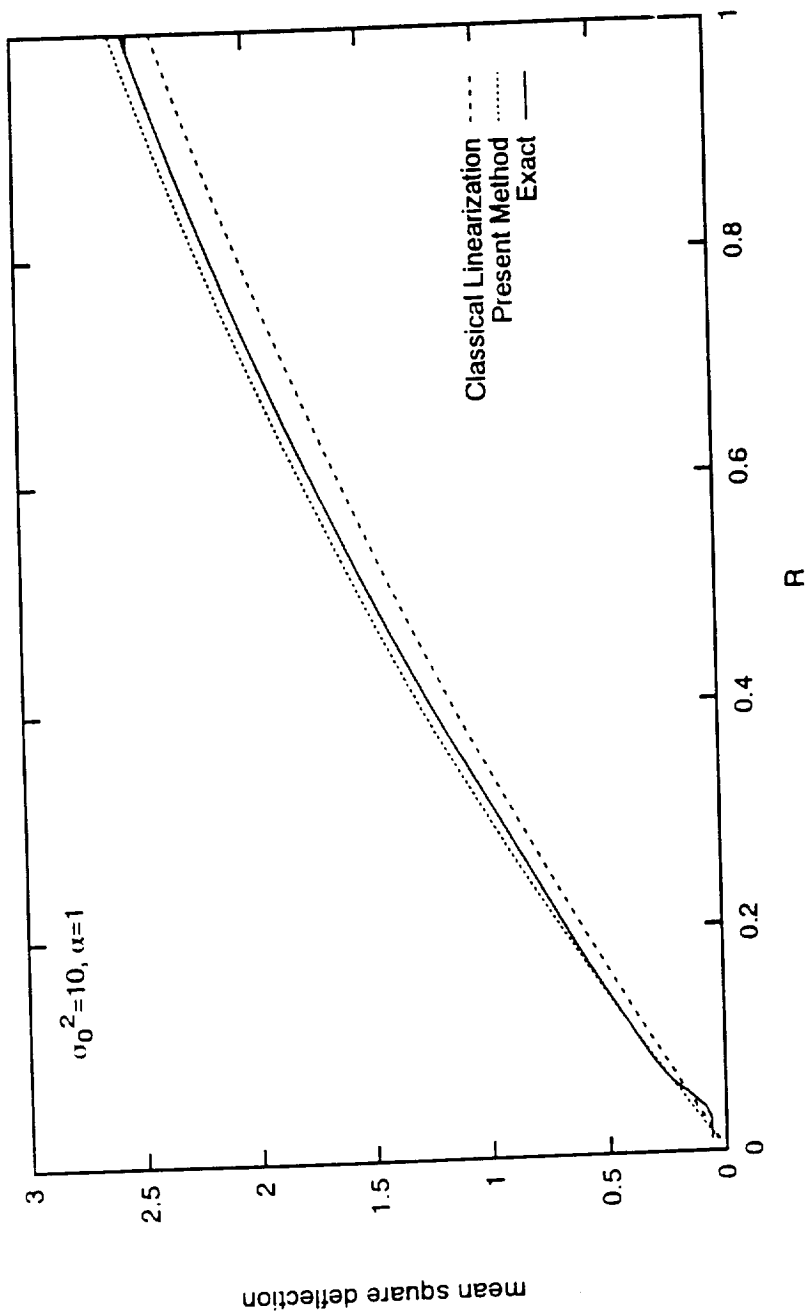

Fig. 4 Effect of nonlinearity (R) on mean square deflection at the midspan of the simply supported beam ($\sigma_0^2 = 10$, $\alpha = 1$) (space-wise white noise loading).

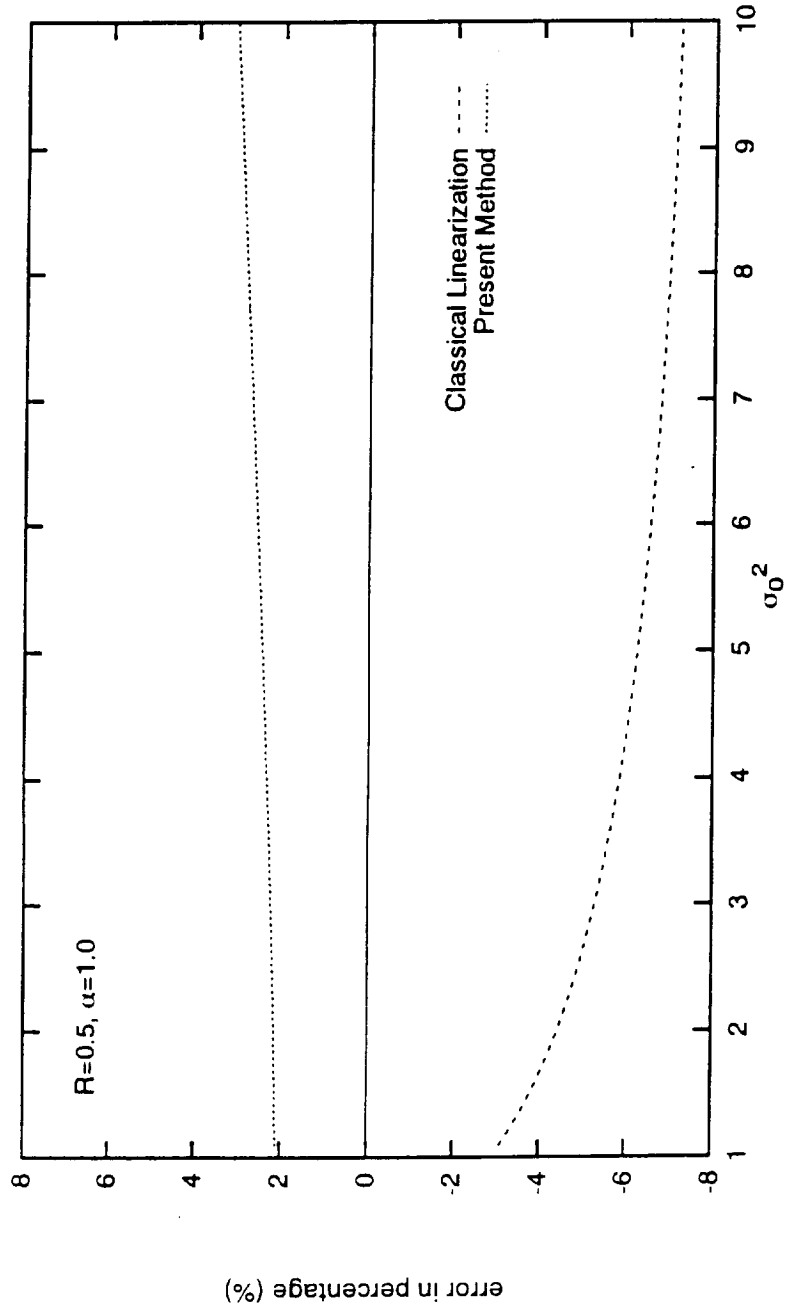

Fig. 5 Percentage error in determination of mean square deflection by the two methods in comparison with exact solution (space-wise white noise loading).

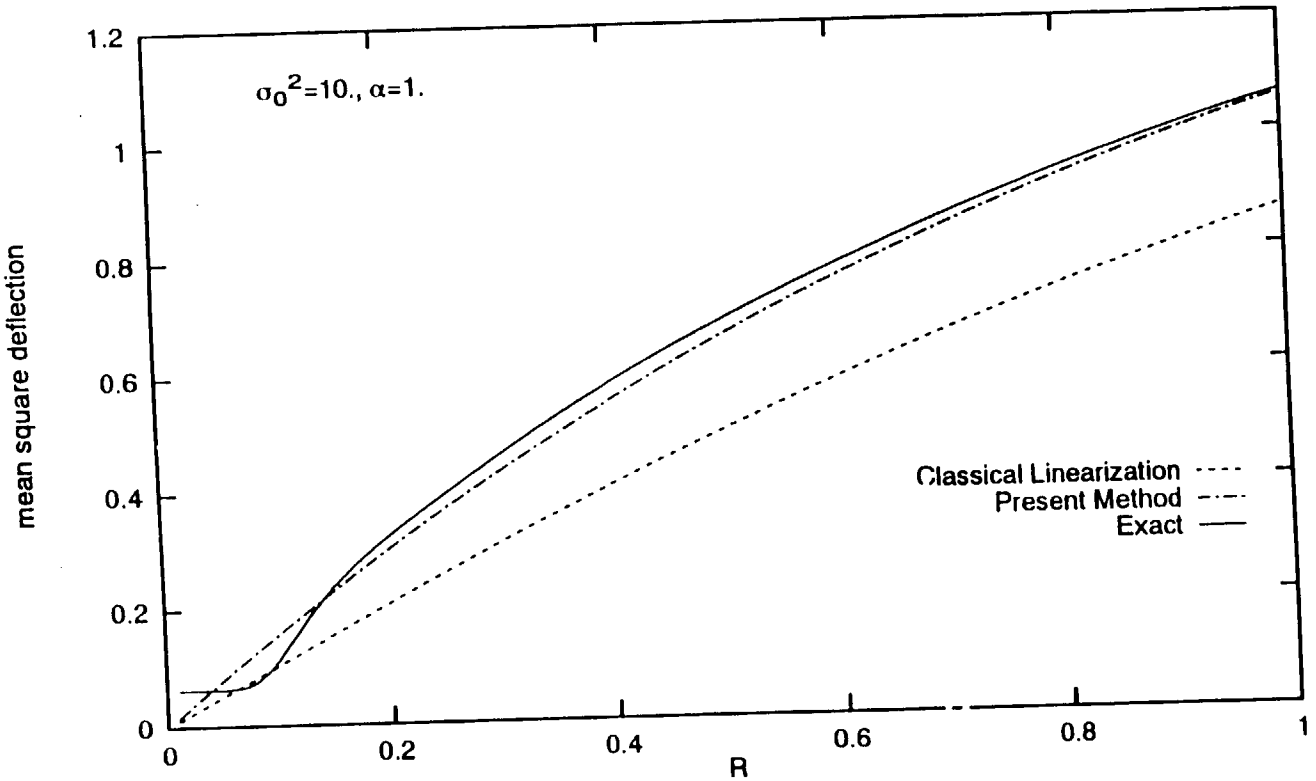

Fig. 6 Effect of nonlinearity (R) on mean square deflection at the midspan of the beam clamped at both ends ($\sigma_0^2 = 10,\ \alpha = 1$) (space-wise white noise loading).

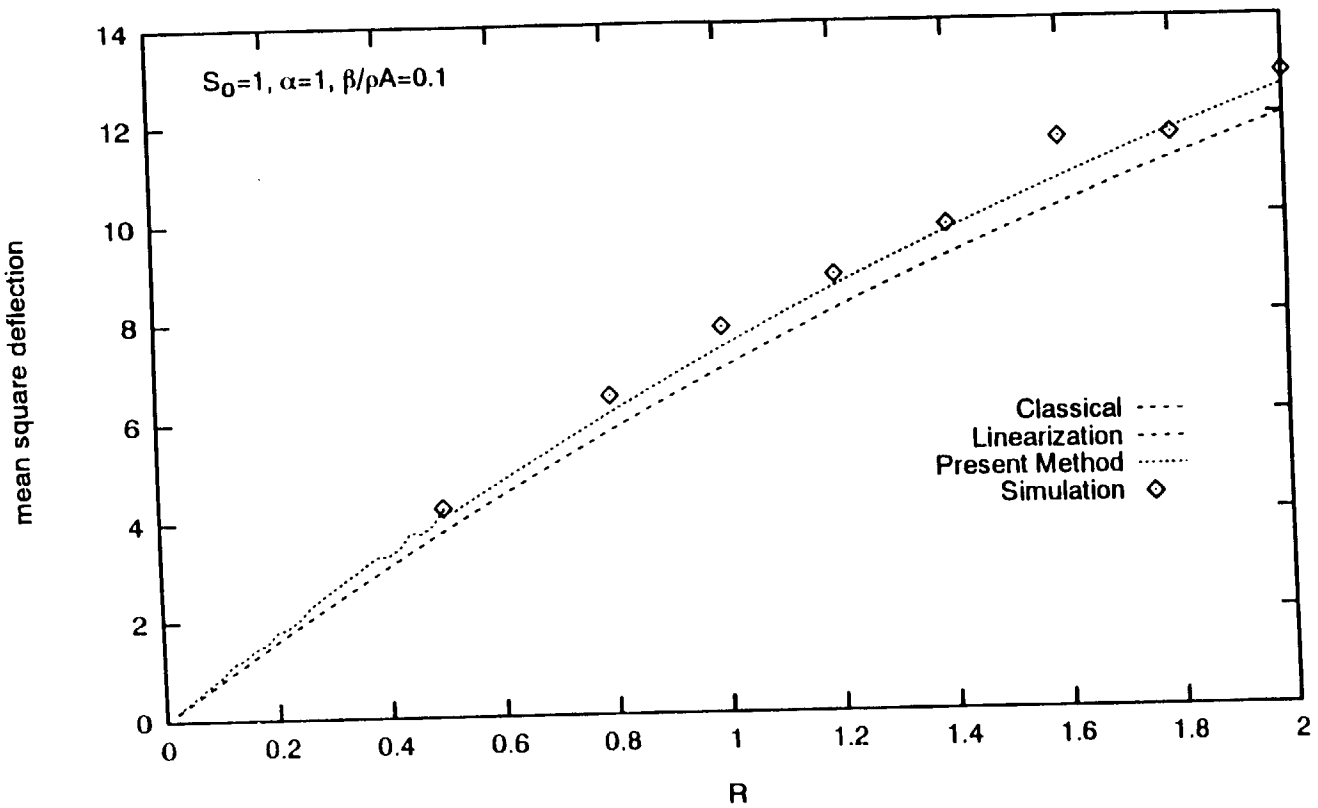

Fig. 7 The variation of the mean square deflection at the mid-span of the simply supported beam with the nonlinearity coefficient R (space-wise uniformly distributed load).

CHAPTER # 9

Approximate Solution for Random Vibrations of Nonlinearly Damped Systems by Partial Stochastic Linearization

Approximate Solution for Random Vibrations of Nonlinearly Damped Systems by Partial Stochastic Linearization

I. Elishakoff and G. Q. Cai

Center for Applied Stochastics Research and Department of Mechanical Engineering

Florida Atlantic University, Boca Raton, FL 33431-0991, USA

ABSTRACT The accuracy of the stochastic linearization method is improved by the proposed method of partial stochastic linearization, in which only the nonlinear damping force in the original system is replaced by a linear viscous damping, while the nonlinear restoring force remains unchanged. The replacement is based on the criterion of equal mean work, performed by the nonlinear damping force in the original system and its linear counterpart. The resulting nonlinear stochastic differential equation is then solved exactly, keeping the equivalent damping coefficient as a parameter, which can be determined for a specific system by solving a nonlinear algebraic equation.

INTRODUCTION

There exist very few nonlinear stochastic problems amenable to exact solutions. Therefore, the

investigators are resorting to various approximate techniques. One of the most popular techniques is the method of stochastic linearization [1-6]. This method has many drawbacks however. For example, the tail probabilities for the Duffing oscillator, predicted by the approximation may differ form the exact value by a factor as large as 250[7], and the first excursion probability may be in error by several orders of magnitudes[8].

Recently, an alternative technique, called "stochastic nonlinearization" has been suggested[9-13], in which one replaces the original nonlinear stochastic differential equation by another "close" nonlinear equation, possessing an exact solution. In some cases, however, this method is not amenable to closed form solution.

This study combines the stochastic linearization and nonlinearization techniques. It is specially designed for systems with both nonlinear damping and nonlinear restoring force. Instead of the classical stochastic linearization technique, where both nonlinear damping and nonlinear restoring force are replaced by their respective linear counterparts, here we use only a *partial* linearization, namely, we linearize only the damping. The equation thus obtained is amenable to an exact solution. The equivalent damping parameter is obtained by solving a nonlinear algebraic equation either analytically or numerically. For the system with nonlinear damping but with linear restoring force, the present method coincides with the usual stochastic linearization. For the system with both nonlinear damping and nonlinear restoring force, it represents a natural generalization of the stochastic linearization. The proposed procedure considerably *improves* the accuracy of the stochastic linearization and yields *simple* equations to determine the desired probabilistic characteristics.

BASIC EQUATIONS

Consider the following nonlinear equation

$$\ddot{X} + f(X,\dot{X}) + g(X) = W(t) \tag{1}$$

Here $f(X,\dot{X})$ is associated generally with nonlinear damping and $g(X)$ is associated with nonlinear restoring force. The excitation W(t) is assumed to be a Gaussian white noise. We replace the nonlinear damping force $f(X,\dot{X})$ by an equivalent linear one,

$$\ddot{X} + \beta_e \dot{X} + g(X) = W(t) \tag{2}$$

Thus, the key issue is to determine the equivalent damping coefficient β_e for the substituting system (2). The criterion for selecting β_e is that the average energy dissipation remains the same[11,12], namely,

$$E[\dot{X} f(X,\dot{X})] = \beta_e E[\dot{X}^2] \tag{3}$$

The left and right hand sides of equation (3) represent the average work per unit time performed by the original nonlinear damping force and the equivalent linear damping force, respectively. It is noted that the stochastic linearization uses the least mean square criterion, namely,

$$E\{[\, f(X,\dot{X}) - \beta_e \dot{X}]^2\} = \textit{minimum} \tag{4}$$

which also leads to equation (3). Although the formally identical criterion (3) is used in both stochastic linearization and partial linearization, the ensemble averaging in equation (3) is performed with different probability densities for these two methods. In the stochastic linearization, the probability density is assumed to be Gaussian, while in the present partial linearization method, it is generally not Gaussian.

We now calculate the left hand side of equation (3). Equation (1) can be written in the following Itô differential equation form

$$dX_1 = X_2 dt \tag{5a}$$

$$dX_2 = [-f(X_1,X_2) - g(X_1)]dt + \sqrt{2\pi K}\, dB(t) \tag{5b}$$

where $X_1 = X$, $X_2 = \dot{X}$, K is the spectral density of the white noise excitation $W(t)$, and $B(t)$ is a unit Wiener's process. According to the Itô differential rule[14],

$$\frac{d}{dt}X_2^2 = -2X_2[f(X_1,X_2) + g(X_1)] + 2\pi K + 2\sqrt{2\pi K}\,X_2 dB(t) \tag{6}$$

Ensemble averaging of equation (6) results in

$$\frac{d}{dt}E[X_2^2] = -2E\{X_2[f(X_1,X_2) + g(X_1)]\} + 2\pi K \tag{7}$$

which reduces to

$$E[X_2 f(X_1,X_2)] = \pi K \tag{8}$$

for the stationary state. Equation (8) leads to a remarkable conclusion: for any oscillator with only an additive white noise excitation, the average work done by the damping force per unit time depends only on the spectral density of the excitation, regardless the damping mechanism. The same conclusion was reached by Karnopp[15] by using a different proof. Hence, from equations (3) and (8)

$$\beta_e = \frac{E[\dot{X} f(X,\dot{X})]}{E[\dot{X}^2]} = \frac{\pi K}{E[\dot{X}^2]} \tag{9}$$

We will make use of the fact that the exact stationary probabilistic solution of equation

(2) is a classical result of the random vibration; it reads[3,4]

$$p(x,\dot{x}) = C\exp\{-\frac{\beta_e}{\pi K}[\frac{\dot{x}^2}{2} + \int_0^x g(u)\,du]\} \tag{10}$$

where C is a constant determined from the normalization condition

$$C = \left\{\int_{-\infty}^{\infty}\int_{-\infty}^{\infty}\exp\{-\frac{\beta_e}{\pi K}[\frac{\dot{x}^2}{2} + \int_0^x g(u)\,du]\}dx\,d\dot{x}\right\}^{-1} \tag{11}$$

Equation (10) shows that the velocity of system (2) is a Gaussian random variable, while the displacement is not. The probability density (10) can be considered as an approximate one for the response of the original system and can be used in equation (8) to yield

$$C\int_{-\infty}^{\infty}\int_{-\infty}^{\infty}\dot{x}f(x,\dot{x})\exp\{-\frac{\beta_e}{\pi K}[\frac{\dot{x}^2}{2} + \int_0^x g(u)\,du]\}dx\,d\dot{x} = \pi K \tag{12}$$

Substituting Eq. (11) into Eq. (12), we obtain

$$\int_{-\infty}^{\infty}\int_{-\infty}^{\infty}[\dot{x}f(x,\dot{x}) - \pi K]\exp\{-\frac{\beta_e}{\pi K}[\frac{\dot{x}^2}{2} + \int_0^x g(u)\,du]\}dx\,d\dot{x} = 0 \tag{13}$$

This is a nonlinear algebraic equation for β_e which can be solved analytically or numerically for a given system. Once β_e is determined, it can be substituted into equation (10) for the approximate joint probability density.

If the nonlinear damping force depends only on the velocity, namely, $f(X,\dot{X}) = f(\dot{X})$, then equation (13) is reduced to

$$\int_{-\infty}^{\infty} [\dot{x} f(\dot{x}) - \pi K] \exp(-\frac{\beta_e \dot{x}^2}{2\pi K}) d\dot{x} = 0 \qquad (14)$$

Equation (14) can often be solved analytically for β_e.

It can be seen that if the damping force depends on both the displacement and velocity, then the equivalent damping coefficient calculated from (13) is different from that obtained from equivalent linearization, because the displacement is not a Gaussian random variable. When the damping force is dependent solely on velocity, both methods yield the same equivalent damping coefficient from equation (14) since the velocity is Gaussian. However, the present method is simpler than the stochastic linearization method since only an equivalent damping coefficient needs to be calculated.

It is noted that Caughey[10] proposed an approximation scheme to replace the original nonlinear damping by an energy-dependent nonlinear damping by using the least mean square criterion. But his method was only applied to systems with linear restoring force. Lin[13] extended Caughey's method to the case of nonlinear restoring force. However, the determination of the replacement nonlinear damping force usually requires numerical calculations.

As expected, the partial linearization method yields more accurate results than the equivalent linearization since it retains one of the characteristics of the original nonlinear system, namely the nonlinear restoring force. However, the method is expected to be less accurate than the energy dissipation balancing method in which the equivalent damping force is selected from a larger class of linear and nonlinear damping forces, rather than from the sub-class of linear damping. Therefore, the selected equivalent damping using the energy dissipation balancing method is generally "closer" to the original damping. Nevertheless, we pay a penalty of more

numerical computations for obtaining more accurate results, when the approximate probability density has to be calculated numerically at every point in the energy dissipation balancing method, as shown in the illustrative example. One can visualize that for the preliminary design of structures, one may need a sufficiently accurate analytical technique such as the proposed partial linearization rather than a fully numerical technique. For final design of the structure once its parameters are nominally chosen based on partial linearization, one may use a refined analysis of the structure vis the dissipation energy balancing method.

MOMENTWISE CONSISTENCY OF THE PROPOSED METHOD

It is of interest to note that, in terms of certain statistical moments of the response, the partial linearization method is a consistent approximation procedure. Consider $M(X_1,X_2) = X_1^i X_2^j$ where i and j are nonnegative integers. An equation for $E[M]$ can be obtained by using Itô's differential rule for M, and then taking the ensemble averaging, resulting in

$$\frac{d}{dt}E[M] = E\left[X_2\frac{\partial M}{\partial X_1}\right] + E\left\{\left[-f(X_1,X_2) - g(X_1)\right]\frac{\partial M}{\partial X_2}\right\} + \pi KE\left[\frac{\partial^2 M}{\partial X_2^2}\right] \qquad (15)$$

The left hand side of (15) is a time derivative of a nth ($n=i+j$) order moment, while the form of the right hand side depends on functions f and g. It contains only the nth and lower order moments if both f and g are linear; however, it also contains moments of orders higher than n if at least one of the f and g functions is a nonlinear polynomial. In either case, equation (15) represents a set of relations among moments.

When the system response eventually attains the stationary state after a sufficiently long exposure to Gaussian white noise excitations, the moment equations of the form (15) are reduced

to algebraic equations as follows

$$E\left[X_2\frac{\partial M}{\partial X_1}\right] + E\left\{\left[-f(X_1,X_2) - g(X_1)\right]\frac{\partial M}{\partial X_2}\right\} + \pi K E\left[\frac{\partial^2 M}{\partial X_2^2}\right] = 0 \tag{16}$$

Letting $M = X_1$, X_2, X_1^2, X_1X_2 and X_2^2, we obtain from (16) the following relations:

$$E[X_2] = 0 \tag{17a}$$

$$E[f(X_1,X_2) + g(X_1)] = 0 \tag{17b}$$

$$E[X_1X_2] = 0 \tag{17c}$$

$$E[X_2^2] = E\{X_1[f(X_1,X_2) + g(X_1)]\} \tag{17d}$$

$$E\{X_2[f(X_1,X_2) + g(X_1)]\} = \pi K \tag{17e}$$

Equations (17a)-(17e) are satisfied if the true stationary probability density of the system response is used when performing the ensemble averaging. They may or may not be satisfied if an approximate probability density is used.

Yet, the use of the approximate probability density (10) guarantees that equations (17a)-(17e) are also satisfied provided that $g(X_1)$ is an odd function, and $f(X_1, X_2)$ is an odd function of X_2 and an even function of X_1, which is true for most physical systems. The validity of the above assertion is obvious for equation (17a)-(17c). Equation (17e) is also satisfied by virtue of equation (12). Lastly, equation (17d) can be verified by noting that $E[X_1 f(X_1,X_2)] = 0$ and $E[X_1 g(X_1)] = E[X_2^2]$ upon the following integrations by parts:

$$C\int_{-\infty}^{\infty}\int_{-\infty}^{\infty} x_1 g(x_1)\exp\{-\frac{\beta_e}{\pi K}[\frac{x_2^2}{2}+\int_0^{x_1} g(u)\,du]\}dx_1 dx_2 = \frac{\pi K}{\beta_e} \tag{18}$$

and

$$C\int_{-\infty}^{\infty}\int_{-\infty}^{\infty} x_2^2\exp\{-\frac{\beta_e}{\pi K}[\frac{x_2^2}{2}+\int_0^{x_1} g(u)\,du]\}dx_1 dx_2 = \frac{\pi K}{\beta_e} \tag{19}$$

ILLUSTRATIVE EXAMPLE

For illustration, consider a system governed by

$$\ddot{X} + \beta\dot{X} + \alpha\dot{X}^3 + \gamma X + \delta X^3 = W(t) \tag{20}$$

The stochastic linearization yields

$$p(x,\dot{x}) = C\exp[-\frac{\beta_e}{\pi K}(\frac{1}{2}\dot{x}^2 + \frac{1}{2}k_e x^2)] \tag{21}$$

where

$$\beta_e = \frac{\beta}{2} + \sqrt{(\frac{\beta}{2})^2 + 3\alpha\pi K} \tag{22}$$

and

$$k_e = \frac{\gamma}{2} + \sqrt{(\frac{\gamma}{2})^2 + \frac{3\pi K\delta}{\beta_e}} \tag{23}$$

With partial linearization method, only the same β_e is needed to evaluate a "better" probability density

$$p(x,\dot{x}) = C_1 \exp[-\frac{\beta_e}{\pi K}(\frac{1}{2}\dot{x}^2 + \frac{1}{2}\gamma x^2 + \frac{1}{4}\delta x^4)] \tag{24}$$

In this example, the present method is simpler and more accurate than the equivalent linearization.

Let us contrast now the partial and "full" stochastic linearization[1-6,16,17] methods with the more accurate energy dissipation method[11]. The probability density is found to be

$$p(x,\dot{x}) = C_2 \exp\left\{-\frac{\beta}{\pi K}\lambda - \frac{\alpha}{\pi K}\int \frac{\int_{-A}^{A}(2\lambda - \gamma x^2 - \frac{1}{2}\delta x^4)^{\frac{3}{2}}dx}{\int_{-A}^{A}(2\lambda - \gamma x^2 - \frac{1}{2}\delta x^4)^{\frac{1}{2}}dx} d\lambda\right\} \tag{25}$$

where λ is the total energy given by

$$\lambda = \frac{1}{2}\dot{x}^2 + \frac{1}{2}\gamma x^2 + \frac{1}{4}\delta x^4 \tag{26}$$

and

$$A = \begin{cases} \sqrt{\sqrt{(\frac{\gamma}{\delta})^2 + 4\frac{\lambda}{\delta}} - \frac{\gamma}{\delta}}, & \delta \neq 0 \\ \sqrt{2\frac{\lambda}{\gamma}}, & \delta = 0,\ \gamma \neq 0 \end{cases} \tag{27}$$

The integrals in equation (25) cannot be obtained in closed form if both δ and γ are nonzero.

By using the method proposed by Caughey[10] and Lin[13] and choosing two coefficients in the replacing nonlinear damping force, the approximate probability density is obtained as

$$p(x,\dot{x}) = C_2 \exp\left[-\frac{1}{\pi K}(c_{01}\lambda + c_{03}\lambda^2)\right] \tag{28}$$

where λ is shown in (26), and the two coefficients c_{01} and c_{03} satisfy

$$m_{02}c_{01} + (m_{04} + \gamma m_{22} + \frac{1}{2}\delta m_{42})c_{03} = \beta m_{02} + \alpha m_{04} \tag{29a}$$

$$(m_{04} + \gamma m_{22} + \frac{1}{2}\delta m_{42})c_{01} + (m_{06} + \gamma^2 m_{42} + \frac{1}{4}\delta^2 m_{82} + 2\gamma m_{24} + \delta m_{44} + \delta\gamma m_{62})c_{03}$$

$$= \beta(m_{04} + \gamma m_{22} + \frac{1}{2}\delta m_{42}) + \alpha(m_{06} + \gamma m_{24} + \frac{1}{2}\delta m_{44}) \tag{29b}$$

where $m_{ij} = E[X_i \dot{X}_j]$. Equations (28) and (29) can be solved together for c_{01} and c_{03}.

The approximate results (25) and (28) may improve the accuracy by introducing a higher order term of λ. However, numerical computations have to be performed to obtain the approximate results.

In Figs. 1 and 2, the stationary mean square values of the displacement X for system (20) are plotted against the stiffness nonlinearity parameter δ and the damping nonlinearity parameter α, respectively. Results computed from both the "full" linearization and partial linearization are shown and compared with the Monte-Carlo simulation results. It is seen that considerably higher accuracy can be achieved with the present method as compared to the "full" linearization procedure.

CONCLUSIONS

For a single-degree-of-freedom nonlinear oscillator subjected to an external Gaussian white noise

excitation, the partial linearization method not only yields more accurate results than those obtained from the full linearization method, but also requires less computation. It is also shown that the partial linearization method is a consistent approximation scheme in the sense that the obtained approximate probability density satisfies certain exact relationships for certain statistical moments of the system response.

ACKNOWLEDGEMENT

This study has been supported by the NASA Kennedy Space Center, through Cooperative Agreement No. NCC10-000,S1, Technical Monitor Mr. R. Caimi. This support is gratefully appreciated. We are also grateful to Professor Y. K. Lin for constructive comments.

REFERENCES

1 Caughey, T. K. Equivalent linearization techniques, *Journal of Acoustical Society of America,* 1963, **35**, 1706-1711.

2 Crandall, S. H. On statistical linearization for nonlinear oscillators, in "*Nonlinear System Analysis and Synthesis: Volume 2 - Techniques and Applications*", (R.V. Ramnath, J. Hedrick and H. M. Paynther, eds.), ASME 1980, 199-209.

3 Lin, Y. K. *Probabilistic Theory of Structural Dynamics,* McGraw Hill, New York, 1967 (Second edition: Robert Krieger Company, Malabar, FL, 1976).

4 Bolotin, V. V. *Random Vibrations of Elastic Systems,* Martinus Nijhoff Publishers, The Hague, 1984.

5 Spanos, P. D. Stochastic linearization in structural dynamics, *Applied Mechanics Reviews,*

1981, **34**(10), 1-8.

6 Roberts, J. B. and Spanos, P. D. *Random Vibration and Statistical Linearization,* Wiley, New York, 1990.

7 Hampl, N. C. Non-Gaussian stochastic analysis of nonlinear systems, in "*Proceedings of the 2nd International Workshop on Stochastic Methods in Structural Mechanics*", (F. Casciati and L. Faravelli, eds.), University of Pavia, 1986, 243-254.

8 Schuëller G. I. and Bucher, C. G. Nonlinear damping and its effects on the reliability estimates of structures, in "*Random Vibration-Status and Recent Developments*", (I. Elishakoff and R. H. Lyon, eds.), Elsevier Science Publishers, Amsterdam, 1986, 389-402.

9 Lutes, L. D. Approximate technique for testing random vibration of hysteretic systems, *Journal of Acoustical Society of America,* 1970, **48**, 299-306.

10 Caughey, T. K. On response of non-linear oscillators to stochastic excitation, *Probabilistic Engineering Mechanics,* 1986, **1**, 2-4.

11 Cai, G. Q. and Lin, Y. K. A new approximate technique for randomly excited nonlinear oscillators, *International Journal of Nonlinear Mechanics,* 1988, **23**, 409-420.

12 Cai, G. Q., Lin, Y. K. and Elishakoff, I. A new approximate technique for randomly excited nonlinear oscillators, Part II, *International Journal of Nonlinear Mechanics,* to apper, 1991.

13 Lin, A. A numerical evaluation of the method of equivalent nonlinearization, *Ph. D. Dissertation,* Califorlia Institute of Technology, 1988.

14 Itô, K. On a formula concerning stochastic differentials, *Nagoya Math. J.,* 1951, **3**, 55-

65.

15 Karnopp, D. Power balance method for nonlinear random vibration, *Journal of Applied Mechanics,* 1967, **34**, 212-214.

16 Elishakoff, I. and Zhang, X. An appraisal of different stochastic linearization techniques, *Journal of Sound and Vibration,* to appear, 1991.

17 Elishakoff, I. Stochastic linearization: revised and improved, in "*Computational Stochastic Mechanics*", (P. D. Spanos and C. A. Brebbia, eds.), Elsevier, London, 1991, 101-110.

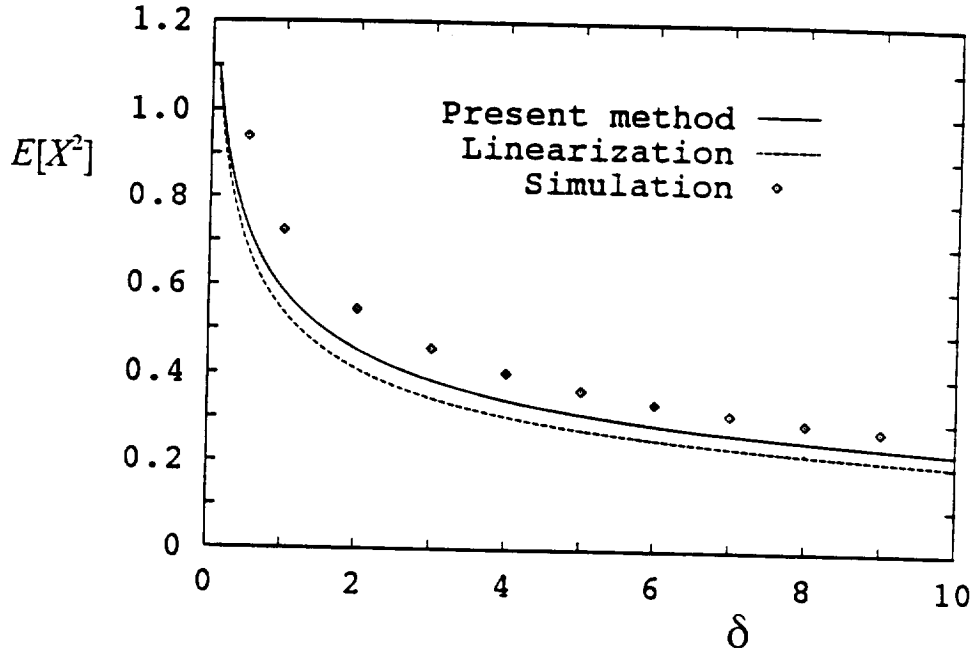

Fig. 1. *Mean square displacement with respect to stiffness nonlinearity; $K=1$, $\beta=0.1$, $\alpha=0.5$, $\gamma=1$*

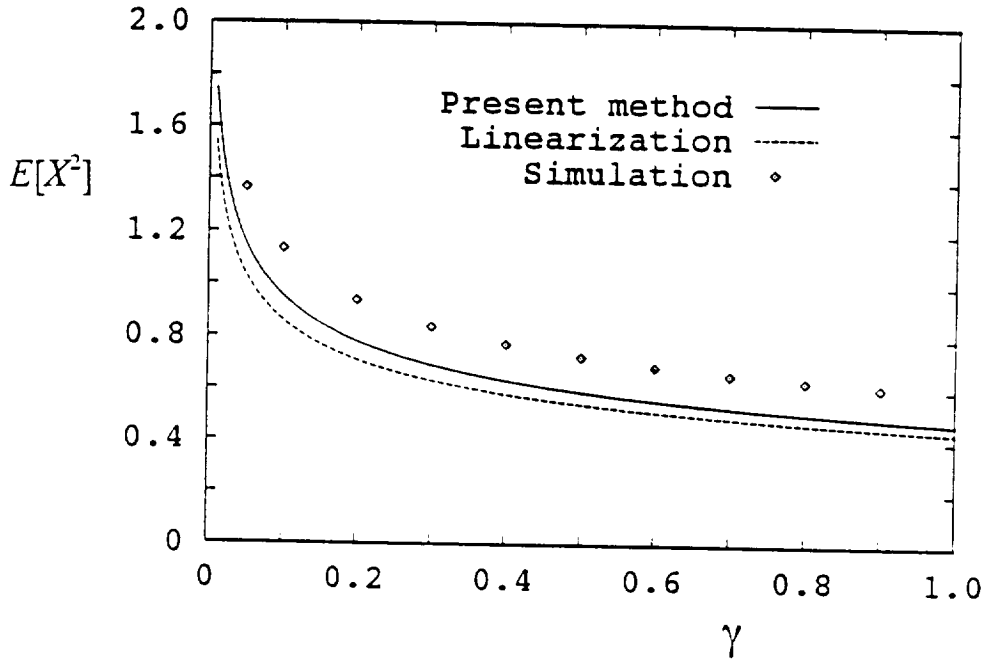

Fig. 2. *Mean square displacement with respect to damping nonlinearity; $K=1$, $\beta=0.1$, $\delta=1$, $\gamma=1$*